Toward realizable quantum computers

Thesis by
Michael Edward Beverland

In Partial Fulfillment of the Requirements for the
degree of
Doctor of Philosophy

CALIFORNIA INSTITUTE OF TECHNOLOGY
Pasadena, California

2016
Defended (May 20, 2016)

Michael Edward Beverland
ORCID: [Author ORCID]

ACKNOWLEDGEMENTS

I have been very lucky to have been surrounded by many inspiring scientists while a graduate student at Caltech.

Firstly, I would like to thank my advisor, John Preskill, for always finding time to hear me out when I wanted to explain my often underdeveloped ideas. He will always be my role model as a physicist. Along with John, I would also like to thank the rest of my thesis committee: Xie Chen, Alexei Kitaev, and Gil Refael.

I have also received valuable mentorship from my main collaborators Alexey Gorshkov, Gorjan Alagic, Fernando Pastawski, and Krysta Svore. Their guidance has been invaluable.

Special thanks goes to my officemate, collaborator and good friend Aleksander Kubica. I have had many other exceptional collaborators deserve a lot of credit for the work presented in this thesis: Gretchen Campbell, Jeongwan Haah, Ana Maria Rey, Michael Martin, Andrew Koller, Hector Bombin, Robert Koenig, Sumit Sijher, and Oliver Buerschaper.

John's group meetings have been a hub for quantum information and have provided much inspiration. Regular attendees during my time include, Ning Bao, Mario Berta, Thom Bohdanowicz, Peter Brooks, Todd Brun, Darrick Chang, Elizabeth Crosson, Nicolas Delfosse, Andrew Essin, Glen Evenbly, Bill Fefferman, Matthew Fishman, Steve Flammia, Alexey Gorshkov, David Gosset, Nick Hunter-Jones, Joe Iverson, Stacey Jeffery, Stephen Jordan, Isaac Kim, Olivier Landon-Cardinal, Netanel Lindner, Shaun Maguire, Prabha Mandayam, Spiros Michalakis, Roger Mong, Evgeny Mozgunov, Leonid Pryadko, Kirill Shtengel, Sujeet Shukla, Kristan Temme, and Beni Yoshida.

Other people in the field I have learned a lot from include, Sergey Bravyi, Ben Brown, Dan Browne, Tomas Jochym-OConnnor, David Poulin, and Thomas Vidick.

Overall I had an overwhelmingly positive PhD experience. This has largely been due to support and friendships from many friends I have made at Caltech, in Cambridge, and in Belfast and in Medellin. Eduardo Serna has been particularly influential, and has taught me a lot about how to code. Of course my family, and my girlfriend Achiamar, deserve extra thanks for putting up with my slightly unconventional life choices!

ABSTRACT

The work in this thesis splits naturally into two parts: (1) experimentally oriented work consisting of experimental proposals for systems that could be used to implement quantum information tasks with current technology, and (2) theoretical work focusing on universal fault-tolerant quantum computers which we hope can be scaled as experimental capabilities continue to move forward. Chapters one, three, and four are based on published work Michael E. Beverland et al., 2016; Koller et al., 2014; Michael E Beverland et al., 2016; Kubica and M. Beverland, 2015. Chapters two and three cover currently unpublished work (at the time of writing).

In the first chapter we propose trapping cold atoms in a square-well to robustly implement a spin hamiltonian which is naturally protected from the dominant source of noise. The key feature is that the system's Hamiltonian has parameters which are independent of the spatial degrees of atomic motion which is not the case for spin hamiltonians made with other traps or a different type of atom. The Hamiltonian is highly symmetric (invariant under both on-site spin rotations and site permutations), and exactly solvable. This highly symmetric spin model should be experimentally realizable even when the vibrational levels are occupied according to a high-temperature thermal or an arbitrary non-thermal distribution.

After analyzed the experimental aspects of the proposal and a few direct applications in the first chapter, in chapter two we focus on a particular application for which the system is particularly well suited: spectrum estimation of unknown density matrices. The symmetry group of the Hamiltonian is precisely the group which is relevant for the Young diagram algorithm to measure density matrices Keyl and Werner, 2001. The highly entangled Young diagram measurements are performed naturally via standard Ramsey spectroscopy in our system, when prepared with a copy of the unknown density matrix in the nuclear spin of each atom.

In the first chapter of second part of the thesis, we consider the important class of quantum error correcting codes which can be understood as two-dimensional topological quantum field theories. The most promising implementations for quantum computers, such as Kitaev's surface code, are of this type. Importantly, they can be implemented by using local operations on a two-dimensional lattice, yet they can store information non-locally, protecting it from the effects of the most common physical noise (which tends to act locally). These features make such codes ideal

for storing quantum information and can result in high error thresholds. In chapter three, we consider the fault-tolerant processing of information in such codes. As opposed to studying braiding of anyons, about which much was already known, we considered the action of locally generated unitary logical gates. Locally generated logical gates of topological codes are intrinsically fault tolerant because spatially localized errors remain localized, and therefore correctible. They are also expected to be much easier to implement than braiding in some settings. Unfortunately, we find severe limitations on the locally generated logical gates. No code in this class has a universal set of locally generated gates, and topological codes which support anyons which are universal for braiding have no non-trivial locally generated gates. Abelian models have locally generated gates restricted to the Clifford group. We derive these results by relating logical gates of a topological code to automorphisms of the Verlinde algebra of the corresponding anyon model.

Although are results are negative, there are ways around them. Firstly, braiding is known to be universal for some topological codes, although they may be hard to implement in practice. There is a standard approach Sergey Bravyi and Alexei Kitaev, 2005, using resource states, to complete the universal gate set for a code which admits the full (but non-universal) Clifford group. These resource states cannot be fault-tolerantly generated in the code, but they can be distilled so that many noisy resource states can be traded for fewer resource states with less noise. The drawback is that this approach involves very significant overhead, which accounts for the vast majority of the quibits required in the realistic overhead estimates Austin G Fowler et al., 2012.

Although in chapter three we find that two-dimensional topological codes have severe restrictions on the locally generated gates that can occur, in higher dimensional topological codes there is considerably more freedom. In chapter four we describe a three-dimensional topological code for which one can use locally generated unitaries (along with local measurement) to achieve a universal gate set. Our work is based on ideas from Bombín's paper *Gauge Color Codes* [arXiv:1311.0879v3]. We show how to transversally implement the generalized phase gate $R_n = \text{diag}(1, e^{2\pi i/2^n})$ in an n-dimensional color code, which deviates from the method in the aforementioned paper, allowing an arguably simpler proof. We describe how to implement the Hadamard gate H fault-tolerantly by fault-tolerantly switching to another code. In three dimensions, this yields, together with the transversal CNOT , a fault-tolerant universal gate set $\{H, \text{CNOT}, R_3\}$ without using resource states.

Finally, in chapter five we ask if code switching like that described in chapter four involves less overhead than its competitor state distillation. Unfortunately we find that this type of codeswitching does not appear to offer an overhead advantage. This is because the third dimension which must be used to construct the three-dimensional code has to be filled with many qubits – even more qubits than are required to distill resource states. As a part of this work, we found error thresholds of 0.3 % and 4.2 % under circuit-level and phenomenological noise for the two-dimensional color code on the hexagonal lattice using an efficient decoder. These numbers significantly close the gap with the surface code, which (still) has the best known circuit level threshold of ~ 1 %.

PUBLISHED CONTENT AND CONTRIBUTIONS

Beverland, Michael E et al. (2016). "Protected gates for topological quantum field theories". In: *Journal of Mathematical Physics* 57.2, p. 022201.

Beverland, Michael E. et al. (2016). "Realizing exactly solvable $\mathrm{SU}(N)$ magnets with thermal atoms". In: *Phys. Rev. A* 93 (5), p. 051601.

Koller, A. P. et al. (2014). "Beyond the Spin Model Approximation for Ramsey Spectroscopy". In: *Phys. Rev. Lett.* 112, p. 123001.

Kubica, Aleksander and Michael Beverland (2015). "Universal transversal gates with color codes: A simplified approach". In: *Physical Review A* 91.3, p. 032330.

Chapter one was partially motivated by the results in Koller et al., 2014 (to which I was a minor contributor). Chapter one is based on work published in Michael E. Beverland et al., 2016 (to which I was the main contributor). Chapter three is based on work in Michael E Beverland et al., 2016. I began this project by analyzing abelian systems with my Caltech collaborators. We benefited greatly by working with Robert Koenig and his Masters student Sumit Sijher along with Oliver Buerschaper yielding results applicable to non-abelian systems. Chapter four is based on the work with Aleksander Kubica Kubica and M. Beverland, 2015. We both contributed significantly to this work: I focused mainly on the code-switching aspects, and Aleksander focused mainly on the higher dimensional color code. We wrote the paper together.

TABLE OF CONTENTS

Part I

Small quantum computers

Chapter 1

A NATURALLY PROTECTED SYMMETRIC HAMILTONIAN

In this chapter we propose the use of n thermal fermionic alkaline-earth atoms in a flat-bottom trap to robustly implement a spin model which is naturally protected from noise. The key feature is that the system's Hamiltonian has parameters which are independent of the spatial degrees of atomic motion which is not the case for spin hamiltonians made with other traps or a different type of atom. The hamiltonian displays two symmetries: the S_n symmetry that permutes atoms occupying different vibrational levels of the trap and the SU(N) symmetry associated with N nuclear spin states. The high symmetry makes the model exactly solvable, which, in turn, enables the analytic study of dynamical processes such as spin diffusion in this SU(N) system. We also show how to use this system to generate entangled states that allow for Heisenberg-limited metrology.

This highly symmetric spin model should be experimentally realizable even when the vibrational levels are occupied according to a high-temperature thermal or an arbitrary non-thermal distribution.

1.1 Background and Motivation

The study of quantum spin models with ultracold atoms Bloch, Dalibard, and Zwerger, 2008; Bloch, Dalibard, and Nascimbene, 2012 promises to give crucial insights into a range of equilibrium and non-equilibrium many-body phenomena from quantum spin liquids Balents, 2010 and many-body localization Basko, Aleiner, and Altshuler, 2006 to quantum quenches Polkovnikov et al., 2011; Richerme et al., 2014; Jurcevic et al., 2014 and quantum annealing Das and Chakrabarti, 2008. While other approaches exist Wu, 2008; Simon et al., 2011; Pielawa et al., 2011; Schauß et al., 2012, the most common approach to implementing a quantum spin model with ultracold atoms relies on preparing a Mott insulator in an optical lattice, where the internal states of atoms on each site define the effective spin Duan, Demler, and Lukin, 2003; Bloch, Dalibard, and Zwerger, 2008; Trotzky et al., 2008; Fukuhara et al., 2013; Greif et al., 2013; Hild et al., 2014; Hart et al., 2015; R. C. Brown et al., 2015. Virtual hopping processes to neighboring sites and back then give rise to effective superexchange spin-spin interactions. Since the superexchange interactions are typically very weak ($\ll$ kHz) Bloch, Dalibard, and Zwerger, 2008

(unless the traps are operated near surfaces, which can reduce spacings and increase energy scales Gullans et al., 2012; Romero-Isart et al., 2013; González-Tudela et al., 2015), it is a significant challenge in experimental cold atom physics to achieve temperatures and decoherence rates low enough to access superexchange-based quantum magnetism.

Since ultracold atoms can be prepared in specific internal (i.e. spin) states with extremely high precision, spin temperatures that can be realized are much lower than the experimentally achievable motional temperatures. It is therefore tempting to circumvent the problem of high motional temperature by constructing a spin model in such a way that the motional and spin degrees of freedom are effectively decoupled. We provide a recipe for such a decoupling and hence for realizing spin models with thermal atoms.

The first crucial ingredient for implementing such a spin model is to depart from second-order superexchange interactions and use contact interactions to first order Gibble, 2009; A. M. Rey, A. V. Gorshkov, and Rubbo, 2009; Yu and Pethick, 2010; Pechkis et al., 2013; C. Deutsch et al., 2010; Maineult et al., 2012; Hazlett et al., 2013; Martin et al., 2013; Swallows et al., 2011; Koller et al., 2014. As shown in Fig. 1.1(a), this can be achieved if all atoms sit in different orbitals of the same anharmonic trap and remain in these orbitals throughout the evolution, which is a good approximation for weak interactions Martin et al., 2013; Swallows et al., 2011;

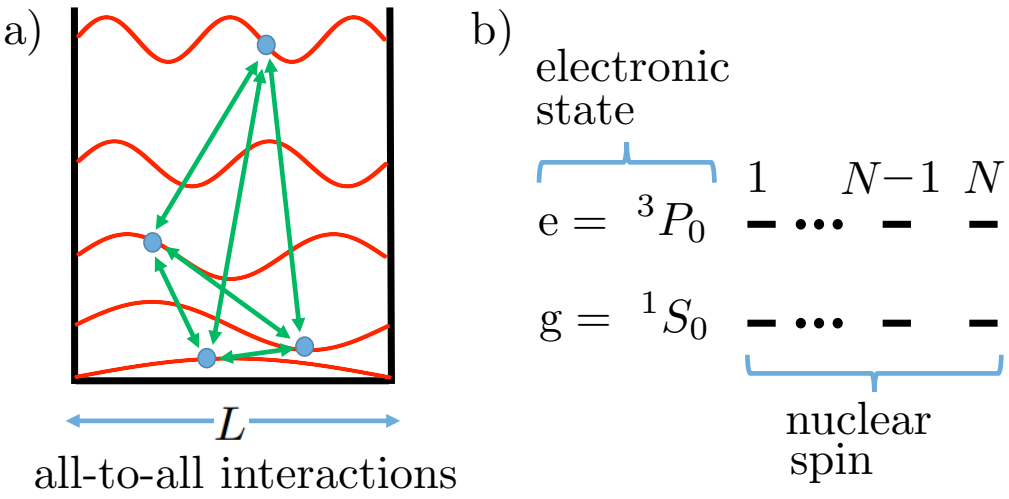

Figure 1.1: (a) Contact interactions between atoms in the orbitals of a one-dimensional infinite square well of width L are all-to-all with equal strength. (b) Thanks to the nuclear spin I, each of the electronic clock states g and e of fermionic alkaline-earth atoms can offer N degenerate states, with $N \leq 2I + 1$.

Gibble, 2009; A. M. Rey, A. V. Gorshkov, and Rubbo, 2009; Yu and Pethick, 2010. In that case, the occupied orbitals play the role of the sites of the spin Hamiltonian. However, because of high motional temperature in such systems, every run of the experiment typically yields a different set of populated orbitals and hence a different spin Hamiltonian Martin et al., 2013. Thus, unless the dynamics are constrained to states symmetric under arbitrary exchanges of spins Martin et al., 2013, every run of the experiment would lead to different spin dynamics.

The second crucial ingredient of our proposal to decouple spin and motion is therefore to use an infinite one-dimensional square-well potential as the anharmonic trap, with the motion frozen along the other two directions. The interaction terms in the spin Hamiltonian H are proportional to the squared overlap of pairs of distinct sinusoidal orbitals, and are thus all of equal strength. Therefore $\hat{H}$ is independent of which orbitals are occupied, leading to spin-motion decoupling and temperature independent predictions, as well as opening up the possibility of precise control. Moreover, since $\hat{H}$ is invariant under any relabeling of the n occupied orbitals, $\hat{H}$ has S_n permutation symmetry.

Alkaline-earth atoms enrich the symmetry. In such atoms, the vanishing electronic angular momentum J in the electronic clock states $g = {}^1S_0$ and $e = {}^3P_0$ results in the decoupling of the nuclear spin I from J [Fig. 1.1(b)]. This endows $\hat{H}$ with an additional $SU(N)$ spin-rotation symmetry, where N can be tuned between 2 and $2I + 1$ by choosing the initial state A. V. Gorshkov, Hermele, et al., 2010; M. A. Cazalilla, Ho, and Ueda, 2009; X. Zhang et al., 2014; Scazza et al., 2014; Guido Pagano et al., 2014; Cappellini et al., 2014. Restricted to g, $\hat{H}$ is just the sum of spin-swaps over all pairs of occupied orbitals and can be diagonalized in terms of irreducible representations of the group of symmetries $G = S_n \times SU(N)$.

Motional-temperature-insensitive spin models can also be realized using long-range interactions between ions in Paul traps Sorensen and Klaus Molmer, 1999, Penning traps Richerme et al., 2014; Jurcevic et al., 2014; Britton et al., 2012, and also between molecules Micheli, Brennen, and Zoller, 2006; Barnett et al., 2006; A. V. Gorshkov, Manmana, et al., 2011; Yan et al., 2013 or Rydberg atoms Schauß et al., 2012 pinned at different sites of an optical lattice. However, the realization of $SU(N)$-symmetric spin models in such systems requires a great deal of fine tuning Alexey V. Gorshkov, Hazzard, and Ana Maria Rey, 2013.

Motivated by the exploration of how quantum systems evolve after quantum quenches and whether (or how) they equilibrate and/or thermalize Eisert, Friesdorf, and

Gogolin, 2015, especially in the presence of long-range interactions Richerme et al., 2014; Jurcevic et al., 2014, we first study spin diffusion Sommer et al., 2011; Koschorreck et al., 2013; Yan et al., 2013 in a system of g atoms only. Due to crucial use of representation-theoretic techniques, our calculations are not only exponentially faster than naive exact diagonalization but also, for $N = 2$, yield a closed-form expression for all n. We then present a protocol that employs both g and e states to create Greenberger-Horne-Zeilinger (GHZ) states Greenberger, Horne, and Zeilinger, 1989, which could be used to approach the Heisenberg limit for metrology and clock precision Bollinger et al., 1996.

1.2 Spin Hamiltonian: ground electronic level only

A single mass-M fermionic alkaline-earth atom (for now, in its ground electronic state g) trapped in a 1D spin-independent potential $V(x)$ has real orbitals $\phi_j(x)$ with energies E_j satisfying $\left[-(\hbar^2/2M)\partial^2/\partial x^2 + V(x)\right]\phi_j(x) = E_j\phi_j(x)$. The operator $\hat{c}^\dagger_{jp}$ creates an atom from the vacuum in $\phi_j(x)$ with nuclear spin state $p \in 1, 2, ..., N$. For n identical atoms in the same potential with contact s-wave interactions, the Hamiltonian is $\hat{H} = \sum_{jp} E_j \hat{c}^\dagger_{jp}\hat{c}_{jp} + \sum_{p<q}\sum_{jkj'k'} U_{jkj'k'}\hat{c}^\dagger_{jp}\hat{c}_{j'p}\hat{c}^\dagger_{kq}\hat{c}_{k'q}$, where

$$U_{jkj'k'} = 4\pi\hbar\omega_\perp a_{gg}\int_{-\infty}^{\infty} dx\phi_j(x)\phi_k(x)\phi_{j'}(x)\phi_{k'}(x), \tag{1.1}$$

and a_{gg} is the 3D-scattering length, and a potential with frequency $\omega_\perp$ freezes out transverse motion.

To obtain the desired highly symmetric Hamiltonian, we specialize to the case where $V(x)$ is a width-L infinite square well, with well-known eigenstates $\phi_j(x) = \sqrt{2/L}\sin(j\pi x/L)$ for $0 \le x \le L$, with energy $E_j = (\pi j/L)^2/2M$. Then $U_{jkj'k'}$ is zero unless (i): $(j \pm k) = \pm(j' \pm k')$; to first order in the interaction, we can also set $U_{jkj'k'} \to 0$ unless $\sum_{jp} E_j\hat{c}^\dagger_{jp}\hat{c}_{jp}$ is conserved, which occurs when (ii): $j^2 + k^2 = j'^2 + k'^2$. Conditions (i) and (ii) are both satisfied if and only if $(j', k') = (j, k)$ or $(k', j') = (j, k)$. As the system conserves orbital occupancies, it can be described by a spin model. Assuming orbitals are at most singly occupied ($\hat{n}_j = \sum_p \hat{c}^\dagger_{jp}\hat{c}_{jp} \le 1$ for all j) [1], the spin Hamiltonian is:

$$\hat{H} = -U\sum_{j<k}\hat{s}_{jk}, \tag{1.2}$$

[1] For temperatures far from degeneracy, the probability of multiple occupancy will be small. Alternatively, absence of multiple occupancy is guaranteed by Pauli exclusion for nuclear-spin polarized states.

where $\hat{s}_{jk} \equiv \sum_{pq} \hat{c}^\dagger_{jp}\hat{c}_{jq}\hat{c}^\dagger_{kq}\hat{c}_{kp}$ swaps spins j and k, and the sum is over occupied orbitals. Crucially, $U \equiv 4\pi a_{gg}\hbar\omega_\perp/L$ is independent of j and k. We dropped a constant $\sum_j E_j + n(n-1)U/2$, which will have no effect on spin dynamics. For a fixed set of occupied orbitals, $\hat{H}$ has N^n basis states $|p_1, p_2, ..p_n\rangle$ with $p_j \in 1, ..., N$.

1.3 Exact eigenenergies and eigenstates

For $N = 2$, the spin-swap can be written in terms of the Pauli operators: $\hat{s}_{jk} = 1/2 + (\hat{\sigma}^x_j\hat{\sigma}^x_k + \hat{\sigma}^y_j\hat{\sigma}^y_k + \hat{\sigma}^z_j\hat{\sigma}^z_k)/2$, allowing Eq. (1.2) to be written as $\hat{H} = -U\left[\vec{S}^2 + \frac{n}{4}(n-4)\right]$, where $\vec{S} = \frac{1}{2}\sum_j \vec{\sigma}_j$. The eigenstates of $\hat{H}$ for $N = 2$ are therefore the well-known Dicke Dicke, 1954 states $|S, S_z, k\rangle$, with energies

$$E(S) = -U\left[S(S+1) + \frac{n}{4}(n-4)\right].$$

The quantum number k labels distinct states with the same $\vec{S}^2$ and $\hat{S}^z$ eigenvalues. We now describe the general case for arbitrary N.

The Hamiltonian in equation (1.2) has two obvious symmetries: permutations in S_n of the n occupied orbitals, and application of the same unitary in $SU(N)$ to all of the spins. Define a unitary $\hat{U}(\hat{V}, \sigma)$ which permutes occupied orbitals by $\sigma \in S_n$ and implements the spin rotation $\hat{V} \in SU(N)$:

$$\hat{U}(\hat{V}, \sigma)\ |p_1\rangle|p_2\rangle...|p_n\rangle \quad \equiv \quad \hat{V}|p_{\sigma^{-1}(1)}\rangle\hat{V}|p_{\sigma^{-1}(2)}\rangle...\hat{V}|p_{\sigma^{-1}(n)}\rangle. \tag{1.3}$$

These unitaries (for all $\hat{V} \in SU(N)$ and $\sigma \in S_n$) form a well-understood representation of the group $G = S_n \times SU(N)$. Each unitary $\hat{U}(\hat{V}, \sigma)$ commutes with $\hat{H} = -U\sum_{j\neq k}\hat{s}_{jk}$. Irreps of $SU(N)$ and S_n are both uniquely labeled by Young diagrams. A *Young diagram* is a pictorial representation of $\vec{\lambda}$ consisting of a row of λ_1 boxes above a row of λ_2 boxes, which is above a row of λ_3 boxes etc. It is also useful to define $\vec{\gamma} = (\gamma_1, \gamma_2, ..., \gamma_{\lambda_1})$ as the column heights of the Young diagram $\vec{\lambda}$. Figure 2.3(a) shows an example with $n = 7$ and $N = 3$.

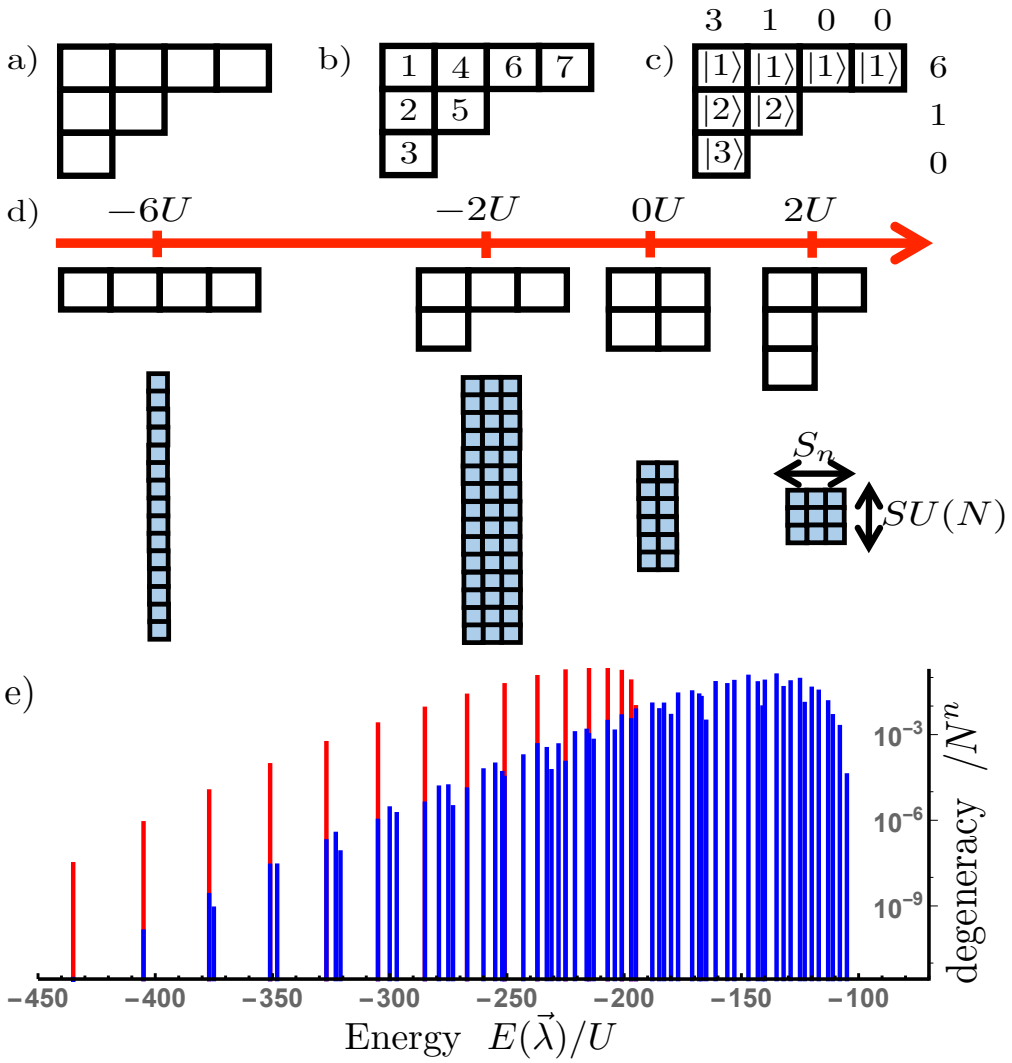

Figure 1.2: (a) An example Young diagram $\vec{\lambda} = (4,2,1)$ [with $\vec{\gamma} = (3,2,1,1)$] for $n = 7, N = 3$. (b) A labeling of boxes in $\vec{\lambda}$ from 1 to n, increasing down columns, starting at the left. (c) Orbitals associated with boxes in the pth row of the Young diagram are put in spin state $|p\rangle$ to form basis state $|T\rangle = |1231211\rangle$ [spins ordered as in (b)], used to construct eigenstate $|\vec{\lambda}\rangle = |\mathcal{A}\{123\}\rangle|\mathcal{A}\{12\}\rangle|11\rangle$ with $E(\vec{\lambda})/(-U) = \sum_i \binom{\lambda_i}{2} - \sum_j \binom{\gamma_j}{2} = 6+1+0-3-1-0-0 = 3$. (d) The set of all Young diagrams for $n = 4$ and $N = 3$, with energies above. Below each diagram, every eigenstate is represented by a colored box: starting with any given eigenstate, rotations in $SU(N)$ generate linear combinations of eigenstates in the same column, while permutations in S_n generate linear combinations of eigenstates in the same row. Representative states are found using the prescribed construction to be $|1111\rangle$, $(|12\rangle - |21\rangle)\,|11\rangle$, $(|12\rangle - |21\rangle)(|12\rangle - |21\rangle)$, and $(|123\rangle + |312\rangle + |231\rangle - |132\rangle - |213\rangle - |321\rangle)\,|1\rangle$, respectively. (e) Spectrum for $n = 30$ with $N = 2$ (red), and $N = 3$ (blue).

A Young diagram $\vec{\mu}$ labels an Irrep of $SU(N)$ if and only if it has at most N rows: $\vec{\mu} = (\mu_1, \mu_2, ..\mu_N)$. On the other hand, a Young diagram $\vec{\nu}$, labels an Irrep of S_n if and only if its elements sum to n: $\sum_i \nu_i = n$.

Each irrep of the product group $G = S_n \times SU(N)$ is the tensor product of an irrep of $SU(N)$ and an irrep of S_n and is therefore uniquely labeled by a pair $(\vec{\mu}, \vec{\nu})$. A consequence of Schur-Weyl duality is that representation (1.3) block-diagonalizes into exactly one copy of each irrep of G satisfying $\vec{\mu} = \vec{\nu}$, and no other irreps Bacon, I. L. Chuang, and Harrow, 2007; Fulton and Harris, 1991. Therefore for each Young diagram $\vec{\lambda} = (\lambda_1, \lambda_2, .., \lambda_N)$ such that $\sum_i \lambda_i = n$, there is a subspace of constant energy $E(\vec{\lambda})$. One can form an unnormalized projection operator $\hat{\Pi}_{L(\vec{\lambda})}$ into the $\vec{\lambda}$ subspace Fulton and Harris, 1991:

$$\hat{\Pi}_{L(\vec{\lambda})} = \sum_{\substack{c \in \text{col}(T) \\ r \in \text{row}(T)}} \text{sgn}(c)\ \ \hat{U}(\hat{I}, c)\, \hat{U}(\hat{I}, r). \tag{1.4}$$

Here, $L(\vec{\lambda})$ is the labeling of boxes in the Young diagram $\vec{\lambda}$ from 1 to n as shown in Fig. 2.3(b), and row(L) (col(L)) is the group of all permutations of the numbers 1 to n that preserve the contents of rows (columns) of $L(\vec{\lambda})$. Applying $\hat{\Pi}_{L(\vec{\lambda})}$ to any state that it does not annihilate returns an eigenstate of energy $E(\vec{\lambda})$. For concreteness we use $|T\rangle \equiv |1, 2, ..., \gamma_1\rangle\ |1, 2, ..., \gamma_2\rangle ... \ |1, 2, ..., \gamma_{\lambda_1}\rangle$, where we also define $\vec{\gamma} = (\gamma_1, \gamma_2, ..., \gamma_{\lambda_1})$ as the column heights of the Young diagram $\vec{\lambda}$. For each $\vec{\lambda}$ we obtain an explicit eigenstate: $|\vec{\lambda}\rangle = \hat{\Pi}_{L(\vec{\lambda})}|T\rangle$. Now we describe how to obtain the eigenvalue $E(\vec{\lambda})$ such that:

$$\hat{H}|\vec{\lambda}\rangle = E(\vec{\lambda})|\vec{\lambda}\rangle. \tag{1.5}$$

Premultiplying by $\langle T|$ we obtain: $E(\vec{\lambda}) = \langle T|\hat{H}|\vec{\lambda}\rangle = -U \sum_{j \neq k} \langle T|\hat{s}_{jk}|\vec{\lambda}\rangle$, noting that $\langle T|\vec{\lambda}\rangle = 1$. For j, k in the same column of the labeled Young diagram $L(\vec{\lambda})$, we know that $\hat{s}_{jk}|\vec{\lambda}\rangle = -|\vec{\lambda}\rangle$. Similarly for j, k in the same row of $L(\vec{\lambda})$ we have $\langle T|\hat{s}_{jk} = \langle T|$. Thus pairs (j, k) in columns contribute -1 to $E(\vec{\lambda})$ and pairs (j, k) in rows contribute $+1$. The number of such pairs can be counted, hence:

$$E(\vec{\lambda})/(-U) = \sum_{i=1}^{N} \binom{\lambda_i}{2} - \sum_{j=1}^{\lambda_1} \binom{\gamma_j}{2} + \sum_{\{j \neq k\}_{\text{diagonal}}} \langle T|\hat{s}_{jk}|\vec{\lambda}\rangle, \tag{1.6}$$

The swap $\hat{s}_{jk}$, where j and k are neither in same column nor in same row in $L(\vec{\lambda})$, can always be written as $\hat{s}_{jk} = \hat{s}_{jm}\hat{s}_{km}\hat{s}_{jm} = \hat{s}_{km}\hat{s}_{jm}\hat{s}_{km}$, where m is chosen such that (j, m) and (k, m) lie in a row and a column of $L(\vec{\lambda})$, respectively (it

suffices to consider the case $j > k$). Therefore, $\langle T|\hat{s}_{jk}|\vec{\lambda}\rangle = \langle T|\hat{s}_{km}\hat{s}_{jm}|\vec{\lambda}\rangle = -\langle T|\hat{s}_{km}\hat{s}_{jm}|\vec{\lambda}\rangle = 0$, implying $E(\vec{\lambda})/(-U) = \sum_{i=1}^{N}\binom{\lambda_i}{2} - \sum_{j=1}^{\lambda_1}\binom{\gamma_j}{2}$. Therefore the energy of the Hamiltonian is simply the number of ways of choosing two boxes in the same row of $\vec{\lambda}$, minus the number of ways of choosing two boxes in the same column. This is in line with the intuition that the swap picks up $-U$ for each symmetric pair and $+U$ for each antisymmetric pair in the Young diagram. In terms of $\vec{\lambda}$,

$$E(\vec{\lambda}) = -\frac{U}{2}\sum_{i=1}^{N}(\lambda_i - 2i + 1)\,\lambda_i. \tag{1.7}$$

Figure 2.3(d) illustrates the eigenvalues and eigenstates of $\hat{H}$ for the simple case of $n = 4$ and $N = 3$, along with the corresponding Young diagrams. There is an equivalence for the $SU(2)$ case between Young diagram (λ_1, λ_2) and angular momentum quantum number S given by $S = (\lambda_1 - \lambda_2)/2 = (2\lambda_1 - n)/2$.

Now we show how to create an eigenstate in any $\vec{\lambda}$-subspace. First consider the basis state: $|T\rangle \equiv |1, 2, ..., \gamma_1\rangle\ |1, 2, ..., \gamma_2\rangle ...\ |1, 2, ..., \gamma_{\lambda_1}\rangle$, which is chosen by associating orbitals with boxes of the Young diagram as in Fig. 2.3(b), and putting those orbitals in spin states as in Fig. 2.3(c). We form $|\vec{\lambda}\rangle$ (which is one of many eigenstates in the $\vec{\lambda}$-subspace) by antisymmetrizing $|T\rangle$ over orbitals associated with boxes in each column of $\vec{\lambda}$:

$$|\vec{\lambda}\rangle = |\mathcal{A}\{12...\gamma_1\}\rangle|\mathcal{A}\{12...\gamma_2\}\rangle...|\mathcal{A}\{12...\gamma_{\lambda_1}\}\rangle, \tag{1.8}$$

where $\mathcal{A}\{...\}$ antisymmetrizes its argument, for example: $|\mathcal{A}\{123\}\rangle = |123\rangle + |312\rangle + |231\rangle - |132\rangle - |321\rangle - |213\rangle$. The normalization constant is fixed by $\langle\vec{\lambda}|\vec{\lambda}\rangle = \gamma_1!\,\gamma_2!\,...\gamma_{\lambda_1}!$.

To understand and label the other eigenstates in the $\vec{\lambda}$-subspace, we note that there are three (equivalent) views of how the full N^n dimensional Hilbert space $\mathcal{H}$ decomposes. Firstly, $\mathcal{H}$ decomposes into a single copy of each $\vec{\lambda}$-irrep of the group $S_n \times SU(N)$ for each valid Young diagram $\vec{\lambda}$. Secondly, $\mathcal{H}$ decomposes into $\|\vec{\lambda}_{S_n}\|$ copies of each $\vec{\lambda}$-irrep of $SU(N)$ for each valid Young diagram $\vec{\lambda}$. Thirdly, $\mathcal{H}$ decomposes into $\|\vec{\lambda}_{SU(N)}\|$ copies of each $\vec{\lambda}$-irrep of S_n for each valid Young diagram $\vec{\lambda}$. Here, $\|\vec{\lambda}_{S_n}\|$ and $\|\vec{\lambda}_{SU(N)}\|$ are the dimensions of $\vec{\lambda}$ irreps of S_n and $SU(N)$, respectively.

An instructive picture is that of Schur states represented by boxes, and grouped together into blocks of equal $\vec{\lambda}$ [Fig. 2.3(d)]. Renaming the state we constructed

$|\vec{\lambda},1,1\rangle = |\vec{\lambda}\rangle$ in the $\vec{\lambda}$-subspace, one can obtain the set of orthonormal states $\{|\vec{\lambda},1,b\rangle\}$ for $b = 1,2,...,\|\vec{\lambda}_{S_n}\|$ from linear combinations of $\hat{U}(\hat{I},\sigma)|\vec{\lambda},1,1\rangle$ for $\sigma \in S_n$. Similarly, from each state $|\vec{\lambda},1,b\rangle$, one can form the set of orthonormal states $\{|\vec{\lambda},a,b\rangle\}$ for $a = 1,2,...,\|\vec{\lambda}_{SU(N)}\|$ from linear combinations of $\hat{U}(\hat{V},I)|\vec{\lambda},1,b\rangle$ for $\hat{V} \in SU(N)$. For $N = 2$, this picture is the familiar *D*icke ladder, in which states are grouped into blocks of equal S, with S_z increasing downwards and k increasing to the right.

The dimensions of each block can be calculated using the standard hook-length formulae Sagan, 2000 for any given Young diagram $\vec{\lambda}$. In particular, the ground-state spaces for $U > 0$ (ferromagnetic interaction) and $U < 0$ (antiferromagnetic interaction) are $\vec{\lambda}_F = (n,0,0,...,0)$ and $\vec{\lambda}_{AF} = (n/N,n/N,...,n/N)$ and have dimensions D_F and D_{AF}, respectively:

$$D_F = \frac{(n+N-1)!}{n!\,(N-1)!}, \qquad D_{AF} = \frac{n!}{[(n/N)!]^N}\prod_{i=1}^{N-1}\frac{i!}{[n/N+i]}. \tag{1.9}$$

1.4 Robustness to imperfections

In this Section, we consider deviation from a perfect infinite square-well potential $V(x)$. For simplicity, we consider the case in which all atoms are in the ground electronic state. The interaction Hamiltonian Eq. (1.2) becomes: $\hat{H}' = -\sum_{j<k} U_{jk}\hat{s}_{jk}$, where $U_{jk} = (UL/2)\int \phi_j^2(x)\phi_k^2(x)dx$, and $\phi_j(x)$ is a single-particle orbital, which is a sine function in the ideal case. As $\hat{H}'$ is a weighted sum of terms $\hat{s}_{jk}$ and therefore has $SU(N)$ symmetry, it cannot mix states in different $\vec{\lambda}$-subspaces. However as $\hat{H}'$ does not exhibit S_n symmetry, the $\vec{\lambda}$ subspace does not have a single energy - but breaks into $D(\vec{\lambda})$ energy subspaces, $D(\vec{\lambda})$ is the dimension of the $\vec{\lambda}$ irrep of S_n. We write the eigenenergies of $\hat{H}'$ as $E'(\vec{\lambda},b)$, with b labeling distinct energies.

Provided that the inhomogeneity in U_{jk} is small, i.e. that $|U_{jk}-U| \ll U$, the energy splittings $E'(\vec{\lambda},b)$ within each $\vec{\lambda}$ subspace will be small compared to energy separations between different $\vec{\lambda}$ subspaces. Exact determination of $E(\vec{\lambda},b)$ can be carried out by projecting $\hat{H}'$ onto the $\vec{\lambda}$ subspace and solving the resulting matrix equation, which is computationally difficult as the matrices have dimension $O(\exp(n))$. Here we are satisfied with an indication of the magnitude of deviation from the ideal energy eigenvalues. We seek the offset: $\Delta E(\vec{\lambda}) \equiv \frac{1}{D(\vec{\lambda})}\sum_{b=1}^{D(\vec{\lambda})}\left[E'(\vec{\lambda},b) - E(\vec{\lambda})\right]$ and the variance: $\sigma^2(\vec{\lambda}) \equiv \frac{1}{D(\vec{\lambda})}\sum_{b=1}^{D(\vec{\lambda})}\left[\Delta E(\vec{\lambda},b) - \Delta E(\vec{\lambda})\right]^2$. Defining $E(\vec{\lambda}_0) =$

$-Un(n-1)/2$, where $\vec{\lambda}_0 = (n, 0, 0, .., 0)$, one can show that

$$\Delta E(\vec{\lambda}) = -\left(\frac{E(\vec{\lambda})}{E(\vec{\lambda}_0)}\right)\sum_{j<k}(U_{jk} - U). \tag{1.10}$$

Note that $\left|\frac{E(\vec{\lambda})}{E(\vec{\lambda}_0)}\right| \leq 1$ for all $\vec{\lambda}$. The main technical lemma used to prove this is that for any operator $\hat{O}$,

$$\sum_{b=1}^{D(\vec{\lambda})}\langle\vec{\lambda}, b|\hat{O}|\vec{\lambda}, b\rangle = \frac{D(\vec{\lambda})}{n!}\sum_{\sigma\in S_n}\langle\vec{\lambda}, b'|\sigma^{-1}\hat{O}\sigma|\vec{\lambda}, b'\rangle, \tag{1.11}$$

where the latter sum is over all permutations σ in the symmetric group S_n. Modeling U_{jk} as a set of $n(n-1)/2$ independent random variables with mean U, one can similarly show that

$$\sigma^2(\vec{\lambda}) = \left[1 - \left(\frac{E(\vec{\lambda})}{E(\vec{\lambda}_0)}\right)^2\right]\sum_{j<k}\langle(U_{jk} - U)^2\rangle, \tag{1.12}$$

where $\langle\rangle$ indicates that we have taken the ensemble average over realizations **footnote2** of ΔU_{jk}, which simply allows us to set $\langle\Delta U_{jk}\Delta U_{j'k'}\rangle = 0$ where $j, k \neq j', k'$. These results indicate that the deviations in energy levels from those for the exact case caused by inhomogeneity in U_{jk} generically behave as $\sim n\Delta U$. This is because, to estimate $\Delta E(\vec{\lambda})$, we assume that $\sum_{j<k}(U_{jk} - U)$ is the sum of $n(n-1)/2$ uncorrelated positive and negative terms each of magnitude $\sim \Delta U$, and similarly for the variance $\sigma^2(\vec{\lambda})$, except all terms are positive. We therefore expect that, in order to see p revivals of the kind shown in Fig. 1.3 of the main text, we need to pick up small phase errors $n\Delta U t \lesssim 1$ over time $t \sim p/U$, which corresponds to $\Delta U/U \lesssim 1/(np)$.

However, note that most symmetric $\vec{\lambda}$ subspaces (which have $E(\vec{\lambda})/E(\vec{\lambda}_0)$ close to unity), experience less splitting due to inhomogeneity in U_{jk}, although they do experience an overall shift. For the GHZ protocol, the $\vec{\lambda}$ subspaces involved are $(n, 0)$, $(n-1, 1)$ and $(n-2, 2)$, which will shift relative to one another under inhomogeneity in U_{jk} by an amount independent of n for large n.

To obtain some concrete estimates of the effects of an imperfect square-well potential, we consider the following example: a perfect square well, plus an additional harmonic perturbing potential $V_1(x) = \alpha x^2$ (which in effect "rounds off" the boundary of the well somewhat). With first-order corrections, the single-particle wave

functions $\phi_j(x)$ are

$$\phi_j(x) = \sqrt{\frac{2}{L}} \sin\left(j\pi x/L\right) + \frac{8}{\pi^2}\left(\alpha L^2/\frac{\hbar^2\pi^2}{2ML^2}\right) \sum_{k\ k\neq j} \frac{jk(-1)^{j+k}}{(j^2-k^2)^3} \sqrt{\frac{2}{L}} \sin\left(k\pi x/L\right).$$

Substitution into $U_{jk} = UL\int \phi_j^2(x)\phi_k^2(x)dx$ yields exact expressions for the first order corrections to U, which (for all j and k) satisfy: $|U_{jk}-U| < 10^{-2}\left(\alpha L^2/\frac{\hbar^2\pi^2}{2ML^2}\right)U + O(\alpha^2)$. The inhomogeneity is therefore strictly less than one percent if the magnitude of the perturbation is approximately of the same order as the characteristic energy of the square well. The size of the deviations fall off at the fourth power of j, k, such that for ensembles of atoms, ΔU is typically much better than this bound suggests.

1.5 Experimental proposal: spin diffusion dynamics

Spin diffusion is the process by which evolution under a generic spin Hamiltonian causes initially ordered states to diffuse Sommer et al., 2011; Koschorreck et al., 2013; Yan et al., 2013. We take initial state $|\psi(0)\rangle = |1\rangle^{\otimes m_1}|2\rangle^{\otimes m_2}...|N\rangle^{\otimes m_N}$. Note that any computational basis state can be changed to this form by reordering occupied orbitals. We consider the time evolution of observable $\hat{Q} = \sum_{j=1}^{m_1}|1\rangle_j\langle 1|_j$: the number of the first m_1 orbitals in spin-state $|1\rangle$. This is the simplest observable capturing the broken symmetry of the initial state. The expectation of $\hat{Q}$ evolves according to: $Q(t) \equiv \langle\psi(0)|e^{i\hat{H}t}\hat{Q}e^{-i\hat{H}t}|\psi(0)\rangle$, omitting $\hbar$ where convenient from here on.

Calculation of such a time evolution for a generic Hamiltonian requires matrix diagonalization, which scales exponentially with n (for fixed N). Using the symmetry of Hamiltonian (1.2) and the Wigner-Eckart theorem for $SU(N)$, we obtain an explicit sum (see section 1.6) for $Q(t)$ in terms of Clebsch-Gordan and recoupling coefficients. For the case of $N = 2$, with initial state of $m_1 = m$ spin up and $m_2 = n-m$ spin down orbitals, using well-known closed forms for the Clebsch-Gordan and recoupling coefficients:

$$Q(t) = m + \sum_{S=|n-2m|/2+1}^{n/2} \gamma(S)[\cos\left(2SUt\right) - 1], \tag{1.13}$$

where $\gamma(S) = \frac{4S^2-(n-2m)^2}{4S}\binom{n}{n/2+S}/\binom{n}{n-m}$. For $N > 2$, closed forms for the required coefficients are not known to the authors, but can be calculated efficiently using standard algorithms as in Ref. Alex et al., 2011. In Fig. 1.3, we compare the

evolution of the same operator and total particle number for initial states with $N = 2$ spin states and $N = 3$ spin states. The oscillations are much less pronounced and spin diffusion occurs more fully (Q drops lower) for the latter state. With this model, looking at times away from the multiples of the revival time $2\pi/U$, one could study apparent near-equilibration of some observables (such as Q in the $N = 3$ case) acting on the first m_1 spins. Perturbations could be added to the system to remove revivals and potentially allow for the thermalization of the first m_1 spins.

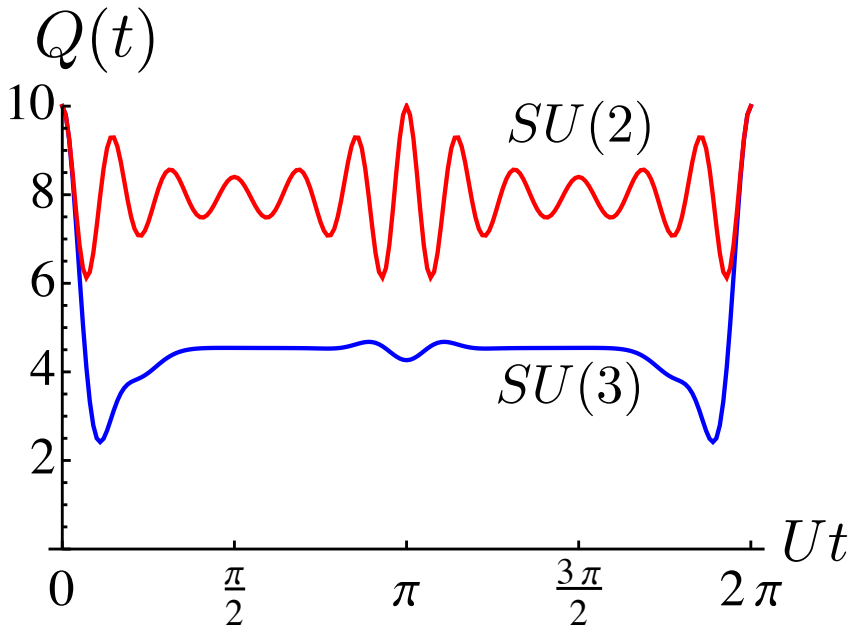

Figure 1.3: Exact time evolution under $\hat{H}$ of an operator $\hat{Q} = \sum_{j=1}^{10} |1\rangle_j\langle 1|_j$, which counts the number of the first ten orbitals in spin state $|1\rangle$. Two initial states are compared: $|1\rangle^{\otimes 10}|2\rangle^{\otimes 20}$ for $SU(2)$ and $|1\rangle^{\otimes 10}|2\rangle^{\otimes 10}|3\rangle^{\otimes 10}$ for $SU(3)$. Although the evolution is the same for short times, the $SU(3)$ case results in significantly more diffusion of spin state $|1\rangle$ out of the first four orbitals at later times. Since all $E(\vec{\lambda})$ are integer multiples of U, complete revival occurs at $Ut = 2\pi$. In the $SU(2)$ case, the oscillation is dominated by the smallest S in Eq. (1.13). This is consistent with the fact that for fixed S_z, the size of the eigenspaces decreases with S, causing overlap to be larger with subspaces of small S generically.

1.6 Derivation of spin-diffusion dynamics

In this Section, we present the derivation of the spin-diffusion dynamics, first for $N = 2$and then for general N.

We are concerned with observable $\hat{Q} = \sum_{j=1}^{m_1} |1\rangle_j\langle 1|_j$. In this section, we use the notation that for any operator $\hat{A}$, $A(t) \equiv \langle\psi(0)|e^{i\hat{H}t}\hat{A}e^{-i\hat{H}t}|\psi(0)\rangle$, where $|\psi(0)\rangle = |1\rangle^{\otimes m_1}|2\rangle^{\otimes m_2}...|N\rangle^{\otimes m_N}$. As most readers are assumed to be familiar with spin-$1/2$

systems, we outline the $N = 2$ case first before covering the general case more abstractly.

For $N = 2$, we can choose the angular momentum (Dicke) basis to span the Hilbert space: $|S, S_z, k\rangle$, which diagonalizes the Hamiltonian: $\hat{H}|S, S_z, k\rangle = -US(S+1)|S, S_z, k\rangle$ (dropping a constant energy). The initial state is $|\psi(0)\rangle = |\uparrow\rangle^{\otimes m} |\downarrow\rangle^{\otimes n-m}$ where we used $|\uparrow\rangle$ and $|\downarrow\rangle$ in place of $|1\rangle$ and $|2\rangle$. This state can be understood as a tensor product of two Dicke states on subsets of spins: $|\psi(0)\rangle = |m/2, m/2\rangle \otimes |(n-m)/2, -(n-m)/2\rangle$, where there is no need for a k quantum number since states with $|S_z| = S$ have no additional degeneracy. The tensor product of two angular momentum states can be written as a sum of "total" angular momentum states: $|\psi(0)\rangle = \sum_S C(S)|S, S_z{=}m{-}n/2, \alpha(S)\rangle$, where $C(S)$ is a Clebsch-Gordan coefficient, and $\alpha(S)$ represents the fact that $|S, S_z{=}m{-}n/2, \alpha(S)\rangle$ is some specific linear combination of Dicke states with the same S and S_z, but different k's. Hence, $Q(t) = \sum_{S,S'} C(S')^* C(S) e^{iUt[S(S+1)-S'(S'+1)]} \langle S', S_z, \alpha(S')|\hat{Q}|S, S_z, \alpha(S)\rangle$. Note that $\hat{Q} = m\hat{I} + \hat{S}^z_m$ with $\vec{S}_m = \sum_{j=1}^m \vec{S}_j$, and $\hat{S}^z_m$ is the 0-component of the $(S = 1)$-spherical tensor $\hat{\mathbb{T}} \equiv \{\hat{S}^{-1}_m, \hat{S}^z_m, \hat{S}^{+1}_m\}$, with $\hat{S}^{\pm 1}_m = \mp(\hat{S}^x_m \pm i\hat{S}^y_m)/\sqrt{2}$. We first apply the Wigner-Eckart theorem to write the matrix element in terms of the reduced matrix element and a Clebsch-Gordan coefficient. Then, since $\hat{\mathbb{T}} \equiv \hat{\mathbb{T}}_m \otimes \hat{I}$ acts only on the first m spins, we rewrite Rose, 1957; J. Brown and Carrington, 2003 the reduced matrix element on the full system in terms of one on the first m spins and a recoupling coefficient:

$$\begin{aligned} \langle S', S'_z, \alpha(S')|\hat{Q}|S, S_z, \alpha(S)\rangle &= m\delta_{S,S'} \\ +\langle m/2||\hat{\mathbb{T}}_L||m/2\rangle \begin{Bmatrix} 1 & m/2 & m/2 \\ (n-m)/2 & S' & S \end{Bmatrix} &(\langle 1, 0| \otimes \langle S, S_z|)\ |S', S'_z\rangle, \end{aligned} \tag{1.14}$$

where $(\langle 1, 0| \otimes \langle S, S_z|)\ |S', S'_z\rangle$ is a Clebsch-Gordan coefficient and $\langle m/2||\hat{\mathbb{T}}_L||m/2\rangle$ is the reduced matrix element of $\hat{\mathbb{T}}_L$ on the $S = m/2$ state of the first m spins. The recoupling coefficient $\begin{Bmatrix} S_A & S_B & S_{AB} \\ S_C & S & S_{BC} \end{Bmatrix} \equiv \langle S, S_z, (S_{AB}, S_C)|S, S_z, (S_A, S_{BC})\rangle$ is the overlap between two states of given S and S_z formed from the tensor product of three subsystems with S_A, S_B and S_C in two different ways: by combining A and B to form S_{AB} first, and by combining B and C to form S_{BC} first. Substitution of the Clebsch-Gordan and recoupling coefficients into the matrix element gives Eq. (1.13).

Now we proceed with the calculation for arbitrary N, simplifying our notation by dropping hats and vectors. The initial state [see Fig. 1.4(a)] can be written

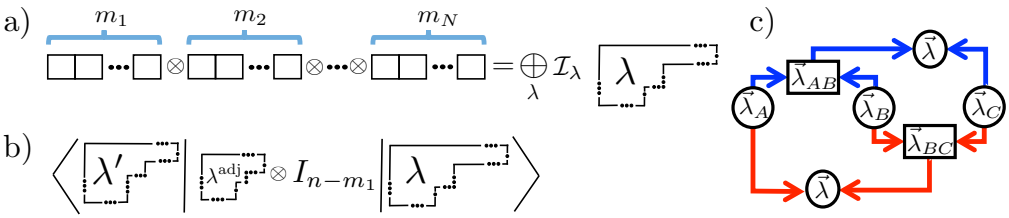

Figure 1.4: (a) Initial state $|\psi(0)\rangle$ can be written in terms of energy eigenstates: $|\psi(0)\rangle = |11...1\rangle|22...2\rangle...|NN...N\rangle = \sum_{\lambda,a,\alpha} C(\lambda,a,\alpha)|\lambda,a,\alpha\rangle$. (b) Key simplifications arise in the matrix element $\langle\lambda',a',\alpha|Q|\lambda,a,\alpha\rangle$ (which is used to calculate $Q(t)$) since: $\hat{Q}$ is a component of a "spherical tensor" for $SU(N)$ (allowing us to make use of the Wigner-Eckart theorem) and has support only on the first m_1 sites. (c) The recoupling coefficient is defined by taking the direct product of three irreps A, B and C, and finding the overlap between two copies of the same irrep found in two ways: by combining A and B first (top), and by combining B and C first (bottom).

as a direct product of spin-symmetric states $|\psi(0)\rangle = \otimes_{j=1}^{m_1}|1\rangle \otimes_{j=1}^{m_2}|2\rangle... \otimes_{j=1}^{m_N} |N\rangle = |\kappa_1,a_1\rangle|\kappa_2,a_2\rangle...|\kappa_N,a_N\rangle$, where a_i labels the particular state in the $\kappa_i \equiv (m_i,0,...0)$ irrep which corresponds to $|i\rangle^{\otimes m_i}$. The product of $\kappa = (m,0,...,0)$ with any irrep λ' has no multiplicity Bacon, I. L. Chuang, and Harrow, 2007: $|\kappa,a\rangle|\lambda',a'\rangle = \sum_{\lambda'',a''} C(\lambda'',a'')|\lambda'',a''\rangle$, where each irrep λ'' appears at most once and $C(\lambda'',a'') \equiv \langle\lambda'',a''|\left(|\kappa,a\rangle|\kappa',a'\rangle\right)$ is a Clebsch-Gordan coefficient. Applying this iteratively, starting from the right, $|\psi(0)\rangle = \sum_{\lambda,a,\alpha} C(\lambda,a,\alpha)|\lambda,a,\alpha\rangle$, where α labels the set of intermediate irreps, $C(\lambda,a,\alpha)$ can be expressed in terms of Clebsch-Gordan coefficients, and $|\lambda,a,\alpha\rangle$ are orthogonal eigenstates: $H|\lambda,a,\alpha\rangle = E(\lambda)|\lambda,a,\alpha\rangle$. Note: $a \in 1,2,...,\dim[\lambda_{SU(N)}]$ labels a basis state within the λ-irrep of $SU(N)$, and each α labels one distinct copy (out of $\dim[\lambda_{S_n}]$ copies) of the λ-irrep of $SU(N)$ in the Hilbert space $\mathcal{H} = (\mathbb{C}_N)^{\otimes n}$ (all copies of irrep λ of $SU(N)$ in $\mathcal{H}$ sit inside a single copy of irrep λ of $S_n \times SU(N)$). Therefore: $Q(t) = \sum_{\lambda,\lambda',a,a',\alpha} C^*(\lambda',a',\alpha)C(\lambda,a,\alpha)e^{i[E(\lambda')-E(\lambda)]t}\langle\lambda',a',\alpha|Q|\lambda,a,\alpha\rangle$, where we set $\alpha' = \alpha$ since Q has support only on the first m_1 spins. We now outline tools to determine the matrix element $\langle\lambda',a',\alpha|Q|\lambda,a,\alpha\rangle$.

The states $|\lambda,a,\alpha\rangle$ transform according to matrix irrep D^λ of $SU(N)$: $V^{\otimes n}|\lambda,a,\alpha\rangle = \sum_{a'} D^\lambda_{a'a}(V)|\lambda,a',\alpha\rangle$. For each N, there is a set of single-spin operators which generate $SU(N)$: $\tau^{\text{adj}} \equiv \{t_1,t_2,...,t_{N^2-1}\}$ which transform according to D^{adj} (the *adjoint irrep* λ_{adj}): $V^{\otimes n}t_aV^{\dagger\otimes n} = \sum_{a'} D^{\text{adj}}_{a'a}(V)t_{a'}$. The set $\{t_1,t_2,...,t_{N^2-1},\hat{I}\}$ forms a basis for $N \times N$ Hermitian matrices: therefore, any single-atom spin observable can be written as $\hat{q} = c_0\hat{I} + \sum_a c_a t_a$ for some real constants c_a. Therefore

$\langle \lambda', a', \alpha | Q | \lambda, a, \alpha \rangle = c_0 + \sum_{a''} c_{a''} \langle \lambda', a', \alpha | T^{\text{adj}}_{a''} | \lambda, a, \alpha \rangle$, where $T^{\text{adj}}_a = \sum_{j=1}^{m_1} t_{a\,j}$ and $Q = \sum_{j=1}^{m_1} |1\rangle_j \langle 1|_j \equiv \sum_{j=1}^{m_1} \hat{q}_j$. We now prove a generalization of Eq. (1.14) to determine the matrix element $\langle \lambda', a', \alpha' | T^{\text{adj}}_{a''} | \lambda, a, \alpha \rangle$ [see Fig. 1.4(b)]. We will need the Wigner-Eckart theorem and recoupling coefficients for $SU(N)$:

$$\langle \lambda', a', \alpha' | T^{\lambda''}_{a''} | \lambda, a, \alpha \rangle = \sum_{\mathcal{I}} \left(\langle \lambda', a', \mathcal{I} || \lambda'', a'' \rangle | \lambda, a \rangle \right) \langle \lambda', \alpha' || T^{\lambda''} || \lambda, \alpha \rangle_{\mathcal{I}}, \quad (1.15)$$

$$\left\{ \begin{array}{ccc} \lambda_A & \lambda_B & \lambda_{AB} \\ \lambda_C & \lambda & \lambda_{BC} \end{array} \right\}_{\mathcal{I}_{AB},\mathcal{I}_C;\mathcal{I}_{BC},\mathcal{I}_A} \equiv \langle \lambda, a, (\lambda_{AB}, \mathcal{I}_{AB}, \mathcal{I}_C) | \lambda, a, (\lambda_{BC}, \mathcal{I}_{BC}, \mathcal{I}_A) \rangle. \quad (1.16)$$

Note that multiplicity $\mathcal{I}$ appears in the Wigner Eckart theorem for $N > 2$ [Eq. (1.15)], since the tensor product of irreps can include multiple appearances of the same irrep. The recoupling coefficient defined in Eq. (1.16) relates two copies of the same irrep λ formed from the tensor product of three irreps: λ_A, λ_B, and λ_C, but combined in different orders [see Fig. 1.4(c)]. To define notation: λ_A and λ_B are combined to make λ_{AB}, whose different copies are labeled by $\mathcal{I}_{AB}$, while $\mathcal{I}_C$ labels different copies of λ when λ_{AB} is combined with λ_C.

One can decompose $|\lambda, a, \alpha\rangle = \sum_{a_1,a_2} \mathcal{C}^{\lambda,a}_{\kappa_1,a_1;\lambda_2,a_2} |\kappa_1, a_1\rangle |\lambda_2, a_2\rangle$, where λ_2 is specified by α, and

$$\mathcal{C}^{\lambda,a}_{\kappa_1,a_1;\lambda_2,a_2} \equiv (\langle \kappa_1, a_1 | \langle \lambda_2, a_2 |) | \lambda, a, \alpha \rangle \quad (1.17)$$

Substituting into $\langle \lambda', a', \alpha | T^{\text{adj}}_{a''} | \lambda, a, \alpha \rangle$ and applying Eq. (1.15) to the first m_1 spins:

$$\langle \lambda', a', \alpha | T^{\text{adj}}_{a''} | \lambda, a, \alpha \rangle = \langle \kappa_1 || \mathbb{T}^{\text{adj}} || \kappa_1 \rangle \sum_{a_1,a_1',a_2} \bar{\mathcal{C}}^{\lambda',a'}_{\kappa_1,a_1';\lambda_2,a_2} \mathcal{C}^{\lambda,a}_{\kappa_1,a_1;\lambda_2,a_2} \mathcal{C}^{\kappa_1,a_1}_{\kappa_1,a_1';\lambda^{\text{adj}},a''}$$

$$= \langle \kappa_1 || \mathbb{T}^{\text{adj}} || \kappa_1 \rangle \sum_{\mathcal{I}_1} \left\{ \begin{array}{ccc} \lambda^{\text{adj}} & \kappa_1 & \kappa_1 \\ \lambda_2 & \lambda' & \lambda \end{array} \right\}^*_{\mathcal{I}_1} \mathcal{C}^{\lambda',a',\mathcal{I}_1}_{\lambda^{\text{adj}},a'';\lambda,a}. \quad (1.18)$$

The second line represents the generalization of Eq. (1.14). To derive Eq. (1.18), we return to the abstract scenario of three irreps λ_A, λ_B and λ_C used to define recoupling coefficients in Eq. (1.16). First write $|\lambda, a, (\lambda_{AB})\rangle$ as a linear combination of $|\lambda, a, (\lambda_{BC}, \mathcal{I}_A)\rangle$ with Eq. (1.16) as coefficients in the special case where $\lambda_B = \lambda_{AB} = \kappa$ (allowing us to drop $\mathcal{I}_{AB}$, $\mathcal{I}_C$ and $\mathcal{I}_{BC}$). Rewriting states on both sides as the direct product of states in each of the three subsystems, multiplying by $\mathcal{C}^{\lambda_C,a_C}_{\lambda'_{BC},a_{BC};\lambda_B,a_B}$, summing over λ'_{BC}, and using orthogonality gives:

$$\sum_{a_{AB},a_B,a_C} \mathcal{C}^{\lambda,a}_{\lambda_{AB},a_{AB};\lambda_C,a_C} \mathcal{C}^{\lambda_{AB},a_{1AB}}_{\lambda_A,a_A;\lambda_B,a_B} \mathcal{C}^{\lambda_C,a_C}_{\lambda_{BC},a_{BC};\lambda_B,a_B} =$$

$$\sum_{\mathcal{I}_A} \left\{ \begin{array}{ccc} \lambda_A & \kappa & \kappa \\ \lambda_C & \lambda & \lambda_{BC} \end{array} \right\}^*_{\mathcal{I}_A} \mathcal{C}^{\lambda,a}_{\lambda_A,a_A;\lambda_{BC},a_{BC}}. \quad (1.19)$$

Using Eq. (1.18), the time evolution $T_a(t) \equiv \langle\psi(0)|\exp(iHt)T_a\exp(-iHt)|\psi(0)\rangle$, and therefore $Q(t)$, is written as an efficiently computable sum (containing $poly(n)$ terms Alex et al., 2011, each calculated in $poly(n)$ operations):

$$T_a(t) = \langle\kappa_1||\mathbb{T}^{\text{adj}}||\kappa_1\rangle \sum_{\lambda_1',a_1',\lambda_1,a_1;\alpha} C^*(\lambda_1',a_1',\alpha)\, C(\lambda_1,a_1,\alpha) e^{(i[E(\lambda_1')-E(\lambda_1)]t)} \quad (1.20)$$
$$\times \sum_{\mathcal{I}_1} \left\{ \begin{array}{ccc} \lambda^{\text{adj}} & \kappa_1 & \kappa_1 \\ \lambda_2 & \lambda_1' & \lambda_1 \end{array} \right\}_{\mathcal{I}_1} \left[\langle\lambda_1',a_1',\mathcal{I}_1|\left(|\lambda^{\text{adj}},j\rangle|\lambda_1,a_1\rangle\right)\right].$$

The group-theoretic method presented in this Section was crucial for obtaining the analytical result for $SU(2)$ [Eq. (1.13)]. It is also crucial for doing numerics for $SU(N>2)$ for large n. However, for sufficiently small n, such as the one shown in Fig. 3, one can do the $SU(N>2)$ numerics using the following simpler method. One first constructs a complete basis of fully symmetric states for the first m_1 spins, for the next m_2 spins, for the next m_3 spins, etc... Then one combines them into a basis for the full system and keeps only those states that have m_1 1's, m_2 2's, m_3 3's, etc... It is straightforward to evaluate the Hamiltonian in this reduced basis and then numerically exponentiate it to calculate time evolution.

1.7 Spin Hamiltonian: ground and first excited electronic levels

In this section, we derive the Hamiltonian describing identical (bosonic or fermionic) multi-component particles in an infinite square well interacting via s-wave interactions. We then specialize to the case of fermionic alkaline-earth atoms. This section generalizes the hamiltonian derived in Section 1.2 to the case of multiple energy levels, which will be needed in the following section on the proposal for producing GHZ states.

Contact interactions between two identical multi-component fermionic (bosonic) atoms are described by the Hamiltonian

$$\hat{H}_{int}^{12} = 4\pi\hbar\omega_\perp\delta(x_1-x_2)\otimes\hat{A}, \quad (1.21)$$

where the operator $\hat{A}$ only has a physical effect on exchange antisymmetric (symmetric) two-particle internal states because exchange symmetric (antisymmetric) spatial states do not interact. In second quantized form, where $\hat{c}_{jr}^\dagger$ creates an atom in internal state r and orbital $\phi_j(x)$ with non-interacting energy E_j, and $W_{k'j'jk} = (4\pi\hbar\omega_\perp)\int_0^L dx\ \phi_{k'}(x)\phi_{j'}(x)\phi_j(x)\phi_k(x)$. The interaction becomes: $\hat{H}_{int} = \sum_{j',k',j,k} W_{k'j'jk}\sum_{r',s',r,s}\langle s',r'|\hat{A}|r,s\rangle\ \hat{c}_{j'r'}^\dagger\hat{c}_{k's'}^\dagger\hat{c}_{jr}\hat{c}_{ks}$. Specializing to the

infinite square well of width L, to first order in the interaction, only terms satisfying $(j', k') = (j, k)$ or $(j', k') = (k, j)$ survive. Additionally assuming no multiple occupancies, we obtain $W_{kjjk} = W_{jkjk} = W \equiv (4\pi\hbar\omega_\perp)/L$ for $j \neq k$, and the Hamiltonian becomes:

$$\begin{aligned}\hat{H} &= \sum_{j,r} E_j \hat{c}^\dagger_{jr}\hat{c}_{jr} \\ &\quad + W \sum_{j,k} \sum_{r',s',r,s} \langle s', r'|\hat{A}|r, s\rangle \left(\hat{c}^\dagger_{jr'}\hat{c}^\dagger_{ks'}\hat{c}_{jr}\hat{c}_{ks} + \hat{c}^\dagger_{kr'}\hat{c}^\dagger_{js'}\hat{c}_{jr}\hat{c}_{ks}\right).\end{aligned} \tag{1.22}$$

Now we specialize to the case focused on in our work. For fermionic alkaline-earth atoms, $\hat{A}$ cannot depend on nuclear spin; therefore (denoting the identity on nuclear spin by $\hat{I}_N$),

$$\hat{A} = \left(a_{ee}|e, e\rangle\langle e, e| + a_{gg}|g, g\rangle\langle g, g| + a^+_{eg}|e, g\rangle_+\langle e, g|_+ + a^-_{eg}|e, g\rangle_-\langle e, g|_-\right) \otimes \hat{I}_N,$$

where $|e, g\rangle_\pm = (|e, g\rangle \pm |g, e\rangle)/\sqrt{2}$ A. V. Gorshkov, Hermele, et al., 2010. Under these conditions, and applying a strong magnetic field (which to first order in perturbation theory prevents exchanges $|ep, gq\rangle \leftrightarrow |eq, gp\rangle$ for $p \neq q$), we obtain Eq. (5) with $U_{1g2g} = U_{2g1g} = U_{gg} \equiv 4\pi\omega_\perp a_{gg}/L$, $U_{1e2e} = U_{2e1e} = U_{ee} \equiv 4\pi\omega_\perp a_{ee}/L$, $U_{1g1e} = U_{2g2e} = 4\pi\omega_\perp a^-_{eg}/M$, $U_{1g2e} = U_{2g1e} = 2\pi\omega_\perp(a^+_{eg} + a^-_{eg})/M$. Recently discovered orbital Feshbach resonances may be used to further tune the values of U_{1g2e} and U_{2g1e} R. Zhang et al., 2015; G. Pagano et al., 2015; Höfer et al., 2015.

1.8 Experimental proposal: GHZ state preparation

Highly entangled states could lead to short-term applications in metrology Bollinger et al., 1996; Sackett et al., 2000, and long-term applications in quantum information M. A. Nielsen and I. L. Chuang, 2000; Dutta, Mukherjee, and Sengupta, 2013. It is particularly timely to design ways for implementing entanglement-assisted – and hence more accurate – clocks with alkaline-earth atoms Gil et al., 2014; Olmos et al., 2013 since such atoms recently gave rise to the world's best clock and have nearly approached the quantum projection noise limit for unentangled atoms Bloom et al., 2014; Nicholson et al., 2014. We will now show that the quantum spin models studied in the present manuscript offer a natural way to produce metrologically relevant entanglement (in the form of GHZ states) in alkaline-earth clock experiments. It is indeed the experimental realization of quantum spin models in alkaline-earth clock experiments Martin et al., 2013 and the potential application of these spin models to improve the clocks that motivated this work.

To create a GHZ state, we allow atoms in the excited electronic state e with an energy ω_{eg} above the ground electronic state g [see Fig. 1.1(b)]. First assume $N = 2$. An applied magnetic field adds Zeeman spin-splittings $B_g \neq B_e$ Boyd, Zelevinsky, Ludlow, Foreman, et al., 2006 to both g and e states. To first order in the interaction strength, the spin Hamiltonian is (see section 1.9 for details) :

$$\hat{H} = \hat{H}_{sp} + \sum_{\alpha<\beta} U_{\alpha\beta} \left(\hat{n}_\alpha \hat{n}_\beta - \sum_{j\neq k} \hat{c}^\dagger_{j\alpha} \hat{c}_{j\beta} \hat{c}^\dagger_{k\beta} \hat{c}_{k\alpha} \right). \tag{1.23}$$

The single-particle Hamiltonian is $\hat{H}_{sp} = \omega_{eg}\hat{n}_e + B_g(\hat{n}_{1g} - \hat{n}_{2g}) + B_e(\hat{n}_{1e} - \hat{n}_{2e})$, the sum $\alpha < \beta$ is over distinct pairs of $1g$, $1e$, $2g$ and $2e$, and the constants $U_{\alpha\beta}$ are derived in terms of (electronic-state dependent) scattering lengths. Note that $\hat{n}_{1g}$, $\hat{n}_{2g}$, $\hat{n}_{1e}$ and $\hat{n}_{2e}$ are separately conserved by Hamiltonian (1.23). As shown in Fig. 1.5, to create the n-particle GHZ state $(|1g1g..1g\rangle + |2g2g..2g\rangle)$ from $|1g1g..1g\rangle$, three consecutive pulses should be applied:

1. Spatially inhomogeneous, weak, many-body $\pi/2$ pulse

$$e^{-i\nu_{eg}t} \sum_j \Omega^{eg}_j (|1e\rangle_j\langle 1g|_j + |2e\rangle_j\langle 2g|_j) + h.c.$$

   with frequency $\nu_{eg} = \omega_{eg} + (B_e - B_g) + nU_{1e1g}$.

2. Spatially uniform, weak, single-atom π pulse $e^{-i\nu_{12}t}\Omega^{12}\sum_j(|2g\rangle_j\langle 1g|_j + |2e\rangle_j\langle 1e|_j) + h.c.$ with frequency $\nu_{12} = 2B_g$.

3. Pulse 1, but for pulse area π, not $\pi/2$.

The frequency of the first pulse picks out an effective two-level system consisting of $|1g1g..1g\rangle$ and $|\{1e1g..1g\}\rangle \propto \sum_{jp}(\Omega^{eg}_j - \bar{\Omega}^{eg})|1e\rangle_j\langle 1g|_j|1g1g..1g\rangle$ (we defined $\bar{\Omega}^{eg} \equiv \sum_j \Omega^{eg}_j/n$.). The pulse must be spatially inhomogeneous to make Ω^{eg}_j j-dependent and to be thus able to access eigenstates with interaction-dependent energies (i.e. not fully symmetric eigenstates). The precise form of the inhomogeneity is unimportant, as all $n-1$ non-symmetric states with a single e atom are degenerate in $\hat{H}$ due to its S_n symmetry. The curly bracket notation signifies the state is a linear combination of $|1e1g..1g\rangle$ and permutations. No state $|\{1e1e..1g\}\rangle$ is coupled by pulse 1 because the first e atom blockades the addition of another by energy $2U_{1e1g}$. The second pulse has no effect on $|\{1e1g..1g\}\rangle$ because the e atom blockades transition to any state $|\{1e2g..1g\}\rangle$. The final pulse does not affect the

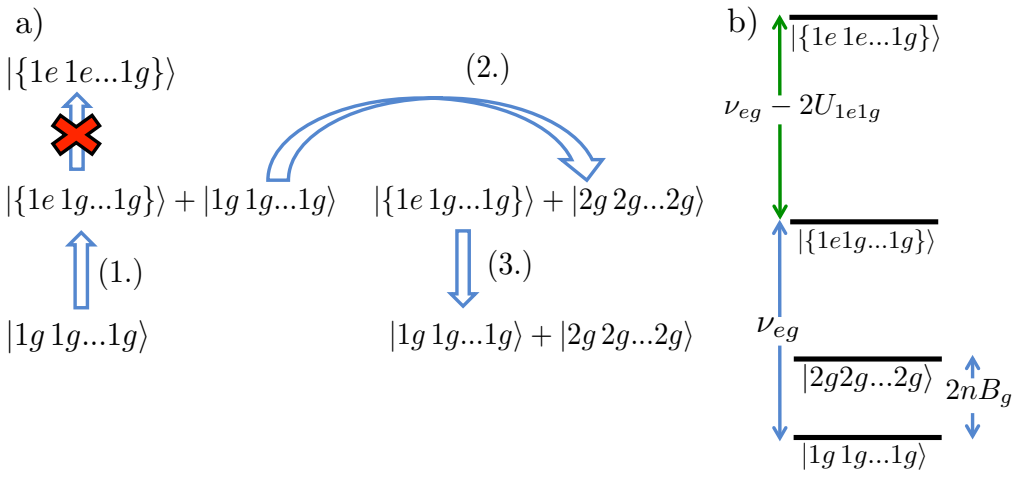

Figure 1.5: (a) System is prepared in $|1g1g..1g\rangle$, and spatially inhomogeneous pulse (1.) results in an equal superposition of this state and $|\{1e1g..1g\}\rangle$, which has one e atom. An interaction blockade prevents coupling to states with two e atoms. Pulse (2.) flips the spins of the all-g state. The initial pulse is reversed in pulse (3.), resulting in the GHZ state. (b) Relevant energy levels of the Hamiltonian with e and g states and the magnetic field. Note that pulses (1.) and (3.), which involve states $|1g1g..1g\rangle$ and $|\{1e1g..1g\}\rangle$, do not couple to state $|\{1e1e..1g\}\rangle$ since there is a blockade of $2U_{1e1g}$. Similarly, during pulse (2.), blockade prevents the excitation of state $|\{1e1g..1g\}\rangle$.

$|2g2g..2g\rangle$ state because the pulse is off-resonant by energy of order $(B_e - B_g)$. Note that although the precise form of the inhomogeneity in the first pulse is unimportant, the final pulse and the first pulse must have the same inhomogeneity. Since all three pulses rely on blockade, each pulse must take time $\gg 1/U$. Curiously, the fact that the interactions in our spin model have effectively infinite range makes our spins analogous to long-range interacting Rydberg atoms, for which a similar protocol exists for generating maximally entangled states Saffman and K. Molmer, 2009. Note that we have designed the protocol to have at most one e atom at any time, which avoids the potential problem of inelastic e-e collisions Traverso et al., 2009, while g-e losses are negligible Bishof et al., 2011; X. Zhang et al., 2014.

For integer m such that $N \geq 2^m$, it is possible to create m GHZ states provided one has sufficient control A. V. Gorshkov, A. M. Rey, et al., 2009 over the nuclear spin states coupled by the pulses. We describe the procedure here for $m = 2$ (which generalizes directly for larger m). First create a regular GHZ state as described above ($|1g1g..1g\rangle + |2g2g..2g\rangle$) from initial state $|1g...1g\rangle$. Then, apply pulse 1 of two different frequencies to $|1g1g..1g\rangle$ and to $|2g2g..2g\rangle$, resulting in

$(|1e1g..1g\rangle + |1g1g..1g\rangle + |2e2g..2g\rangle + |2g2g..2g\rangle)$. Now, instead of applying pulse 2, apply a pulse which implements $|p\rangle \mapsto |p+2\rangle$ (for $p = 1, 2$), but only to atoms in a many-body state containing no e atoms. The resulting state is $(|1e1g..1g\rangle + |3g3g..3g\rangle + |2e2g..2g\rangle + |4g4g..4g\rangle)$. Finally, apply pulse 3 of two different frequencies to yield $(|1g1g..1g\rangle + |2g2g..2g\rangle + |3g3g..3g\rangle + |4g4g..4g\rangle)$. This is precisely equivalent to two GHZ states, which can be seen by defining the basis $\{|\Downarrow\Downarrow\rangle, |\Downarrow\Uparrow\rangle, |\Uparrow\Downarrow\rangle, |\Uparrow\Uparrow\rangle \equiv \{|1\rangle, |2\rangle, |3\rangle, |4\rangle\}\}$. Then $(|11..1\rangle + |22..2\rangle + |33..3\rangle + |44..4\rangle) = (|\Downarrow\Downarrow .. \Downarrow\rangle + |\Uparrow\Uparrow .. \Uparrow\rangle)(|\Downarrow\Downarrow .. \Downarrow\rangle + |\Uparrow\Uparrow .. \Uparrow\rangle)$. The process could be continued, where in the ith iteration, the second pulse involves $|p\rangle \mapsto |p + 2^i\rangle$ (for $p = 1, 2, 3...2^i$).

Several GHZ states can be used to create a single GHZ state of better fidelity via entanglement pumping Aschauer, Dur, and Briegel, 2005; A. V. Gorshkov, A. M. Rey, et al., 2009.

1.9 Derivations for GHZ state preparation

In this Section, we present the details behind the GHZ state preparation protocol.

The state $|A\rangle = |1g\,1g...1g\rangle$ has energy $E_A = nB_g$. The state $|B\rangle = |\{1e\,1g...1g\}\rangle$ lies in the same energy manifold as the state $(|1g\,1e\rangle - |1e\,1g\rangle)|1g...1g\rangle$, which has energy $E_B = \omega_{eg} + (n-1)B_g + B_e + [(n-1) - (-1)]U_{1g\,1e}$. Similarly, $|C\rangle = |\{1e\,1e...1g\}\rangle$ has the same energy as $(|1g\,1e\rangle - |1e\,1g\rangle)(|1g\,1e\rangle - |1e\,1g\rangle)|1g...1g\rangle$, with energy $E_C = 2\omega_{eg} + (n-2)B_g + 2B_e + [2(n-2) - (-2)]U_{1g\,1e}$. Driving with frequency $(E_B - E_A)$ forms an effective two-level system: $\{|A\rangle \leftrightarrow |B\rangle \not\leftrightarrow |C\rangle\}$ since $(E_B - E_A) = \omega_{eg} - B_g + B_e + nU_{1g\,1e} \neq (E_C - E_B) = \omega_{eg} - B_g + B_e + (n-2)U_{1g\,1e}$.

Now we explain why transition $|A\rangle \to |D\rangle \equiv |2g\,2g...2g\rangle$ occurs, while the transition $|B\rangle \not\to |x\rangle$ is blocked for any energy eigenstate $|x\rangle$. First note that the transition $|A\rangle \to |D\rangle$ actually passes through a ladder of intermediate energy eigenstates: $|A\rangle \equiv |1g\,1g...1g\rangle \to |\mathcal{S}\{2g\,1g...1g\}\rangle \to |\mathcal{S}\{2g\,2g...1g\}\rangle \to ... \to |2g\,2g...2g\rangle \equiv |D\rangle$, where $\mathcal{S}$ symmetrizes its argument. Each state in the ladder has energy $2B_g$ more than the last, and is connected to the previous through the operator $\hat{P} = \sum_j (|2g\rangle_j\langle 1g|_j + |2e\rangle_j\langle 1e|_j)$, which is applied as a pulse with frequency $2B_g$. To show that $|B\rangle$ does not transition to any other state under the action of this pulse, we must prove that *there exists no state* $|x\rangle$ *such that* $\hat{H}|x\rangle = (E_B + 2B_g)|x\rangle$ *and* $\langle x|\hat{P}|B\rangle \neq 0$. We will assume that $n > 2$, $B_e \neq B_g$ and either $|U_{gg}| > 0$ or $|U_{eg}| > 0$.

Our proof has the following structure: we find four orthonormal states such that $\hat{P}|B\rangle \in \text{span}\{|\phi_1\rangle, |\phi_2\rangle, |\phi_3\rangle, |\phi_4\rangle\} \equiv \mathcal{H}_0$, where subspace $\mathcal{H}_0$ is closed under the action of $\hat{H}$ (i.e. for all $|\psi\rangle \in \mathcal{H}_0,\ \hat{H}|\psi\rangle \in \mathcal{H}_0$). Any eigenstate $|x\rangle$ of $\hat{H}$ coupled to $|B\rangle$ through $\hat{P}$ must be in $\mathcal{H}_0$, but we show the four eigenvalues E_i of $\hat{H}$ in $\mathcal{H}_0$ satisfy $E_i \neq (E_B - 2B_g)$.

To complete the proof, we must present $\{|\phi_1\rangle, |\phi_2\rangle, |\phi_3\rangle, |\phi_4\rangle\}$ explicitly, and show that $E_i \neq (E_B - 2B^g)$ for all four eigenstates ($i = 1, 2, 3, 4$). Without loss of generality, take $|B\rangle = (|1g\,1e\rangle - |1e\,1g\rangle)|1g...1g\rangle$, thus $\hat{P}|B\rangle = \sqrt{2(n-2)}|\phi_1\rangle + \sqrt{2}|\phi_3\rangle + \sqrt{2}|\phi_4\rangle$, where $|\phi_1\rangle \equiv \frac{1}{\sqrt{2(n-2)}}(|1g\,1e\rangle - |1e\,1g\rangle)|\mathcal{S}\{1g2g...1g\}\rangle$, $|\phi_2\rangle \equiv \frac{1}{\sqrt{2}}(|2g\,1e\rangle - |1e\,2g\rangle)|1g1g...1g\rangle$, $|\phi_3\rangle \equiv \frac{1}{\sqrt{2(n-2)}}(|1g\,2g\rangle - |2g\,1g\rangle)|\mathcal{S}\{1g1e...1g\}\rangle$, and $|\phi_4\rangle \equiv \frac{1}{\sqrt{2}}(|1g\,2e\rangle - |2e\,1g\rangle)|1g1g...1g\rangle$ (note that $|\phi_4\rangle$ is an energy eigenstate). $\hat{H}$ is closed on subspace $\mathcal{H}_0$ and takes the form:

$$\hat{H} = (E_B - 2B_g) + \begin{pmatrix} 0 & -\sqrt{n-2}U_{gg} & -U_{ge} & 0 \\ -\sqrt{n-2}U_{gg} & (n-2)U_{gg} & \sqrt{n-2}U_{ge} & 0 \\ -U_{ge} & \sqrt{n-2}U_{ge} & (n-1)U_{gg} - U_{ge} & 0 \\ 0 & 0 & 0 & 2(B_g - B_e) \end{pmatrix}. \tag{1.24}$$

The matrix written explicitly in Eq. (1.24) can be shown to have non-zero determinant (and therefore no vanishing eigenvalues) provided $n > 2$, $B_e \neq B_g$ and either $|U_{gg}| > 0$ or $|U_{eg}| > 0$, which completes our proof.

1.10 Experimental Details

We use the example of ^{87}Sr to describe how to experimentally access the physics we discuss in this work.

The key requirements of this proposal are as follows. Firstly, the x and y degrees of freedom must be frozen and the dynamics occur along the z direction, forming a 1D interacting system. Secondly, $U = (4\pi a_{gg}\hbar\omega_\perp)/L$ should be less than the single-particle energy separations, the smallest of which is $3\hbar^2(\pi/L)^2/M$, thus ensuring the validity of the first-order perturbation theory in our derivation of Eq. (1.2). This constrains the relative sizes of L and $\omega_\perp$. Thirdly, variations in U_{jkjk}, with standard deviation ΔU, give rise to variations in eigenergies $\sim n\Delta U$ (see below). Therefore, we also require $\Delta U/U < 1/n$.

To meet these requirements, we propose an optical lattice potential formed by two magic-wavelength (813 nm) Ye, Kimble, and Katori, 2008 orthogonal standing

waves in x and y. This could be achieved with a pair of angled beams Nelson, Li, and Weiss, 2007 for each standing wave, in bow tie configuration [see Fig. 1.6].

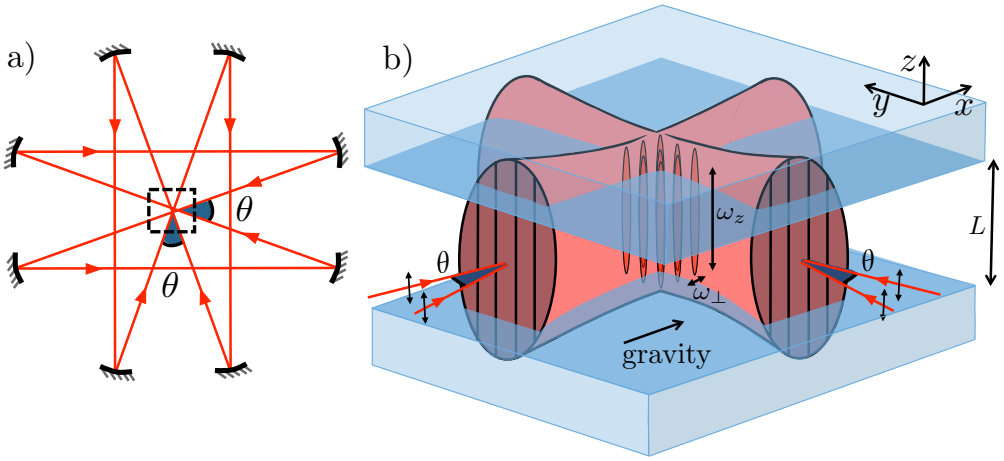

Figure 1.6: Layout of suggested experimental implementation. a) The beam configuration is achieved using a bow tie arrangement (view from above). Two pairs of beams are aimed at a vacuum chamber. In each pair, the two beams have a difference in k vector direction of $\theta = 30^{\circ}$, causing an in-plane standing wave to form in the direction perpendicular to that pair's net k vector direction. The pair of perpendicular standing waves forms an attractive lattice. b) The two-dimensional lattice of attractive-potential tubes forms with transverse vibrational frequency $\omega_\perp$ and lattice constant Δx. The finite beam width results in a weak potential in the z direction with vibrational frequency ω_z. Gravity is in the beam plane to avoid a potential gradient along the tubes. Blue-detuned light outside the central region of width L forms caps for the tubes. We obtain $\omega_\perp \simeq 2\pi \times 10$ kHz, $\Delta x \simeq 3$ μm, $\omega_z \simeq 2\pi \times 100$ Hz, and $L \simeq 10$ μm.

An additional blue-detuned optical potential at 394 nm, the Sr blue magic wavelength, is applied to form approximate 1D square wells from the resulting tubes. The potential could be formed from a projected image of a Gaussian beam with waist 30 μm and total power 400 mW screened in the center by a rectangular mask of width L = 10 μm. Imperfect cap potentials, along with a finite curvature of the flat potential, contribute to ΔU and are analyzed below.

With these parameters, and $a_{gg} = 5.1$ nm Martinez de Escobar et al., 2008, one obtains $U/\hbar = (4\pi a_{gg}\omega_\perp)/L \approx 2\pi \times 10$ Hz, and should be able to meet all three of the aforementioned key requirements with $\lesssim 20$ atoms in a single tube. Such values of $U_{\alpha\beta} \sim U$ X. Zhang et al., 2014 can potentially allow for the preparation of the GHZ state on a time scale comparable to the $\sim$1s experimental cycle time for state-of-the-art clocks Bloom et al., 2014, and may thus provide a practical advantage

over the use of unentangled atoms.

To observe spin diffusion, the most straightforward way of preparing the initial state and measuring observable $\hat{Q}$ involves cooling a spin-polarized system to the limit where the lowest n orbitals are occupied. One could also potentially consider taking advantage of large N for better cooling Hazzard et al., 2012; Taie et al., 2012. One can then address different orbitals either spatially with spin-changing pulses which only couple to certain orbitals (for example using pulses focused on the center of the well and hence decoupled from orbitals that vanish there), or energetically by temporarily transferring atoms to another electronic state subject to a different potential. To observe spin diffusion with thermal atoms, one could rely on the fact that about half of the occupied orbitals are odd, and the other half are even, which becomes statistically more accurate for larger n. It is possible to address only the even orbitals by using a beam focused at the center of the well, since the odd orbitals vanish there. This could be extended to larger N by using additional beams focused on other points in the well.

The bow tie configuration build-up cavity of attractive magic-wavelength (λ =813 nm) beams shown in Fig. 1.6 results in orthogonal standing waves in the x-y plane, whose intensity maxima are spaced by $\simeq$ 3 μm, with beam waist of 100 μm at the intersection of the two beams. The build-up cavity will increase the beams' intensity by a factor of $\sim$ 100 with a circulating power of 25 W. The resulting 1D trap sites have $\omega_\perp \simeq 2\pi \times 88$ kHz for the initial loading and cooling phase of the experiment. The (much weaker) longitudinal trapping frequency that results is $\omega_z \simeq 2\pi \times 880$ Hz.

The additional blue-detuned optical potential at 394 nm, the Sr blue magic wavelength, creates sharp caps on the resulting tubes. This potential could be formed by a projected image of a Gaussian beam with waist 30 μm and total power 400 mW screened in the center by a rectangular mask of width L = 10 μm.

The large $\omega_\perp$ enforces a pseudo one-dimensional system as only the lowest radial energy level will be populated. However, the desired condition that $U = (4\pi a_{gg}\hbar\omega_\perp)/L < 3\hbar^2(\pi/L)^2/M$ is not satisfied with this large $\omega_\perp$. After loading into the hybrid red- and blue-detuned optical potential, we propose to ramp the red-detuned optical lattice potentials adiabatically from the 25 W circulating power to 300 mW, resulting in $\omega_\perp \simeq 2\pi \times 10$ kHz and $\omega_z \simeq 2\pi \times 100$ Hz. The adiabatic nature of the ramp ensures that the x and y degrees of freedom remain frozen.

Imperfections on the mask that creates the flat potential and imperfect edges of the trap from the blue-detuned potential contribute to ΔU. In Section 1.4 we give an analytic bound that a harmonic perturbation of frequency ω_z small enough that $M\omega_z^2 L^2 < \frac{\hbar^2\pi^2}{ML^2}$ leads to $\Delta U/U < 10^{-2}$. Exact diagonalization of the 1D potential confirms that $\Delta U/U$ is even less sensitive to ω_z: our parameters correspond to $M\omega_z^2 L^2 \approx 750\frac{\hbar^2\pi^2}{2ML^2}$, yet $\Delta U/U$ remains below one percent. The imaging system used to form the potential contributes much more significantly to ΔU. With an imaging point spread function of full width at half maximum (FWHM) of 1 μm with atoms at 1 μK, exact diagonalization results in $\Delta U/U \lesssim 5\%$.

Therefore with these parameters, one obtains $U/\hbar = (4\pi a_{gg}\omega_\perp)/L \approx 2\pi \times 10$ Hz, and should be able to meet all three of the key requirements stated above with $\lesssim 20$ atoms in a single tube. In addition, as the pulses in the GHZ protocol should resolve U, they should have a sufficiently long duration $\gg 0.1$ s. With additional effort, it should be possible to reach a regime of higher U and n while satisfying these requirements. By shaking the trap during preparation with frequencies low enough to depopulate the lowest m energy orbitals, the restrictions on L and $\omega_\perp$ from the requirement that $U = (4\pi a_{gg}\hbar\omega_\perp)/L < 3\hbar^2(\pi/L)^2/M$ is relaxed to $(4\pi a_{gg}\hbar\omega_\perp)/L < [(m+2)^2-(m+1)^2]\hbar^2(\pi/L)^2/M$. Decreasing the ratio between the spatial imperfections of the potential and L will reduce $\Delta U/U$. For example, reducing the FWHM of the point spread function in our numerical calculations described above from 1 μm to 0.5 μm yields $\Delta U/U < 2\%$. Approaches for creating subwavelength potentials can also be envisioned Jendrzejewski, 2014.

Beyond the three key requirements given at the start of this section, there are a number of other considerations which we now address. Taking a typical recombination rate constant $K_3 \approx 10^{-28}$ cm^6/s for $n = 20$ particles, it should take approximately 1 second before a single particle is lost. This loss time is 10 times longer than the coherent interaction time $2\pi\hbar/U$, a ratio that is comparable (or even superior) to the ratio of the decoherence time to the spin-spin interaction time in superexchange-based systems Trotzky et al., 2008; R. C. Brown et al., 2015. Tunneling between the tubes is negligible due to the large 3 μm spacing between tubes. The approximate magnitude of p-wave terms involving occupied orbitals j and k is $\pi^2(j^2+k^2)(b_{gg}/L)^2(b_{gg}/a_{gg})\,U$, where b_{gg}^3 is the scattering volume for p-wave interactions. This remains small for $j, k < 300$, taking $b_{gg} \approx 3.9$ nm X. Zhang et al., 2014 for ^{87}Sr. Vector and tensor light shifts Boyd, Zelevinsky, Ludlow, Blatt, et al., 2007 in principle break $SU(N)$ symmetry, but tensor polarizability in our system

is negligible, while vector shifts can be avoided with the use of linear polarization. Specifically, to ensure any breaking of the $SU(N)$ symmetry is far below a level which could affect our proposal, beam circularity of below a few percent should be sufficient. An appropriate choice of linear polarization of the blue-detuned beam will ensure minimal longitudinal field components (and hence minimal circularity) induced by imaging the mask.

1.11 Outlook

The proposed system opens a wide range of research and application avenues beyond those discussed above. For the case of $N = 2$, our $S_n \times SU(N)$-symmetric Hamiltonian can be used for decoherence-resistant entanglement generation A. M. Rey, Jiang, et al., 2008, a method whose generalization to $N > 2$ we postpone to future work. Furthermore, by comparing with the exact solutions presented here or those derived in the limit of strong interactions Volosniev et al., 2015; Deuretzbacher et al., 2014 one could verify the performance of the proposed experimental system as a quantum simulator. The system can then be used to reliably study more general regimes where complexity theory might rule out efficient classical solutions. In particular, deviations from the square-well potential will break S_n [but not $SU(N)$] symmetry. This will for example lift the degeneracy of the most antisymmetric spin state (highest energy eigenspace for $U > 0$). Depending on how this degeneracy is lifted, exotic many-body states might arise Miguel A Cazalilla and Ana Maria Rey, 2014; A. M. Rey, A. V. Gorshkov, Kraus, et al., 2014.

Finally, thanks to its high $S_n \times SU(N)$ symmetry, the present system allows one to implement powerful quantum information protocols, such as the density matrix spectrum estimation protocol of Keyl and Werner Keyl and Werner, 2001, which is the topic of Chapter 2.

Chapter 2

SPECTRUM ESTIMATION

In Chapter 1, we studied an atomic system which gives rise to a highly symmetric nuclear spin Hamiltonian which is decoupled from the spatial degrees of freedom. The decoupling arose because the trap used forces the Hamiltonian to have parameters which are symmetric under exchange of spatial states.

In this chapter, we argue that standard Ramsey spectroscopy on this system, enabled by its' high symmetry, provides an efficient and accurate estimate for the eigenspectrum of a density matrix whose n copies are stored in the nuclear spins of n such atoms.

2.1 Motivation and Background

The eigenspectrum of an N-dimensional density matrix $\hat{\rho}$ of a system characterizes the entanglement of the system with its environment Horodecki et al., 2009. As it gives access to quantities such as purity, entanglement entropy, and more generally Renyi entropies, the eigenspectrum is an indispensable tool for studying many-body quantum states and processes in general and quantum information processors in particular Eisert, Cramer, and Plenio, 2010; M. A. Nielsen and I. L. Chuang, 2000.

One can learn about the spectrum of $\hat{\rho}$ by making measurements on n copies of the state. To characterize the efficiency of a particular measurement strategy for this task, one can consider the sample complexity: i.e. the number n of copies required to obtain an estimate $\vec{q}$ of the spectrum $\vec{p}$ of an arbitrary N dimensional density matrix, such that the one-norm deviation is below a certain threshold $||\vec{q}-\vec{p}||_1 < \epsilon$. Normally one considers the asymptotic scaling of n with N and ϵ, ignoring prefactors. It is not currently known how many copies are necessary and sufficient to estimate the spectrum of any dimension N density operator to ϵ-accuracy, but the best known strategy scales O'Donnell and Wright, 2015 as $\tilde{\Theta}(N^2/\epsilon^2)$, where log factors have been dropped. This strategy is the empirical Young diagram (EYD) algorithm, performs a single joint entangled measurement on all n copies Alicki, Rudnicki, and Sadowski, 1988; Keyl and Werner, 2001; Hayashi, 2002; Keyl, 2006; Christandl and Mitchison, 2006; O'Donnell and Wright, 2015. It is natural that an optimal measurement should be invariant under arbitrary permutations [symmetry

group S_n] and arbitrary simultaneous rotations [symmetry group $SU(N)$] of all n copies. Indeed the EYD algorithm simply projects the initial state onto irreducible representations of $S_n \times SU(N)$.

The best known strategy for spectrum estimation without joint measurements, is an adaptive two-stage protocol in which an asymptotically vanishing fraction of the copies are used with full tomography to estimate the eigenbasis of the state, which is used as a measurement basis on the remaining copies Ballester, 2006. It is unclear if this strategy has the same sample complexity as the EYD strategy, but the author argues to be asymptotically as good under a different notion of performance. In any case, for the overhead involved for moderate numbers of copies could be prohibitive in practice.

However prohibitive the number of copies required for spectrum estimation using separable measurements, one may expect that the difficulty involved in making joint measurements of many quantum systems renders the EYD scheme highly impractical. Here we show that, surprisingly, Ramsey spectroscopy of fermionic alkaline-earth atoms in a square-well trap naturally performs the highly entangled EYD measurement on n copies of $\hat{\rho}$ stored in the d-dimensional nuclear spin of n such atoms.

Spectrum estimation could be a useful tool in these experimental systems. Two unique features of fermionic alkaline-earth atoms are the metastability of the optically excited state $|e\rangle = {}^3\mathrm{P}_0$ and the decoupling of the nuclear spin from the ($J = 0$) electrons in both the ground state $|g\rangle = {}^1\mathrm{S}_0$ and in $|e\rangle$. Thanks to these two features, alkaline-earth atoms have given rise to the world's best atomic clocks Bloom et al., 2014; Nicholson et al., 2014 and hold great promise for quantum information processing with nuclear and optical electronic qubits Childress et al., 2005; Reichenbach and I. H. Deutsch, 2007; Hayes, Julienne, and I. H. Deutsch, 2007; Daley et al., 2008; A. V. Gorshkov, A. M. Rey, et al., 2009; Daley, 2011 and for quantum simulation of two-orbital, high-symmetry magnetism A. V. Gorshkov, Hermele, et al., 2010; M. A. Cazalilla, Ho, and Ueda, 2009; Miguel A Cazalilla and Ana Maria Rey, 2014; X. Zhang et al., 2014; Scazza et al., 2014; Cappellini et al., 2014. Spectrum estimation of $\hat{\rho}$, using a copy of $\hat{\rho}$ stored in the nuclear spin of each of n $|g\rangle$ atoms, would be of great value in all of these applications. First, it can determine whether $\hat{\rho}$ describes a pure state, in which case the fermions would be identical and s-wave scattering would not interfere with clock operation. Second, it can be used to assess how faithfully the nucleus stores quantum information as

one manipulates the electron Childress et al., 2005; Reichenbach and I. H. Deutsch, 2007; A. V. Gorshkov, A. M. Rey, et al., 2009. Finally, this procedure can be used to characterize the entanglement of a given nuclear spin with others in a many-atom state obtained via evolution under a spin Hamiltonian Honerkamp and Hofstetter, 2004; A. V. Gorshkov, Hermele, et al., 2010; M. A. Cazalilla, Ho, and Ueda, 2009; Miguel A Cazalilla and Ana Maria Rey, 2014; X. Zhang et al., 2014; Scazza et al., 2014; Cappellini et al., 2014; we would need n copies of the many-atom state.

2.2 Overview of the proposal

As illustrated in Fig. 2.1(a), to estimate the spectrum of $\hat{\rho}$, whose n copies are stored in the nuclear spins of n $|g\rangle$ atoms, we transfer all n atoms into a single infinite square well, with at most one atom per single-particle orbital.

As detailed in Chapter 1, for sufficiently weak interactions, due to energy conservation and the anharmonicity of the trap, the n occupied orbitals of the well remain unchanged throughout the experiment and play the role of sites. Thanks to the decoupling of the N-dimensional nuclear spin from the electrons, s-wave interactions give rise to a spin Hamiltonian with nuclear-spin-rotation $SU(N)$ symmetry A. V. Gorshkov, Hermele, et al., 2010; M. A. Cazalilla, Ho, and Ueda, 2009. Furthermore, the interaction strength between square-well orbitals labeled by positive integers $p \neq q$ is proportional to $\int_0^\pi dx \sin^2(px)\sin^2(qx) = \pi/4$ and is thus independent of p and q, giving rise to the site-permutation symmetry S_n **beverland16** The resulting $S_n \times SU(N)$ symmetric Hamiltonian,

$$\hat{H} = U\sum_{j<k}(1-\hat{s}_{jk}), \tag{2.1}$$

is therefore diagonal in the EYD measurement basis, naturally turning Ramsey spectroscopy of this system into an implementation the EYD algorithm. As in Chapter 1, $\hat{s}_{jk}$ swaps spins j and k, and the sum is over occupied orbitals. Here, we have explicitly restored the constant $Un(n-1)/2$ which was omitted in Equation 1.2 as it will be relevant here.

To include the first excited electronic state, one should use the prescription of Section 1.7. For simplicity, we instead make the modeling assumption that atoms only interact if they are in the ground electronic state, such that the Hamiltonian is

$$\hat{H}_{\mathrm{D}} = U\sum_{j<k}\hat{\sigma}^j_{gg}\hat{\sigma}^k_{gg}(1-\hat{s}_{jk}) - \delta\sum_k \hat{\sigma}^k_{ee}, \tag{2.2}$$

where σ_{gg}^j projects the atom in the jth orbital into the ground electronic state, and δ is an energy offset of the electronically excited level. This Hamiltonian would occur for particular (unrealistic) values of the scattering constants, or could be enforced by using different traps for the ground and excited electronic states, such that the density in the confined directions is much lower for atoms in the excited (rather than ground) electronic states.

At the start of the Ramsey sequence, the initial state of the n-atom system is $|G\rangle\langle G| \otimes \rho^{\otimes n}$, where $|G\rangle = |g \dots g\rangle$ and each nuclear spin is in the same state $\hat{\rho}$. The first Ramsey pulse of area β between $|g\rangle$ and $|e\rangle$ [Fig. 2.1(b)] is implemented over short time $t_P = \beta/\Omega$ (so that interactions can be ignored), using Hamiltonian $\hat{H}_P = \frac{\Omega}{2}\sum_k \left(\hat{\sigma}_{eg}^k + \hat{\sigma}_{ge}^k\right)$ with Rabi frequency Ω and $\hat{\sigma}_{\mu\nu}^k = |\mu\rangle_k\langle\nu|$. Then the system is allowed to evolve under $\hat{H}_\mathrm{D}$ for a dark time t_D. After the second Ramsey pulse of area $-\beta$, the state is

$$\hat{\rho}' = \hat{U}_p^\dagger \hat{U}_D \hat{U}_p |G\rangle\langle G| \hat{\rho}^{\otimes n} (\hat{U}_p^\dagger \hat{U}_D \hat{U}_p)^\dagger,$$

where $\hat{U}_p = \exp[-it_P \hat{H}_P]$ and $\hat{U}_D = \exp[-i\tau \hat{H}_D]$. Finally, the number of $|e\rangle$ atoms $\langle \hat{n}_e \rangle = \mathrm{Tr}\left[\hat{n}_e \hat{\rho}'\right]$ is measured, where $\hat{n}_e = \sum_j \hat{\sigma}_{ee}^j$. We will show below that

$$\frac{\langle \hat{n}_e \rangle}{n} = \frac{\sin^2\beta}{2}\left[1 - \sum_{r=1}^{N} p_r \cos\left(\omega_r \tau\right)\right] + \mathcal{O}\left(\frac{1}{\sqrt{n}}\right), \tag{2.3}$$

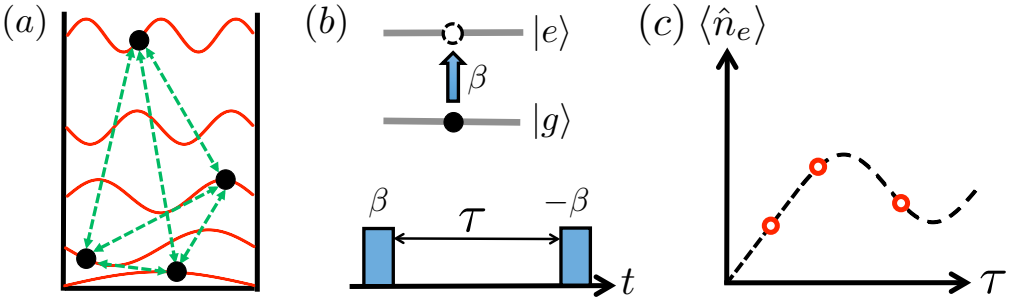

Figure 2.1: Optimal spectrum estimation with alkaline-earth atoms. (a) n copies of an N-dimensional density matrix $\hat{\rho}$ are stored in the nuclear spin of n fermionic alkaline-earth atoms trapped in the same square-well trap and prepared in their ground electronic state $|g\rangle$. (b) A Ramsey sequence is applied consisting of two pulses of area β and $-\beta$, respectively, coupling $|g\rangle$ to the first excited electronic state $|e\rangle$. (c) The number $\langle \hat{n}_e \rangle$ of $|e\rangle$ atoms is measured for $\mathcal{O}(N)$ different dark times τ (red circles) between the pulses and allows to extract the eigenspectrum of $\hat{\rho}$.

where $\omega_r = Un(1-p_r)\cos^2\frac{\beta}{2} + \delta$ and $(p_1, p_2, \ldots, p_N)$ is the eigenspectrum of $\hat{\rho}$, ordered for future convenience as $p_1 \geq p_2 \geq \cdots \geq p_N$. Moreover, as n increases, the distribution of measurement outcomes $\hat{n}_e/n$ becomes tightly peaked about its expectation value $\langle \hat{n}_e \rangle / n$. As the measurement destroys $\hat{\rho}$, we envisage starting with $\mathcal{O}(N)$ sets of n atoms, each with nuclear spin state $\hat{\rho}$. Performing the Ramsey protocol on each set for different times τ [Fig. 2.1(c)] and comparing to Eq. (2.3) allows one to infer the spectrum of $\hat{\rho}$. Notice an important difference from the usual Ramsey spectroscopy where the entire $\langle \hat{n}_e \rangle$ curve as a function of τ is typically measured and each point on the curve requires many measurements.

The limiting cases of Eq. (2.3) make sense. Indeed, Rabi π-pulses ($\beta = \pi$) give zero since $\hat{H}_D \to -n\delta$, so $\hat{U}_p^\dagger \hat{U}_D \hat{U}_p = \exp[in\delta\tau]$. Similarly, $\langle \hat{n}_e \rangle = 0$ in the absence of Rabi pulses ($\beta = 0$) since no $|e\rangle$ atoms are ever created. If $\hat{\rho}$ describes a pure state, in which case one of the p_r is unity while the rest vanish, the interaction U drops out (as it should for identical fermions) and we recover the familiar non-interacting expression. When $\hat{\rho}$ is maximally mixed, the system behaves as a non-interacting system with a frequency shift $-Un\frac{N-1}{N}\cos^2\frac{\beta}{2}$. When N is large and all $p_r \ll 1$, the system behaves as a non-interacting system with a frequency shift $-Un\cos^2\frac{\beta}{2}$.

2.3 Spectrum estimation for $N = 2$

To describe the physics behind our Ramsey-based spectrum estimation protocol and behind Eq. (2.3), we start by reviewing the original EYD spectrum estimation algorithm for the familiar case of qubits ($N = 2$, or, equivalently, spin-$1/2$). The algorithm states: Letting $(p, 1-p)$ with $p \geq 1/2$ be the spectrum of $\hat{\rho}$, in the limit $n \to \infty$, a single measurement on $\hat{\rho}^{\otimes n}$ of the total spin $\hat{S}^2$ [with possible outcomes $S(S+1)$ with nonnegative $S = n/2, n/2-1, \ldots$] gives an outcome satisfying $p = 1/2 + S/n + \mathcal{O}(1/\sqrt{n})$. This result follows from the fact that for large n the measurement outcome distribution $\Pr(S|n,p)$ becomes peaked with mean and standard deviation $(p-1/2)n$ and $\sqrt{p(1-p)n}$ to leading order in n, as shown in Fig. 2.2(a). The mean value can be understood from the fact that $\langle \hat{S}_z \rangle = (p-1/2)n$ for $\hat{\rho} = p\,|\uparrow\rangle\langle\uparrow| + (1-p)\,|\downarrow\rangle\langle\downarrow|$.

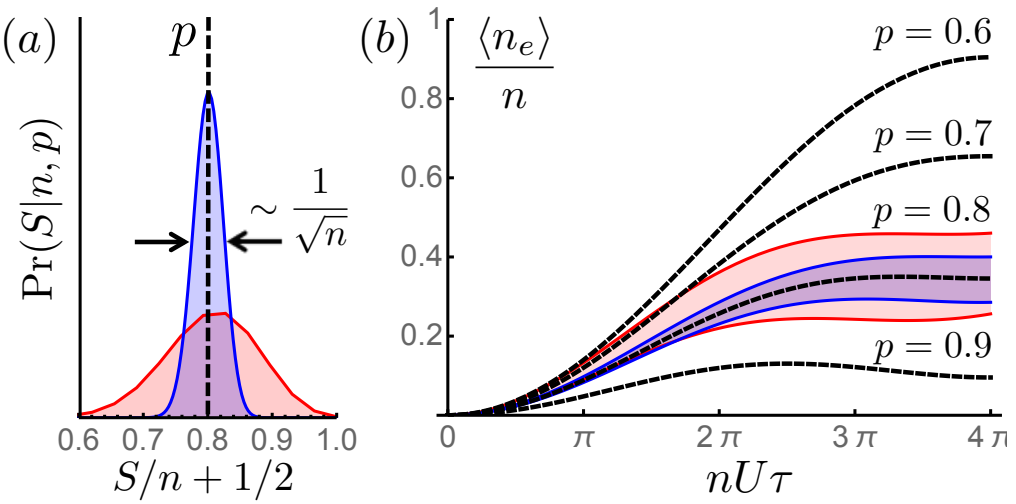

Figure 2.2: (a) The normalized probability distribution $\Pr(S|n,p)$ for obtaining a measurement outcome S (and the estimate $S/n+1/2$ for p) for $n=30$ and $n=300$ copies of $\hat{\rho}$ with spectrum $(p,1-p)$ with $p=0.8$. The standard deviation of the p estimate scales as $\sim 1/\sqrt{n}$. (b) The dashed curves represent the Ramsey signal $\langle \hat{n}_e\rangle/n$, in the limit $n\to\infty$, for $\beta=\pi/2$ and $N=2$, for different values of p [Eq. (2.3)]. For finite n, the measurement outcomes $n_e(\tau,S)$ are distributed around $\langle \hat{n}_e\rangle$ according to the probability distribution $\Pr(S|n,p)$ [Eq. 2.4]. For $n=300$ ($n=30$), the blue (blue and red) region around the $p=0.8$ asymptotic curve corresponds to the range of $\hat{n}_e/n$ outcomes observed with probability $2/3$. For all curves, $\delta=0$.

In our system, the interaction $\hat{H}_D$ has $S_n\times SU(2)$ symmetry, implying that, when all atoms are in $|g\rangle$, it can be re-expressed in terms of $\hat{S}^2$. So the eigenspaces of $\langle G|\,\hat{H}_D\,|G\rangle$ are in one-to-one correspondence with the EYD measurement basis. Ramsey spectroscopy, which is known to access properties of many-body systems Knap et al., 2013, provides a natural tool for accessing these $\hat{S}^2$ eigenspaces.

We write the result of the Ramsey measurement as

$$\frac{\langle \hat{n}_e\rangle}{n} = \frac{\mathrm{Tr}\left(\hat{\rho}^{\otimes n}\,\hat{n}_e(\tau)\right)}{n} = \sum_S \Pr(S|n,p)\frac{n_e(\tau,S)}{n}, \tag{2.4}$$

where $\hat{n}_e(\tau)\equiv\langle G|U_p^\dagger U_D^\dagger U_p \hat{n}_e U_p^\dagger U_D U_p|G\rangle$ is the time-evolved measurement operator projected onto $|G\rangle$. As $\hat{n}_e(\tau)$ acts only on the nuclear spins, and is manifestly $S_n\times SU(2)$ symmetric, it is therefore diagonal in the $\hat{S}^2$ eigenbasis, with eigenvalue $n_e(\tau,S)$.

As we will the expectation value $\langle \hat{n}_e\rangle/n$ is a function of τ that depends on p, allowing one to learn about the spectrum p through Ramsey spectroscopy [see Fig. 2.2(b)]. We will see that for arbitrary N, the variation of $\langle \hat{n}_e\rangle/n$ with the spectrum $\vec{p}$ is

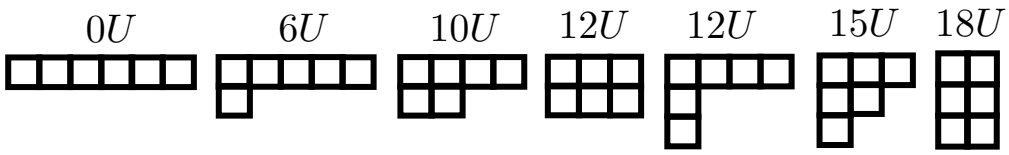

Figure 2.3: The Young diagrams $\vec{\lambda} = (\lambda_1, \lambda_2, ..., \lambda_N)$ for $n = 6$, $N = 3$. With all atoms in $|g\rangle$, the interaction Hamiltonian $\langle G| \hat{H}_D |G\rangle = U \sum_{j<k}(1 - \hat{s}_{jk})$ has $S_n \times SU(N)$ symmetry and is therefore diagonal in $\vec{\lambda}$-subspaces. The energy in $\langle G| \hat{H}_D |G\rangle$ is displayed above each Young diagram. Notice two of the Young diagrams correspond to the same energy.

sufficiently rich to allow inference of the spectrum. In addition to the expectation of the operator $\hat{n}_e/n$, we will also be concerned with its variance $(\langle \hat{n}_e^2 \rangle - (\langle \hat{n}_e \rangle^2)/n^2$, which provides an estimate for how many repetitions are necessary to estimate $\langle \hat{n}_e \rangle/n$ sufficiently accurately.

2.4 Generalization to arbitrary N

We now describe the EYD and Ramsey-based spectrum estimation protocols for arbitrary N. Thanks to Schur-Weyl duality Fulton and Harris, 1991, the irreducible representations (irreps) of $S_n \times SU(N)$ in the N^n-dimensional nuclear-spin Hilbert space $\mathcal{H}$ of n atoms are in one-to-one correspondence with N-row Young diagrams $\vec{\lambda} = (\lambda_1, \lambda_2, \ldots, \lambda_N)$ whose row lengths satisfy $\lambda_1 \geq \lambda_2 \geq \cdots \geq \lambda_N$ and $\sum \lambda_i = n$ [see Fig. 2.3]. We write $\mathcal{H} = \bigoplus_{\vec{\lambda}} \mathcal{H}_{\vec{\lambda}}$, where $\vec{\lambda}$-subspace $\mathcal{H}_{\vec{\lambda}} \subset \mathcal{H}$ supports the $\vec{\lambda}$-irrep. Any operator on $\mathcal{H}$ with $S_n \times SU(N)$ symmetry has $\mathcal{H}_{\vec{\lambda}}$ as eigenspaces.

In the EYD algorithm, one measures the Young diagram on $\hat{\rho}^{\otimes n}$. The distribution of outcomes $\vec{\lambda}$ has a single peak near $n\vec{p}$ with a typical deviation $\sum_i |\frac{\lambda_i}{n} - p_i|$ being $\mathcal{O}(n^{-1/2})$ Christandl and Mitchison, 2006.

Restricted to the ground electronic state, $\langle G| \hat{H}_D |G\rangle = U \sum_{j<k}(1 - \hat{s}_{jk})$ is an operator on $\mathcal{H}$ with $S_n \times SU(N)$ symmetry. The energies $E(\vec{\lambda}) = \frac{U}{2} n(n - 1) - \frac{U}{2} \sum_i \lambda_i(\lambda_i - 2i + 1)$ are not in one-to-one correspondence with subspaces $\mathcal{H}_{\vec{\lambda}}$ for $N > 2$ [see Fig. 2.3 for an example]. Therefore, even if it were possible experimentally, direct measurement of the energy associated with $\langle G| \hat{H}_D |G\rangle$ would not be sufficient to perform the EYD algorithm. We will see that, remarkably, by accessing restrictions of $\hat{H}_D$ to different subsets of g atoms, Ramsey spectroscopy is powerful enough to uniquely identify $\vec{\lambda}$.

For arbitrary N, Eq. (2.4) becomes

$$\frac{\langle \hat{n}_e \rangle}{n} = \frac{\mathrm{Tr}\left(\hat{\rho}^{\otimes n}\, \hat{n}_e(\tau)\right)}{n} = \sum_{\vec{\lambda}} \Pr(\vec{\lambda}|n,\vec{p}) \frac{n_e(\tau,\vec{\lambda})}{n}, \tag{2.5}$$

once again defining $\hat{n}_e(\tau) \equiv \langle G|U_p^\dagger U_D^\dagger U_p \hat{n}_e U_p^\dagger U_D U_p|G\rangle$, which acts on $\mathcal{H}$ and exhibits $S_n \times SU(N)$ symmetry.

2.5 Expectation value of the number operator

We now evaluate the eigenvalues $n_e(\tau,\vec{\lambda}) \equiv \left\langle \vec{\lambda} \right| \hat{n}_e(\tau) \left| \vec{\lambda} \right\rangle$ of $\hat{n}_e(\tau)$. To avoid clutter, we drop hats on operators and arrows on vectors and introduce abbreviations: $\mathfrak{c} \equiv \cos\frac{\beta}{2}$, $\mathfrak{s} \equiv \sin\frac{\beta}{2}$. Expanding $U_p|G\rangle$ in the $|E\rangle$ basis,

$$\begin{aligned} n_e(\tau,\lambda) = \sum_{E',E\in\{0,1\}^n} & i^{|E'|-|E|} \mathfrak{c}^{2n-|E|-|E'|} \mathfrak{s}^{|E|+|E'|} \\ & \times \langle\lambda|\langle E'| U_D^\dagger n_e(\beta) U_D |E\rangle |\lambda\rangle, \end{aligned} \tag{2.6}$$

where $n_e(\beta) \equiv U_p n_e U_p^\dagger$, and where binary vector $E = (E_1, E_2, ..., E_n) \in \{0,1\}^n$ defines $|E\rangle$ with kth atom in electronic state $|g\rangle$ when $E_k = 0$, and $|e\rangle$ when $E_k = 1$. We denote by $|E|$ the number of 1's in E. Since $n_e(\beta)$ is a sum of single-atom operators, terms in which strings E and E' differ on more than one site vanish. When $E' = E$,

$$\begin{aligned} \langle E| U_D^\dagger n_e(\beta) U_D |E\rangle &= \langle E| n_e(\beta) |E\rangle \\ &= (n-|E|)\mathfrak{s}^2 + |E|\mathfrak{c}^2, \end{aligned} \tag{2.7}$$

because $|E\rangle$ is an eigenstate of U_D with eigenvalue $e^{i\delta|E|\tau} \exp\left[-i\alpha \sum_{j<k\in E}(1-\hat{s}_{jk})\right]$, which is an operator acting on the nuclear spins. Here $\alpha = U\tau$, $j<k\in E$ means $j<k$ and $j,k\in E$, and $j\in E$ means $E_j = 0$. Terms with $E' = E$ thereby sum to $2n\mathfrak{c}^2\mathfrak{s}^2 = \frac{n}{2}\sin^2\beta$ in Eq. (2.20).

When E' and E only differ on the kth atom such that $E_k = 1$ and $E'_k = 0$,

$$\langle E'| U_D^\dagger n_e(\beta) U_D |E\rangle = -i\mathfrak{c}\mathfrak{s} \underbrace{e^{i\delta\tau} e^{i\alpha\sum_{j\in E}(1-s_{jk})}}_{\mathcal{A}_E}, \tag{2.8}$$

as $e^{-i\alpha\sum_{j<l\in E'} s_{jl}} e^{i\alpha\sum_{j<l\in E} s_{jl}} = e^{-i\alpha\sum_{j\in E} s_{jk}}$, which holds since the exponents commute. Therefore, the contribution to the sum in Eq. (2.20) of E and E' that

differ on a single atom is

$$-\sum_{k=1}^{n}\sum_{\substack{E\in\{0,1\}^n\\E_k=1}}\mathfrak{c}^{2n-2|E|+2}\mathfrak{s}^{2|E|}\left\langle\lambda\right|\mathcal{A}_E+\mathcal{A}_E^\dagger\left|\lambda\right\rangle. \tag{2.9}$$

For integer $w=0,1,...,n-1$, define the operator $\mathcal{A}_w\equiv\sum_{k=1}^{n}\sum_{E;E_k=1,|E|=w+1}\mathcal{A}_E$. Note that $\mathcal{A}_w$ consists of $n\binom{n-1}{w}$ terms, and has $S_n\times SU(N)$ symmetry. It has (scaled) eigenvalues

$$\begin{aligned}A_w(\lambda)&\equiv\frac{1}{n\binom{n-1}{w}}\left\langle\lambda\right|\mathcal{A}_w\left|\lambda\right\rangle=\frac{1}{n\binom{n-1}{w}}\frac{1}{\|\lambda\|}\operatorname{tr}_\lambda\mathcal{A}_w\\&=\frac{1}{\|\lambda\|}\operatorname{tr}_\lambda e^{i\delta\tau}e^{i\alpha\sum_{j=1}^{n-1-w}(1-s_{jn})},\end{aligned} \tag{2.10}$$

where $\|\lambda\|$ is the dimension of the λ irrep of S_n, and in the last equality we used the conjugation invariance of tr to choose a convenient expression. Note that we ignored the $SU(N)$ Hilbert space and considered S_n alone since $\mathcal{A}_E$ is written in terms of elements of S_n, which are each themselves $SU(N)$ symmetric. In terms of $A_w(\lambda)$,

$$\frac{n_e(\tau,\lambda)}{n}=\frac{\sin^2\beta}{2}\left[1-\sum_{w=0}^{n-1}\Pr(w|n,\beta)\,\mathfrak{Re}\,A_w(\lambda)\right], \tag{2.11}$$

where $\Pr(w|n,\beta)\equiv\binom{n-1}{w}\mathfrak{c}^{2(n-w-1)}\mathfrak{s}^{2w}$ is the binomial distribution obtained from expanding $(\mathfrak{s}^2+\mathfrak{c}^2)^{n-1}=1$. Now we show

$$A_w(\lambda)=e^{i\delta\tau+i\alpha(n-w-1)}\sum_{\xi}\Pr(\xi|w,\lambda)\sum_{r=1}^{N}\frac{\|\xi^{-r}\|}{\|\xi\|}e^{-i\alpha(\xi_r-r)}, \tag{2.12}$$

where the sum is over all irreps ξ of S_{n-w}, and $\Pr(\xi|w,\lambda)\equiv\frac{m(\lambda,\xi)\|\xi\|}{\|\lambda\|}$ is a probability distribution defined in terms of *branching rules* $m(\lambda,\xi)$ that we define shortly. From Eq. (2.10), we must evaluate $\operatorname{tr}_\lambda[\mathcal{B}_w]$, where $\mathcal{B}_w\equiv e^{-i\alpha\sum_{j=1}^{n-w-1}s_{jn}}$. The operator $\mathcal{B}_w$ is composed of permutations in the subgroup S_{n-w} of the first $n-w-1$ sites, along with the nth site. From this observation, we regard the representation space λ as a representation of S_{n-w}, to obtain a *reducible* representation $\lambda|^n_{n-w}$ of S_{n-w}. This decomposes into a direct sum of irreps ξ of S_{n-w} as $\lambda|^n_{n-w}\cong\bigoplus_\xi m(\lambda,\xi)\xi$. The branching rule $m(\lambda,\xi)$ is the multiplicity, calculated iteratively from the fact that the restriction of an irrep λ of S_l to S_{l-1} consists of distinct irreps λ^{-r} of S_{l-1} with multiplicity 1, i.e., $\lambda|^l_{l-1}\cong\bigoplus_r\lambda^{-r}$, where λ^{-r} is obtained by removing a box from the rth row of λ Diaconis, 1988. λ^{-r} is zero if the diagram becomes an invalid

Young diagram after removing the box. Since $\mathcal{B}_w$ is invariant under permutation of the first $n-w-1$ sites, we can finally diagonalize $\mathcal{B}_w$ by further restricting each ξ-irrep of S_{n-w} to subgroup $S_{n-w-1} \subset S_{n-w}$; $\mathcal{B}_w$ must have each ξ^{-r}-subspace as an eigenspace. Below, we show that the eigenvalue of the ξ^{-r}-subspace is $e^{-i\alpha(\xi_r - r)}$, resulting in Eq. (2.12).

So far, we have introduced three probability distributions $\Pr(\lambda|n,p)$, $\Pr(w|n,\beta)$, and $\Pr(\xi|w,\lambda)$, all of which turn out to be unimodal for large n. The first one $\Pr(\lambda|n,p)$ is concentrated at $\lambda \simeq n\vec{p}$ with the deviation of $\|\vec{\lambda}/n - \vec{p}\|$ being $\mathcal{O}(n^{-\frac{1}{2}})$ by the result of the EYD algorithm Keyl and Werner, 2001; Christandl and Mitchison, 2006. The second distribution $\Pr(w|n,\beta)$ is a familiar binomial distribution with the deviation being $\mathcal{O}(n^{-\frac{1}{2}})$ relative to the mean $w = n\sin^2\frac{\beta}{2}$. The third distribution $\Pr(\xi|w,\lambda)$ is concentrated at $\xi \simeq \frac{n-w}{n}\lambda$ with the deviation of $\|\frac{\vec{\xi}}{n-w} - \frac{\vec{\lambda}}{n}\|$ being $\mathcal{O}(n^{-\frac{1}{2}})$ (see Section **??** for explicit calculations). Thus, the unimodality together with the fact that $\frac{\|\xi^{-r}\|}{\|\xi\|} \to \frac{\xi_r}{\sum_j \xi_j}$ for large n imply our main result Eq. (2.3).

Diagonalizing the operator $\mathcal{B}_w$

Here we prove,

$$\mathrm{tr}_\lambda\left[\mathcal{B}_w\right] = \sum_\xi m(\lambda,\xi) \sum_{r=1}^{N} \frac{\|\xi^{-r}\|}{\|\lambda\|} e^{-i\alpha(\xi_r - r)}, \tag{2.13}$$

where the sum is over all irreps ξ of S_{n-w}. Here, $\|X\| = \dim X$ denotes the dimension of the vector space.

For completeness, we repeat parts of the argument from above. The operator $\mathcal{B}_w$ is composed of permutations in the subgroup S_{n-w} of the first $n-1-w$ sites, along with the nth site. By regarding the representation space λ of S_n as a representation of the subgroup S_{n-w}, one obtains a *r*educible representation $\lambda|^n_{n-w}$ of S_{n-w}. This is a direct sum of irreps ξ of S_{n-w} as $\lambda|^n_{n-w} \cong \bigoplus_\xi m(\lambda,\xi)\xi$. The *b*ranching rules $m(\lambda,\xi)$ (multiplicity) are calculated iteratively from the fact for any positive integer l, the restriction of irrep λ of S_l to S_{l-1} yields $\lambda|^l_{l-1} \cong \bigoplus_r \lambda^{-r}$, where λ^{-r} is an irrep of S_{l-1} associated with the Young diagram obtained by removing one box from the row r of the λ-Young diagram. λ^{-r} is zero whenever removing a box from λ-Young diagram makes the diagram invalid. (Recall that a valid Young diagram is one in which the number of boxes in a row is non-increasing.) The multiplicity for nonzero λ^{-r} is precisely 1.

$\mathcal{B}_w$ is invariant under permutation of the first $n-w-1$ sites. So, within an irreducible space under these permutations, $\mathcal{B}_w$ acts as a scalar. In other words,

under the further restriction $\xi|^{S_{n-w}}_{S_{n-w-1}} = \bigoplus_r \xi^{-r}$, the operator $\mathcal{B}_w$ has ξ^{-r} as an eigenspace, with the eigenvalue $v_r(\xi) \equiv \frac{\mathrm{tr}_{\xi^{-r}}[\mathcal{B}_w]}{\|\xi^{-r}\|}$. Therefore,

$$\mathrm{tr}_\lambda [\mathcal{B}_w] = \sum_\xi m(\lambda, \xi) \sum_{r=1}^{N} \frac{\|\xi^{-r}\|}{\|\lambda\|} v_r(\xi). \tag{2.14}$$

In order to compute $v_r(\xi)$, it is necessary to understand the irrep ξ^{-r} of S_{l-1} inside the irrep ξ of S_l, where $l = n - w$. To this end, we construct a series of spaces of tabloids. Recall that given a Young diagram $\xi = (\xi_1, ..., \xi_N)$ with $\sum_r \xi_r = l$, a *Y*oung tableau t is formed by inserting integers in the boxes of ξ. Here we consider those Young tableaux with each number from 1 to l appearing in precisely one box of ξ. A *t*abloid $\{t\}$ is an equivalence class of Young tableaux t, where two tableaux are equivalent if one is obtained from another by permuting within each row. In other words, if A_t is the *g*roup of all row-preserving permutations of t, then $\{t\} = \{\alpha t : \alpha \in A_t\}$. The symmetric group S_l acts on the set of all tabloids by permuting numbers; it can be verified that $\{\pi t\} = \{\pi \alpha t\}$ for any $\alpha \in A_t$ and $\pi \in S_l$, and hence the notation $\pi\{t\}$ makes sense. Let B_t be the *g*roup of all column-preserving permutations of t, and define

$$e_t = \sum_{\beta \in B_t} \mathrm{sgn}(\beta) \beta \{t\},$$

which is called a *p*olytabloid. The action of S_l on the span of all polytabloids is isomorphic to the irrep ξ. A basis for this irrep can be chosen to be $\{e_t : t \text{ is a standard Young tableau}\}$. (A *s*tandard tableau is one in which numbers are increasing in each row and column.)

Define V_i to be the span of e_t where t is a standard Young tableau with l in one of the rows $1, \ldots, i$. Certainly, $V_1 \subseteq V_2 \subseteq \cdots V_N = \xi$. Observe that V_i is a representation space of S_{l-1} because the position of the number l is fixed by S_{l-1}. It is known that V_i/V_{i-1} is isomorphic to ξ^{-i} Fulton and Harris, 1991. Define $h \equiv \sum_{j=1}^{l-1} s_{jl}$. Note that h preserves each V_i, because V_i and its orthogonal complement contain distinct irreps of S_{l-1}, and the projection Π_{V_i} onto V_i from ξ can be written by some element of $\mathbb{C}S_{l-1}$, which implies that h commutes with the projector Π_{V_i}.

The eigenvalue v_r is determined by $he_t = u_r e_t + w$, with $v_r = \exp(-i\alpha u_r)$, for some $e_t \in V_r \setminus V_{r-1}$ and $w \in V_{r-1}$. We will read off the coefficient of $\{t\}$, where 'l' is placed in the row i of a standard tableau t. (If it is not possible for such t to be

standard, then $V_r/V_{r-1} = 0$.) Since

$$he_t = \sum_{\tau\in h,\ \beta\in B_t} \mathrm{sgn}(\sigma)\tau\beta\{t\}, \tag{2.15}$$

we see that the coefficient of $\{t\}$ in he_t is

$$u_r = \sum_{\tau\in h,\ \beta\in B_t\ :\ \tau\beta\{t\}=\{t\}} \mathrm{sgn}(\beta) = \sum_{\tau\in h,\ \beta\in B_t\ :\ \tau\beta\in A_t} \mathrm{sgn}(\beta). \tag{2.16}$$

In order to make a nonzero contribution to the sum, τ must be a member of $B_t \cdot A_t$. If both $\alpha \in B_t$ and $\beta \in A_t$ are nontrivial, then $\beta\alpha$ cannot be a transposition. Thus, $\tau = \beta\alpha$ must be a member of either A_t, in which case $\mathrm{sgn}(\beta = 1) = 1$, or B_t, in which case $\mathrm{sgn}(\beta) = \mathrm{sgn}(\tau) = -1$. There are $\xi_r - 1$ terms of h that belong to A_t, and $r - 1$ terms of h that belong to B_t. Therefore,

$$u_r = (\xi_r - 1)(+1) + (r - 1)(-1) = \xi_r - r. \tag{2.17}$$

Hence $v_r(\xi) = e^{-i\alpha(\xi_r - r)}$ as promised.

2.6 Variance of the number operator (ongoing work)

We now study the variance of the operator $\hat{n}_e/n$. More precisely, we study $(\langle\hat{n}_e^2\rangle - \langle\hat{n}_e\rangle^2)/n^2$, where the expectation value $\langle\hat{n}_e\rangle$ was the object of study in the previous section, and

$$\frac{\langle\hat{n}_e^2\rangle}{n} \;=\; \frac{\mathrm{Tr}\,(\hat{\rho}^{\otimes n}\ \hat{n}_e^2(\tau))}{n} = \sum_{\vec{\lambda}} \mathrm{Pr}(\vec{\lambda}|n,\vec{p})\frac{n_e^2(\tau,\vec{\lambda})}{n}, \tag{2.18}$$

defining $\hat{n}_e^2(\tau) \equiv \langle G|U_p^\dagger U_D^\dagger U_p \hat{n}_e^2 U_p^\dagger U_D U_p|G\rangle$, which acts on $\mathcal{H}$ and exhibits $S_n \times SU(N)$ symmetry.

We now evaluate the eigenvalues $n_e^2(\tau,\vec{\lambda}) \equiv \left\langle\vec{\lambda}\right| \hat{n}_e^2(\tau) \left|\vec{\lambda}\right\rangle$ of $\hat{n}_e^2(\tau)$. We take abbreviations: $\mathfrak{c} \equiv \cos\frac{\beta}{2}$, $\mathfrak{s} \equiv \sin\frac{\beta}{2}$ and drop arrows on vectors and hats on operators. Expanding $U_p\,|G\rangle$ in the $|E\rangle$ basis,

$$\begin{aligned} n_e^2(\tau,\lambda) = \sum_{E',E\in\{0,1\}^n} & i^{|E'|-|E|}\mathfrak{c}^{2n-|E|-|E'|}\mathfrak{s}^{|E|+|E'|} \\ & \times \langle\lambda|\,\langle E'|\,U_D^\dagger n_e^2(\beta) U_D\,|E\rangle\,|\lambda\rangle\,, \end{aligned} \tag{2.19}$$

where $n_e^2(\beta) \equiv U_p n_e^2 U_p^\dagger$. Since $n_e^2(\beta) = (\sum_j \sigma_{ee}^j)^2$ is a sum of one- and two-atom operators, terms in which strings E and E' differ on more than two sites vanish.

Since the expectation of λ is permutation invariant, we can choose those two sites to be the last two without loss of generality. We also order the remaining $n-2$ entries of E and E',

$$n_e^2(\tau,\lambda) = \sum_{w=0}^{n-2} \binom{n-2}{w} \mathfrak{c}^{2(n-w)} \mathfrak{s}^{2w} \sum_{l_1,l_2,l_1',l_2' \in \{0,1\}} i^{l_1'+l_2'-l_1-l_2} \mathfrak{c}^{2(l_1-l_2-l_1'-l_2')} \mathfrak{s}^{l_1+l_2+l_1'+l_2'} \times \langle\lambda| \left\langle 0^{n-2-w}, 1^w, l_1', l_2' \right| U_D^\dagger n_e^2(\beta) U_D \left| 0^{n-2-w}, 1^w, l_1, l_2 \right\rangle |\lambda\rangle , \tag{2.20}$$

There are 2^4 cases for the different l values. We make critical use of the fact that $|E\rangle$ is an eigenstate of U_D with eigenvalue $e^{i\delta|E|\tau} \exp\left[-i\alpha \sum_{j<k\in E}(1-\hat{s}_{jk})\right]$, which is an operator acting on the nuclear spins.

In the four terms where $(l_1', l_2') = (l_1, l_2)$, the result has trivial action on the nuclear spin degrees

$$\left\langle 0^{n-2-w}, 1^w, l_1, l_2 \right| U_D^\dagger n_e^2(\beta) U_D \left| 0^{n-2-w}, 1^w, l_1, l_2 \right\rangle \tag{2.21}$$

$$= (n-w-l_1-l_2)\mathfrak{s}^2 + (w+l_1+l_2)\mathfrak{c}^2 \tag{2.22}$$

$$+ (n-w-l_1-l_2)(n-w-l_1-l_2-1)\mathfrak{s}^4 \tag{2.23}$$

$$+ (w+l_1+l_2)(w+l_1+l_2-1)\mathfrak{c}^4. \tag{2.24}$$

The remaining 12 terms can be split into four cases (up to complex conjugate). The first two cases have familiar forms,

$$\begin{aligned} &\left\langle 0^{n-2-w}, 1^w, 0, 0 \right| U_D^\dagger n_e^2(\beta) U_D \left| 0^{n-2-w}, 1^w, 0, 1 \right\rangle \\ &= -i\mathfrak{c}\mathfrak{s} e^{i\delta\tau} e^{i\alpha[(1-s_{n-1,n})+\sum_{j=1}^{n-2-w}(1-s_{jn})]} \left[1 + (n-w-1)\mathfrak{s}^2 + w\mathfrak{c}^2\right], \quad \text{and,} \end{aligned} \tag{2.25}$$

$$\begin{aligned} &\left\langle 0^{n-2-w}, 1^w, 1, 0 \right| U_D^\dagger n_e^2(\beta) U_D \left| 0^{n-2-w}, 1^w, 1, 1 \right\rangle \\ &= -i\mathfrak{c}\mathfrak{s} e^{i\delta\tau} e^{i\alpha\sum_{j=1}^{n-2-w}(1-s_{jn})} \left[1 + (n-w-2)\mathfrak{s}^2 + (w+1)\mathfrak{c}^2\right]. \end{aligned} \tag{2.26}$$

These can both be analyzed precisely as in the previous section. Next is

$$\begin{aligned} &\left\langle 0^{n-2-w}, 1^w, 0, 0 \right| U_D^\dagger n_e^2(\beta) U_D \left| 0^{n-2-w}, 1^w, 1, 1 \right\rangle \\ &= -2\mathfrak{s}^2\mathfrak{c}^2 e^{2i\delta\tau} e^{i\alpha[(1-s_{n-1,n})+\sum_{1\le j<k\le n-w-2}(1-s_{jk})+\sum_{j\le n-w-2}(1-s_{j,n-1})+\sum_{j\le n-w-2}(1-s_{jn})]} \\ &\quad \times e^{-i\alpha\sum_{1\le j<k\le n-w-2}(1-s_{jk})} \end{aligned} \tag{2.27}$$

$$= -2\mathfrak{s}^2\mathfrak{c}^2 e^{2i\delta\tau} \underbrace{e^{-i\alpha[-(1-s_{n-1,n})+\sum_{j=1}^{n-w-2}(s_{j,n-1}+s_{j,n})]}}_{\mathcal{C}_w} \tag{2.28}$$

To obtain the second equality, note that the second exponent commutes with each sum in the first exponent, implying that they can be combined. This operator can be attacked as in the previous section. We defer the evaluation of $\mathrm{tr}_\lambda[\mathcal{C}_w]$ for now, but it should clear that it can be approached in a similar way to $\mathrm{tr}_\lambda[\mathcal{B}_w]$.

The final (and most problematic) term to be analyzed is,

$$\begin{aligned}
&\left\langle 0^{n-2-w}, 1^w, 0, 1\right| U_D^\dagger n_e^2(\beta) U_D \left|0^{n-2-w}, 1^w, 1, 0\right\rangle \\
=&2\mathfrak{s}^2\mathfrak{c}^2 e^{i\alpha[\sum_{1\le j<k\le n-w-2}(1-s_{jk})+\sum_{j\le n-w-2}(1-s_{j,n-1})]} \\
&\times e^{-i\alpha[\sum_{1\le j<k\le n-w-2}(1-s_{jk})+\sum_{j\le n-w-2}(1-s_{j,n})]} \qquad (2.29)\\
=&2\mathfrak{s}^2\mathfrak{c}^2 e^{-i\alpha\sum_{j\le n-w-2} s_{j,n-1}} e^{i\alpha\sum_{j\le n-w-2} s_{j,n}} \qquad (2.30)\\
& \qquad (2.31)
\end{aligned}$$

Define $b_{n-1} := \sum_{j\le n-w-2} s_{j,n-1}$ and $b_n := \sum_{j\le n-w-2} s_{j,n}$. A barrier to proceed with an analysis of the previous form is that $[b_{n-1}, b_n] \neq 0$ preventing us from combining the exponents directly.

2.7 Experimental Considerations

In Chapter 1, we give details on how one could implement this core experimental system. Here we expand upon the major modifications to that set-up which is that here we assumed that only g-g interactions contribute, and that there are no e-g or e-e interactions.

This could in principle be enforced by using a weaker transverse trap for the excited electronic state than the ground electronic state. Alternatively, to avoid e-e collisions, instead of temporarily loosening the e trap during the dark time, one could keep both traps loose but temporarily tighten the g trap during the dark time. The latter approach allows one to minimize lossy e-e collisions during the counting of e atoms. We expect that the inclusion of nonzero elastic g-e interactions will modify the dynamics, but we expect that it would not change the fact that the Ramsey signal depends strongly on the spectrum of the nuclear spin density matrix, since the $S_n \times SU(N)$ symmetry of the dynamics would still hold.

An experimentally simpler approach is to use β sufficiently small as to make e-e interactions negligible; this will, however, decrease the signal requiring additional repetitions of the experiment and will require the inclusion of e-g collisions in our treatment.

2.8 Outlook

We have shown that alkaline-earth atoms can be used as a special-purpose quantum computer capable of performing the highly-entangled EYD measurement for spectrum estimation. It is possible that many other useful quantum information tasks can be accessed in similar systems with special symmetry properties. In particular, an important extension of our work would be to find an efficient implementation of full-state tomography in current experimental systems. On the other hand, it would also be interesting to know if one can improve on our proposal if one seeks to measure a simpler quantity than the full spectrum O'Donnell and Wright, 2015, such as the purity.

We thank S. P. Jordan, J. Preskill, K. R. A. Hazzard, M. Foss-Feig, P. Richerme, M. Maghrebi,... for discussions. This work was supported by NSF IQIM-PFC-1125565, NSF JQI-PFC-0822671, NSF JQI-PFC-1430094, NSF JILA-PFC-1125844, NSF-PIF, NIST, ARO, ARL, ARO-DARPA-OLE, AFOSR, AFOSR MURI, and the Lee A. DuBridge and Gordon and Betty Moore foundations. MEB and AVG acknowledge the Centro de Ciencias de Benasque Pedro Pascual for hospitality. JH is supported by Pappalardo Fellowship in Physics at MIT.

Part II

Scalable quantum computers

Chapter 3

GATES FOR TOPOLOGICAL QUANTUM ERROR CORRECTING CODES

We study restrictions on locality-preserving unitary logical gates for topological quantum codes in two spatial dimensions. A locality-preserving operation is one which maps local operators to local operators — for example, a constant-depth quantum circuit of geometrically local gates, or evolution for a constant time governed by a geometrically-local bounded-strength Hamiltonian. Locality-preserving logical gates of topological codes are intrinsically fault tolerant because spatially localized errors remain localized, and hence sufficiently dilute errors remain correctable. By invoking general properties of two-dimensional topological field theories, we find that the locality-preserving logical gates are severely limited for codes which admit non-abelian anyons; in particular, there are no locality-preserving logical gates on the torus or the sphere with M punctures if the braiding of anyons is computationally universal. Furthermore, for Ising anyons on the M-punctured sphere, locality-preserving gates must be elements of the logical Pauli group. We derive these results by relating logical gates of a topological code to automorphisms of the Verlinde algebra of the corresponding anyon model, and by requiring the logical gates to be compatible with basis changes in the logical Hilbert space arising from local F-moves and the mapping class group.

3.1 Introduction

In order to reliably compute, it is necessary to protect information against noise. For quantum computations, this is particularly challenging because noise in the form of decoherence threatens the very quantum nature of the process. Adding redundancy by encoding information into a quantum error-correcting code is a natural, conceptually appealing approach towards building noise-resilient scalable computers based on imperfect hardware.

Among the known quantum error-correcting codes, the class of so-called topological codes stands out. Examples in 2D include the toric code and quantum double models A. Y. Kitaev, 2003, the surface codes S. Bravyi and A. Y. Kitaev, 1998, the 2D color codes H. Bombin and M. Martin-Delgado, 2006, variants of these codes H. Bombin, 2010; A. G. Fowler, A. M. Stephens, and Groszkowski, 2009, and the

Levin-Wen model Levin and X.-G. Wen, 2005. In 3D, known examples are Bombin and Martin-Delgado's 3D color code H. Bombin and M.A. Martin-Delgado, 2007, as well as Haah's Haah, 2011 and Michnicki's Michnicki, 2012 models. These codes are attractive for a number of reasons: their code space is topologically protected, meaning that small local deformations or locally acting noise do not affect encoded information. The degree of this protection (measured in information-theoretic notions in terms of code distance, and manifesting itself in physical properties such as gap stability) scales with the system size: in other words, robustness essentially reduces to the question of scalability. Finally, the code space of a topological code is the degenerate ground space of a geometrically local Hamiltonian: this means that syndrome information can be extracted by local measurements, an important feature for actual realizations. Furthermore, this implies that a topological code is essentially a phase of a many-body system and can be characterized in terms of its particle content, their statistics, and the quantum field theory emerging in the continuum limit. In particular, the quantum field theory provides a description of such systems which captures all universal features, independently of microscopic details.

While quantum error-correcting codes can provide the necessary protection of information against noise, a further requirement for quantum computation is the ability to execute gates in a robust manner. Again, topological codes stand out: they usually provide certain intrinsic mechanisms for executing gates in a robust way. More precisely, there are sequences of local code deformations, under which the information stays encoded in a code with macroscopic distance, but undergoes some unitary transformation. In principle, this provides a robust implementation of computations by sequences of local, and hence, potentially experimentally realizable actions. In the case of $2D$-topological codes described by topological quantum field theories, this corresponds to adiabatic movement (braiding) of quasi-particle excitations (also called anyons).

Unfortunately, as is well known, braiding (by which we mean the movement either around each other or more generally around non-trivial loops) of anyons does not always give rise to a universal gate set. Rather, the set of gates is model-dependent: braiding of $D(\mathbb{Z}_2)$-anyons generates only global phases on the sphere, and elements of the Pauli group on non-zero genus surfaces. Braiding of Ising anyons gives Clifford gates, whereas braiding of Fibonacci anyons generates a dense subgroup of the set of unitaries (and is therefore universal within suitable subspaces of the

code space). In other words, braiding alone, without additional tricks such as magic state distillation Sergey Bravyi and Alexei Kitaev, 2005 (which has a large overhead Austin G Fowler et al., 2012), is not in general sufficient to provide universal fault-tolerant computation; unfortunately, the known systems with universal braiding behavior are of a rather complex nature, requiring e.g., 12-body interactions among spins Levin and X.-G. Wen, 2005. Even ignoring the question of universality, the use of braiding has some potentially significant drawbacks: in general (for non-abelian anyons), it requires an amount of time which scales with the system size (or code distance) to execute a single logical gate. (Mathematically, this is reflected by the fact that string-operators cannot be implemented in constant depth for general non-abelian anyon models – in contrast to e.g., the toric code[1].) This implies that error-correction steps will be necessary even during the execution of such a gate (see e.g., Pedrocchi and DiVincenzo, 2015; Hutter and Wootton, 2015; Burton, Brell, and Flammia, 2015; Brell et al., 2014 for a recent discussion of the robustness of braiding). This may pose an additional technological challenge, for example, if the intermediate topologies are different.

Given the limitations of braiding, it is natural to look for other mechanisms for implementing robust gates in topological codes. For stabilizer quantum codes, the notion of transversal gates has traditionally been used almost synonymously with fault-tolerant gates: their key feature is the fact that they do not propagate physical errors. More generally, for topological stabilizer codes, we can consider logical gates implementable by constant-depth quantum circuits as a proxy for robust gates: they can increase the weight of a physical error only by a constant, and are thus sufficiently robust when combined with suitable error-correction gadgets. Note that finite-depth local circuits represent a much broader class than transversal gates.

Gate restrictions on transversal, as well as constant-depth local circuits have been obtained for stabilizer and more general codes. Eastin and Knill Eastin and Knill, 2009 argued that for any code protected against local errors, transversal gates can only generate a finite group and therefore do not provide universality. Bravyi and König Sergey Bravyi and König, 2013 consider the group of logical gates that may be implemented by such constant-depth local circuits on geometrically local topological stabilizer codes. They found that such gates are contained in $\mathcal{P}_D$, the D-th level of the Clifford hierarchy, where D is the spatial dimension in which the

[1] In the language of this paper, braiding/mapping class group elements belong to locality-preserving unitaries if the model is abelian. However, for a general non-abelian model, braiding is not locality-preserving according to our definition.

stabilizer code is geometrically local.

In this work, we characterize the set of gates implementable by a locality-preserving unitary in a system described by a 2D TQFT. By doing so, we both specialize and generalize the results of Sergey Bravyi and König, 2013: we restrict our attention to dimension 2, but go beyond the set of local stabilizer codes in two significant ways.

First, we obtain statements which are independent of the particular realization (e.g., the toric code model) but are instead phrased in terms of the TQFT (i.e., the anyon model describing the system). In this way, we obtain a characterization which holds for a gapped phase of matter, rather than just for a particular code representing that phase. On a conceptual level, this is similar in spirit to the work of Else et al., 2012, where statements on the computational power for measurement-based quantum computation were obtained that hold throughout a certain phase. Here we use the term phase loosely – we say that two systems are in the same phase if they have the same particle content. To avoid having to make any direct reference to an underlying lattice model, we replace the notion of a constant-depth local circuit by the more general notion of a locality-preserving unitary: this is a unitary operation which maps local operators to local ones.

Second, our results and techniques also apply to non-abelian anyon models (whereas stabilizer codes only realize certain abelian models, unless e.g., domain walls or 'twists' are added H. Bombin, 2010 that break homogeneity). In particular, we obtain statements that can be applied, e.g., to the Levin-Wen models Levin and X.-G. Wen, 2005, as well as chiral phases. For such systems, restrictions on protected gates were previously not known. Again, knowledge of the underlying microscopic model is unnecessary to apply our results, which only depend on the type of anyons present in the system. Our approach relates locality-preserving unitaries to certain symmetries of the underlying anyon model; this imposes constraints on the allowed operations. We consider the Fibonacci and Ising models as paradigmatic examples and find that there are no non-trivial gates in the former, and only Pauli operations in the latter case. Our focus on these anyons models is for concreteness only, but our methods and conclusions apply more generally. Some of our more general conclusions are that

(i) protected gates generically (see Section 3.4 discussing the necessity of certain technical assumptions) form only a finite group and

(ii) when the representation of the mapping class group is computationally universal (i.e., forms a dense subgroup), then there are no non-trivial protected gates.

Our observations are summarized in Table 3.1. According to our results, the class of locality-preserving unitaries (which is distinguished from the point of view of error correction) is too restricted and needs to be supplemented with alternative mechanisms to achieve universality.

Model	mapping class group contained in	locality-preserving unitaries contained in
$D(\mathbb{Z}_2)$	Pauli group	restricted Clifford group
abelian anyon model	generalized Pauli group	generalized Clifford group
Fibonacci model	universal	global phase (trivial)
general anyon model	universal	global phase (trivial)
Ising model	Clifford group	Pauli group
generic anyon model	model-dependent	finite group

Table 3.1: We study different anyon models (first column). The second column describes the properties of the unitary group generated by the (projective) representation of the mapping class group (see Section 3.2) – this corresponds to braiding for punctured spheres. The third column characterizes the set of protected gates. Our results suggest a trade-off between the computational power of the mapping class group representation and that of gates implementable by locality-preserving unitaries.

Finally, let us comment on limitations, as well as open problems arising from our work. The first and most obvious one is the dimensionality of the systems under consideration: our methods apply only to $2D$ TQFTs. The mathematics of higher-dimensional TQFTs is less developed, and currently an active research area (see e.g., Kong and X.-G. Wen, 2014). While the techniques of Sergey Bravyi and König, 2013, which have recently been significantly strengthened by Pastawski and Yoshida F. Pastawski and B. Yoshida, 2014, also apply to higher-dimensional codes (such as Haah's), they are restricted to the stabilizer formalism (but importantly, F. Pastawski and B. Yoshida, 2014 also obtain statements for subsystem codes). Obtaining non-abelian analogues of our results in higher dimensions appears to be a challenging research problem. A full characterization of the case $D = 3$ is particularly desirable from a technological viewpoint.

Even in $2D$, there are obvious limitations of our results: the systems we consider are essentially "homogenous" lattices with anyonic excitations in the bulk. We are not considering defect lines, or condensation of anyons at boundaries; for example, our discussion excludes the quantum double models constructed in Beigi, P. W. Shor, and Whalen, 2011, which have domain walls constructed from condensation at boundaries using the folding trick. Again, we expect that obtaining statements on protected gates for these models requires additional technology in the form of more refined categorical notions, as discussed by Kitaev and Kong A. Y. Kitaev and Kong, 2012. Also, although we identify possible locality preserving logical unitaries, our arguments do not show that these can necessarily be realized, either in general TQFTs or in specific models that realize TQFTs. Lastly, our work is based on the (physically motivated) assumption that a TQFT description is possible and the underlying data is given. For a concrete lattice model of interacting spins, the problem of identifying this description (or associated invariants A. Kitaev and J. Preskill, 2006; Levin and X.-G. Wen, 2006; Haah, 2014), as well as constructing the relevant string-operators (as has been done for quantum double models A. Y. Kitaev, 2003; H. Bombin and M. A. Martin-Delgado, 2008 as well as the Levin-Wen models Levin and X.-G. Wen, 2005), is a problem in its own right.

Rough statement of problem

Our results concern families of systems defined on any 2-dimensional orientable manifold (surface) Σ, which we will take to be closed unless otherwise stated. Typically, such a family is defined in terms of some local physical degrees of freedom (spins) associated with sites of a lattice embedded in Σ. We refer to the joint Hilbert space $\mathcal{H}_{\text{phys},\Sigma}$ of these spins as the 'physical' Hilbert space. The Hamiltonian H_Σ on $\mathcal{H}_{\text{phys},\Sigma}$ is local, i.e., it consists only of interactions between "neighbors" within constant-diameter regions on the lattice. More generally, assuming a suitable metric on Σ is chosen, we may define locality in terms of the distance measure on Σ.

We are interested in the ground space $\mathcal{H}_\Sigma$ of H_Σ. For a topologically ordered system, this ground space is degenerate with dimension growing exponentially with the genus of Σ, and is therefore suitable for storing and manipulating quantum information. We will give a detailed description of this space below (see Section 3.2); it has a preferred basis consisting of labelings associated with some set $\mathbb{A}$. This is a finite set characterizing all distinct types of anyonic quasiparticle excitations of H_Σ in the relevant low energy sector of $\mathcal{H}_{\text{phys},\Sigma}$.

Importantly, the form of $\mathcal{H}_\Sigma$ is independent of the microscopic details (in the definition of H_Σ): it is fully determined by the associated TQFT. In mathematical terms, it can be described in terms of the data of a modular tensor category, which also describes fusion, braiding and twists of the anyons. We will refer to $\mathcal{H}_\Sigma$ as the TQFT Hilbert space.

The significance of $\mathcal{H}_\Sigma$ is that it is protected: local observables can not distinguish between states belonging to $\mathcal{H}_\Sigma$. This implies that $\mathcal{H}_\Sigma$ is an error-correcting code with the property that local regions are correctable: any operator supported in a small region which preserves the code space must act trivially on it (otherwise it could be used to distinguish between ground states).

To compute fault-tolerantly, one would like to operate on information encoded in the code space $\mathcal{H}_\Sigma$ by acting with a unitary $U : \mathcal{H}_{\text{phys},\Sigma} \to \mathcal{H}_{\text{phys},\Sigma}$ on the physical degrees of freedom[2]. There are a number of features that are desirable for such a unitary to be useful – physical realizability being an obvious one. For fault-tolerance, two conditions are particularly natural:

(i) the unitary U should preserve the code space, $U\mathcal{H}_\Sigma = \mathcal{H}_\Sigma$ so that the information stays encoded. We call a unitary U with this property an automorphism of the code and denote its restriction to $\mathcal{H}_\Sigma$ by $[U] : \mathcal{H}_\Sigma \to \mathcal{H}_\Sigma$. The action $[U]$ defines the logical operation or gate that U realizes.

(ii) typical errors should remain correctable under the application of the unitary U. In the context of topological codes, which correct sufficiently local errors, and where a local error model is usually assumed, this condition is satisfied if U does not significantly change the locality properties of an operator: if an operator X has support on a region $\mathcal{R} \subset \Sigma$, then the support of $UXU^\dagger$ is contained within a constant-size neighborhood of $\mathcal{R}$. We call such a unitary a locality-preserving unitary.

We call a unitary U satisfying (i) and (ii) a locality-preserving unitary automorphism of the code (or simply a topologically protected gate). Our goal is to characterize

[2] In principle, we could consider unitaries/isometries (or sequences thereof) of the form $U : \mathcal{H}_{\text{phys},\Sigma} \to \mathcal{H}'_{\text{phys},\Sigma'}$ which map between *different* systems $\mathcal{H}_{\text{phys},\Sigma}$ and $\mathcal{H}'_{\text{phys},\Sigma'}$. By a slight modification of the arguments here, we could then obtain restrictions on locality-preserving isomorphisms (instead of automorphisms, cf. Section 3.3). Such a scenario was discussed in Sergey Bravyi and König, 2013 in the context of stabilizer codes. Here we restrict to the case where the systems (and associated ground spaces) are identical for simplicity, since the main conclusions are identical.

the set of logical operations that have the form $[U]$ for some locality-preserving[3] unitary automorphism U. For example, if $\mathcal{H}_\Sigma$ is a topologically ordered subspace of $\mathcal{H}_{\text{phys},\Sigma}$, the Hilbert space of a spin lattice, then (ii) is satisfied if U is a constant-depth local circuit. Another important example is the constant-time evolution $U = \mathcal{T}\exp[-i\int dt H(t)]$ of a system through a bounded-strength geometrically-local Hamiltonian $H(t)$. Here, Lieb-Robinson bounds Lieb and Robinson, 1972; S. Bravyi, Hastings, and Verstraete, 2006 provide quantitative statements on how the resulting unitary may be exponentially well approximated by a locality-preserving unitary. This is relevant since it describes the time evolution of a physical system and can also be used to model adiabatic transformations of the Hamiltonian Chen, Gu, and Xiao-Gang Wen, 2010.

From a computational point of view, the group

$$\langle \{[U] \mid U \text{ locality-preserving unitary automorphism}\} \rangle$$

generated by such gates is of particular interest: it determines the computational power of gates that are implementable fault-tolerantly with locality preserving automorphisms.

Outline

In Section 3.2, we provide a brief introduction to the relevant concepts of TQFTs. We then derive our main results on the characterization of protected gates in Section 3.3. Further restrictions on the allowed protected gates are provided in Sections 3.4 and 3.5. In Section 3.6, we apply our results to particular models, deriving in particular our characterizations for Ising and Fibonacci anyons. Finally, in Section 3.7 we use additional properties of abelian models to show that their protected gates must be contained within a proper subgroup of the generalized Clifford group, which is similar to the result of Sergey Bravyi and König, 2013, but goes further.

[3] As a side remark, we mention that our terminology is chosen with spin lattices in mind. However, the notion of locality-preservation can be relaxed. As will become obvious below, our results apply more generally to the set of *homology-preserving* automorphisms U. The latter can be defined as follows: if the support of an operator X is contained in a region $\mathcal{R} \subset \Sigma$ which deformation retracts to a closed curve C, then the support of $UXU^\dagger$ must be contained in a region $\mathcal{R}' \subset \Sigma$ which deformation retracts to a curve C' in the same homology class as C. For example, for a translation-invariant system, translating by a possibly extensive amount realizes such a homology-preserving (but not locality-preserving) automorphism.

3.2 TQFTs: background

In this section, we provide the necessary background on topological quantum field theories (TQFTs). Our discussion will be rather brief; for a more detailed discussion of topological quantum computation and anyons, we refer to J. Preskill, 2004. Following Witten's work Witten, 1989, TQFTs have been axiomatized by Atiyah Atiyah, 1989 based on Segal's work Segal, 2004 on conformal field theories. Moore and Seiberg Moore and Seiberg, 1998 derived the relations satisfied by the basic algebraic data of such theories (or more precisely, a modular functor). Here we borrow some of the terminology developed in full generality by Walker K., 1991 (see also M. H. Freedman, A. Y. Kitaev, and Z. Wang, 2002). For a thorough treatment of the category-theoretic concepts, we recommend the appendix of A. Y. Kitaev, 2006.

Our focus is on the Hilbert space $\mathcal{H}_\Sigma$ spanned by the vacuum states of a TQFT defined on the orientable surface Σ. Recall that this is generally a subspace $\mathcal{H}_\Sigma \subset \mathcal{H}_{\text{phys},\Sigma}$ of a Hilbert space of physical degrees of freedom. The TQFT is specified by a finite set of anyon labels $\mathbb{A} = \{1, a, b, c \dots\}$, their *fusion rules* (described using a non-negative integer N_{ab}^c for each triple of anyons a, b, c, called fusion multiplicities), along with S, F, R and T matrices (complex valued matrices with columns and rows indexed by anyon labels). If the TQFT arises from taking continuous limits of a local Hamiltonian model such as the toric code, the anyons are simply the elementary excitations of the model, and the fusion rules and matrices can be understood in terms of creating, combining, moving and annihilating anyons in the surface. The anyon set must contain a trivial particle $1 \in \mathbb{A}$ such that when combined with any particle, the latter remains unchanged $N_{a1}^c = N_{1a}^c = \delta_a^c$, and each particle $a \in \mathbb{A}$ must have an antiparticle $\overline{a} \in \mathbb{A}$ such that $N_{a\overline{a}}^1 \neq 0$. We will restrict our attention to models where $N_{ab}^c \in \{0, 1\}$ for all $a, b, c \in \mathbb{A}$ for simplicity (our results generalize with only minor modifications).

String-like operators and relations

We are interested in the algebra $\mathcal{A}_\Sigma$ of operators $X : \mathcal{H}_{\text{phys},\Sigma} \to \mathcal{H}_{\text{phys},\Sigma}$ which preserve the subspace $\mathcal{H}_\Sigma$. We call such an element $X \in \mathcal{A}_\Sigma$ an automorphism and denote by $[X] : \mathcal{H}_\Sigma \to \mathcal{H}_\Sigma$ the restriction to $\mathcal{H}_\Sigma$. We call X a representative (or realization) of $[X]$. Operators of the form $[X]$, where $X \in \mathcal{A}_\Sigma$, define an associative $*$-algebra $[\mathcal{A}_\Sigma]$ with unit and multiplication $[X][Y] = [XY]$. The unit element in $[\mathcal{A}_\Sigma]$ is represented by the identity operator id on the whole space $\mathcal{H}_{\text{phys},\Sigma}$.

Our constraints on protected gates are derived by studying how they transform certain operators acting on $\mathcal{H}_{phys,\Sigma}$ (see Fig. 3.1). To define the latter, fix a simple closed curve $C : [0,1] \to \Sigma$ on the surface and an "anyon label" $a \in \mathbb{A}$. (The set of labels $\mathbb{A}$ is determined by the underlying model.) Then there is a "string-operator" $F_a(C)$ acting on $\mathcal{H}_{\text{phys},\Sigma}$, supported in a constant-diameter neighborhood of C. It corresponds to the process of creating a particle-antiparticle-pair $(a, \overline{a})$, moving a along C, and subsequently fusing to the vacuum. The last step in this process involves projection onto the ground space, which is not trivial in general: the operator $F_a(C)$ can involve post-selection, in which case it is a non-unitary element of $\mathcal{A}_\Sigma$.

The operators $\{F_a(C)\}_{a\in\mathbb{A}}$ form a closed subalgebra $\mathcal{A}(C) \subset \mathcal{A}_\Sigma$: they preserve the ground space and satisfy

$$\begin{aligned} F_a(C)F_b(C) &= \sum_n N_{ab}^n F_n(C) \,, \\ F_a(C)^\dagger &= F_{\overline{a}}(C) \\ F_1(C) &= \mathrm{id}_{\mathcal{H}_{\text{phys}}} \end{aligned} \tag{3.1}$$

for the fusion multiplicities N_{ab}^n (see Section 3.2). In addition, reversing the direction of C, i.e., considering $C^{-1}(t) \equiv C(1-t)$, is equivalent to exchanging the particle with its antiparticle, i.e.,

$$F_a(C^{-1}) = F_{\overline{a}}(C) \,. \tag{3.2}$$

Here $a \mapsto \overline{a}$ is an involution on the set of particle labels $\mathbb{A}$, again defined by the underlying model. Properties (3.1) and (3.2) of the string-operators can be shown in the diagrammatic formalism mentioned below (but this is not needed here; we will use them as axioms).

We denote the restriction of $F_a(C)$ to the code space $\mathcal{H}_\Sigma$ by $[F_a(C)]$. Note that, while $[F_a(C)]$ is unitary in abelian anyon models, this is not the case in general.

Example 3.1 ($D(G)$ and Kitaev's toric code)**.** As an example, consider a model described by the quantum double $D(G)$ of a finite group G, for which Kitaev has constructed a lattice model A. Y. Kitaev, 2003. In the case where G is abelian, we have $D(G) \cong G \times G$, i.e., the particles and fusion rules are simply given by the product group $\mathbb{A} = G \times G$.

Specializing to $G = \mathbb{Z}_2$ gives the particles commonly denoted by $1 = (0,0)$ (vacuum), $m = (1,0)$, $e = (0,1)$ and $\epsilon = m \times e = (1,1)$. For the toric code

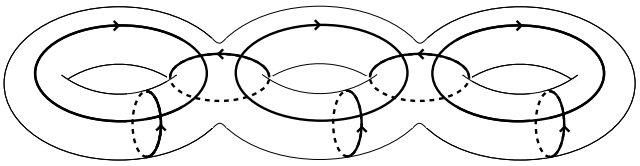

Figure 3.1: Closed 2-manifolds are characterized by their genus g. The figure illustrates the 3-handled torus Σ_g corresponding to $g = 3$. A canonical set of $3g - 1$ generators of the mapping class group of the surface Σ_g can be specified in terms of a set $\mathcal{G} = \{C_j\}_{j=1}^{3g-1}$ of loops (each associated with a Dehn twist). Dragging an anyon a around such loop $C : [0, 1] \to \Sigma_g$ and fusing to the vacuum implements an undetectable operator $F_a(C)$; homologically non-trivial loops realize logical operations. The full algebra of logical operators is generated by the set of operators $\{F_a(C)\}_{a\in\mathbb{A},C\in\mathcal{G}}$. However, these operators are generally not independent.

model, the associated ribbon operators are

$$F_1(C) = \mathrm{id} \quad F_e(C) = \bar{X}(C) \quad F_m(C) = \bar{Z}(C) \quad F_\epsilon(C) = \bar{X}(C)\bar{Z}(C)\,,$$

where $\bar{X}(C) = \otimes_{j\in\partial_+ C} X_j$ and $\bar{Z}(C) = \otimes_{j\in\partial_- C} Z_j$ are appropriate tensor products of Pauli-X and Pauli-Z-operators along C (as specified in A. Y. Kitaev, 2003).

Specializing to $G = \mathbb{Z}_N$, with $\omega_N = \exp(2\pi i/N)$ and generalized N-dit Pauli operators X and Z (and their inverses), defined by their action

$$X\,|j\rangle = |j + 1 \mod N\rangle \qquad Z\,|j\rangle = \omega_N^j\,|j\rangle$$

on computational basis states $\{|j\rangle\}_{j=0,\ldots,N-1}$, we can consider such a model (the $\mathbb{Z}_N$-toric code) with generalized ribbon operators. Here

$$F_{(a,a')}(C) = \bar{X}(C)^a \bar{Z}(C)^{a'},$$

where $\bar{X}(C)$ is a tensor product of Pauli-X and its inverse depending on the orientation of the underlying lattice, and similarly for $\bar{Z}(C)$.

It is easy to check that operators associated with the same loop commute, i.e.,

$$[F_{(a,a')}(C), F_{(b,b')}(C)] = 0\,, \tag{3.3}$$

and since $Z^a X^b = \omega_N^{ab} X^b Z^a$, we get the commutation relation

$$F_{(a,a')}(C_1)F_{(b,b')}(C_2) = \omega_N^{ab'-a'b} F_{(b,b')}(C_2)F_{(a,a')}(C_1) \tag{3.4}$$

for any two strings C_1, C_2 intersecting once.

Returning to the general case, the algebra of string operators does not necessarily satisfy relations as simple as (3.3) and (3.4). Nevertheless, some essential features hold under very general assumptions. We express these as postulates; they can be seen as a subset of the isotopy-invariant calculus of labeled ribbon graphs associated with the underlying category (see e.g., M. Freedman et al., 2008 for a discussion of the latter). That is, the properties expressed by our postulates are a subset of the axioms formalizing TQFTs, and serve to capture the essential features in an algebraic manner. For particular systems (such as the toric code or the quantum double models), these postulates can be rigorously established (see A. Y. Kitaev, 2003; H. Bombin and M. A. Martin-Delgado, 2008), whereas in other cases, only partial results are known (see e.g., the discussion in Z. Wang, 2010, p. 107) but they are conjectured to hold. We sidestep the independent important and challenging problem of rigorously establishing these postulates, and instead derive some consequences. Throughout our work, we hence assume that the models under consideration satisfy our postulates.

Postulate 3.1 (Completeness of string-operators)**.** Consider an operator U with support in some region $\mathcal{R}$ which preserves the code space $\mathcal{H}_\Sigma$. Then its action on the code space is equivalent to that of a linear combination of products of operators of the form $F_a(C)$, for a closed loop $C : [0,1] \to \mathcal{R}$ which is supported in $\mathcal{R}$. That is, we have

$$[U] = \sum_j \beta_j \prod_k [F_{a_{j,k}}(C_{j,k})] \,.$$

This postulate essentially means that, as far as the logical action is concerned, we may think of $[U]$ as a linear combination of products of closed-loop string operators. Such products $F_{a_m}(C_m) \cdots F_{a_1}(C_1)$ can conveniently be thought of as 'labeled' loop gases embedded in the three-manifold $\Sigma \times [0,1]$, where, for some $0 < t_1 < \cdots < t_m < 1$, the operator $F_{a_j}(C_j)$ is applied at 'time' t_j (and hence a labeled loop is embedded in the slice $\Sigma \times \{t_j\}$). Diagrammatically, one represents such a product by the projection onto Σ with crossings representing temporal order, as in

$F_{a_2}(C_2)F_{a_1}(C_1) \quad =$ 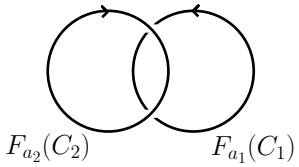

(3.5)

One may manipulate every term in a linear combination representing U without changing the logical action according to certain local 'moves'; in particular, the

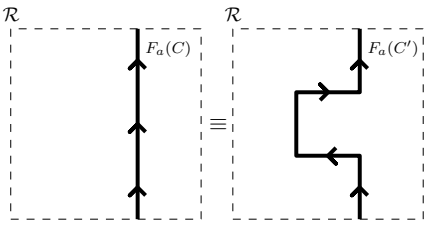

Figure 3.2: The content of Postulate 3.2: We can deform a line without changing the logical action of the string-operator.

order of application of these moves is irrelevant (a fact formalized by MacLane's theorem Lane, 1998).

For our purposes, we only require the following 'local' moves, which relate two products U and U' of string-operators given by diagrams such as (3.5). More generally, they may be applied term-by-term to any linear combination if each term contains the same local sub-diagram.

Postulate 3.2 (String deformation (see Fig. 3.2))**.** Suppose operators $U, U' \in \mathcal{A}_\Sigma$ are identical on the complement of some region $\mathcal{R}$. Assume further that inside $\mathcal{R}$, both U and U' contain a single string describing the dragging of the same anyon type along a path C and C', respectively, where C' can be locally deformed into C. Then the logical action of U and U' must be equivalent: $[U] = e^{i\theta}[U']$ for some unimportant phase $e^{i\theta}$ (Fig. 3.2).

In particular, this postulate implies that if C and C' are two closed homologically equivalent loops and a is an arbitrary anyon label, then the operators $F_a(C)$ and $F_a(C')$ realized by "dragging" the specified anyon along C and C' respectively have equivalent logical action on the code space, $[F_a(C)] = e^{i\theta}[F_a(C')]$.

The next postulate involves local operators, and essentially states that the space $\mathcal{H}_\Sigma$ is a quantum error-correcting code protecting against local errors. While we may state it in a form only referring to local operators, we will find it more intuitive to combine it with the deformation postulate: this extends correctability from small regions to contractible loops (i.e., loops that are homotopic to a point).

Postulate 3.3 (Error correction postulate)**.** If C is a contractible loop, then for each $a \in \mathbb{A}$, the operator $F_a(C)$ has trivial action on the space $\mathcal{H}_\Sigma$ up to a global

constant d_a, that is,

$$[F_a(C)] = d_a \mathrm{id}_{\mathcal{H}_\Sigma} \ . \tag{3.6}$$

This postulate essentially means that we may remove certain closed loops from diagrams such as (3.5).

An immediate consequence of these postulates is the following statement.

Proposition 3.2.1 (Local completeness of string operators)**.** Consider an operator $O \in \mathcal{A}_\Sigma$ whose support is contained within a constant-diameter neighborhood of a simple loop C. Then $[O] = [\tilde{X}]$ for some $\tilde{X} \in \mathcal{A}(C)$. In other words, the logical action of O is identical to that of a linear combination of string-operators $F_a(C)$.

This proposition can be seen as a consequence of the completeness condition for strings (Postulate 3.1), the string deformation Postulate 3.2 and (3.1). A similar argument leads us to the following conclusion.

Proposition 3.2.2 (Global completeness of few homology classes)**.** The full logical algebra $[\mathcal{A}_\Sigma]$ is generated by the logical algebras $[\mathcal{A}(C)]$ associated with a finite number of inequivalent non-contractible simple loops C.

Proof. That the algebra $[\mathcal{A}_\Sigma]$ is finite-dimensional can be seen from the finite dimensionality of the code space $\mathcal{H}_\Sigma$. By Postulate 3.1, the algebra $[\mathcal{A}_\Sigma]$ is generated by $\{\mathcal{A}(C)\}_C$. Let us start from a trivial algebra and build up $[\mathcal{A}_\Sigma]$ from a finite number of loops. As long as the algebra is not complete, we may include additional loops C such that $[\mathcal{A}(C)]$ is not included in the partially generated algebra. Such a loop C must be inequivalent to the previously included loops due to Postulate 3.2. After a number of steps no greater than the square of the ground space dimension, we will have constructed the complete algebra. □

Therefore there exists a finite, *minimal* set of loops which is sufficient to span $[\mathcal{A}_\Sigma]$.

The Verlinde algebra

It is convenient to formally introduce some algebraic data defined by the underlying anyon model. We will return to the discussion of string-operators in the next section and relate them to this algebraic language.

As before, let $\mathbb{A}$ be the set of particle labels (generally a finite set), and let $a \mapsto \overline{a}$ be the involution giving the antiparticle associated with particle a. The *fusion rules*

of the model are encoded in integers N_{ab}^c, which are called fusion multiplicites. We will restrict our attention to models where $N_{ab}^c \in \{0,1\}$ for all $a,b,c \in \mathbb{A}$ for simplicity (our results generalize with only minor modifications).

The *Verlinde algebra* Ver is the commutative associative $*$-algebra spanned by elements $\{\mathbf{f}_a\}_{a\in\mathbb{A}}$ satisfying the relations

$$\mathbf{f}_a\mathbf{f}_b = \sum_c N_{ab}^c \mathbf{f}_c \qquad \text{and} \qquad \mathbf{f}_a^\dagger = \mathbf{f}_{\overline{a}} \,. \tag{3.7}$$

Note that $\mathbf{f}_1 = \mathrm{id}$ is the identity element because the numbers $\{N_{ab}^c\}$ satisfy $N_{a1}^c = N_{1a}^c = \delta_{ac}$.

Since every anyon model is braided by definition, one indeed has $N_{ab}^c = N_{ba}^c$ and the algebra Ver is a finite-dimensional commutative C^*-algebra. Therefore $\mathsf{Ver} \cong \mathbb{C}^{\oplus(\dim \mathsf{Ver})}$ is a direct sum of copies of $\mathbb{C}$. The fusion multiplicity N_{ab}^c may also be written in terms of the modular S-matrix, whose matrix elements are, in the diagrammatic calculus, given by the Hopf link and the total quantum dimension $\mathcal{D}$ by

$S_{ab} = \frac{1}{\mathcal{D}}$ 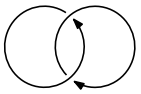 .

We consider (and restrict our attention to) the case where the S-matrix is unitary: here the isomorphism $\mathsf{Ver} \cong \mathbb{C}^{\oplus(\dim \mathsf{Ver})}$ can be made explicit thanks to the *Verlinde formula* Verlinde, 1988

$$N_{ab}^c = \sum_x \frac{S_{ax}S_{bx}S_{\overline{c}x}}{S_{1x}} \,, \tag{3.8}$$

as the proof of the following Proposition 3.2.3 shows. (Note that $S_{1x} = d_x/\mathcal{D}$ where $\mathcal{D} = \sqrt{\sum_a d_a^2}$.) For this purpose, we define the elements

$$\mathbf{p}_a = S_{1a} \sum_b \overline{S_{ba}} \mathbf{f}_b \qquad \text{for all } a \in \mathbb{A} \,. \tag{3.9}$$

This relation can be inverted by making use of unitarity of the S-matrix

$$\mathbf{f}_b = \sum_a \frac{S_{ba}}{S_{1a}} \mathbf{p}_a \qquad \text{for all } a \in \mathbb{A} \,. \tag{3.10}$$

The main statement we use is the following:

Proposition 3.2.3 (Primitive idempotents)**.** The elements $\{\mathbf{p}_a\}_{a\in\mathbb{A}}$ are the unique complete set of orthogonal minimal idempotents spanning the Verlinde algebra,

$$\mathsf{Ver} = \bigoplus_a \mathbb{C}\mathbf{p}_a \,. \tag{3.11}$$

Furthermore, they satisfy

$$\sum_a \mathbf{p}_a = \mathbf{f}_1 = \mathrm{id}\ . \tag{3.12}$$

Proof. That $\{\mathbf{p}_a\}_{a\in\mathbb{A}}$ span the algebra Ver is evident from the fact that $\{\mathbf{f}_a\}_{a\in\mathbb{A}}$ span the algebra, and each $\mathbf{f}_a$ can be written in terms of $\{\mathbf{p}_a\}_{a\in\mathbb{A}}$ via Eq. (3.10). To show they are orthogonal idempotents $\mathbf{p}_a\mathbf{p}_b = \delta_{a,b}\mathbf{p}_a$, first note that

$$\begin{aligned}
\mathbf{p}_a\mathbf{p}_b &= S_{1a}S_{1b}\sum_{g,h}\overline{S_{ga}S_{hb}}\mathbf{f}_g\mathbf{f}_h \\
&= S_{1a}S_{1b}\sum_{g,h,j}\overline{S_{ga}S_{hb}}N_{gh}^{j}\mathbf{f}_j \\
&= S_{1a}S_{1b}\sum_{g,h,j,x}\overline{S_{ga}S_{hb}}\frac{S_{gx}S_{hx}S_{\bar{j}x}}{S_{1x}}\mathbf{f}_j
\end{aligned}$$

where we used the Verlinde formula (3.8) in the second step. With the unitarity of the S-matrix, we then obtain

$$\begin{aligned}
\mathbf{p}_a\mathbf{p}_b &= S_{1a}S_{1b}\sum_{j,x}\delta_{a,x}\delta_{b,x}\frac{S_{\bar{j}x}}{S_{1x}}\mathbf{f}_j \\
&= \delta_{a,b}S_{1a}^2\sum_{j}\frac{S_{\bar{j}a}}{S_{1a}}\mathbf{f}_j \\
&= \delta_{a,b}S_{1a}\sum_{j}S_{\bar{j}a}\mathbf{f}_j\ .
\end{aligned}$$

It follows that $\mathbf{p}_a\mathbf{p}_b = \delta_{a,b}\mathbf{p}_a$ from the symmetry property $S_{\bar{j}a} = \overline{S_{ja}}$, see e.g., A. Y. Kitaev, 2006, Eq. (224). It remains to verify that the set of projectors is unique. Consider $\mathbf{q}_b = \sum_a \alpha_{ba}\mathbf{p}_a$ for some constants $\alpha_{ba} \in \mathbb{C}$, such that $\mathbf{q}_a\mathbf{q}_b = \delta_{a,b}\mathbf{q}_a$. This implies

$$\begin{aligned}
\mathbf{q}_a\mathbf{q}_b &= \sum_{dc}\alpha_{ac}\alpha_{bd}\mathbf{p}_c\mathbf{p}_d \\
&= \sum_{c}\alpha_{ac}\alpha_{bc}\mathbf{p}_c = \delta_{a,b}\sum_{c}\alpha_{ac}\mathbf{p}_c,
\end{aligned}$$

which implies $\alpha_{ac}\alpha_{bc} = \delta_{a,b}\alpha_{ac}$ for all $a, c \in \mathbb{A}$ by linear independence of the $\mathbf{p}_a$'s. This implies $\alpha_{ac} = 0, 1$, and can only form a complete basis for the algebra Ver if α_{ac} is a permutation matrix, implying $\{\mathbf{q}_a\}_{a\in\mathbb{A}} \equiv \{\mathbf{p}_a\}_{a\in\mathbb{A}}$.

□

As explained in the next section, the string operators of anyons around a loop C give rise to a representation of the Verlinde algebra. While the projections (introduced in Eq. (3.14) below) associated with the idempotents are not a basis for the logical algebra $[\mathcal{A}_\Sigma]$, they are a basis of a subalgebra $[\mathcal{A}_\Sigma(C)]$ isomorphic to the Verlinde algebra. This algebra must be respected by the locality-preserving unitaries, and this is best understood in terms of the idempotents. This is the origin of the non-trivial constraints we obtain on the realizable logical operators.

Bases of the Hilbert space $\mathcal{H}_\Sigma$

Eq. (3.1) shows that the collection of operators $\{[F_a(C)]\}_{a\in\mathbb{A}}$ form a representation of the Verlinde (fusion) algebra Ver. By linear independence of operators $\{[F_a(C)]\}_{a\in\mathbb{A}}$, we see that the representation is faithful, such that the logical loop algebra is isomorphic to the Verlinde algebra

$$[\mathcal{A}(C)] \cong \mathsf{Ver}. \tag{3.13}$$

This will be central in the following development. Considering the primitive idempotents (3.9), it is natural to consider the corresponding operators in this representation, that is, we set

$$[P_a(C)] = S_{1a} \sum_b \overline{S_{ba}} [F_b(C)] \, . \tag{3.14}$$

Since the set $\{[F_a(C)]\}_{a\in\mathbb{A}}$ forms a representation of the Verlinde algebra, the $\{[P_a(C)]\}_{a\in\mathbb{A}}$ are orthogonal projectors as a consequence of Proposition 3.2.3. The inverse relation to (3.14) is given by

$$[F_b(C)] = \sum_a \frac{S_{ba}}{S_{1a}} [P_a(C)] \, . \tag{3.15}$$

While the projectors $[P_a(C)]$ associated with a loop do not span the full logical algebra, they do span the local logical algebra of operators supported along C which must be respected by locality preserving unitaries. Intuitively, $\{P_a(C)\}_{a\in\mathbb{A}}$ are projectors onto the smallest possible sectors of the Hilbert space which can be distinguished by a measurement supported on C.

A state in the image of $P_a(C)$ has the interpretation of carrying flux a through the loop C. In particular, since the code space $\mathcal{H}_\Sigma$ corresponds to the vacua of a TQFT, there are no anyons present on Σ, however, there can be flux associated to non-contractible loops. We can use the operators $\{P_a(C)\}_{a,C}$ to define bases of the Hilbert space $\mathcal{H}_\Sigma$.

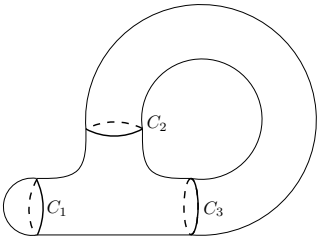

Figure 3.3: A simple DAP decomposition of a torus utilizing a disc enclosed by C_1, an annulus enclosed by $\{C_2, C_3\}$ and a pair of pants enclosed by $\{C_1, C_2, C_3\}$. This decomposition is not minimal in that the same manifold could have been decomposed using a single loop.

Let us first define the Hilbert space $\mathcal{H}_\Sigma$ in more detail.

Definition 3.4 (DAP-decomposition)**.** Consider a minimal collection $\mathcal{C} = \{C_j \mid C_j : [0,1] \to \Sigma\}_j$ of pairwise non-intersecting non-contractible loops, which cut the surface Σ into a collection of surfaces homeomorphic to discs, annuli and pants. We call $\mathcal{C}$ a DAP-decomposition.

A *labeling* $\ell \colon \mathcal{C} \mapsto \mathbb{A}$ is an assignment of an anyon label $\ell(C)$ to every loop $C \in \mathcal{C}$ of a DAP decomposition. We call ℓ fusion-consistent if it satisfies the following conditions:

(i) for every loop $C \in \mathcal{C}$ enclosing a disc on Σ, $\ell(C) = 1$, the vacuum label of the anyon model.

(ii) for every pair of loops $\{C_2, C_3\} \subset \mathcal{C}$ defining an annulus in Σ, $\ell(C_2) = \overline{\ell(C_3)}$ assuming the loops are oriented such that the annulus is found to the left.

(iii) for every triple $\{C_1, C_2, C_3\} \subset \mathcal{C}$ defining a pair of pants in Σ, the labeling ℓ satisfies the fusion rule

$$N_{\ell(C_1),\ell(C_2)}^{\overline{\ell(C_3)}} \neq 0,$$

where the loops are oriented such that the pair of pants is found to the left.

Here we may assume $\ell(C^{-1}) = \overline{\ell(C)}$, where C^{-1} denotes the loop coinciding with C but with opposite orientation.

Now fix any DAP-decomposition $\mathcal{C}$ of Σ and let $\mathsf{L}(\mathcal{C}) \subset \mathbb{A}^{|\mathcal{C}|}$ be the set of fusion-consistent labelings. The Hilbert space $\mathcal{H}_\Sigma$ is the formal span of elements of $\mathsf{L}(\mathcal{C})$

$$\mathcal{H}_\Sigma := \sum_{\ell \in \mathsf{L}(\mathcal{C})} \mathbb{C}\ell = \sum_{\ell \in \mathsf{L}(\mathcal{C})} \mathbb{C}\,|\ell\rangle\,.$$

Any fusion-consistent labeling $\ell \in \mathsf{L}(\mathcal{C})$ defines an element $|\ell\rangle \in \mathcal{H}_\Sigma$ such that the vectors $\{|\ell\rangle\}_{\ell \in \mathsf{L}(\mathcal{C})}$ are an orthonormal basis (which we call $\mathcal{B}_\mathcal{C}$) of $\mathcal{H}_\Sigma$, and this defines the inner product.

It is important to remark that this construction of $\mathcal{H}_\Sigma$ is independent of the DAP-decomposition $\mathcal{C}$ of Σ in the following sense: if $\mathcal{C}$ and $\mathcal{C}'$ are two distinct DAP-decompositions, then there is a unitary basis change between the bases $\mathcal{B}_\mathcal{C}$ and $\mathcal{B}_{\mathcal{C}'}$. In most cases under consideration, this basis change can be obtained as a product of unitaries associated with local "moves" connecting two DAP decompositions $\mathcal{C}$ and $\mathcal{C}'$. One such basis change is associated with a four-punctured sphere (the F-move), and specified by the unitary F-matrix in Fig. 3.4. Another matrix of this kind, the S-matrix (which also arose in our discussion of the Verlinde algebra), connects the two bases $\mathcal{B}_\mathcal{C}$ and $\mathcal{B}_{\mathcal{C}'}$ of $\mathcal{H}_{\text{torus}}$ associated with the first and second non-trivial cycles on the torus (Fig. 3.4). In this case, writing $\mathcal{B}_\mathcal{C} = \{|a\rangle_\mathcal{C}\}_a$ and $\mathcal{B}_{\mathcal{C}'} = \{|a\rangle_{\mathcal{C}'}\}_a$ since each basis element $|\ell\rangle$ is specified by a single label $\ell(C), \ell(C') \in \mathbb{A}$, we have the relation

$$|a\rangle_{\mathcal{C}'} = \sum_b S_{ba}\,|b\rangle_\mathcal{C}\ . \tag{3.16}$$

Other unitary basis changes arise from the representation of the mapping class group, as discussed in Section 3.2. All these basis changes constitute the second ingredient for the non-trivial constraints we obtain on the realizable logical operators.

A basis element $|\ell\rangle \in \mathcal{B}_\mathcal{C}$ associates the anyon label $\ell(C)$ with each curve $C \in \mathcal{C}$. The vector $|\ell\rangle$ is the (up to a phase) unique simultaneous $+1$-eigenvector of all the projections $\{P_\ell(C)\}_{C \in \mathcal{C}}$. It is also a simultaneous eigenvector with respect to Dehn-twists along each curve $C \in \mathcal{C}$ with eigenvalue $e^{i\theta_{\ell(C)}}$. The action of Dehn-twists along curves C' not belonging to $\mathcal{C}$ can be obtained by applying the local moves to change into a basis $\mathcal{B}_{\mathcal{C}'}$ associated with a DAP-decomposition $\mathcal{C}'$ containing C'.

Open surfaces: labeled boundaries

So far, we have been discussing the Hilbert space $\mathcal{H}_\Sigma$ associated with closed surfaces; this does not cover the physically important case of pinned localized excitations (which correspond to punctures/holes in the surface). Here we describe the

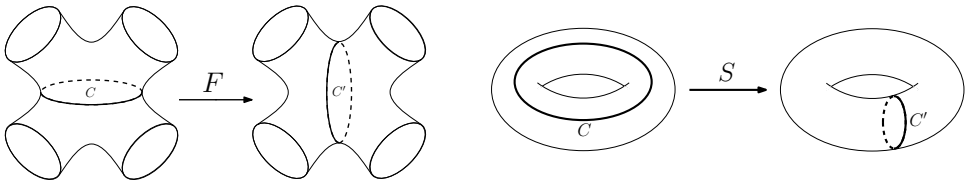

Figure 3.4: Two DAP-decompositions $\mathcal{C} = \{C\}$ and $\mathcal{C}' = \{C'\}$ of either the 4-punctured sphere (left), or the torus (right), are related by an F-move or an S-move, respectively.

modifications necessary to deal with surfaces with boundaries. We assume that the boundary $\partial\Sigma = \bigcup_{\alpha=1}^{M} \hat{C}_\alpha$ is the disjoint union of M simple closed curves, and assume that an orientation $\hat{C}_\alpha : [0,1] \to \partial\Sigma$ has been chosen for each boundary component $\hat{C}_\alpha$ such that Σ is found to the left. In addition, we fix a label $a_\alpha \in \mathbb{A}$ for every boundary component $\hat{C}_\alpha$. We call this a labeling of the boundary. Let us write $\Sigma(a_1, \ldots, a_M)$ for the resulting object (i.e., the surfaces, its oriented boundary components, and the associated labels). We call $\Sigma(a_1, \ldots, a_M)$ a surface with labeled boundary components; slightly abusing notation, we sometimes write $\Sigma = \Sigma(a_1, \ldots, a_M)$ when the presence of boundaries is understood/immaterial.

A TQFT associates to every surface $\Sigma(a_1, \ldots, a_M)$ with labeled boundary components a Hilbert space $\mathcal{H}_{\Sigma(a_1,\ldots,a_M)}$. The construction is analogous to the case of closed surfaces and based on DAP-decompositions. The only modification compared to the case of closed surfaces is that only DAP-decompositions including the curves $\{\hat{C}_\alpha\}_{\alpha=1}^{M}$ are allowed; furthermore, the labeling on these boundary components is fixed by $\{a_\alpha\}_{\alpha=1}^{M}$. That is, "valid" DAP-decompositions are of the form $\mathcal{C} = \{C_1, \ldots, C_N, \hat{C}_1, \ldots, \hat{C}_M\}$ with curves $\{C_j\}_{j=1}^{N}$ "complementing" the boundary components, and valid labelings are fusion-consistent, i.e., $\ell \in \mathsf{L}(C)$ with the additional condition that they agree with the boundary labels, $\ell(\hat{C}_\alpha) = a_\alpha$ for $\alpha = 1, \ldots, M$. To simplify the discussion, we will often omit the boundary components $\{\hat{C}_\alpha\}_\alpha$ and focus on the remaining degrees of freedom associated with the curves $\{C_j\}_j$. It is understood that boundary labelings have to be fusion-consistent with the labeling $\{a_\alpha\}_\alpha$ of the boundary under consideration.

As a final remark, note that boundary components labeled with the trivial particle $1 \in \mathbb{A}$ correspond to contractible loops in a surface without this boundary (i.e., obtained by "gluing in a disc"). This means that they can be omitted: we have the isomorphism

$$\mathcal{H}_{\Sigma(1)} \cong \mathcal{H}_{\Sigma'} ,$$

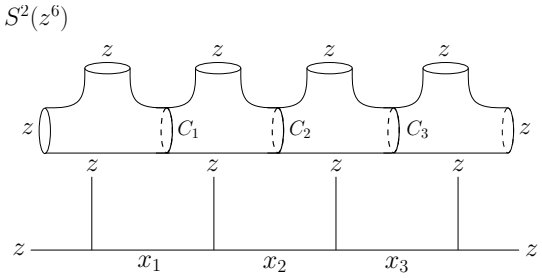

Figure 3.5: The 'standard' DAP-decomposition of the 6-punctured sphere, and the corresponding fusion-tree notation representing the labeling which assigns $\ell(C_i) = x_i$.

where Σ' is the surface with one boundary component less that of Σ.

Example: the M-anyon Hilbert space

A typical example we are interested in is the labeled surface

$$S^2(z^M) = S^2(\underbrace{z, \ldots, z}_{M \text{ times}}) \,,$$

where $S^2(\ ,\ ,\ \ldots\ ,\ ,\ )$ is the punctured sphere, and $z \in \mathbb{A}$ is some fixed anyon type (we assume that each boundary component has the same orientation). The Hilbert space $\mathcal{H}_{S^2(z^M)}$ is the space of M anyons of type z. When $M = N + 3$ for some $N \in \mathbb{N}$, we can choose a 'standard' DAP-decomposition $\mathcal{C} = \{C_j\}_{j=1}^N$ as shown in Fig. 3.5. A fusion-consistent labeling ℓ of the standard DAP-decomposition $\mathcal{C}$ corresponds to a sequence $(x_1, \ldots, x_N) = (\ell(C_1), \ldots, \ell(C_N))$ such that

$$N_{zz}^{x_1} = N_{x_N z}^{\bar{z}} = 1 \qquad \text{and} \qquad N_{x_j z}^{x_{j+1}} = 1 \qquad \text{for all } j = 1, \ldots, N-1, \quad (3.17)$$

as illustrated by Fig. 3.5.

The gluing axiom

Consider a closed curve C embedded in Σ. We will assume that C is an element of a DAP-decomposition $\mathcal{C}$; although this is not strictly necessary, it will simplify our discussion. Now consider the surface Σ' obtained by cutting Σ along C. Compared to Σ, this is a surface with two boundary components C_1', C_2' (both isotopic to C) added. We will assume that these have opposite orientation. A familiar example is

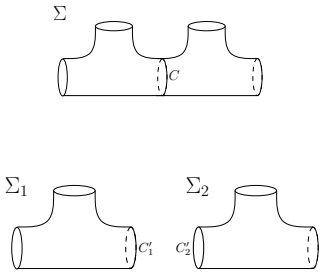

Figure 3.6: Cutting a surface Σ along some closed curve C of a DAP-decomposition yields a disconnected surface $\Sigma' = \Sigma_1 \cup \Sigma_2$ having additional boundary components C_1' and C_2'.

the case where cutting Σ along C results in two disconnected surfaces $\Sigma' = \Sigma_1 \cup \Sigma_2$, as depicted in Fig. 3.6 in the case where Σ is the 4-punctured sphere.

Let a be a particle label. We will denote by $\mathcal{H}_{\Sigma'(a,\overline{a})}$ the Hilbert space associated with the open surface Σ', where boundary C_1' is labeled by a and boundary C_2' by $\overline{a}$. The gluing axiom states that the Hilbert space of the surface Σ has the form

$$\mathcal{H}_\Sigma \cong \bigoplus_a \mathcal{H}_{\Sigma'(a,\overline{a})} \tag{3.18}$$

where the direct sum is over all particle labels a that occur in different fusion-consistent labelings of $\mathcal{C}$. In the special case where cutting along C gives two components Σ_1, Σ_2, we have $\mathcal{H}_\Sigma \cong \bigoplus_a \mathcal{H}_{\Sigma_1(a)} \otimes \mathcal{H}_{\Sigma_2(\overline{a})}$.

The isomorphism (3.18) can easily be made explicit. A first observation is that $\mathcal{H}_\Sigma$ decomposes as $\mathcal{H}_\Sigma = \bigoplus_a \mathcal{H}_{a,\Sigma}(C)$, where

$$\mathcal{H}_{a,\Sigma}(C) \coloneqq \mathsf{span}\{|\ell\rangle \mid \ell \in \mathsf{L}(\mathcal{C}), \ell(C) = a\} \tag{3.19}$$

is the space spanned by all labelings which assign the label a to C. It therefore suffices to argue that

$$\mathcal{H}_{a,\Sigma}(C) \cong \mathcal{H}_{\Sigma'(a,\overline{a})} \,. \tag{3.20}$$

To do so, observe that the DAP-decomposition $\mathcal{C}$ of Σ gives rise to a DAP-decomposition $\mathcal{C}' = \mathcal{C} \backslash \{C\}$ of Σ'. Any labeling $\ell \in \mathsf{L}(\mathcal{C})$ with $\ell(C) = a$ restricts to a labeling $\ell' \in \mathsf{L}(\mathcal{C}')$ of the labeled surface $\Sigma'(a, \overline{a})$. Conversely, any labeling $\ell' \in \mathsf{L}(\mathcal{C}')$ of the surface $\Sigma'(a, \overline{a})$ provides a labeling $\ell \in \mathsf{L}(\mathcal{C})$ (by setting $\ell(C) = a$). This defines the isomorphism (3.20) in terms of basis states $\{|\ell\rangle\}_{\ell \in \mathsf{L}(\mathcal{C})}$ and $\{|\ell'\rangle\}_{\ell' \in \mathsf{L}(\mathcal{C}')}$.

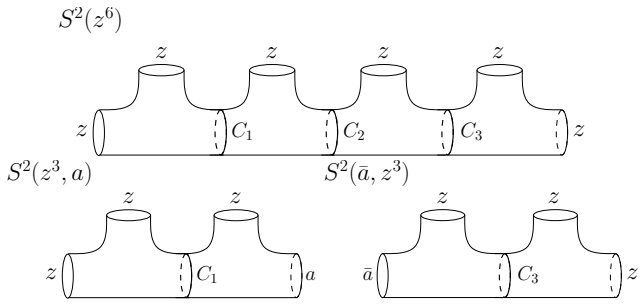

Figure 3.7: The 6-punctured sphere $S^2(z^6)$ shown with three curves $C_1, C_2, C_3 \in \mathcal{C}$ of a DAP-decomposition. Cutting along C_2 with labeling $\ell(C_2) = a$ results in the two surfaces $S^2(z^3, a)$ and $S^2(\overline{a}, z^3)$.

Example: decomposing the M-anyon Hilbert space

Consider the M-punctured sphere $\Sigma = S^2(z^M)$ with the standard DAP decomposition of Fig. 3.5 and boundary labels z (corresponding to M anyons of type z). Cutting $S^2(z^M)$ along C_j gives a surface Σ'_j which is the disjoint union of two punctured spheres, with $j+2$ and $M-j$ punctures, respectively. The resulting surface labelings are $S^2(z^{j+1}, a)$ and $S^2(\overline{a}, z^{M-1-j})$. That is, if $\Sigma = S^2(z^M)$ is the original surface and $\Sigma'_j(a, \overline{a})$ is the resulting one, then

$$\mathcal{H}_{\Sigma'_j(a,\overline{a})} = \mathcal{H}_{S^2(z^{j+1},a)} \otimes \mathcal{H}_{S^2(\overline{a},z^{M-1-j})} \ . \tag{3.21}$$

This is illustrated in Fig. 3.7 for the case $M = 6$ and $j = 2$.

The mapping class group

In the following, we denote by MCG_Σ the *mapping class group* of the surface Σ. Physically, a mapping class group element for a surface Σ gradually deforms the surface, but returns to the original configuration. For the n-punctured sphere, the mapping class group includes braiding of the punctures. For the torus, a Dehn twist is an element of the mapping class group. More formally, elements of MCG_Σ are isotopy classes of orientation-preserving diffeomorphisms of Σ preserving labels and commuting with boundary parametrization (see e.g., M. H. Freedman, A. Y. Kitaev, and Z. Wang, 2002). Slightly abusing notation, we will often simply write $\vartheta \in \mathsf{MCG}_\Sigma$ for an equivalence class represented by a map $\vartheta : \Sigma \to \Sigma$. If Σ is the torus, then the mapping class group is generated by two elements, $\mathsf{MCG}_\Sigma = \langle s, t \rangle$

where s and t are the standard generators of the modular group. For the M-punctured sphere $S^2(z^M)$, we will also need the $M-1$ elements $\{\sigma_j\}_{j=1}^{M-1}$, where σ_j braids holes j and $j+1$.

The Hilbert space $\mathcal{H}_\Sigma$ is equipped with a projective unitary representation

$$\begin{array}{ccc} \mathsf{MCG}_\Sigma & \to & \mathsf{U}(\mathcal{H}_\Sigma) \\ \vartheta & \mapsto & \mathbf{V}(\vartheta) \end{array} \tag{3.22}$$

of the mapping class group MCG_Σ. For example, for the torus, $\mathbf{V}(s) = S$ and $\mathbf{V}(t) = T$ are the usual S- and T-matrices defined by the modular tensor category. For the M-punctured sphere $S^2(z^M)$ with $M = N+3$, we again use the standard DAP-decomposition with associated basis $\{|x\rangle\}_x$. Here the sequences $x = (x_1, \ldots, x_N)$ are subject to the fusion rules (see (3.17)) and the action on such vectors is

$$\begin{aligned} \mathbf{V}(\sigma_1)\,|x\rangle &= R^{zz}_{x_1}\,|x\rangle\,, \\ \mathbf{V}(\sigma_k)\,|x\rangle &= \sum_{x'} B(x_{k-1}, x_{k+1})_{x' x_k}\,|x_1, \ldots, x_{k-1}, x', x_{k+1}, \ldots, x_N\rangle \\ &\qquad\qquad\qquad\qquad\qquad\qquad \text{for } k = 2, \ldots, N+1, \\ \mathbf{V}(\sigma_{N+2})\,|x\rangle &= \overline{R^{zz}_{x_1}}\,|x\rangle\,, \end{aligned}$$

where $B(a,b) = \tilde{F}^{-1}\tilde{R}\tilde{F}$ is the braid matrix. Here the matrices $\tilde{F}$ and $\tilde{R}$ are given in terms of the tensors F and R associated with the TQFT[4].

3.3 Constraints on locality-preserving automorphisms

In this section, we derive restrictions on topologically protected gates for general non-abelian models. Our strategy will be to consider what happens to string-operators. We will first consider operators associated with a single loop C, and derive restrictions on the map $F_a(C) \mapsto U F_a(C) U^\dagger$, or, more precisely, its effect on logical operators, $[F_a(C)] \mapsto [U F_a(C) U^\dagger]$. We will argue that this map implements an isomorphism of the Verlinde algebra and exploit this fact to derive a constraint which is 'local' to a specific loop. We will subsequently consider more 'global' constraints arising from fusion rules, as well as basis changes.

We would like to characterize locality-preserving unitary automorphisms $U \in \mathcal{A}_\Sigma$ in terms of their logical action $[U]$. For example in the toric code, where the physical

[4] More precisely, for $B(x_{k-1}, x_{k+1})$, the relevant matrices are $\tilde{F}_{x',x} = F^{z x_{k-1} x_k}_{x_{k+1} z x'}$ and $\tilde{R}$ is diagonal with entries $\tilde{R}_{x,x} = R^{zz}_x$. Here F is the F-matrix associated with basis changes on the four-punctured sphere (see Section 3.5), whereas R^{xy}_z determines an isomorphisms between certain Hilbert spaces associated with the three-punctured sphere. We refer to e.g., J. Preskill, 2004, p. 48 for a derivation of these expressions.

qubits are imbedded in the edges of the square lattice, the locality preserving unitaries include the well-known transversal gates of single-qubit unitaries applied to each qubit. More general examples of locality preserving unitaries in the toric code are finite depth circuits composed of gates of arbitrary unitaries applied to physical qubits in geometrically-local patches of fixed diameter.

A first goal is to characterize the map

$$\begin{array}{rccc} \rho_U : & [\mathcal{A}_\Sigma] & \to & [\mathcal{A}_\Sigma] \\ & [X] & \mapsto & [UXU^{-1}] \,, \end{array} \tag{3.23}$$

which determines the evolution of logical observables in the Heisenberg picture. (Clearly, this does not depend on the representative, i.e., if $[X] = [X']$, then $\rho_U([X]) = \rho_U([X'])$.) In fact, the map (3.23) fully determines U up to a global phase since $[\mathcal{A}_\Sigma]$ contains an operator basis for linear maps on $\mathcal{H}_\Sigma$. However, it will often be more informative to characterize the action of $[U]$ on basis elements of $\mathcal{H}_\Sigma$. This will require additional effort.

The main observation is that the map (3.23) defines an automorphism of $[\mathcal{A}_\Sigma]$, since

$$\rho_U([X])\rho_U([X']) = \rho_U([X][X']) \qquad \text{for all } X, X' \in \mathcal{A}_\Sigma \qquad \text{and} \qquad \rho_U^{-1} = \rho_{U^{-1}} \,. \tag{3.24}$$

Combined with the locality of U, (3.24) severly constrains ρ_U. Using this fact, we obtain a number of very general constraints, which will be worked out in more detail in the following.

A local constraint from a simple closed loop

Specifying the action of ρ_U on all of $[\mathcal{A}_\Sigma]$ completely determines $[U]$ up to a global phase. However, this is not entirely straightforward; instead, we fix some simple closed curve C and characterize the restriction to the subalgebra $\mathcal{A}(C) \subset \mathcal{A}_\Sigma$, i.e., the map

$$\begin{array}{rccc} \rho_U(C) : & [\mathcal{A}(C)] & \to & [\mathcal{A}(C)] \\ & [X] & \mapsto & [UXU^{-1}] \,, \end{array} \tag{3.25}$$

Observe that this map is well-defined since UXU^{-1} is supported in a neighborhood of C (by the locality-preservation of U), and hence $[UXU^{-1}] = [X']$ for some operator $X' \in \mathcal{A}(C)$ (here we have used Proposition 3.2.1). It is also easy to see that it defines an automorphism of the subalgebra $[\mathcal{A}(C)]$.

As we argued above, the algebra $\mathcal{A}(C)$ is isomorphic to Ver. This carries over to $[\mathcal{A}(C)] \cong \mathsf{Ver} \cong \mathbb{C}^{\oplus|\mathbb{A}|}$. As Ver has idempotents $\mathbf{p}_{a\in\mathbb{A}}$, the logical algebra for loop C has idempotents $\{[P_a(C)]\}_{a\in\mathbb{A}}$. Note that the idempotents $\{[P_a(C)]\}_{a\in\mathbb{A}}$ in the logical algebra are unique, in that there is no linear combination of these idempotents which yields a distinct, complete set of idempotents. At the physical level however, there can be huge redundency, with many different physical operators corresponding to the same logical operator, i.e. $[P_a(C)] = [P'_a(C)]$, for $P_a(C) \neq P'_a(C)$. We use the following fact:

Lemma 3.5. The set of automorphisms of the algebra Ver is in one-to-one correspondence with the permutations $S_{|\mathbb{A}|}$. For $\pi \in S_{|\mathbb{A}|}$, the associated automorphism $\rho_\pi : \mathsf{Ver} \to \mathsf{Ver}$ is defined by its action on the central idempotents $\mathbf{p}_a$

$$\rho_\pi(\mathbf{p}_a) = \mathbf{p}_{\pi(a)} \qquad \text{for } a \in \mathbb{A} \tag{3.26}$$

Proof. It is clear that (3.26) defines an automorphism for every $\pi \in S_{|\mathbb{A}|}$. Also, from Eq. (3.24) we see that $\mathbf{p}_a\mathbf{p}_b = \delta_{ab}\mathbf{p}_b$ implies $\rho(\mathbf{p}_a)\rho(\mathbf{p}_b) = \delta_{ab}\rho(\mathbf{p}_b)$, such that $\rho(\mathbf{p}_a) \in \mathsf{Ver}$ are a complete set of projectors (Proposition 3.2.3). As there is a unique set of complete projectors for Ver, we conclude that $\rho(\mathbf{p}_a) = \mathbf{p}_{\pi(a)}$ for some permutation $\pi \in S_{|\mathbb{A}|}$. □

Applying this to $[\mathcal{A}(C)]$ shows that a locality-preserving unitary automorphism realizes, up to*important* phases, a a permutation of labelings. Let us emphasize that it is the projectors (idempotents) $[P_a(C)]$ which are being permuted, and not the string operators $[F_a(C)]$.

Proposition 3.3.1 (Local constraint)**.** Let U be a locality-preserving automorphism of the code, and let $\rho_U([X]) = [UXU^{-1}]$.

(i) For each simple closed loop C on Σ, there is a permutation $\pi^C : \mathbb{A} \to \mathbb{A}$ of the particle labels such that

$$\begin{array}{rccll} \rho_U : & [\mathcal{A}(C)] & \to & [\mathcal{A}(C)] & \\ & [P_a(C)] & \mapsto & [P_{\pi^C(a)}(C)] & \text{for all } a \in \mathbb{A}\,, \end{array} \tag{3.27}$$

(and linearly extended to all of $[\mathcal{A}(C)]$).

(ii) For some anyon model $\mathbb{A}$ with an associated S matrix, let $D_{a,b} = \delta_{a,b} \cdot d_a$ be the diagonal matrix with the quantum dimensions on the diagonal. Let

$\pi^C\colon \mathbb{A} \to \mathbb{A}$ be a permutation associated with a loop C as in (i), and let Π be the matrix defined by $\Pi_{x,y} \coloneqq \delta_{x,\pi^C(y)}$. Define the matrix

$$\Lambda \coloneqq S\Pi^{-1}D\Pi D^{-1}\Pi^{-1}S^{-1} \,. \tag{3.28}$$

Then

$$\rho_U([F_b(C)]) = \sum_{b'} \Lambda_{b,b'}[F_{b'}(C)] \,. \tag{3.29}$$

Proof. We have already argued that (i) holds. For the proof of (ii), we use the relationship between $\{P_a(C)\}_a$ and $\{F_a(C)\}_a$ (cf. (3.14) and (3.15)) to get (suppressing the dependence on the loop C)

$$\rho_U([F_b]) = \sum_a \frac{S_{b,a}}{S_{1,a}}[P_{\pi^C(a)}] = \sum_{b'} \left(\sum_a \frac{S_{b,a}}{S_{1,a}} S_{1,\pi^C(a)} \overline{S_{b',\pi^C(a)}} \right) [F_{b'}] \,.$$

The claim (3.29) follows from this using $(\Pi^{-1}S^{-1})_{a,b'} = (S^{-1})_{\pi^C(a),b'} = \overline{S_{b',\pi^C(a)}}$ by the unitarity of S, as well as the fact that $S_{1,a} = d_a/\mathcal{D}$ and hence $\frac{S_{b,a}}{S_{1,a}} S_{1,\pi^C(a)} = (S\Pi^{-1}D\Pi D^{-1})_{b,a}$. □

Global constraints from DAP-decompositions, fusion rules and the gluing axiom

For higher-genus surfaces, we can obtain information by applying Proposition 3.3.1 to all loops of a DAP-decomposition; these must then satisfy the following consistency condition.

Proposition 3.3.2 (Global constraint from fusion rules)**.** Let U be a locality-preserving automorphism of the code. Let $\mathcal{C}$ be a DAP-decomposition of Σ, and consider the family of permutations $\vec{\pi} = \{\pi^C\}_{C\in\mathcal{C}}$ defined by Proposition 3.3.1. Then this defines a permutation $\vec{\pi}\colon \mathsf{L}(\mathcal{C}) \to \mathsf{L}(\mathcal{C})$ of the set of fusion-consistent labelings via

$$\vec{\pi}(\ell)(C) \coloneqq \pi^C[\ell(C)] \tag{3.30}$$

for all $C \in \mathcal{C}$. We have

$$U\,|\ell\rangle = \mathrm{e}^{\mathrm{i}\varphi(\ell)}\,|\vec{\pi}(\ell)\rangle \qquad \text{for all } \ell \in L(\mathcal{C}) \tag{3.31}$$

with some phase $\mathrm{e}^{\mathrm{i}\varphi(\ell)}$ depending on ℓ.

Proof. Let us fix some basis element $|\ell\rangle \in \mathcal{B}_{\mathcal{C}}$. The vector $|\ell\rangle$ is a $+1$-eigenvector of $P_{\ell(C)}(C)$ for each $C \in \mathcal{C}$; hence according to (3.27), the vector $U\,|\ell\rangle$ is a $+1$-eigenvector of $P_{\pi^C[\ell(C)]}(C) = P_{\vec{\pi}(\ell)(C)}(C)$ for every $C \in \mathcal{C}$. This implies that it is

proportional to $|\vec{\pi}(\ell)\rangle$, hence we obtain (3.31). Fusion-consistency of $\vec{\pi}(\ell)$ follows because $U\,|\ell\rangle$ must be an element of $\mathcal{H}_\Sigma$. □

Proposition (3.3.2) expresses the requirement that a locality-preserving automorphism U maps the set of fusion-consistent labelings into itself.

In fact, we can say more: it must be an isomorphism between the subspaces of $\mathcal{H}_\Sigma$ arising from the gluing axiom (i.e., Eq. (3.18)). This allows us to constrain the set of allowed permutations $\vec{\pi} = \{\pi^C\}_{C\in\mathcal{C}}$ arising from locality-preserving automorphisms even further:

Proposition 3.3.3 (Global constraint from gluing)**.** Let C be an element of a DAP-decomposition of Σ. Recall that

$$\mathcal{H}_\Sigma = \bigoplus_a \mathcal{H}_{a,\Sigma}(C)\,, \tag{3.32}$$

where the subspaces in the direct sum are defined by labelings associating a to C. Let U be a locality-preserving automorphism of the code and let $\pi^C\colon \mathbb{A}\to\mathbb{A}$ be the permutation associated with C by Proposition 3.3.1. Then for every $a\in\mathbb{A}$ occuring in Eq. (3.32), the restriction of U to $\mathcal{H}_{a,\Sigma}(C)$ defines an isomorphism

$$\mathcal{H}_{a,\Sigma}(C) \cong \mathcal{H}_{\pi^C(a),\Sigma}(C)\,. \tag{3.33}$$

In particular, if Σ' is the surface obtained by cutting Σ along C, then

$$\mathcal{H}_{\Sigma'(a,\bar{a})} \cong \mathcal{H}_{\Sigma'(\pi^C(a),\overline{\pi^C(a)})} \tag{3.34}$$

for every $a\in\mathbb{A}$ occuring in the sum (3.32).

The reason we refer to Proposition (3.3.3) as a global constraint (even though it superficially only concerns a single curve C) is that the surface Σ' and hence the spaces (3.34) depend on the global form of the surface Σ outside the support of C.

Proof. Proposition (3.3.2) implies that $U\mathcal{H}_{a,\Sigma}(C)\subset\mathcal{H}_{\pi^C(a),\Sigma}(C)$ for any a in expression (3.32). Since U acts unitarily on the whole space $\mathcal{H}_\Sigma$, this is compatible with (3.32) only if $U\mathcal{H}_{a,\Sigma}(C)=\mathcal{H}_{\pi^C(a),\Sigma}(C)$ for any such a. This proves (3.33). Statement (3.34) then immediately follows from (3.20). □

A simple but useful implication of Proposition 3.3.3 is that

$$\dim\left(\mathcal{H}_{\Sigma'(a,\bar{a})}\right) = \dim\left(\mathcal{H}_{\Sigma'(\pi^C(a),\overline{\pi^C(a)})}\right) \tag{3.35}$$

is a necessary condition that π^C has to satisfy.

Global constraints from basis changes

Eq. (3.27) essentially tells us that a locality-preserving protected gate U can only permute particle labels; it indicates that such a gate U is related to certain symmetries of the anyon model. But (3.27) does not tell us what phases basis states may acquire. We show how to obtain constraints on these phases by considering basis changes. This also further constrains the allowed permutations on the labels of the idempotents.

Consider two DAP-decompositions $\mathcal{C}$ and $\mathcal{C}'$. Expressed in the first basis $\mathcal{B}_{\mathcal{C}}$, we have

$$U\,|\ell\rangle = \mathrm{e}^{\mathrm{i}\varphi(\ell)}\,|\vec{\pi}(\ell)\rangle \tag{3.36}$$

for some unknown phase $\varphi(\ell)$ depending only on the labeling $\ell \in \mathsf{L}(\mathcal{C})$. This means that with respect to the basis elements of $\mathcal{B}_{\mathcal{C}}$, the operator U is described by a matrix $\boldsymbol{U} = \boldsymbol{\Pi}\boldsymbol{D}(\{\varphi(\ell)\}_\ell)$, where $\boldsymbol{\Pi}$ is a permutation matrix (acting on the fusion-consistent labelings $\mathsf{L}(\mathcal{C})$), and $\boldsymbol{D}$ is a diagonal matrix with entries $\{\mathrm{e}^{\mathrm{i}\varphi(\ell)}\}_\ell$ on the diagonal.

Analogously, we can consider the operator U expressed as a matrix $\boldsymbol{U}'$ in terms of the basis elements of $\mathcal{B}_{\mathcal{C}'}$. We conclude that $\boldsymbol{U}' = \boldsymbol{\Pi}'\boldsymbol{D}(\{\varphi'(\ell)\}_\ell)$, for $\ell \in \mathsf{L}(\mathcal{C}')$, with a (potentially different) permutation matrix $\boldsymbol{\Pi}'$, and (potentially different) phases $\{\varphi'(\ell)\}_\ell$.

Let $\boldsymbol{V}$ be the unitary change-of-basis matrix for going from $\mathcal{B}_{\mathcal{C}}$ to $\mathcal{B}_{\mathcal{C}'}$. Then we must have

$$\boldsymbol{V}\boldsymbol{U} = \boldsymbol{U}'\boldsymbol{V}. \tag{3.37}$$

We show below that this equation strongly constrains the phases as well as the permutations in (3.31). More specifically, we will examine constraints arising when using basis changes $\mathbf{V}$ defined by F-moves in Section 3.5. In Section 3.4, we consider basis changes $\mathbf{V}$ defined by elements of the mapping class group.

3.4 Global constraints from the mapping class group

The following is based on the simple observation that we must have consistency conditions of the form (3.37) for more general basis changes (in particular, basis changes not made up of F-moves only). We are particularly interested in the case where the basis change is the result of applying a mapping class group element.

Basis changes defined by the mapping class group

A key property of the representation (3.22) of the mapping class group MCG_Σ is that it maps idempotents according to

$$V(\vartheta)P_a(C)V(\vartheta)^\dagger = P_a\big(\vartheta(C)\big)\ . \tag{3.38}$$

Let us fix a 'standard' DAP-decomposition $\mathcal{C}$, and let $\mathcal{B}_\mathcal{C} = \{|\ell\rangle_\mathcal{C}\}_\ell$ be the corresponding standard basis.

Let ϑ be an arbitrary element of MCG_Σ. Consider the basis

$$\mathcal{B}_{\vartheta(\mathcal{C})} \coloneqq \{V(\vartheta)\,|\ell\rangle\}_\ell.$$

Because of (3.38), this basis is a simultaneous eigenbasis of the complete set of commuting observables associated with the DAP decomposition $\vartheta(\mathcal{C}) \coloneqq \{\vartheta(C_j)\}_{j=1}^M$. The change of basis from $\mathcal{B}_\mathcal{C}$ to $\mathcal{B}_{\vartheta(\mathcal{C})}$ is given by the image $V(\vartheta)$ of the mapping class group element ϑ.

In particular, if $\mathbf{V}(\vartheta)$ is the matrix representing $V(\vartheta)$ in the standard basis, then (3.37) implies

$$\mathbf{V}(\vartheta)\mathbf{\Pi}\mathbf{D} = \mathbf{\Pi}(\vartheta)\mathbf{D}(\vartheta)\mathbf{V}(\vartheta) \tag{3.39}$$

for some permutation matrix $\mathbf{\Pi}(\vartheta)$ and a diagonal matrix $\mathbf{D}(\vartheta)$ consisting of phases.

Some terminology will be useful: Let Δ be the set of matrices of the form $\mathbf{\Pi}\mathbf{D}$, where $\mathbf{\Pi}$ is a permutation of fusion-consistent labelings, and $\mathbf{D}$ is a diagonal matrix with phases (these are sometimes called *unitary monomial matrices*). For $\mathbf{U} \in \Delta$ and $\vartheta \in \mathsf{MCG}_\Sigma$, we say that $\mathbf{U}$ intertwines with ϑ if

$$\mathbf{V}(\vartheta)\mathbf{U}\mathbf{V}(\vartheta)^\dagger \in \Delta\ .$$

Let $\Delta_\vartheta \subset \Delta$ be the set of matrices that intertwine with ϑ, and let

$$\Delta_{\mathsf{MCG}_\Sigma} = \bigcap_{\vartheta\in\mathsf{MCG}_\Sigma} \Delta_\vartheta$$

be the matrices that are intertwiners of the whole mapping class group representation. We have shown the following:

Theorem 3.6. Let $\mathbf{U}$ be the matrix representing a protected gate U in the standard basis. Then $\mathbf{U} \in \Delta_{\mathsf{MCG}_\Sigma}$.

As an example, consider the torus: since $T = \mathbf{V}(t)$ is diagonal, it is easy to see that for any $\mathbf{\Pi D} \in \Delta$, we have $T\mathbf{\Pi D}T^{-1} = \mathbf{\Pi D}'$ for some $\mathbf{D}'$. This implies that $\Delta_t = \Delta$ is generally not interesting, i.e., $\mathbf{U} \in \Delta_t$ does not impose an additional constraint. In contrast, mapping class group elements such as s and st generally give different non-trivial constraints.

Density of the mapping class group representation and absence of protected gates

The following statement directly links computational universality of the mapping class group representation to the non-existence of protected gates.

Corollary 3.7. Suppose the representation of MCG_Σ is dense in the projective unitary group $\mathsf{PU}(\mathcal{H}_\Sigma)$. Then there is no non-trivial protected gate.

Proof. Let U be an arbitrary protected gate and let $\mathbf{U} \in \Delta$ be the matrix representing it in the standard basis. Assume for the sake of contradiction that U is non-trivial. Then $\mathbf{U}$ is a unitary with at least two different eigenvalues λ_1, $\lambda_2 \in \mathrm{U}(1)$. In particular, there is a diagonalizing unitary $\mathbf{V}_1$ such that $\mathbf{V}_1\mathbf{U}\mathbf{V}_1^\dagger = \mathsf{diag}(\lambda_1, \lambda_2) \oplus \tilde{\mathbf{U}}$ for some matrix $\tilde{\mathbf{U}}$. Setting $\mathbf{V}_2 = H \oplus I$, where H is the Hadamard matrix

$$H = \frac{1}{\sqrt{2}} \begin{pmatrix} 1 & 1 \\ 1 & -1 \end{pmatrix},$$

and $\mathbf{V} = \mathbf{V}_2\mathbf{V}_1$, we obtain that

$$\mathbf{V}\mathbf{U}\mathbf{V}^\dagger \notin \Delta \tag{3.40}$$

because this matrix contains both diagonal and off-diagonal elements. Note that if $\lambda_2 = -\lambda_1$ one may use the matrix

$$\frac{1}{2} \begin{pmatrix} 1 & -\sqrt{3} \\ \sqrt{3} & 1 \end{pmatrix}$$

instead of H.

Observe also that (3.40) stays valid if we replace $\mathbf{V}$ by a sufficiently close approximation (up to an irrelevant global phase) $\tilde{\mathbf{V}} \approx \mathbf{V}$. In particular, by the assumed density, we may approximate $\mathbf{V}$ by a product $\tilde{\mathbf{V}} = \mathbf{V}(\vartheta_1) \cdots \mathbf{V}(\vartheta_m)$ of images of $\vartheta_1, \ldots, \vartheta_m \in \mathsf{MCG}_\Sigma$. But then we have

$$\mathbf{U} \notin \Delta_{\vartheta_1 \cdots \vartheta_m} ,$$

which contradicts Theorem 3.6. □

Note that in general, the mapping class group is only dense on a subspace $\mathcal{H}_0 \subset \mathcal{H}_\Sigma$. This is the case for example when the overall system allows for configurations where anyons can be present or absent (e.g., a boundary may or may not carry a topological charge). In such a situation, $\mathcal{H}_\Sigma$ decomposes into superselection sectors which are defined by the gluing axiom (i.e., having fixed labels associated with certain closed loops associated). Corollary 3.7 can be adapted to this situation, e.g., as explained in Appendix 3.8 (Lemma 3.22).

Characterizing diagonal protected gates

Fix a DAP-decomposition $\mathcal{C}$ and let $\vartheta \in \mathsf{MCG}_\Sigma$. Let us call two (fusion-consistent) labelings ℓ_1, ℓ_2 *connected by* ϑ (denoted $\ell_1 \Leftrightarrow_\vartheta \ell_2$) if there is a labeling ℓ such that

$$0 \neq \langle \ell | V(\vartheta) | \ell_m \rangle \qquad \text{for } m = 1, 2 \, .$$

(Here $|\ell\rangle$ is the associated basis element of $\mathcal{B}_\mathcal{C}$.) More generally, let us say ℓ_1, ℓ_2 are connected (written $\ell_1 \Leftrightarrow \ell_2$) if there exists an element $\vartheta \in \mathsf{MCG}_\Sigma$ such that $\ell_1 \Leftrightarrow_\vartheta \ell_2$. Clearly, this notion is symmetric in ℓ_1, ℓ_2, and furthermore, it is reflexive, i.e., $\ell_1 \Leftrightarrow \ell_1$ since $\ell_1 \Leftrightarrow_{\mathrm{id}} \ell_1$. We can therefore define an equivalence relation on the set of labelings: we write $\ell_1 \sim \ell_2$ if there are labelings $k_1, \ldots, k_m$ such that $\ell_1 \Leftrightarrow k_1 \Leftrightarrow \cdots \Leftrightarrow k_m \Leftrightarrow \ell_2$. We point out (for later use) that we can always find a finite collection $\{\vartheta_k\}_{k=1}^M \subset \mathsf{MCG}_\Sigma$ that generates the relation $\sim$ in the sense that $\ell_1 \sim \ell_2$ if and only if $\ell_1 \Leftrightarrow_{\vartheta_k} \ell_2$ for some k (after all, we only have a finite set of labelings ℓ).

Observe that if the representation of MCG_Σ has a non-trivial invariant subspace, then there is more than one equivalence class. We discuss an example of this below (see Section 3.4). However, in important special cases such as the Fibonacci or Ising models, there is only one equivalence class for the relation $\sim$, i.e., any pair of labelings are connected (see Lemma 3.13 and Lemma 3.14 below).

Lemma 3.8. Consider a protected gate U acting diagonally in the basis $\mathcal{B}_\mathcal{C}$ as $U|\ell\rangle = \mathrm{e}^{\mathrm{i}\varphi(\ell)}|\ell\rangle$.

(i) Suppose that U also acts diagonally in the basis $\mathcal{B}_{\vartheta(\mathcal{C})}$. Then $\varphi(\ell_1) = \varphi(\ell_2)$ for any pair $\ell_1 \Leftrightarrow_\vartheta \ell_2$ connected by ϑ.

(ii) Suppose that $\{\vartheta_k\}_{k=1}^M \subset \mathsf{MCG}_\Sigma$ generates the relation $\sim$, and U acts diagonally in each basis $\mathcal{B}_{\vartheta_k(\mathcal{C})}$. Then φ assigns the same value to every element of the same equivalence class under $\sim$.

We will refer to a protected gate U with property (ii) as a $\sim$-trivial gate. One implication of Lemma 3.8 is that any protected gate which is close to the identity acts as a $\sim$-trivial gate (see the proof of Theorem 3.10). In Section 3.4, we will show how to use this statement to prove that the set of protected gates is finite up to irrelevant phases.

Proof. Consider two labelings ℓ_1, ℓ_2 satisfying $\ell_1 \Leftrightarrow_\vartheta \ell_2$. Then, writing $\mathbf{V} = \mathbf{V}(\vartheta)$, we know that

$$\mathbf{V}_{\ell,\ell_1} \neq 0 \qquad \text{and} \qquad \mathbf{V}_{\ell,\ell_2} \neq 0 \tag{3.41}$$

for some labeling ℓ, where $\mathbf{V}_{\ell,k} = \langle \ell | V(\vartheta) | k \rangle$. Since U acts diagonally in both bases $\mathcal{B}_\mathcal{C}$ and $\mathcal{B}_{\vartheta(\mathcal{C})}$ by assumption, (3.39) becomes simply

$$\mathbf{V}\mathbf{D}\mathbf{V}^\dagger = \mathbf{D}(\vartheta) \tag{3.42}$$

when written in the standard basis. Here the diagonal matrices are given by $\mathbf{D} = \mathrm{diag}(\{\varphi(\ell)\}_\ell)$ and $\mathbf{D}(\vartheta) = \mathrm{diag}(\{\varphi'(\ell)\}_\ell)$. Taking the diagonal entry at position (ℓ, ℓ) in the matrix equation (3.42), we get the identity

$$\sum_k \mathrm{e}^{\mathrm{i}(\varphi(k) - \varphi'(\ell))} |\mathbf{V}_{\ell,k}|^2 = 1. \tag{3.43}$$

By unitarity of the mapping class group representation, we also have

$$\sum_k |\mathbf{V}_{\ell,k}|^2 = 1. \tag{3.44}$$

By taking the real part of (3.43), it is straightforward to see that compatibility with (3.44) imposes that $\cos\big(\varphi(k) - \varphi'(\ell)\big) = 1$ whenever $|\mathbf{V}_{\ell,k}| \neq 0$ or

$$\varphi(k) \equiv \varphi'(\ell) \mod 2\pi \qquad \text{for all } k \text{ with } |\mathbf{V}_{\ell,k}| \neq 0.$$

With (3.41), we conclude that $\varphi(\ell_1) = \varphi'(\ell) = \varphi(\ell_2)$, which proves claim (i).

The claim (ii) immediately follows from (i). □

We will show how to apply this result to the Fibonacci model in Section 3.6. Note that Lemma 3.8 does not generally rule out the existence of non-trivial diagonal protected gates in the standard basis (an example is a Pauli-Z in the Ising model, see Section 3.6): it is important that the protected gate is diagonal in *several* different bases $\{\mathcal{B}_{\vartheta_k(\mathcal{C})}\}_k$.

A simple consequence of Lemma 3.8 is that any protected gate has a finite order up to certain phases:

Lemma 3.9. There is a finite n_0 (depending only on the dimension of $\mathcal{H}_\Sigma$) such that for every protected gate U, there is an $n \leq n_0$ such that U^n is a $\sim$-trivial phase gate.

Proof. Consider an arbitrary DAP-decomposition $\mathcal{C}$ and suppose U acts as (3.31) in the basis $\mathcal{B}_\mathcal{C}$. Since the permutation $\vec{\pi}$ acts on the finite set $\mathsf{L}(\mathcal{C})$ of fusion-consistent labelings, it has finite order $n_\mathcal{C}$. This means that $U^{n_\mathcal{C}}$ acts diagonally in the basis $\mathcal{B}_\mathcal{C}$.

Assume $\{\vartheta_k\}_{k=1}^M \subset \mathsf{MCG}_\Sigma$ generate the relation $\sim$. Setting $n = \mathsf{lcm}(n_{\vartheta_1(\mathcal{C})}, \ldots, n_{\vartheta_M(\mathcal{C})})$, we can apply Lemma 3.8 to U^n to reach the conclusion that U^n is $\sim$-trivial. Furthermore, since the number n depends only on the permutation $\vec{\pi}$, and there are only finitely many such permutations, there is a finite n_0 with the claimed property. □

Finiteness of the set of protected gates

In the following, we will ignore phase differences that are "global" to subspaces of vectors defined by the equivalence classes of $\sim$. That is, we will call two protected gates U_1 and U_2 equivalent (written $U_1 \sim U_2$) if

$$\begin{aligned} \mathbf{U}_1 &= \mathbf{\Pi}\mathbf{D}_1 \\ \mathbf{U}_2 &= \mathbf{\Pi}\mathbf{D}_2 \end{aligned} \qquad \text{and} \qquad (\mathbf{D}_2)_{\ell,\ell} = \mathrm{e}^{\mathrm{i}\varphi([\ell])}(\mathbf{D}_1)_{\ell,\ell} \,,$$

i.e., they encode the same permutation of fusion-consistent labels, and their phases only differ by a phase $\varphi([\ell])$ depending on the equivalence class $[\ell]$ that ℓ belongs to. This is equivalent to the statement that $\mathbf{U}_1^{-1}\mathbf{U}_2 = \mathbf{D}_1^{-1}\mathbf{D}_2$ acts as a phase dependent only on the equivalence class, i.e., $U_1^{-1}U_2$ is a $\sim$-trivial phase gate.

We obtain an Eastin and Knill **EastinKnill2009** type statement, which is one of our main conclusions.

Theorem 3.10 (Finite group of protected gates)**.** The number of equivalence classes of protected gates is finite.

In particular, this means that locality-preserving automorphisms on their own do not provide quantum computational universality.

Proof. Assume that there are infinitely many equivalence classes of protected gates. Then we can choose a sequence $\{U_n\}_{n\in\mathbb{N}}$ of protected gates indexed by integers and belonging to different equivalence classes each. Since the number of permutations of fusion-consistent labels is finite, there exists at least one permutation matrix $\mathbf{\Pi}$ such that there is an infinite subsequence of protected gates U_n with $\mathbf{U}_n = \mathbf{\Pi}\mathbf{D}_n$, i.e.,

they act with the same permutation. Applying the Bolzano-Weierstrass theorem to this subsequence, we conclude that there is a convergent subsequence of protected gates $\{U_{n_j}\}_{j\in\mathbb{N}}$ such that $\mathbf{U}_{n_j} = \mathbf{\Pi}\mathbf{D}_{n_j}$ for all j. Let $U = \lim_{j\to\infty} U_{n_j}$ be the corresponding limit, and let us define $\tilde{U}_j \coloneqq U^{-1}U_{n_j}$. Clearly, each $\tilde{U}_j$ is a protected gate and

$$\tilde{\boldsymbol{U}}_j = \mathbf{D}^{-1}\mathbf{D}_{n_j} \tag{3.45}$$

acts non-trivially on subspaces defined by equivalence classes, i.e., $\tilde{U}_j$ is a $\sim$-non-trivial phase gate. This is because of the assumption that the original sequence $\{U_n\}_{n\in\mathbb{N}}$ has elements belonging to different equivalence classes. Furthermore, we have that

$$\lim_{j\to\infty} \tilde{\boldsymbol{U}}_j = \mathbf{I}\,, \tag{3.46}$$

where $\mathbf{I}$ is the identity matrix.

For a mapping class group element $\vartheta \in \mathsf{MCG}_\Sigma$, the matrix expressing the action of $\tilde{U}_j$ in the basis $\mathcal{B}_{\vartheta(\mathcal{C})}$ is given by $\mathbf{V}(\vartheta)\tilde{\boldsymbol{U}}_j\mathbf{V}(\vartheta)^\dagger$. Because $\tilde{U}_j$ is a protected gate, we get

$$\mathbf{V}(\vartheta)\tilde{\boldsymbol{U}}_j\mathbf{V}(\vartheta)^\dagger = \tilde{\mathbf{\Pi}}_j\tilde{\mathbf{D}}_j \tag{3.47}$$

for some permutation matrix $\tilde{\mathbf{\Pi}}_j$ and a diagonal matrix $\tilde{\mathbf{D}}_j$ of phases. Combining (3.46), (3.47), using the unitarity of $\mathbf{V}(\vartheta)$ and continuity, we conclude that there exists some $N_0 = N_0(\vartheta)$ such that $\tilde{\mathbf{\Pi}}_j = \mathbf{I}$ for all $j \geq N_0$, i.e., $\mathbf{V}(\vartheta)\tilde{\boldsymbol{U}}_j\mathbf{V}(\vartheta)^\dagger$ is diagonal for sufficiently large j. Equivalently, for all $j \geq N_0$, $\tilde{U}_j$ acts diagonally in the basis $\mathcal{B}_{\vartheta(\mathcal{C})}$, as well as in the basis $\mathcal{B}_\mathcal{C}$ (by (3.45)).

The latter conclusion can be extended uniformly to a finite collection $\{\vartheta_k\}_{k=1}^M \subset \mathsf{MCG}_\Sigma$ of mapping class group elements: there is a constant $N = N(\vartheta_1, \ldots, \vartheta_M)$ such that for all $j \geq N$, the protected gate $\tilde{U}_j$ acts as a diagonal matrix in all bases $\mathcal{B}_\mathcal{C}$, $\mathcal{B}_{\vartheta_1(\mathcal{C})}$, ..., $\mathcal{B}_{\vartheta_M(\mathcal{C})}$. Taking a finite collection $\{\vartheta_k\}_{k=1}^M \subset \mathsf{MCG}_\Sigma$ that generates the relation $\sim$ and applying Lemma 3.8, we reach the conclusion that $\tilde{U}_j$ is a $\sim$-trivial phase gate for all $j \geq N$. This contradicts the fact that each $\tilde{U}_j$ is a $\sim$-non-trivial phase gate, as argued above. □

Necessity of restricting to equivalence classes

Here we briefly argue that without imposing $\sim$-equivalence on protected gates, one can end up with infinitely many protected gates (that are, however, not very interesting).

Concretely, consider a model such as the toric code, with local commuting projector Hamiltonian $H_{top} = -\sum_j \Pi_j$ acting on spins which we collectively denote by A. Let $\mathcal{H}_\Sigma$ be its ground space. We introduce a local spin-degree of freedom B_j associated with each term in the Hamiltonian, and let $B = \bigotimes_j B_j$ the space of these auxiliary degrees of freedom. Define an Ising-like Hamiltonian $H_I = -\sum_{\langle j,j'\rangle} Z_j Z_{j'}$ coupling all nearest neighbors in B (according to some notion). Finally, consider the following Hamiltonian:

$$H = J \cdot H_I - \sum_j \Pi_j \otimes |0\rangle\langle 0|_{B_j} - \sum_j \Pi_j \otimes |1\rangle\langle 1|_{B_j} \,. \tag{3.48}$$

This Hamiltonian is local, and for large J, has a ground space of the form

$$(\mathcal{H}_\Sigma \otimes |00\cdots 0\rangle) \oplus (\mathcal{H}_\Sigma \otimes |11\cdots 1\rangle) \,. \tag{3.49}$$

In other words, the ground space (and similarly the low-energy subspace) splits as $\mathcal{H}_\Sigma^{(0)} \oplus \mathcal{H}_\Sigma^{(1)}$ into two isomorphic copies of the space $\mathcal{H}_\Sigma$.

Now take two arbitrary protected gates $U^{(0)}, U^{(1)}$ for H_{top} (these may be global phases, i.e., trivial), implementing logical operations $\overline{U}^{(0)}$, $\overline{U}^{(1)}$. Let us assume that they are implemented by circuits acting locally, i.e., they can be written (arbitrarily – the details do not matter) in the form

$$U^{(m)} = U^{(m)}_{j_1} U^{(m)}_{j_2} \cdots U^{(m)}_{j_{M_m}}$$

with each unitary U_j local near the support of Π_j. Then we can define the unitary

$$U = \prod_{k=1}^{M_0} \left(U^{(0)}_{j_k} \otimes |0\rangle\langle 0|_{B_{j_k}} + \mathrm{id} \otimes |1\rangle\langle 1|_{B_{j_k}} \right) \prod_{k=1}^{M_1} \left(\mathrm{id} \otimes |0\rangle\langle 0|_{B_{j_k}} + U^{(1)}_{j_k} \otimes |1\rangle\langle 1|_{B_{j_k}} \right)$$

on $A \otimes B$. It is easy to check that U is a protected gate and its logical action is

$$\overline{U} = \overline{U}^{(0)} \oplus \overline{U}^{(1)} \,.$$

In particular, such a unitary can introduce an arbitrary relative phase between the "superselection" sectors $\mathcal{H}_\Sigma^{(0)}$, $\mathcal{H}_\Sigma^{(1)}$: we can choose $U^{(0)} = I$ and $U^{(1)} = e^{i\varphi} I$. The construction here corresponds to the direct sum of two TQFTs; the mapping class group representation is reducible and basis elements belonging to different sectors are inequivalent. Imposing the relation $\sim$ on the set of protected gates renders all such relative-phase gates equivalent.

A small caveat is in order here concerning the given microscopic example. The Hamiltonian (3.48) indeed has (3.49) as its ground space. However, the latter is not

an error-correcting code: whether a state belongs to $\mathcal{H}_\Sigma^{(0)}$ or $\mathcal{H}_\Sigma^{(1)}$ can be determined by a local measurement. Thus information should only be encoded in either one of the superselection sectors, and this renders the introduction of (arbitrary) relative phases between two superselection sectors computationally trivial. The example given here is mainly intended to give a concrete realization of the space (3.49) as the ground space of a local Hamiltonian, and to illustrate the fact that reducibility of the mapping class group representation has important consequences on the form of protected gates.

3.5 Global constraints from F-moves on the n-punctured sphere

We first consider the four-punctured sphere, where there are two inequivalent DAP-decompositions related by an F-move (i.e., the basis change $\mathbf{V}$ is the F-matrix). More generally (e.g., for the 5-punctured sphere), we need to consider several different F-moves and obtain a constraint of the form (3.37) for every pair of bases related by such moves. We describe such global constraints in Section 3.5. The results obtained by considering F-moves are summarized in Section 3.5: there we outline a general procedure for characterizing protected gates.

The consideration of/restriction to n-punctured spheres is motivated by the fact that they correspond to $n-1$ anyons situated on a disc. Realizing such a system appears to be more feasible experimentally than designing e.g., a higher-genus surface. For this reason, the n-punctured sphere is most commonly considered in the context of topological quantum computation. We point out, however, that our techniques immediately generalize to other (higher-genus) surfaces with or without punctures (although basis changes other than those given by the F-matrix need to be considered).

Determining phases for the four-punctured sphere: fixed boundary labels

For a four-punctured sphere Σ, we can fix the labels on the punctures to $i, j, k, l \in \mathbb{A}$. The corresponding space $\mathcal{H}_{\Sigma(i,j,k,l)}$ associated to this open surface with labeled boundary components is the fusion space V_{kl}^{ij}. (In the non-abelian case, this space can have dimension larger than 1.) We have two bases $\mathcal{B}_\mathcal{C}$, $\mathcal{B}_{\mathcal{C}'}$ of this fusion space, corresponding to two different DAP-decompositions differing by one loop (Fig. 3.4). We can enumerate basis elements by the label assigned to this loop. Let $\{|a\rangle_\mathcal{C}\}_a$ and $\{|a\rangle_{\mathcal{C}'}\}_a$ be the elements of the bases $\mathcal{B}_\mathcal{C}$ and $\mathcal{B}_{\mathcal{C}'}$, respectively. Note that a ranges over all elements consistent with the fusion rules.

For the models considered in this article, these are $N_{ij}^a = N_{kl}^a = 1$. Let $Q =$

$Q(i,j,k,l)$ be the set of such elements. The basis change is given by the F-matrix

$$|m\rangle_{\mathcal{C}'} = \sum_n F^{ijm}_{kln} \, |n\rangle_{\mathcal{C}} \, .$$

Considering a locality-preserving automorphism which preserves the boundary labels (this is reasonable if we think of them as certain boundary conditions of the system), we can apply the procedure explained above to find the action

$$U \, |a\rangle_{\mathcal{C}} = \mathrm{e}^{\mathrm{i}\varphi(a)} \left|\pi^C(a)\right\rangle_{\mathcal{C}}$$

on basis states. Here $\pi^C \colon Q \to Q$ permutes fusion-consistent labels. To apply the reasoning above, we have to use the $|Q \times Q|$-basis change matrix $\boldsymbol{V}$ defined by $\boldsymbol{V}_{m,n} = F^{ijm}_{kln}$.

Solving the consistency relation (3.37) (for the permutations π^C, $\pi^{C'}$ and phases $\{\varphi(a)\}_a, \{\varphi'(a)\}_a$) shows that for any permutation π^C that is part of a solution, the function φ takes the form

$$\varphi(a) = \eta + f(a) \, , \tag{3.50}$$

where η is a global phase and f belongs to a certain set of functions which we denote

$$\mathsf{Iso}\left(\begin{array}{ccccc} & i & & l & \\ j & | & \cdot & | & k \\ \multicolumn{5}{c}{\underline{\qquad\qquad\qquad\qquad}} \end{array} \rightarrow \begin{array}{ccccc} & i & & l & \\ j & | & \pi^C(\cdot) & | & k \\ \multicolumn{5}{c}{\underline{\qquad\qquad\qquad\qquad}} \end{array} \right) . \tag{3.51}$$

(The reason for this notation will become clearer when we discuss isomorphisms in the next section; here we are concerned with relative phases arising from automorphisms.) In summary, we have

$$\begin{aligned} U \, |a\rangle_{\mathcal{C}} \;\; &= \;\; e^{i\eta} e^{if(a)} \left|\pi^C(a)\right\rangle_{\mathcal{C}} \\ &\text{where } f \in \mathsf{Iso}\left(\begin{array}{ccccc} & i & & l & \\ j & | & \cdot & | & k \\ \multicolumn{5}{c}{\underline{\qquad\qquad\qquad\qquad}} \end{array} \rightarrow \begin{array}{ccccc} & i & & l & \\ j & | & \pi^C(\cdot) & | & k \\ \multicolumn{5}{c}{\underline{\qquad\qquad\qquad\qquad}} \end{array} \right) . \end{aligned} \tag{3.52}$$

Here the set (3.51) can be computed by solving the consistency relation

$$\boldsymbol{V}\boldsymbol{\Pi}\boldsymbol{D}(\{\varphi(a)\}_a) = \boldsymbol{\Pi}'\boldsymbol{D}(\{\varphi'(a)\}_a)\boldsymbol{V} \tag{3.53}$$

with $\boldsymbol{V}_{m,n} = F^{ijm}_{kln}$. This scenario is a special case of the commutative diagram displayed in Fig. 3.8.

Determining phases for the four-punctured sphere in general

Consider the four-punctured sphere Σ with fixed labels $i, j, k, l \in \mathbb{A}$ on the punctures. Let $\tilde{\imath}, \tilde{\jmath}, \tilde{k}, \tilde{l}$ be another set of labels such that the spaces $\mathcal{H}_{\Sigma(i,j,k,l)}$ and $\mathcal{H}_{\Sigma(\tilde{\imath},\tilde{\jmath},\tilde{k},\tilde{l})}$ are isomorphic. In this situation, we can try to characterize locality-preserving isomorphisms between two systems defined on $\Sigma(i, j, k, l)$ and $\Sigma(\tilde{\imath}, \tilde{\jmath}, \tilde{k}, \tilde{l})$, respectively. This situation is slightly more general than what we considered before (automorphisms of the same system), but it is easy to see that all arguments applied so far extend to this situation. Note that we could have phrased our whole discussion in terms of isomorphisms between different spaces. However, we chose not to do so to minimize the amount of notation required; instead, we only consider this situation in this section. This generalization for the 4-punctured sphere is all we need to treat automorphisms on higher-genus surfaces.

For $\mathcal{H}_{\Sigma(i,j,k,l)}$, we have two bases $\mathcal{B}_\mathcal{C}$, $\mathcal{B}_{\mathcal{C}'}$, corresponding to two different DAP-decompositions differing by one loop. Similarly, for $\mathcal{H}_{\Sigma(\tilde{\imath},\tilde{\jmath},\tilde{k},\tilde{l})}$, we have two bases $\tilde{\mathcal{B}}_\mathcal{C}$, $\tilde{\mathcal{B}}_{\mathcal{C}'}$, corresponding to two different DAP-decompositions differing by one loop. We can enumerate the basis elements by the label assigned to this loop. Let $\{|a\rangle_\mathcal{C}\}_a$ and $\{|a\rangle_{\mathcal{C}'}\}_a$ be the elements of the basis $\mathcal{B}_\mathcal{C}$ and $\mathcal{B}_{\mathcal{C}'}$, respectively. Here a ranges over the set $Q = Q(i, j, k, l) \subset \mathbb{A}$ of all elements consistent with the fusion rules, i.e., we must have $N_{ij}^a = N_{kl}^a = 1$. Similarly, let $\{|\tilde{a}\rangle_\mathcal{C}\}_{\tilde{a}}$ and $\{|\tilde{a}\rangle_{\mathcal{C}'}\}_{\tilde{a}}$ be the elements of the basis $\tilde{\mathcal{B}}_\mathcal{C}$ and $\tilde{\mathcal{B}}_{\mathcal{C}'}$, respectively, where now $\tilde{a} \in \tilde{Q} = Q(\tilde{\imath}, \tilde{\jmath}, \tilde{k}, \tilde{l})$.

In this situation, we have two basis changes,

$$\begin{aligned} |m\rangle_{\mathcal{C}'} &= \sum_n \boldsymbol{V}_{m,n} |n\rangle_\mathcal{C} \text{ where } \boldsymbol{V}_{m,n} = F_{kln}^{ijm}, \\ |\tilde{m}\rangle_{\mathcal{C}'} &= \sum_{\tilde{n}} \tilde{V}_{\tilde{m},\tilde{n}} |\tilde{n}\rangle_\mathcal{C} \text{ where } \tilde{\boldsymbol{V}}_{\tilde{m},\tilde{n}} = F_{\tilde{k}\tilde{l}\tilde{n}}^{\tilde{\imath}\tilde{\jmath}\tilde{m}}. \end{aligned}$$

Now consider a locality-preserving isomorphism U which takes the boundary labels (i, j, k, l) to $(\tilde{\imath}, \tilde{\jmath}, \tilde{k}, \tilde{l})$. We can then apply the framework above to find the action

$$U |a\rangle_\mathcal{C} = \mathrm{e}^{\mathrm{i}\varphi(a)} \left|\pi^C(a)\right\rangle_\mathcal{C} \qquad \text{or} \qquad U |a\rangle_{\mathcal{C}'} = \mathrm{e}^{\mathrm{i}\varphi'(a)} \left|\pi^{C'}(a)\right\rangle_{\mathcal{C}'}$$

on basis states. Here $\pi^C, \pi^{C'} \colon Q \to \tilde{Q}$ take fusion-consistent labels on $\Sigma(i, j, k, l)$ to fusion-consistent labels on $\Sigma(\tilde{\imath}, \tilde{\jmath}, \tilde{k}, \tilde{l})$. Because the spaces are isomorphic, we must have $|Q| = |\tilde{Q}|$, hence $\pi^C, \pi^{C'}$ can be represented by permutation matrices $\boldsymbol{\Pi}, \boldsymbol{\Pi}'$ in the basis pairs $(\mathcal{B}_\mathcal{C}, \tilde{\mathcal{B}}_\mathcal{C})$ or $(\mathcal{B}_{\mathcal{C}'}, \tilde{\mathcal{B}}_{\mathcal{C}'})$, respectively. Proceeding similarly with $\boldsymbol{U}$, we get the consistency equation $\tilde{V}\mathbf{U} = \mathbf{U}'\mathbf{V}$ or

$$\tilde{V}\boldsymbol{\Pi}\boldsymbol{D}(\{\varphi(a)\}_a) = \boldsymbol{\Pi}'\boldsymbol{D}(\{\varphi'(a)\}_a)\boldsymbol{V}, \tag{3.54}$$

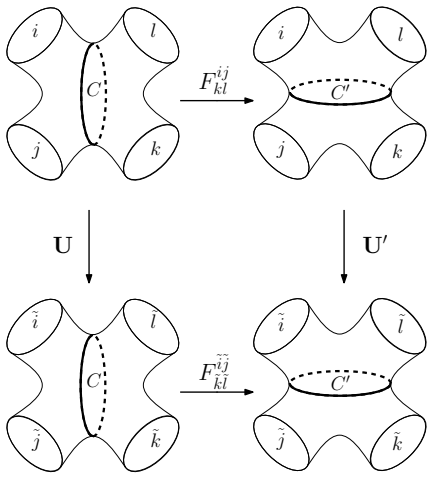

Figure 3.8: An isomorphism $\mathcal{H}_{\Sigma(i,j,k,l)} \to \mathcal{H}_{\Sigma(\tilde{\imath},\tilde{\jmath},\tilde{k},\tilde{l})}$ of two 4-punctured spheres can be given as either $\mathbf{U}$, which relates the bases $\mathcal{B}_C$ of $\mathcal{H}_{\Sigma(i,j,k,l)}$ to $\tilde{\mathcal{B}}_C$ of $\mathcal{H}_{\Sigma(\tilde{\imath},\tilde{\jmath},\tilde{k},\tilde{l})}$, or as $\mathbf{U}'$ relating different bases $\mathcal{B}_{C'}$ of $\mathcal{H}_{\Sigma(i,j,k,l)}$ to $\tilde{\mathcal{B}}_{C'}$ of $\mathcal{H}_{\Sigma(\tilde{\imath},\tilde{\jmath},\tilde{k},\tilde{l})}$. The bases of $\mathcal{H}_{\Sigma(i,j,k,l)}$ and $\mathcal{H}_{\Sigma(\tilde{\imath},\tilde{\jmath},\tilde{k},\tilde{l})}$ are related through the F-moves F^{ij}_{kl} and $F^{\tilde{\imath}\tilde{\jmath}}_{\tilde{k}\tilde{l}}$, respectively. The consistency equation (3.54) can be expressed as a commutative diagram. In the case where $\Sigma(i,j,k,l) = \Sigma(\tilde{\imath},\tilde{\jmath},\tilde{k},\tilde{l})$ have identical boundary labels such an isomorphism becomes an automorphism, and this reduces to the consistency equation (3.53).

which is expressed in the form of a commutative diagram as in Fig. 3.8. Equation (3.54) only differs from equation (3.37) in allowing boundary labels to change and the basis transformation matrix $\tilde{V}$ must change accordingly.

For a given set of boundary labels (i,j,k,l), $(\tilde{\imath},\tilde{\jmath},\tilde{k},\tilde{l})$, and a fixed choice of π^C (which fixes $\mathbf{\Pi}$), any solution $(\mathbf{\Pi}', \{\varphi(a)\}_a, \{\varphi'(a)\}_a)$ of (3.54) has phases $\{\varphi(a)\}_a$ of the "universal" form

$$\varphi(a) = \eta + f(a) \qquad \text{for all } a \in Q(i,j,k,l)\ , \tag{3.55}$$

where $\eta \in [0, 2\pi)$ is an arbitrary global phase independent of a, and f belongs to a set $\mathsf{Iso}\left(\begin{smallmatrix} & i & & l & \\ j & | & \cdot & | & k \end{smallmatrix} \to \begin{smallmatrix} & \tilde{\imath} & & \tilde{l} & \\ \tilde{\jmath} & | & \pi^C(\cdot) & | & \tilde{k} \end{smallmatrix}\right)$ of functions that can be computed from (3.54) as discussed below.

In summary, we have shown that U acts as

$$\begin{aligned} U\,|a\rangle_{\mathcal{C}} \;&=\; e^{i\eta}e^{if(a)}\,\big|\pi^C(a)\big\rangle_{\mathcal{C}} \\ &\text{with}\ \ f \in \mathsf{Iso}\left(\begin{smallmatrix} & i & & l & \\ j & | & \cdot & | & k \end{smallmatrix} \to \begin{smallmatrix} & \tilde{\imath} & & \tilde{l} & \\ \tilde{\jmath} & | & \pi^C(\cdot) & | & \tilde{k} \end{smallmatrix}\right), \end{aligned} \tag{3.56}$$

and where the latter set can be determined by solving the consistency relation (3.54).

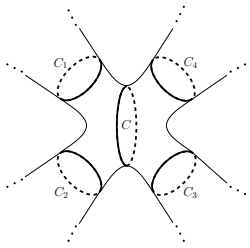

Figure 3.9: For some DAP-decomposition $\mathcal{C}$ of a surface Σ, a curve $C \in \mathcal{C}$ is considered internal if its neighbors $N(C) = \{C_1, C_2, C_3, C_4\}$ define the boundaries of a 4-punctured sphere.

Localization of phases for higher-genus surfaces

We now argue that the phases appearing in Eq. (3.31) of Proposition 3.3.2 also factorize into certain essentially local terms, similar to how the overall permutation $\vec{\pi}$ of fusion-consistent labelings decomposes into a collection $\vec{\pi} = \{\pi^C\}_{C\in\mathcal{C}}$ of permutations of labels. More precisely, we will argue that conclusion (3.57) can be extended to more general surfaces.

Consider a fixed DAP-decomposition $\mathcal{C}$ of Σ. We call a curve $C \in \mathcal{C}$ *internal* if the intersection of Σ with a ball containing C has the form of a 4-punctured sphere with boundary components C_1, C_2, C_3, C_4 consisting of curves 'neighboring' C in the DAP decomposition. We call $N(C) = \{C_1, C_2, C_3, C_4\}$ the neighbors (or neighborhood) of C as illustrated in Fig. 3.9. Key to the following observations is that a basis vector $|\ell\rangle$ whose restriction to these neighbors is given by $\ell \restriction N(C) = \big(\ell(C_1), \ldots, \ell(C_4)\big)$ gets mapped under U to a vector proportional to $|\vec{\pi}(\ell)\rangle$, which assigns the labels $\vec{\pi}(\ell) \restriction N(C) = \big(\pi^{C_1}[\ell(C_1)], \ldots, \pi^{C_4}[\ell(C_4)]\big)$ to the same curves. This means that the restriction of U to this subspace satisfies similar consistency conditions as the isomorphisms between Hilbert spaces associated with the 4-punctured spheres $\Sigma(\ell \restriction N(C))$ and $\Sigma\big(\vec{\pi}(\ell) \restriction N(C)\big)$ studied in Section 3.5. In particular, for a fixed labeling ℓ the dependence of the phase $\varphi(\ell)$ on the label $\ell(C)$ is given by a function from the set $\mathsf{Iso}\left(\underline{j \mid \cdot \mid k}^{\,i \quad l} \to \underline{\tilde{\jmath} \mid \pi^C(\cdot) \mid \tilde{k}}^{\,\tilde{\imath} \quad \tilde{l}}\right)$, where $(i, j, k, l) = \ell \restriction N(C)$ and $(\tilde{\imath}, \tilde{\jmath}, \tilde{k}, \tilde{l}) = \vec{\pi}(\ell) \restriction N(C)$. In the following, we simply write $\mathsf{Iso}\left(\ell \restriction N(C) \overset{\pi^C}{\to} \vec{\pi}(\ell) \restriction N(C)\right)$ for this set.

Proposition 3.5.1 (Localization of internal phases)**.** Let U be a locality-preserving automorphism. Let $\mathcal{C}$ be a DAP-decomposition of Σ, and let $\vec{\pi} = \{\pi^C\}_{C\in\mathcal{C}}$ be the family of permutations defined by Proposition 3.3.1. Let $\varphi(\ell)$ for $\ell \in \mathsf{L}(\mathcal{C})$ be

defined by (3.31). If $C \in \mathcal{C}$ is internal, then

$$\varphi(\ell) = \eta(\ell\restriction \mathcal{C}\backslash\{C\}) + f_{\vec{\pi}\restriction N(C)}(\ell \restriction N(C), \ell(C))$$

for some functions η and f. Furthermore, we have

$$f_{\vec{\pi}\restriction N(C)}(\ell \restriction N(C), \cdot) \in \mathsf{Iso}\left(\ell \restriction N(C) \stackrel{\pi^C}{\to} \vec{\pi}(\ell) \restriction N(C)\right) .$$

In particular, the dependence of $\varphi(\ell)$ on $\ell(C)$ is "local" and "controlled" by the labeling $\ell \restriction N(C)$ of the neighbors.

In other words, if we fix a family of permutations $\vec{\pi}$, and the labels on the neighbors $N(C)$, then the dependence on the label $\ell(C)$ of the internal edge is essentially fixed.

Proof. We will focus our attention on the subspace $\mathcal{H}_{(i,j,k,l,\star)} \subseteq \mathcal{H}_\Sigma$ spanned by labelings ℓ with

$$(\ell(C_1), \ell(C_2), \ell(C_3), \ell(C_4)) = (i,j,k,l), \tag{3.57}$$

$$\ell \restriction \mathcal{C}\backslash\{C, C_1, C_2, C_3, C_4\} = \star, \tag{3.58}$$

fixed (arbitrarily). For the purpose of this proof, it will be convenient to represent basis vectors $|\ell\rangle$ associated with such a labeling $\ell \in \mathsf{L}(C)$ as a vector

$$|\ell\rangle = |\ell(C), \ell(C_1), \ell(C_2), \ell(C_3), \ell(C_4), \star\rangle = |a,i,j,k,l,\star\rangle \ .$$

Defining $\tilde{\imath} = \pi^{C_1}(i)$, $\tilde{\jmath} = \pi^{C_2}(j)$, $\tilde{k} = \pi^{C_3}(k)$, $\tilde{l} = \pi^{C_4}(l)$, we can rewrite (3.31) in the form

$$U\,|a,i,j,k,l,\star\rangle = \mathrm{e}^{\mathrm{i}\varphi(a,i,j,k,l,\star)}\left|\pi^C(a), \tilde{\imath}, \tilde{\jmath}, \tilde{k}, \tilde{l}, \tilde{\star}\right\rangle \ ,$$

where $\tilde{\star} = \vec{\pi}_\restriction(\star)$ for some map $\vec{\pi}_\restriction$ taking labelings of the set $\mathcal{C}\backslash\{C, C_1, C_2, C_3, C_4\}$ consistent with (i,j,k,l) to those consistent with $(\tilde{\imath}, \tilde{\jmath}, \tilde{k}, \tilde{l})$. We conclude that the restriction of U to $\mathcal{H}_{(i,j,k,l,\star)}$ implements an isomorphism $\mathcal{H}_{(i,j,k,l,\star)} \cong \mathcal{H}_{(\tilde{\imath},\tilde{\jmath},\tilde{k},\tilde{l},\tilde{\star})}$. Since these spaces are isomorphic to $\mathcal{H}_{\Sigma(i,j,k,l)}$ and $\mathcal{H}_{\Sigma(\tilde{\imath},\tilde{\jmath},\tilde{k},\tilde{l})}$, respectively, we can apply the result of Section 3.5. Indeed, the consistency relation imposed by the F-move is entirely local, not affecting labels associated with curves not belonging to $\{C, C_1, C_2, C_3, C_4\}$. We conclude from (3.57) that

$$\varphi(a,i,j,k,l,\star) = \eta(i,j,k,l,\star) + f(a),$$
$$\text{where } f \in \mathsf{Iso}\left(\underline{j \;\; i \;\; . \;\; l \;\; k} \;\to\; \underline{\tilde{\jmath} \;\; \tilde{\imath} \;\; \pi^C(\cdot) \;\; \tilde{l} \;\; \tilde{k}} \right).$$

Since $(a,i,j,k,l,\star)$ were arbitrary, this proves the claim. □

For example, for $S^2(z^{N+3})$ (as described above), we can apply Proposition 3.5.1 to the j-th internal edge C_j to obtain

$$\varphi(x) = \eta_j(x_1, \ldots, \widehat{x}_j, \ldots, x_N) + f_j(x_{j-1}, x_j, x_{j+1}), \tag{3.59}$$

where

$$f_j(x_{j-1}, \cdot, x_{j+1}) \in \mathsf{Iso}\left(\underline{\overset{z}{x_{j-1}} \quad \cdot \quad \overset{z}{x_{j+1}}} \to \underline{\overset{z}{\tilde{x}_{j-1}} \; \pi^{C_j}(\cdot) \; \overset{z}{\tilde{x}_{j+1}}} \right),$$

and

$$\tilde{x}_{j-1} = \pi^{C_{j-1}}(x_{j-1}), \qquad \tilde{x}_{j+1} = \pi^{C_{j+1}}(x_{j+1}).$$

Here, we use $\hat{x}_j$ to indicate that this argument is omitted.

Characterizing protected gates on the M-punctured sphere using F-moves

The results in this section give the following procedure for characterizing protected gates associated with $\mathcal{H}_{S^2(z^M)}$, the Hilbert space of $M = N+3$ anyons of type z. We know from Proposition 3.3.2 that the action $U|\ell\rangle = \mathrm{e}^{\mathrm{i}\varphi(\ell)}|\vec{\pi}(\ell)\rangle$ on fusion-consistent labelings is parametrized by certain families $\vec{\pi} = \{\pi^C\}_{C\in\mathcal{C}}$ of permutations, as well as a function φ describing the phase-dependence. To characterize the latter, we

(i) determine the set of allowed 'local' permutations π^C and associated phases f for any occuring internal curve C. This amounts to solving the consistency equation (3.54) for the four-punctured sphere, with appropriate boundary labels. For the standard pants decomposition of the $N+3$-punctured sphere, this means finding all pairs

$$\left(\pi^{C_j}, f_j\right) \quad \text{where } f_j \in \mathsf{Iso}\left(\underline{\overset{z}{x_{j-1}} \quad \cdot \quad \overset{z}{x_{j+1}}} \to \underline{\overset{z}{\tilde{x}_{j-1}} \; \pi^{C_j}(\cdot) \; \overset{z}{\tilde{x}_{j+1}}} \right).$$

These correspond to isomorphisms between the Hilbert spaces associated with the labeled surfaces $S^2(z, x_{j-1}, x_{j+1}, z)$ and $S^2(z, \tilde{x}_{j-1}, \tilde{x}_{j+1}, z)$, where $x_{j-1}, \tilde{x}_{j-1} \in Q(j-1), x_{j+1}, \tilde{x}_{j+1} \in Q(j+1)$.

(ii) we constrain the family $\vec{\pi} = \{\pi^C\}_{C\in\mathcal{C}}$ of allowed permutations by using the global constraints arising from fusion rules and gluing (Proposition 3.3.3). In the case of $N+3$ Fibonacci anyons on the sphere with standard pants decomposition $\mathcal{C}$, dimensional arguments show that all $\pi^{C_j} = \mathrm{id}$ are equal to the identity permutation. For Ising anyons, the fusion rules imply that every permutation with even index is equal to the identity permutation, $\pi^{C_{2j}} = \mathrm{id}$ (in fact, there is only a single allowed label).

(iii) we determine the phases $\varphi(\ell)$ by using the localization property of Proposition 3.5.1 for internal curves C. For $N+3$ anyons of type z on the sphere, this results in the consistency conditions

$$\varphi(x) = \eta_j(x_1, \dots, \widehat{x}_j, \dots, x_N) + f_j(x_{j-1}, x_j, x_{j+1}) \qquad \text{where}$$
$$f_j(x_{j-1}, \cdot, x_{j+1}) \in \mathsf{Iso}\left(\underline{x_{j-1}\overset{z}{|} \quad \cdot \quad \overset{z}{|} x_{j+1}} \to \underline{\tilde{x}_{j-1}\overset{z}{|} \pi^{C_j}(\cdot) \overset{z}{|} \tilde{x}_{j+1}} \right)$$
$$\text{for } j = 1, \dots, N\,. \tag{3.60}$$

In Section 3.6, we apply this procedure to Ising anyons; in this case, the system of equations (3.60) can be solved explicitly.

3.6 The Fibonacci and Ising models

In what follows, we apply the results of the previous sections to the Fibonacci and Ising models. These can be considered as representative examples of non-abelian anyon models. We illustrate the use of the developed constraints in different scenarios:

In Section 3.6, we show that there is no non-trivial gate for the Fibonacci model on the torus. This derivation uses the characterization of protected gates in terms of matrices intertwining with the mapping class group representation obtained in Section 3.4. Note that we cannot apply Corollary 3.7 because the representation of the mapping class group on the torus is finite for the Fibonacci model.

In Section 3.6, we then consider a system with M Fibonacci anyons (where $M \geq 4$ so that the space $\mathcal{H}_{S^2(\tau^M)}$ has non-zero dimension). We establish the following statement:

Theorem 3.11 (Fibonacci anyon model)**.** For $M \geq 4$, any locality-preserving automorphism U on the M-punctured sphere $S^2(\tau^M)$ is trivial (i.e., proportional to the identity).

This proof is a direct consequence of Corollary 3.7 and the known density of braiding Michael H. Freedman, Larsen, and Zhenghan Wang, 2002; Michael H. Freedman, Alexei Kitaev, et al., 2003. We additionally provide an independent proof not relying on this result.

Finally, we consider systems with M Ising anyons; the associated Hilbert space $\mathcal{H}_{S^2(\sigma^M)}$ has non-zero dimension if and only if $M \geq 4$ is even. In this case, there is a natural

isomorphism $\mathcal{H}_{S^2(\sigma^M)} \cong (\mathbb{C}^2)^{\otimes M/2-1}$ (described below, see Eq. (3.66)). Defining the $(M/2-1)$-qubit Pauli group on the latter space in the usual way, we get the following statement:

Theorem 3.12 (Ising anyon model)**.** Any locality-preserving automorphism U of $S^2(\sigma^M)$, where $M \geq 4$ is even, belongs to the $(M/2-1)$-qubit Pauli group.

Our derivation of this result relies on the use of F-moves, as discussed in Section 3.5.

The Fibonacci model

For the Fibonacci model, we have $\mathbb{A} = \{1, \tau\}$ and the only non-trivial fusion rule is $\tau \times \tau = 1 + \tau$ with $d_\tau = \phi = (1+\sqrt{5})/2$.

On the torus

We first consider the torus Σ and show that every protected gate is trivial. We do so by computing some of the sets Δ_ϑ, $\vartheta \in \mathsf{MCG}_\Sigma$ defined in Section 3.4. Recall (see Section 3.2) that the mapping class group of the torus is generated by two elements s, t.

The matrix $\mathbf{V}(s) = S$ representing s is the usual S-matrix (expressed with respect to the ordering $(1, \tau)$)

$$S = \frac{1}{\sqrt{\phi+2}} \begin{pmatrix} 1 & \phi \\ \phi & -1 \end{pmatrix}.$$

In particular, the consistency condition (3.39) becomes

$$S\mathbf{\Pi}\mathbf{D}S^{-1} \in \Delta,$$

In particular, the consistency condition (3.39) becomes

$$S\mathbf{\Pi}\mathbf{D}S^{-1} \in \Delta,$$

where $\mathbf{D} = \mathrm{diag}(\lambda_1, \lambda_\tau)$ and $\lambda_a \in \mathrm{U}(1)$. We consider the two cases:

1. For $\mathbf{\Pi} = I$, we get (using $\phi^2 = \phi + 1$)

$$S\mathbf{\Pi}\mathbf{D}S^{-1} = \frac{1}{\phi+2} \begin{pmatrix} \lambda_1 + \lambda_\tau(\phi+1) & (\lambda_1 - \lambda_\tau)\phi \\ (\lambda_1 - \lambda_\tau)\phi & \lambda_1(\phi+1) + \lambda_\tau \end{pmatrix}.$$

   For this to be a unitary monomial matrix, all entries must have modulus 0 or 1. Since $\phi/(\phi+2) < 1/2$, the off-diagonal elements always have modulus

less than 1, and hence must be zero. That is, we must have $\lambda_1 = \lambda_\tau =: \lambda$, and it follows that the right hand side is in Δ. This implies that $\mathbf{\Pi D} = \lambda I$.

2. For $\mathbf{\Pi} = \begin{pmatrix} 0 & 1 \\ 1 & 0 \end{pmatrix}$, we get

$$S\mathbf{\Pi D}S^{-1} = \frac{1}{\phi+2}\begin{pmatrix} (\lambda_1+\lambda_\tau)\phi & \lambda_1(\phi+1)-\lambda_\tau \\ \lambda_\tau(\phi+1)-\lambda_1 & -(\lambda_1+\lambda_\tau)\phi \end{pmatrix}.$$

To have the absolute value of the first entry equal to 0 (see above), we must have $\lambda_\tau = -\lambda_1$ and we get

$$S\mathbf{\Pi D}S^{-1} = \lambda_1\begin{pmatrix} 0 & 1 \\ -1 & 0 \end{pmatrix},$$

which is a unitary monomial matrix. That is, we have $\mathbf{\Pi D} = \lambda\begin{pmatrix} 0 & 1 \\ -1 & 0 \end{pmatrix}$.

Summarizing, we conclude that

$$\Delta_s = \left\{ \lambda I, \lambda\begin{pmatrix} 0 & 1 \\ -1 & 0 \end{pmatrix} \;\middle|\; \lambda \in \mathrm{U}(1) \right\}. \tag{3.61}$$

The element $t \in \mathsf{MCG}_\Sigma$ defined by twisting along one of the homologically non-trivial cycles is represented by the matrix $\mathbf{V}(t) = T = \mathrm{diag}(1, e^{4\pi i/5})$. We consider the consistency condition (3.39) for the composition $st \in \mathsf{MCG}_\Sigma$:

$$(ST)\mathbf{\Pi D}(ST)^{-1} \in \Delta,$$

where $\mathbf{D} = \mathrm{diag}(\lambda_1, \lambda_\tau)$ and $\lambda_a \in \mathrm{U}(1)$. Again, we consider the following two cases:

1. For $\mathbf{\Pi} = I$, we get

$$(ST)\mathbf{\Pi D}(ST)^{-1} = \frac{1}{\phi+2}\begin{pmatrix} \lambda_1+\lambda_\tau(\phi+1) & (\lambda_1-\lambda_\tau)\phi \\ (\lambda_1-\lambda_\tau)\phi & \lambda_1(\phi+1)+\lambda_\tau \end{pmatrix}.$$

This is identical to the first case above, thus $\mathbf{\Pi D} = \lambda I$.

2. For $\mathbf{\Pi} = \begin{pmatrix} 0 & 1 \\ 1 & 0 \end{pmatrix}$, we get

$$(ST)\mathbf{\Pi}\mathbf{D}(ST)^{-1} = \frac{\zeta}{\phi+2}\begin{pmatrix} (\zeta^3\lambda_1 - \lambda_\tau)\phi & \zeta^3\lambda_1(\phi+1) + \lambda_\tau \\ -\zeta^3\lambda_1 - \lambda_\tau(\phi+1) & -(\zeta^3\lambda_1 - \lambda_\tau)\phi \end{pmatrix},$$

where $\zeta = \mathrm{e}^{\mathrm{i}\pi/5}$. Since $\phi/(\phi+2) < 1/2$, the diagonal elements must vanish, that is, we have $\lambda_\tau = \zeta^3\lambda_1$. This indeed then gives an element of Δ, and $\mathbf{\Pi}\mathbf{D} = \lambda\begin{pmatrix} 0 & \mathrm{e}^{3\pi\mathrm{i}/5} \\ 1 & 0 \end{pmatrix}$.

In summary, we have shown that

$$\Delta_{st} = \left\{ \lambda I, \lambda \begin{pmatrix} 0 & \mathrm{e}^{3\pi\mathrm{i}/5} \\ 1 & 0 \end{pmatrix} \;\middle|\; \lambda \in \mathrm{U}(1) \right\}. \tag{3.62}$$

Combining (3.61) and (3.62), we conclude that

$$\Delta_s \cap \Delta_{st} = \{\lambda I \mid \lambda \in \mathrm{U}(1)\},$$

and this means that $\Delta_{\mathsf{MCG}_\Sigma} \subset \Delta_s \cap \Delta_{st} = \{\lambda I \mid \lambda \in \mathrm{U}(1)\}$. According to Theorem 3.6, this implies that there is no non-trivial protected gate on the torus.

Note that this conclusion is consistent with the form of a Dehn twist, given by the logical unitary $U = \mathrm{diag}(1, e^{4\pi i/5})$ (with the 'topological' phases or twists on the diagonal): Dehn twists do *not* preserve locality! For example, for a Dehn twist along C_1, an operator supported on C_2 may end up with support in the neighborhood of the union $C_1 \cup C_2$ under conjugation by the unitary realizing the Dehn twist.

On the M-punctured sphere

We now provide a proof of Theorem 3.11. As already mentioned, braiding of $M \geq 4$ Fibonacci anyons is known to be universal Michael H. Freedman, Larsen, and Zhenghan Wang, 2002; Michael H. Freedman, Alexei Kitaev, et al., 2003, hence we could invoke Corollary 3.7. Instead, we give a different proof by exploiting the equivalence relation introduced in Section 3.4 and analyzing the dimension of the associated spaces (i.e., using the constraints arising from the gluing axiom, see Section 3.3).

Consider the M-punctured sphere $\Sigma = S^2(\tau^M)$ corresponding to M Fibonacci anyons. We will use as our 'standard' basis the one arising from the standard DAP decomposition $\mathcal{C}$ of the M-punctured sphere introduced in Section 3.2 (see Fig. 3.5). We then have the following statement:

Lemma 3.13. There is only one equivalence class under the relation $\sim$. Furthermore, the set of braids $\{\sigma_j\}_{j=1}^{M-1}$ generates the relation $\sim$.

Proof. Let x and x' be two fusion-consistent labelings that are related by interchanging $\tau = x_j$ and $1 = x'_j$ (or vice versa) in the j-th entry (but are otherwise the same). Fusion-consistency implies that $x_{j-1} = x'_{j-1} = x_{j+1} = x'_{j+1} = \tau$. In particular, the relevant braid matrix describing the action of $V(\sigma_j)$ is $B(\tau, \tau)$ which has non-zero entries everywhere. We conclude that

$$\langle x'|V(\sigma_j)|x\rangle \neq 0 \qquad \text{and} \qquad \langle x'|V(\sigma_j)|x'\rangle \neq 0\,.$$

This implies that $x \Leftrightarrow_{\sigma_j} x'$. Since any fusion-consistent labeling can be obtained from the sequence $\tau^N = (\tau, \ldots, \tau)$ by such interchanges, we conclude that any two fusion-consistent labelings are equivalent. That is, there is only one equivalence class under $\sim$. □

We will now argue that the conditions of Lemma 3.8 (ii) apply in this situation: that is, any protected gate U acts diagonally in any of the bases $\mathcal{B}_{\sigma_j(\mathcal{C})}$ obtained from the standard DAP-decomposition by applying a braid group generator σ_j. In fact, we will argue more generally that U acts diagonally in any basis defined by a DAP-decomposition.

To do so, consider first the standard DAP-decomposition and the spaces $\mathcal{H}_{\Sigma'_j(a,a)}$ for $j \in \{1, \ldots, M-3\}$ and $a \in \{1, \tau\}$ (cf. (3.21)), where Σ'_j is obtained from Σ by cutting along the curve C_j which leaves a $j+2$-punctured and a $(M-j)$-punctured sphere, respectively. Note that τ is its own antiparticle ($\overline{\tau} = \tau$), and hence it suffices to consider $\Sigma'_j(\tau, \tau)$ and $\Sigma'_j(1, 1)$. Our goal is to identify pairs $(a, \tilde{a})$ such that $\mathcal{H}_{\Sigma'_j(a,a)} \cong \mathcal{H}_{\Sigma'_j(\tilde{a},\tilde{a})}$ are isomorphic, this being a necessary condition for a permutation satisfying $\pi^{C_j}(a) = \tilde{a}$ (see Proposition (3.3.3) and Eq. (3.35)). To compute $\dim \mathcal{H}_{\Sigma'_j(a,a)}$ for $a \in \{1, \tau\}$, we make use of the general fact that $\dim \mathcal{H}_{S^2(\tau^M)} = \Phi_{M-1}$ where Φ_M denotes the M-th Fibonacci number, starting with $\Phi_0 = 0$ and $\Phi_1 = 1$ and satisfying the recurrence relation $\Phi_{M+1} = \Phi_M + \Phi_{M-1}$. From (3.21), we obtain $\dim \mathcal{H}_{\Sigma'_j(1,1)} = \Phi_j \Phi_{M-j-2}$ and $\dim \mathcal{H}_{\Sigma'_j(\tau,\tau)} = \Phi_{j+1}\Phi_{M-j-1}$, excluding the case $j = 1 = M-3$ which satisfies $\dim \mathcal{H}_{\Sigma'_1(1,1)} = \Phi_1 \Phi_{M-3} = \dim \mathcal{H}_{\Sigma'_{M-3}(1,1)}$ and $\dim \mathcal{H}_{\Sigma'_1(\tau,\tau)} = \Phi_2 \Phi_{M-2} = \dim \mathcal{H}_{\Sigma'_{M-3}(\tau,\tau)}$, it follows from the monotonicity and positivity of Φ that

$$\dim \mathcal{H}_{\Sigma'_j(1,1)} < \dim \mathcal{H}_{\Sigma'_j(\tau,\tau)} \qquad \text{for } M > 4, \text{ and all } j \in \{1, ..., M-3\}. \quad (3.63)$$

Hence, according to the consistency condition (3.35), for $M > 4$, we only get an isomorphism $\mathcal{H}_{\Sigma'(a,\bar{a})} \cong \mathcal{H}_{\Sigma'(\pi^C(a),\overline{\pi^C(a)})}$ with $\pi^C = \mathrm{id}$ being trivial for any internal loop C in a standard DAP decomposition. This shows that a protected gate acts diagonally in the standard basis.

Observe that this argument only involved the dimensions of the fusion spaces obtained by cutting along a curve C_j in the pants decomposition. Since it is generally true that cutting along a curve will decompose the M-punctured sphere into an $j+2$-punctured and a $(M-j)$-punctured sphere, respectively (for some j), the argument extends to arbitrary DAP-decompositions. In particular, U is diagonal with respect to each of the bases $\mathcal{B}_{\sigma_j(\mathcal{C})}$, as claimed.

We have shown that the conditions of Lemma 3.8 apply. With Lemma 3.13, Theorem 3.11 is immediate.

The Ising model

The Ising anyon model has label set $\mathbb{A} = \{1, \psi, \sigma\}$ and non-trivial fusion rules

$$\psi \times \psi = 1, \;\; \psi \times \sigma = \sigma, \;\; \sigma \times \sigma = 1 + \psi.$$

On the 4-punctured sphere

Consider the possible spaces $\mathcal{H}_{S^2(\sigma,j,k,\sigma)}$ for $\{j,k\} \in \mathbb{A}$, and observe that fusion consistency implies

$$\dim \mathcal{H}_{S^2(\sigma,j,k,\sigma)} = \begin{cases} 0 \text{ if } j \neq k = \sigma \text{ or } k \neq j = \sigma \\ 1 \text{ if } j,k \in \{1,\psi\}, \\ 2 \text{ if } j = k = \sigma. \end{cases}$$

Therefore, the only nontrivial case to consider is $\mathcal{H}_{S^2(\sigma,\sigma,\sigma,\sigma)} = \mathcal{H}_{S^2(\sigma^4)}$ with an ordered basis $\{|1\rangle, |\psi\rangle\}$. A locality-preserving automorphism of $\mathcal{H}_{S^2(\sigma^4)}$ will act as

$$U|a\rangle = e^{i\eta} e^{if(a)} \left|\pi^C(a)\right\rangle$$

where $f \in \mathsf{Iso}\left(\underline{\sigma \;\overset{\sigma}{|}\; \cdot \;\overset{\sigma}{|}\; \sigma} \;\to\; \underline{\sigma \;\overset{\sigma}{|}\; \pi^C(\cdot) \;\overset{\sigma}{|}\; \sigma} \right)$

A valid permutation π^C of $\{1,\psi\}$ that defines the action of U, and the set of phases can be determined as follows. Let $\mathcal{B}_{\mathcal{C}} = \{|1\rangle_{\mathcal{C}}, |\psi\rangle_{\mathcal{C}}\}$ and $\mathcal{B}_{\mathcal{C}'} = \{|1\rangle_{\mathcal{C}'}, |\psi\rangle_{\mathcal{C}'}\}$ be corresponding ordered bases of $\mathcal{H}_{S^2(\sigma^4)}$ for the two DAP-decomposition $\mathcal{C}$ and $\mathcal{C}'$,

respectively. The F-matrix relating these two bases is given in the ordered basis $\mathcal{B}_\mathcal{C}$ as

$$F = \frac{1}{\sqrt{2}} \begin{pmatrix} 1 & 1 \\ 1 & -1 \end{pmatrix}.$$

Now consider some locality-preserving automorphism U expressed in the bases $\mathcal{B}_\mathcal{C}$ and $\mathcal{B}_{\mathcal{C}'}$ as $\mathbf{U} = \mathbf{\Pi}\mathbf{D}$ and $\mathbf{U}' = \mathbf{\Pi}'\mathbf{D}'$ respectively, for some 2×2 permutation matrices $\mathbf{\Pi}, \mathbf{\Pi}'$ and diagonal matrices $\mathbf{D} = \mathrm{diag}(\lambda_1, \lambda_\psi)$ and $\mathbf{D}' = \mathrm{diag}(\lambda'_1, \lambda'_\psi)$ with phases $\lambda_a, \lambda'_a \in \mathrm{U}(1)$. Then the consistency relation takes the form $\mathbf{U}' = F\mathbf{U}F^{-1}$. Next, we find all consistent solutions for a given permutation $\mathbf{\Pi}$.

1. For $\mathbf{\Pi} = I$, we get

$$F\mathbf{\Pi}\mathbf{D}F^{-1} = \frac{1}{2} \begin{pmatrix} \lambda_1 + \lambda_\psi & \lambda_1 - \lambda_\psi \\ \lambda_1 - \lambda_\psi & \lambda_1 + \lambda_\psi \end{pmatrix} = \mathbf{\Pi}'\mathbf{D}'. \tag{3.64}$$

   Suppose that $\mathbf{\Pi}' = I$. Then the consistency relation (3.64) becomes

$$\frac{1}{2} \begin{pmatrix} \lambda_1 + \lambda_\psi & \lambda_1 - \lambda_\psi \\ \lambda_1 - \lambda_\psi & \lambda_1 + \lambda_\psi \end{pmatrix} = \begin{pmatrix} \lambda'_1 & 0 \\ 0 & \lambda'_\psi \end{pmatrix},$$

   which implies $\lambda_1 = \lambda_\psi = \lambda'_1 = \lambda'_\psi =: \mathrm{e}^{\mathrm{i}\eta}$. Therefore U expressed in the basis $\mathcal{B}_\mathcal{C}$ is trivial up to a global phase:

$$\mathbf{U} = \mathrm{e}^{\mathrm{i}\eta} I.$$

   Suppose instead that $\mathbf{\Pi}' = \begin{pmatrix} 0 & 1 \\ 1 & 0 \end{pmatrix}$. The consistency relation (3.64) then becomes

$$\frac{1}{2} \begin{pmatrix} \lambda_1 + \lambda_\psi & \lambda_1 - \lambda_\psi \\ \lambda_1 - \lambda_\psi & \lambda_1 + \lambda_\psi \end{pmatrix} = \begin{pmatrix} 0 & \lambda'_\psi \\ \lambda'_1 & 0 \end{pmatrix},$$

   which implies $\lambda_1 = -\lambda_\psi$ and $\lambda'_1 = \lambda'_\psi = \lambda_1$. Setting $\mathrm{e}^{\mathrm{i}\eta} \coloneqq \lambda_1$, implies that U expressed in the basis $\mathcal{B}_\mathcal{C}$ is given by

$$\mathbf{U} = \mathrm{e}^{\mathrm{i}\eta} \begin{pmatrix} 1 & 0 \\ 0 & -1 \end{pmatrix}.$$

   These two solutions of the consistency relation, for the case $\mathbf{\Pi} = I$, now determine the only two functions of the set

$$\mathsf{Iso}\left(\underline{\sigma \overset{\sigma}{|} \cdot \overset{\sigma}{|} \sigma} \to \underline{\sigma \overset{\sigma}{|} \mathrm{id}(\cdot) \overset{\sigma}{|} \sigma} \right) = \{(f(1), f(\psi))\} = \{(0,0), (0,\pi)\}.$$

2. For $\mathbf{\Pi} = \begin{pmatrix} 0 & 1 \\ 1 & 0 \end{pmatrix}$, corresponding to the transposition $(\psi, 1)$, we get

$$F\mathbf{\Pi}\mathbf{D}F^{-1} = \frac{1}{2}\begin{pmatrix} \lambda_1 + \lambda_\psi & \lambda_1 - \lambda_\psi \\ -\lambda_1 + \lambda_\psi & -\lambda_1 - \lambda_\psi \end{pmatrix} = \mathbf{\Pi}'\mathbf{D}'. \tag{3.65}$$

By taking $\mathbf{\Pi}' = I$, this becomes

$$\frac{1}{2}\begin{pmatrix} \lambda_1 + \lambda_\psi & \lambda_1 - \lambda_\psi \\ -\lambda_1 + \lambda_\psi & -\lambda_1 - \lambda_\psi \end{pmatrix} = \begin{pmatrix} \lambda_1' & 0 \\ 0 & \lambda_\psi' \end{pmatrix},$$

which implies $\lambda_1 = \lambda_\psi = \lambda_1' = -\lambda_\psi'$. Letting $\mathrm{e}^{\mathrm{i}\eta} \coloneqq \lambda_1$ allows U to be expressed in the basis $\mathcal{B}_\mathcal{C}$ by

$$\mathbf{U} = \mathrm{e}^{\mathrm{i}\eta}\begin{pmatrix} 0 & 1 \\ 1 & 0 \end{pmatrix}.$$

Instead, suppose now that $\mathbf{\Pi}' = \begin{pmatrix} 0 & 1 \\ 1 & 0 \end{pmatrix}$. Then the consistency relation (3.65) is of the form

$$\frac{1}{2}\begin{pmatrix} \lambda_1 + \lambda_\psi & \lambda_1 - \lambda_\psi \\ -\lambda_1 + \lambda_\psi & -\lambda_1 - \lambda_\psi \end{pmatrix} = \begin{pmatrix} 0 & \lambda_\psi' \\ \lambda_1' & 0 \end{pmatrix},$$

implying that $\lambda_1 = -\lambda_\psi = -\lambda_1' = \lambda_\psi'$. Let $\mathrm{e}^{\mathrm{i}\eta} \coloneqq \lambda_1$, then this shows that U expressed in the basis $\mathcal{B}_\mathcal{C}$ is given by

$$\mathbf{U} = \mathrm{e}^{\mathrm{i}\eta}\begin{pmatrix} 0 & -1 \\ 1 & 0 \end{pmatrix}.$$

Furthermore, these two solutions completely determine the relevant set of functions (which happens to be the same as the previous case for $\mathbf{\Pi} = I$):

$$\mathsf{Iso}\left(\underline{\sigma \overset{\sigma}{\mid} \cdot \overset{\sigma}{\mid} \sigma} \to \underline{\sigma \overset{\sigma}{\mid} (\psi,1)(\cdot) \overset{\sigma}{\mid} \sigma}\right) = \{(f(1), f(\psi))\} = \{(0,0),(0,\pi)\}.$$

By denoting the single qubit (logical) Pauli group as

$$\mathcal{P} \coloneqq \left\{\lambda\begin{pmatrix} 1 & 0 \\ 0 & 1 \end{pmatrix}, \lambda\begin{pmatrix} 1 & 0 \\ 0 & -1 \end{pmatrix}, \lambda\begin{pmatrix} 0 & 1 \\ 1 & 0 \end{pmatrix}, \lambda\begin{pmatrix} 0 & -\mathrm{i} \\ \mathrm{i} & 0 \end{pmatrix} \;\middle|\; \lambda \in \mathrm{U}(1)\right\},$$

these results can be summarized as follows: If U is a locality-preserving automorphism of the fusion space $\mathcal{H}_{S^2(\sigma^4)}$ of the 4-punctured sphere, then U expressed in the basis $\mathcal{B}_\mathcal{C}$ is in $\mathcal{P}$.

On the M-punctured sphere

Let $M \geq 4$ and consider the $M = N+3$-punctured sphere $S^2(\sigma^M)$ and corresponding space $\mathcal{H}_{S^2(\sigma^M)}$. For the 'standard' DAP-decomposition $\mathcal{C}$ of $S^2(\sigma^M)$, a consistent labeling $\mathsf{L}(\mathcal{C})$ corresponds to a sequence $\big(\ell(C_1), \ldots, \ell(C_N)\big) =: (x_1, \ldots, x_N) =: x$. It is readily observed that $\dim \mathcal{H}_{S^2(\sigma^M)} = 0$ if M is odd, as there are no consistent labelings in this case.

Therefore, in what follows we will restrict our discussion to the $M = N + 3$-punctured sphere where N is any odd positive integer. In this case, any consistent labeling $\ell \in \mathsf{L}(\mathcal{C})$ yields a sequence $(x_1, \ldots, x_N)$ where $x_i \in \{1, \psi\}$ for odd i and $x_i = \sigma$ is fixed for even i. Actually any such labeling of this form is consistent, giving an isomorphism defined in terms of orthonormal basis elements by

$$\begin{array}{rcl} W : \mathcal{H}_{S^2(\sigma^{N+3})} & \to & (\mathbb{C}^2)^{(N+1)/2} \\ |x\rangle & \mapsto & |x_1\rangle \otimes |x_3\rangle \otimes \cdots \otimes |x_N\rangle \ . \end{array} \tag{3.66}$$

Lemma 3.14. Consider the 'standard' basis of the M-punctured sphere $S^2(\sigma^M)$, where $M \geq 4$ is even. Then there is only one equivalence class under the relation $\sim$. Furthermore, the set of braids $\{\sigma_j\}_{j=1}^{M-1}$ generates the relation $\sim$.

Proof. If two fusion-consistent labelings x, x' differ only in location $2j+1$, they can be connected by σ_{2j+1}: the relevant braid matrix is

$$B(\sigma, \sigma) = \frac{\mathrm{e}^{-3\pi \mathrm{i}/8}}{\sqrt{2}} \begin{pmatrix} \mathrm{i} & 1 \\ 1 & \mathrm{i} \end{pmatrix}.$$

We have $x \Leftrightarrow_{\sigma_{2j+1}} x'$, and it follows that there is only one equivalence class under $\sim$. □

Now consider a locality-preserving automorphism U of $\mathcal{H}_{S^2(\sigma^{N+3})}$ and its associated family $\vec{\pi} = \{\pi^{C_j}\}$ of permutations. Because only sequences x with $x_{2j} = \sigma$ for all j are fusion-consistent, and $\vec{\pi}$ is a permutation on $\mathsf{L}(\mathcal{C})$, we conclude that $\pi^{C_{2j}}(\sigma) = \sigma$ for all j. In other words, we can essentially ignore labels carrying even indices. For odd indices, only labels $x_{2j+1} \in \{1, \psi\}$ are allowed, which means that $\pi^{C_{2j+1}} \in \{\mathrm{id}, (\psi, 1)\}$ either leaves the label invariant or interchanges ψ and 1. In conclusion, $\vec{\pi} = \{\pi^{C_j}\}_{j=1}^{N}$ are of the form $\pi^{C_j} \in \{\mathrm{id}, (\psi, 1)\}$ for odd j, and $\pi^{C_j} = \mathrm{id}$ for even j.

For odd $j = 2k+1$, we obtain the constraint

$$\varphi(x) = \eta_{2k+1}(x_1, \ldots, \widehat{x_{2k+1}}, \ldots, x_N) + f_{2k+1}(x_{2k+1}) \quad \text{for } k = 0, \ldots, (N-1)/2$$

where $f_{2k+1} \in \mathsf{Iso}\left(\underline{\sigma \quad | \quad \cdot \quad | \quad \sigma} \to \underline{\sigma \quad | \quad \pi^{C_{2k+1}}(\cdot) \quad \sigma} \right)$ given that for even labels $\pi^{C_{2m}}(x_{2m}) = x_{2m} = \sigma$. Let us write

$$\varphi(x) = \eta(x) + \sum_{m=0}^{(N+1)/2} f_{2m+1}(x_{2m+1}) \tag{3.67}$$

and show that $\eta(x) = \eta$ is actually independent of the labeling x. Indeed, we can write

$$\begin{aligned}\eta(x) &= \big(\varphi(x) - f_{2k+1}(x_{2k+1})\big) - \sum_{m,m\neq k}^{(N+1)/2} f_{2m+1}(x_{2m+1}) \\ &= \eta_{2k+1}(x_1, \ldots, \widehat{x_{2k+1}}, \ldots, x_N) - \sum_{m,m\neq k}^{(N+1)/2} f_{2m+1}(x_{2m+1})\end{aligned}$$

Since this holds for all k, we conclude that $\eta(x) = \eta(\widehat{x}_1, x_2, \widehat{x}_3, x_4, \ldots)$ is a function of the even entries only. But the latter are all fixed as $x_{2m} = \sigma$, hence $\eta(x) = \eta$ is simply a global phase.

We can now combine these results into a general statement concerning locality-preserving automorphisms of the M-punctured sphere $S^2(\sigma^M)$. Again, since $\dim \mathcal{H}_{S^2(\sigma^M)} = 0$ for odd M and $\dim \mathcal{H}_{S^2(\sigma^2)} = 1$, we are only concerned with the cases where $M = N + 3 \geq 4$ is even. Let $\{|x\rangle\}_{x \in \mathsf{L}(\mathcal{C})}$ be a basis of $\mathcal{H}_{S^2(\sigma^M)}$. Then such an automorphism must act on $\mathcal{H}_{S^2(\sigma^M)}$ as

$$U|x\rangle = \mathrm{e}^{\mathrm{i}\varphi(x)} |\vec{\pi}(x)\rangle\,, \qquad \text{where} \qquad \varphi(x) = \eta + \sum_{m=0}^{(N+1)/2} f_{2m+1}(x_{2m+1})$$

and

$$\begin{aligned} f_{2k+1} \in \mathsf{Iso}\left(\underline{\sigma \quad | \quad \cdot \quad | \quad \sigma} \to \underline{\sigma \quad | \quad \pi^{C_{2k+1}}(\cdot) \quad \sigma} \right) \\ = \big\{\big(f(1), f(\psi)\big)\big\} = \{(0,0),(0,\pi)\}.\end{aligned}$$

More explicitly, we have

$$U|x\rangle = e^{i\eta} \left(\prod_{m=1}^{(N+1)/2} e^{i f_{2m+1}(x_{2m+1})} \right) \left|\pi^{C_1}(x_1), x_2, \pi^{C_3}(x_3), x_4, \ldots, \pi^{C_N}(x_N)\right\rangle .$$

In particular, under the isomorphism (3.66), we get

$$WUW^{-1} = e^{i\eta} \bigotimes_{m=1}^{(N+1)/2} U_m \qquad \text{where} \qquad U_m|a\rangle = e^{i f_{2m-1}(a)} \left|\pi^{C_{2m-1}}(a)\right\rangle .$$

From Section 3.6, we know that U_m is a single-qubit Pauli for each m up to a global phase. This concludes the proof of Theorem 3.12.

3.7 Abelian anyon models

Our goal in this section is to characterize topologically protected gates in general abelian anyon models. For simplicity, we will restrict our attention to closed 2-manifolds Σ (see Fig. 3.1). We have seen in Lemma 3.5 that in an arbitrary anyon model, protected gates permute the idempotents along closed loops. In this section we show that for the case of abelian anyon models, the protected gates can only permute the labels of string operators along closed loops (up to phases), which refines Lemma 3.5 for abelian models. To formalize this notion, we introduce the generalized Pauli and Clifford groups in Section 3.7. The main result of this Section, can then be stated as follows:

Theorem 3.15. For an abelian anyon model, any locality-preserving unitary automorphism U acting on $\mathcal{H}_\Sigma$ has logical action $[U] \in \mathsf{Clifford}^\star_\Sigma$.

For abelian anyon models, the set $\mathbb{A}$ of particles is an abelian group and the fusion rules (i.e., the Verlinde algebra (3.7)) are given by the group product, $N_{ab}^c = 1$ if and only if $c = ab$ and $N_{ab}^c = 0$ otherwise. In other words, any two particles a and b fuse to a unique particle $c = ab$, and the identity element $1 \in \mathbb{A}$ is the only particle satisfying $1a = a$ for all $a \in \mathbb{A}$. Another requirement is that the S matrix is composed entirely of phases (divided by the quantum dimension $\mathcal{D}$), and $S_{1a} = S_{a1} = 1/\mathcal{D}$ for all $a \in \mathbb{A}$. Furthermore, the involution $a \mapsto \overline{a}$ defining the antiparticle associated to $a \in \mathbb{A}$ is simple the inverse $\overline{a} = a^{-1}$ with respect to the group multiplication. Note that, by the fundamental theorem of finitely generated abelian groups, the group $\mathbb{A}$ is isomorphic to $\mathbb{Z}_{N_1} \times \mathbb{Z}_{N_2} \times \cdots \times \mathbb{Z}_{N_r}$ for some prime powers N_j. The number $N = \mathsf{lcm}(N_1, \ldots, N_r)$ will play an important role in the following, determining e.g., the order of a protected gate.

It is well known that for abelian anyons a and b, and two inequivalent loops C and C' whose intersection number is 1 in the manifold Σ the relation

$$[F_{\overline{b}}(C')][F_{\overline{a}}(C)][F_b(C')][F_a(C)] = \mathcal{D}S_{ab}[\mathrm{id}] \tag{3.68}$$

holds. As we will see, this provides an additional constraint on the logical action of a protected gate U. The following consistency condition must hold:

Lemma 3.16. Let C and C' be two loops on Σ which intersect once. Consider the action of a locality preserving unitary automorphism of the code on the string operators on C and C', that is

$$\rho_U([F_b(C)]) = \sum_d \Lambda_{b,d}[F_d(C)], \qquad \rho_U([F_b(C')]) = \sum_d \Lambda'_{b,d}[F_d(C')]. \tag{3.69}$$

Then the matrices Λ and Λ' must satisfy the following consistency condition

$$\Lambda_{a,c}\,\Lambda'_{b,d}\,(S_{cd} - S_{ab}) = 0 \quad \forall a, b, c, d \in \mathbb{A}. \tag{3.70}$$

Proof. Since in an abelian anyon model every string operator $[F_a(C)]$ is unitary the relation (3.68) is equivalent to the commutation relation

$$[F_b(C')][F_a(C)] = \mathcal{D}S_{ab}[F_a(C)][F_b(C')].$$

Conjugating this by U and rearranging terms yields

$$0 = \sum_{c,d} \Lambda_{a,c}\,\Lambda'_{b,d}\,(\mathcal{D}S_{cd} - \mathcal{D}S_{ab})\,[F_c(C)][F_d(C')]. \tag{3.71}$$

The claim follows from linear independence of the logical operators $[F_c(C)][F_d(C')]$. □

Invoking our previous result of Lemma 3.5, the following lemma is implied:

Lemma 3.17. The anyon labels of *string* operators along the loop are permuted by U

$$\Lambda_{b,d} = e^{i\phi_b}\delta_{d,\tilde{\pi}(b)}, \tag{3.72}$$

for some phase ϕ_b, and where $\tilde{\pi}$ is a permutation of anyon labels.

Proof. Recall from (3.29) that

$$\Lambda_{b,d} = \sum_a \frac{S_{b,a}}{S_{1,a}} S_{1,\pi^C(a)}\overline{S_{d,\pi^C(a)}} = \sum_a S_{b,a}\overline{S_{d,\pi^C(a)}}, \tag{3.73}$$

where π^C is the permutation of the central idempotents associated with loop C, where the second equality holds for abelian anyons. An analogous equation holds for loop C'. Now sum over all $a \in \mathbb{A}$ in (3.70). To evaluate the sum, we require $\sum_a \Lambda_{a,c}$ and $\sum_a \Lambda_{a,c}S_{ab}$. Firstly,

$$\sum_a \Lambda_{a,c} = \sum_{a,g} S_{a,g}\overline{S_{c,\pi^C(g)}} = \mathcal{D}\sum_g \delta_{g,1}\overline{S_{c,\pi^C(g)}} = \mathcal{D}\overline{S_{c,\pi^C(1)}},$$

where we used unitarity of the S-matrix, $\delta_{1z} = \sum_x \overline{S_{x1}}S_{xz} = \sum_x S_{xz}/\mathcal{D}$. Secondly,

$$\sum_a \Lambda_{a,c}S_{ab} = \sum_{a,g} S_{a,g}\overline{S_{c,\pi^C(g)}}S_{ab} = \sum_{a,g} S_{a,g}\overline{S_{c,\pi^C(g)}S_{a\bar{b}}} = \sum_g \delta_{g,\bar{b}}\overline{S_{c,\pi^C(g)}} = \overline{S_{c,\pi^C(\bar{b})}}.$$

Therefore (3.70) implies

$$\big(\mathcal{D}S_{cd}\overline{S_{c,\pi^C(1)}} - \overline{S_{c,\pi^C(\overline{b})}}\big)\Lambda'_{b,d} = 0 \qquad \forall b, c, d \in \mathbb{A}. \tag{3.74}$$

For any $B \in \mathbb{A}$, there must exist at least one anyon $D \in \mathbb{A}$ such that $\Lambda'_{B,D} \neq 0$. Then

$$\mathcal{D}S_{cD}\overline{S_{c,\pi^C(1)}} - \overline{S_{c,\pi^C(\overline{B})}} = 0 \qquad \forall c \in \mathbb{A}. \tag{3.75}$$

For each $D' \neq D$, there must be some $C \in \mathbb{A}$ such that $S_{CD} \neq S_{CD'}$. Therefore substituting into (3.74) the values $b = B, c = C$ and $d = D'$, the term in brackets must be non-zero, implying $\Lambda'_{B,D'} = 0$ for all $D' \neq D$. Unitarity of U yields the claim for loop C'. □

The generalized Pauli and Clifford groups

Consider the case where $\mathbb{A} = \mathbb{Z}_{N_1} \times \cdots \times \mathbb{Z}_{N_r}$ and set $N = \mathsf{lcm}(N_1, \ldots, N_r)$. We define the following group associated with the surface Σ.

Definition 3.18 (Pauli group)**.** Consider a genus-g surface Σ and let $\mathcal{G} = \{C_j\}_{j=1}^{3g-1}$ be the loops associated with generators of the mapping class group as in Fig. 3.1. The *Pauli group* Pauli_Σ *associated with* Σ is

$$\mathsf{Pauli}_\Sigma \coloneqq \Big\langle \big\{\lambda[F_a(C)] \;\big|\; \lambda \in \langle e^{2\pi i/N}\rangle, a \in \mathbb{A}, C \in \mathcal{G}\big\} \Big\rangle ,$$

i.e., the set of logical operators generated by taking products of string-operators associated with $\mathcal{G}$, where $\langle e^{2\pi i/N}\rangle$ is the subgroup of $\mathrm{U}(1)$ consisting of N-th roots of unity.

According to Eq. (3.68), we can always reorder and write each element $P \in \mathsf{Pauli}_\Sigma$ in the standard form

$$P = \lambda[F_{a_1}(C_1)]\cdots[F_{a_{3g-1}}(C_{3g-1})] \qquad \text{for some } \lambda \in \langle e^{2\pi i/N}\rangle,\ a_j \in \mathbb{A}\,.$$

This shows that the group Pauli_Σ is finite. Furthermore, since $a^N = 1$ for every $a \in \mathbb{A}$, we conclude that $P^N = \lambda[\mathrm{id}]$ is proportional to the identity up to a phase $\lambda \in \langle e^{2\pi i/N}\rangle$. That is, every element of the Pauli group Pauli_Σ has order dividing N.

Given this definition, we can proceed to give the definition of the Clifford group.

Definition 3.19 (Clifford group)**.** The *Clifford group associated with* Σ is the group of logical unitaries

$$\mathsf{Clifford}_\Sigma \coloneqq \{\lambda[U] \mid [U]\mathsf{Pauli}_\Sigma[U]^{-1} \subset \mathsf{Pauli}_\Sigma, \lambda \in \langle e^{2\pi i/N}\rangle\}\,.$$

In this definition, $[U]$ is any logical unitary on the code space.

We can define a 'homology-preserving subgroup' of $\mathsf{Clifford}_\Sigma$. To do so, we first introduce the following subgroup of Pauli_Σ associated with a loop on Σ.

Definition 3.20 (Restricted Pauli group)**.** Let $C \in \mathcal{G}$ be a single closed loop. We set

$$\mathsf{Pauli}_\Sigma(C) \coloneqq \left\langle \left\{ \lambda[F_a(C)] \;\middle|\; \lambda \in \langle e^{2\pi i/N} \rangle, a \in \mathbb{A} \right\} \right\rangle ,$$

i.e., the subgroup generated by string-operators associated with the loop C.

It is straightforward to check that for any $C \in \mathcal{G}$, the subgroup $\mathsf{Pauli}_{\Sigma_g}(C) \subset \mathsf{Pauli}_{\Sigma_g}$ is normal; furthermore, any $P \in \mathsf{Pauli}_{\Sigma_g}(C)$ has the simple form of a product $P = \lambda[F_{a_1}(C)] \cdots [F_{a_r}(C)]$.

Given this definition, we can define a subgroup of Clifford group elements as follows:

Definition 3.21 (Homology-preserving Clifford group)**.** The *homology-preserving Clifford group associated with* Σ is the subgroup

$$\mathsf{Clifford}^\star_\Sigma \coloneqq \{\lambda[U] \mid [U]\mathsf{Pauli}_\Sigma(C)[U]^{-1} \subset \mathsf{Pauli}_\Sigma(C) \text{ for all } C \in \mathcal{G},\ \lambda \in \langle e^{2\pi i/N} \rangle\} .$$

Note that this is a proper subgroup, i.e., $\mathsf{Clifford}^\star_\Sigma \subsetneq \mathsf{Clifford}_\Sigma$, as can be seen from the following example.

Example 3.2. Consider for example Kitaev's $D(\mathbb{Z}_2)$-code on a torus Σ_2 (cf. Example 3.1). In this case, there are two inequivalent homologically non-trivial cycles C_1 and C_2. In the language of stabilizer codes, the logical operators $(\bar{X}_1, \bar{Z}_1) = (F_e(C_1), F_m(C_2))$ and $(\bar{X}_2, \bar{Z}_2) = (F_e(C_2), F_m(C_1))$ are often referred to as the logical Pauli operators associated with the first and second logical qubit, respectively. Consider the logical Hadamard $\bar{H}_1$ on the first qubit, which acts as

$$\bar{H}_1 \bar{X}_1 \bar{H}_1^\dagger = \bar{Z}_1 \qquad \text{and} \qquad \bar{H}_1 \bar{Z}_1 \bar{H}_1^\dagger = \bar{X}_1$$

but leaves $\bar{X}_2$ and $\bar{Z}_2$ invariant. Then $\bar{H}_1$ belongs to the Clifford group, $\bar{H}_1 \in \mathsf{Clifford}_\Sigma$. However, $\bar{H}_1 \notin \mathsf{Clifford}^\star_\Sigma$ because $\bar{X}_1$ and $\bar{Z}_1$ belong to different homology classes (specified by C_1 and C_2, respectively).

In the following, we make use of the existence of a loop C' which intersects with a given loop C exactly once. Note that this is not necessarily given, but works in the special case where C is one of the $3g-1$ curves $\{C_j\}_{j=1}^{3g-1}$ associated with

the generators of the mapping class group of the genus-g surface Σ_g (cf. Fig. 1). We are now ready to prove Theorem 3.15, i.e., that a protected gate U has logical action $[U] \in \mathsf{Clifford}^\star_\Sigma$.

Proof. By Lemma 3.17, we have that $\sum_c \Lambda_{a,c}[F_c(C)] = \lambda[F_b(C)]$ for some $\lambda \in \mathrm{U}(1)$ and $b \in \mathbb{A}$. It remains to show that λ is an N-th root of unity. We have

$$\lambda^N[\mathrm{id}] = \lambda^N[F_b(C)^N] = [\lambda F_b(C)]^N = [U][F_a(C)]^N[U^\dagger] = [\mathrm{id}]$$

because the string operators $F_a(C)$ have order dividing N, thus we must have $\lambda^N = 1$. Because a and C were arbitrary, this concludes the proof that $[U] \in \mathsf{Clifford}^\star_\Sigma$. □

RK and SS gratefully acknowledge support by NSERC, and MB, FP, and JP gratefully acknowledge support by NSF grants PHY-0803371 and PHY-1125565, NSA/ARO grant W911NF-09-1-0442, and AFOSR/DARPA grant FA8750-12-2-0308. RK is supported by the Technische Universität München – Institute for Advanced Study, funded by the German Excellence Initiative and the European Union Seventh Framework Programme under grant agreement no. 291763. OB gratefully acknowledges support by the ERC (TAQ). The Institute for Quantum Information and Matter (IQIM) is an NSF Physics Frontiers Center with support by the Gordon and Betty Moore Foundation. RK and SS thank the IQIM for their hospitality. We thank Jeongwan Haah, Olivier Landon-Cardinal and Beni Yoshida for helpful discussions.

3.8 Density on a subspace and protected gates

Lemma 3.22. Let $\mathcal{H}_0$ be an invariant subspace under the mapping class group representation, and suppose the action of MCG_Σ is dense in the projective unitary group $\mathsf{PU}(\mathcal{H}_0)$. Let $\mathcal{H}_1$ be the orthogonal complement of $\mathcal{H}_0$ in $\mathcal{H}_\Sigma$. Assume that the decomposition $\mathcal{H}_0 \oplus \mathcal{H}_1$ stems from the gluing axiom in the sense that $\mathcal{H}_j = \bigoplus_{\vec{a} \in \Lambda_j} \mathcal{H}_{\Sigma'(\vec{a})}$ for $j = 0, 1$, where Λ_0, Λ_1 are disjoint set of labelings of the boundary components of the surface Σ' obtained by cutting Σ along a family $\vec{C}$ of pairwise non-intersecting curves. If $\dim \mathcal{H}_1 < \dim \mathcal{H}_0$ (or a similar assumption), then any protected gate U leaves $\mathcal{H}_0$ invariant and acts as a global phase on it.

Proof. Extending $\vec{C}$ to a DAP-decomposition $\mathcal{C}$, the unitary U expressed in the (suitably ordered) basis $\mathcal{B}_\mathcal{C}$ takes the form

$$\mathbf{U} = \begin{pmatrix} \mathbf{U}_{00} & \mathbf{U}_{01} \\ \mathbf{U}_{10} & \mathbf{U}_{11} \end{pmatrix},$$

where $\boldsymbol{U}_{jk}$ describes the operator $P_{\mathcal{H}_j} U P_{\mathcal{H}_k}$ obtained by projecting the domain and image of U to $\mathcal{H}_k$ and $\mathcal{H}_j$, respectively.

Consider the Schur decomposition $\mathbf{U}_{00} = \mathbf{W}_{00}\Gamma\mathbf{W}_{00}^\dagger$ of $\mathbf{U}_{00}$, i.e., $\mathbf{W}_{00}$ is a unitary matrix and Γ is upper triangular. There are different cases to consider:

(i) If Γ is diagonal with a single eigenvalue λ, then

$$\mathbf{U} = \begin{pmatrix} \lambda I & \mathbf{U}_{01} \\ \mathbf{U}_{10} & \mathbf{U}_{11} \end{pmatrix} .$$

Assume for the sake of contradiction that $\lambda = 0$. Writing $d_j = \dim \mathcal{H}_j$, the $d_1 \times d_0$-matrix $\mathbf{U}_{10}$, must have exactly d_0 non-zero values, each in a different row because $\mathbf{U} \in \Delta$. This is only possible if $d_1 > d_0$, contradicting our assumption.

We conclude that $\lambda \neq 0$. But then the condition $\mathbf{U} \in \Delta$ requires that $\lambda \in \mathrm{U}(1)$ and $\mathbf{U}_{01} = \mathbf{U}_{10} = 0$ (since we cannot have more than one non-zero entry in each column or row).

(ii) Γ has a non-zero off-diagonal element $\Gamma_{j,k}$, $j < k$. We will show that this is not consistent with the fact that U is a protected gate (i.e., leads to a contradiction). By reordering basis elements of $\mathcal{B}_\mathcal{C}$, we can assume without loss of generality that $\Gamma_{1,2} \neq 0$. By using, e.g., Solovay-Kitaev on $\mathcal{H}_0$, we find a product $\tilde{\mathbf{V}} = \mathbf{V}(\vartheta_1) \cdots \mathbf{V}(\vartheta_m)$ of images of mapping class group elements approximating $\mathbf{V} = \mathbf{W}_{00}^\dagger \oplus \mathbf{W}_{11}$, where $\mathbf{W}_{11}$ is an arbitrary unitary on $\mathcal{H}_1$.

Consider the matrix $\mathbf{VUV}^\dagger$. We have $(\mathbf{VUV}^\dagger)_{j,k} = \Gamma_{j,k}$ for $j, k = 1, \ldots, \dim \mathcal{H}_0$. In particular, $(\mathbf{VUV}^\dagger)_{1,2} \neq 0$ and $(\mathbf{VUV}^\dagger)_{2,1} = 0$.

We claim that we must have $(\mathbf{VUV}^\dagger)_{1,1} = (\mathbf{VUV}^\dagger)_{2,2} = 0$. To show this, assume for the sake of contradiction that one of these diagonal entries is non-zero. Then $\mathbf{VUV}^\dagger \notin \Delta$ since it has two non-zero entries in the same row or column. But this implies $\tilde{\mathbf{V}}\mathbf{U}\tilde{\mathbf{V}}^\dagger \notin \Delta$ since $\tilde{\mathbf{V}}\mathbf{U}\tilde{\mathbf{V}}^\dagger \approx \mathbf{VUV}^\dagger$, a contradiction to the fact that $\mathbf{U} \in \Delta_{\vartheta_1 \cdots \vartheta_m}$.

Now let $X_{j,k} = (\mathbf{VUV}^\dagger)_{j,k}$ for $j, k \in \{1, 2\}$ be the principal minor 2×2 submatrix. We have established that its only non-zero entry is $X_{1,2}$. Using the Hadamard matrix H, we then have $(HXH^\dagger)_{1,1} = X_{1,2}/2 \neq 0$ and $(HXH^\dagger)_{1,2} = -X_{1,2}/2 \neq 0$. Let $\boldsymbol{H} = H \oplus I_{(\dim \mathcal{H}_0 - 2)}$. By Solovay-Kitaev, we can find a product $\tilde{\mathbf{V}}' = \mathbf{V}(\vartheta'_1) \cdots \mathbf{V}(\vartheta'_\ell)$ of images of mapping class group

elements approximating $\mathbf{V}' = \boldsymbol{H} \oplus \mathbf{W}'_{11}$, where $\mathbf{W}'_{11}$ is an arbitrary unitary on $\mathcal{H}_1$. Then we have

$$(\mathbf{V}'\mathbf{V}\mathbf{U}\mathbf{V}^\dagger(\mathbf{V}')^\dagger)_{1,1} = X_{1,2}/2 \neq 0$$
$$(\mathbf{V}'\mathbf{V}\mathbf{U}\mathbf{V}^\dagger(\mathbf{V}')^\dagger)_{1,2} = -X_{1,2}/2 \neq 0\,,$$

which shows that $\mathbf{V}'\mathbf{V}\mathbf{U}\mathbf{V}^\dagger(\mathbf{V}')^\dagger \notin \Delta$. By continuity, this shows that $\tilde{\mathbf{V}}'\tilde{\mathbf{V}}\mathbf{U}\tilde{\mathbf{V}}^\dagger(\tilde{\mathbf{V}}')^\dagger \notin \Delta$, contradicting the fact that $\mathbf{U} \in \Delta_{\vartheta'_1\cdots\vartheta'_\ell\vartheta_1\cdots\vartheta_m}$.

(iii) Γ is diagonal with distinct eigenvalues: in this case we can apply the same kind of argument as in the proof of Corollary 3.7.

□

3.9 Simplifications from excited states

Up until this point, this chapter has presented results from Michael E Beverland et al., 2016. Now we move on to more recent results developed with Gorjan Alagic and Hector Bombin which go beyond what was presented above, and also significantly simplify the anyon-model dependent results.

Recall Proposition 3.3.1, which tells us that given an LPU U, the logical operators associated with loop C transform as

$$[UP_a(C)U^\dagger] = [P_{\pi^C(a)}(C)], \tag{3.76}$$
$$[UF_b(C)U^\dagger] = \sum_{b'} \Lambda_{b,b'}[F_{b'}(C)], \tag{3.77}$$

where π^C is a permutation of anyon labels which can depend on the loop C.

First note that these relations still hold if one extends the notion of a logical operator for an non-contractible loop to a contractible loop C, by considering excited states which are have no local excitations near C. Based on this fact, in the remainder of this section we show that π^C must be the same for all contractible loops C, allowing us to define a permutation $\sigma = \pi^C$ (for contractible C) which depends only on U. Next we argue that the string operators can only be transformed by this permutation up to phase, i.e. that $\Lambda_{b,b'} = e^{i\phi_b}\delta_{b',\sigma(b)}$. Moreover, we show that permutations σ and π^C for any non-contractible loop C must both preserve the quantum dimension of every particle, and that $\sigma(1) = 1$. The phases $e^{i\phi_b}$ for a loop C are fixed completely by π^C and σ and are given in terms of the S matrix as $e^{i\phi_b} = S_{b1}/S_{\sigma(b)\pi(1)}$.

It is clear that these restrictions can be used to simplify many of the previous proofs. For example, it follows that the Fibonacci model can have no non-trivial gates since its two particles have different quantum dimensions and therefore cannot be permuted. Abelian anyons can only have gates in the generalized Clifford group, since string operators can be permuted, with phases which are powers finite root of unity (which appear in the S-matrix).

Lemma 3.23. Let U be an LPU. Then there is a unique permutation $\sigma \in S_{\mathbb{A}}$ such that $\sigma = \pi_C$ for any contractible C.

Proof. Choose a pair of non concentric, non intersecting contractible closed curves C and C', and a contractible closed curve D enclosing C and C'. Consider here only states with local excitations deep inside the regions bounded by C and C', (i.e. not near the curves). Consider an excited state $|\phi\rangle$ is a $+1$ eigenstate of $P_1(E)$ for all contractible closed curves E which enclose regions that exclude those enclosed by C and C', and is also a simultaneous $+1$ eigenstate of $P_a(C)$, $P_{\bar{a}}(C')$ and $P_1(D)$. After the application of U, we obtain $|\phi'\rangle = U|\phi\rangle$, which (rom Proposition 3.3.1, and the fact that U preserves the groundspace) must be a simultaneous $+1$ eigenstate of $P_1(E)$, $P_{\pi_C(a)}(C)$, $P_{\pi_{C'}(\bar{a})}(C)$ and $P_1(D)$. However, to satisfy the fusion rules it must be the case that for some permutations $\pi_C(a) \times \pi_{C'}(\bar{a}) = 1$, which fixes $\pi_{C'}$ given π_C. As this must hold for any choice of closed contractible curve C', the permutation $\pi_{C'}$ must be the same for all such C'. We name the permutation $\sigma = \pi_C$ for any contractible C. □

Lemma 3.24. Let U be an LPU and σ the permutation applied to projection operators for contractible curves afforded by Lemma 3.23. Then $\Lambda_{b,b'} = e^{i\phi_b}\delta_{b',\sigma(b)}$ for some anyon dependent phase e^{ϕ_b}.

Proof. Recall that the string operators are defined in terms of pair creation of b and $\bar{b}$, dragging of a around a closed curve C, and then projecting onto the trivial fusion outcome. We can use the result of Lemma 3.23 to argue that at each step of this process, the action of U would be to replace b by $\sigma(b)$. The only remaining freedom is an overall phase e^{ϕ_b}. □

The following places restrictions on the permutations and phases achievable by LPUs.

Lemma 3.25. Let U be an LPU and fix a simple closed curve C in Σ. Let $\pi, \sigma \in S_{\mathbb{A}}$ and $\{\phi_a : a \in \mathbb{A}\}$ be the permutations and phases (afforded by the above results) satisfying

$$[UP_a(C)U^\dagger] = [P_{\pi(a)}(C)] \qquad \text{and} \qquad [UF_a(C)U^\dagger] = e^{\phi_a}[F_{\sigma(a)}(C)]\,.$$

Then for all $a \in \mathbb{A}$, we have

$$d_{\pi(a)} = d_{\sigma(a)} = d_a \qquad \text{and} \qquad e^{i\phi_a} = \frac{S_{a1}}{S_{\sigma(a)\pi(1)}}. \tag{3.78}$$

Proof. We first recall the definition of the logical projection operators at a simple closed curve $C : [0,1] \to \Sigma$.

$$[P_a(C)] = S_{1a} \sum_b \bar{S}_{ba}[F_b(C)]. \tag{3.79}$$

Applying (3.79) both with and without the above action, we get

$$[P_{\pi(a)}(C)] = S_{1a} \sum_b \bar{S}_{ba} e^{i\phi_b}[F_{\sigma(b)}(C)].$$
$$[P_{\pi(a)}(C)] = S_{1\pi(a)} \sum_b \bar{S}_{b\pi(a)}[F_b(C)].$$

Setting the right hand sides equal to each other,

$$S_{1a} \sum_b \bar{S}_{ba} e^{i\phi_b}[F_{\sigma(b)}(C)] = S_{1\pi(a)} \sum_b \bar{S}_{b\pi(a)}[F_b(C)]\,.$$

$$\sum_b \left(S_{1a}\bar{S}_{ba}e^{i\phi_b} - S_{1\pi(a)}\bar{S}_{\sigma(b)\pi(a)}\right)[F_\sigma(b)(C)] = 0\,.$$

By linear independence of the $[F_b(C)]$, we have that for all $a, b \in \mathbb{A}$,

$$e^{i\phi_b} = \frac{S_{1\pi(a)}\bar{S}_{\sigma(b)\pi(a)}}{S_{1a}\bar{S}_{ba}}. \tag{3.80}$$

Setting $b = 1$ and making use of $\sigma(1) = 1$, it follows that $|S_{1a}|^2 = |S_{1\pi(a)}|^2$. Recalling that $S_{1b} = d_b/\mathcal{D}$ is real for all b, we conclude that $S_{1b} = S_{1\pi(a)}$, and therefore that, $d_a = d_{\pi(a)}$. Substituting $S_{1b} = S_{1\pi(a)}$ into (3.80),

$$e^{i\phi_b} = \frac{\bar{S}_{\sigma(b)\pi(a)}}{\bar{S}_{ba}} = \frac{S_{ba}}{S_{\sigma(b)\pi(a)}}.$$

Setting $a = 1$ yields the claim that $e^{i\phi_b} = S_{b1}/S_{\sigma(b)\pi(1)}$.

To prove that $d_{\sigma(a)} = d_a$, we make the following observation. Consider some new contractible closed curve C' (different from C), along which U implements permutations π' and σ' on the projectors and string operators respectively. We know by Lemma 3.23 and Lemma 3.25 that $\sigma' = \sigma$. We also know that, since C' is contractible, $\pi' = \sigma' = \sigma$. But we have just proven that $d_{\pi'(a)} = d_a$ for any loop C', therefore it must be that $d_{\sigma(a)} = d_a$. □

Chapter 4

CODE SWITCHING

In this chapter, we give a simplified, yet rigorous presentation of the ideas from Bombín's paper *Gauge Color Codes* [arXiv:1311.0879v3]. Our presentation is self-contained, and assumes only basic concepts from quantum error correction. We provide an explicit construction of a family of color codes in arbitrary dimensions and describe some of their crucial properties. Within this framework, we explicitly show how to transversally implement the generalized phase gate $R_n = \text{diag}(1, e^{2\pi i/2^n})$. Our approach differs in aspects from the method in the aforementioned paper, allowing an arguably simpler proof. We describe how to implement the Hadamard gate H fault-tolerantly using code switching. In three dimensions, this yields, together with the transversal CNOT , a fault-tolerant universal gate set $\{H, \text{CNOT}, R_3\}$ without state-distillation.

4.1 Introduction

To build a fully functioning quantum computer, it is necessary to encode quantum information to protect it from noise. In physical systems, one expects noise to act locally. Therefore, *topological codes* A. Y. Kitaev, 2003; Levin and X.-G. Wen, 2005; H. Bombin and M. Martin-Delgado, 2006; Bonderson et al., 2010, which naturally protect against local errors, represent our best hope for storing quantum information. However, a quantum computer must also be capable of processing this information. This motivates the search for topological codes allowing the implementation of a set of gates which (i) can operate in the presence of typical noise without corrupting the stored information, and (ii) can perform any computation on the encoded information. A theoretical framework has been developed around these ideas — a gate which is *fault-tolerant* does not propagate typical errors into uncorrectable errors P. Shor, 1996; J. Preskill, 1998, and therefore satisfies (i). A set of gates which is *universal* can generate any unitary on the code space with arbitrary precision A Yu Kitaev, 1997; M. Nielsen and I. Chuang, 2010, and therefore satisfies (ii).

The known methods of implementing a universal, fault-tolerant gate set in topological codes typically require an enormous amount of overhead. For instance, magic state distillation Sergey Bravyi and Alexei Kitaev, 2005 with the two-dimensional

toric code requires many additional ancilla qubits Austin G Fowler et al., 2012, whereas computing by braiding non-abelian anyons A. Y. Kitaev, 2003; Nayak et al., 2008 requires additional time to move anyons around macroscopic loops Beckman et al., 2001. These forms of overhead can make quantum processing orders of magnitude less efficient than storage alone in topological codes. This may render such approaches impractical given the experimental difficulty of scaling up quantum hardware Austin G Fowler et al., 2012; Devoret and Schoelkopf, 2013; Wecker et al., 2014. In this paper we focus on a new construction by Bombín H. Bombin, 2013, for a universal fault-tolerant gate set with topological color codes. This approach avoids the types of overhead mentioned above. However, a lattice of at least three dimensions is required, limiting the construction's practicality, and there may be other sources of overhead (related to gauge fixing).

Following Bombín's construction, we use the simplest form of fault-tolerant gate — the *transversal gate*, which is a code-space preserving unitary composed of separate unitaries applied to each physical qubit. However, according to a no-go theorem by Eastin and Knill Eastin and Knill, 2009, for any code which protects against arbitrary single-qubit errors, the set of transversal gates forms a finite group and therefore cannot be universal. Some recent approaches to circumvent this no-go theorem in order to implement a universal gate set with transversal gates have been put forward Jochym-O'Connor and Laflamme, 2014; Paetznick and Reichardt, 2013; Jonas T. Anderson, Duclos-Cianci, and Poulin, 2014.

In Ref. H. Bombin, 2013, Bombín applies the approach of *gauge fixing* Paetznick and Reichardt, 2013; Jonas T. Anderson, Duclos-Cianci, and Poulin, 2014 to color codes on a d-dimensional lattice. Color codes were first introduced in two dimensions by Bombín and Martin-Delgado in Ref. H. Bombin and M. Martin-Delgado, 2006. They are *topological stabilizer codes* Gottesman, 1996; Calderbank et al., 1997; A. Y. Kitaev, 2003; Sergey Bravyi and König, 2013, meaning they are defined on a lattice and have macroscopic distance together with geometrically local stabilizer generators. The main new conceptual contribution in Ref. H. Bombin, 2013 is that gauge fixing allows one to fault-tolerantly switch between a (stabilizer) color code on a d-dimensional lattice, in which CNOT and $R_d = \text{diag}\left(1, \exp(\frac{2\pi i}{2^d})\right)$ are transversal, and a different (subsystem) color code on the same lattice, in which H is transversal. Critically, for $d \geq 3$, $\{H, \text{CNOT}, R_d\}$ forms a universal gate set. To the authors' knowledge, this represents the first construction using gauge fixing to achieve a universal gate set in a topological code.

In Ref. H. Bombin, 2013, Bombín argues that for every $d \geq 2$, there exists a d-dimensional color code with a transversal implementation of $R_d \in \mathcal{P}_d \setminus \mathcal{P}_{d-1}$, which is the main technical contribution therein. Here, $\mathcal{P}_d$ is the d^{th} level of the Clifford hierarchy[1] Gottesman and I. L. Chuang, 1999. At the same time, for any topological stabilizer code, Bravyi and König Sergey Bravyi and König, 2013 showed that the group of logical gates implemented transversally must be contained in $\mathcal{P}_d$. These results have been extended beyond the stabilizer code setting Fernando Pastawski and Beni Yoshida, 2014; Michael E Beverland et al., 2016. Color codes are the only family of topological stabilizer codes currently known to saturate the Bravyi-König classification in every dimension $d \geq 2$.

In this paper, we provide a simplified yet rigorous presentation of the ideas in Ref. H. Bombin, 2013. The organization is as follows. First, to build some intuition, we introduce color codes in two dimensions in Section 4.2. We explain how to transversally implement the gate set $\{H, \text{CNOT}, R_2\}$, which generates the Clifford group. Then, we describe the generalization of color codes to d dimensions in Section 4.3. Next, in Section 4.4 we discuss transversal gates in those codes with an emphasis on the phase gate R_n, and show that in certain d-dimensional color codes R_d is transversal. Our construction utilizes the bipartite property of the lattice allowing for a simpler verification than in Ref. H. Bombin, 2013. Finally, in Section 4.5 we explain how to switch between color codes fault-tolerantly using the technique of gauge fixing. In particular, this allows one to implement a fault-tolerant universal gate set $\{H, \text{CNOT}, R_3\}$ in a color code in three dimensions.

4.2 Color code in two dimensions

In this section, we give an explicit construction of a stabilizer color code in two dimensions H. Bombin and M. Martin-Delgado, 2006; Bombín, 2013. We consider a 3-valent lattice formed as a tiling of a sphere, such that faces of the lattice are colored with three colors, where neighboring faces have distinct colors. Qubits are placed at the vertices of this lattice. To define a color code on this lattice, we associate an X- and a Z-type stabilizer generator with every face. This code encodes no logical qubits. A new code, which encodes a single logical qubit, can be formed through the removal of a single physical qubit. We describe the transversal

[1] The Clifford hierarchy is defined sequentially for $j > 1$ according to $\mathcal{P}_j = \{\text{unitary } U | UPU^\dagger \in \mathcal{P}_{j-1} \ \forall P \in \mathcal{P}_1\}$ with $\mathcal{P}_1$ representing the Pauli group. Note that $\mathcal{P}_2$ is the well-known Clifford group.

implementation of the logical gates $\overline{\text{CNOT}}$, $\overline{H}$ and $\overline{R}_2$ in the new code[2].

Color code with no encoded qubits

Color codes in two dimensions are CSS stabilizer codes Gottesman, 1996; Calderbank et al., 1997, and are therefore specified by their stabilizer group $\mathcal{S}$ generated by X- and Z-type stabilizer generators. The code space is the simultaneous $+1$ eigenspace of every stabilizer generator. In the construction, we use a two-dimensional lattice $\mathcal{L}_0^*$, obtained from a tiling of the 2-sphere, and satisfying the following requirements

- valence — every vertex is 3-valent, meaning it belongs to exactly 3 edges,
- colorability — faces can be colored with 3 colors: red, green and blue, such that every two faces sharing an edge have different colors.

An example of such a tiling of the 2-sphere is presented in Fig. 4.1(a). From these properties alone, one can show that the total number of vertices in $\mathcal{L}_0^*$ is even. To see this, note that the Euler characteristic is $V - E + F = 2$, where V, E and F denote the number of vertices, edges and faces in $\mathcal{L}_0^*$, respectively. Since every vertex is 3-valent, we obtain $E = \frac{3}{2}V$, and then $V = 2(F - 2)$, which is even.

At every vertex in $\mathcal{L}_0^*$ we place a qubit. We refer to the set of all qubits by Q, whereas by $\mathcal{Q}(\Pi) \subset Q$ we denote the set of vertices of a face Π. Alternatively, we can think of $\mathcal{Q}(\Pi)$ as the set of qubits belonging to Π. To define the color code, it is sufficient to specify X- and Z-type stabilizer generators. For every face Π, we define an X-type stabilizer generator $X(\Pi)$ to be a tensor product of Pauli X operators supported on qubits $\mathcal{Q}(\Pi)$, similarly for Z-type generators. Then, the stabilizer group $\mathcal{S}$ is generated by

$$\mathcal{S} = \langle X(\Pi), Z(\Pi), \text{for every face } \Pi \text{ in } \mathcal{L}_0^* \rangle. \tag{4.1}$$

To prove that this specifies a well-defined stabilizer code, we must verify that all the generators of $\mathcal{S}$ commute. It is sufficient to check that for any two faces Π_1 and Π_2 in $\mathcal{L}_0^*$, $X(\Pi_1)$ and $Z(\Pi_2)$ commute. First take the case $\Pi_1 \neq \Pi_2$. If Π_1 and Π_2 share no vertices, then $X(\Pi_1)$ and $Z(\Pi_2)$ trivially commute. If they share a vertex, then by 3-valence, they also share an edge. Moreover, due to valence and

[2] We use a bar to indicate action on logical code space. The absence of a bar indicates action on physical qubits.

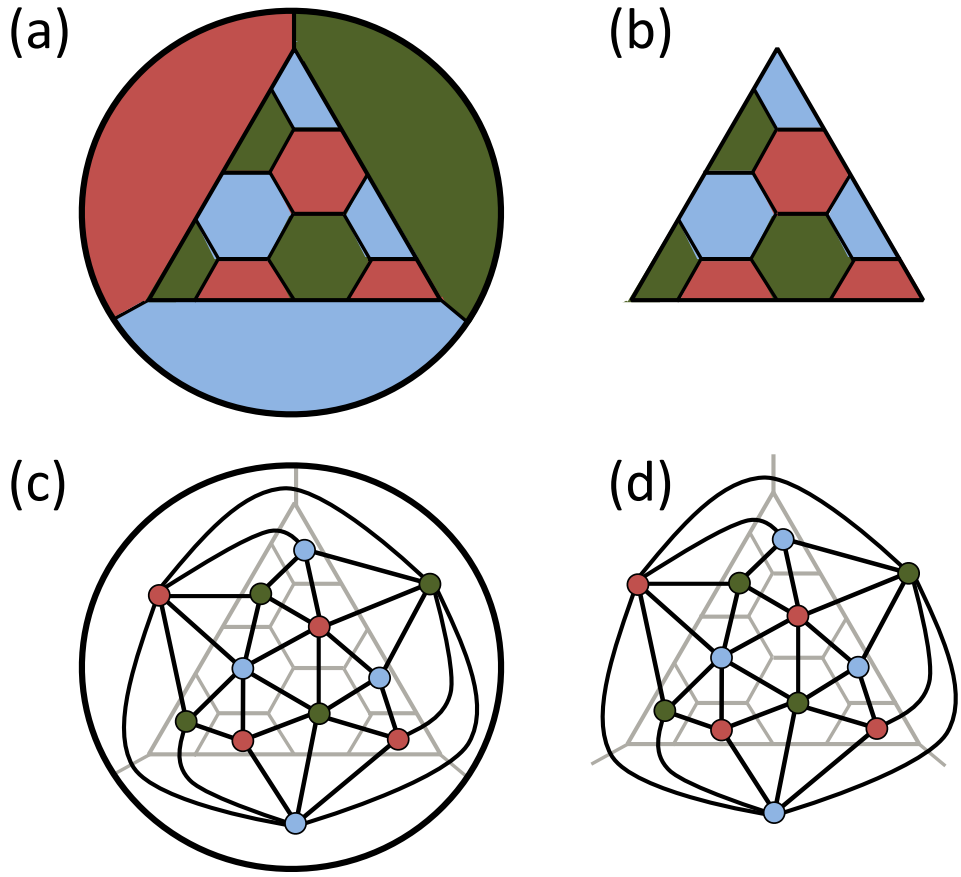

Figure 4.1: (Color online) Construction of color codes in two dimensions. In (a) and (b), qubits are placed at vertices, and X- and Z-type stabilizer generators are associated with faces. In (c) and (d) (the dual picture), qubits are placed on faces, and X- and Z-type stabilizer generators are associated with vertices. (a) Take a lattice $\mathcal{L}_0^*$, which is a tilling of the 2-sphere with 3-colorable faces and 3-valent vertices. The surrounding circle is identified with a vertex v. The color code on $\mathcal{L}_0^*$ encodes no logical qubits. (b) To obtain $\mathcal{L}^*$, remove from $\mathcal{L}_0^*$ the vertex v, together with the three edges and three faces containing it. The color code on $\mathcal{L}^*$ encodes one logical qubit. (c) (Dual) lattice $\mathcal{L}_0$ is obtained from $\mathcal{L}_0^*$ by replacing faces, edges and vertices by vertices, edges and faces, respectively. All faces are triangles, and the vertices are 3-colorable. The color code on $\mathcal{L}_0$ encodes no logical qubits. (d) Lattice $\mathcal{L}$ formed from $\mathcal{L}_0$ by removing a single face. No stabilizer generators are associated with those vertices belonging to the boundary of the removed face. The color code on $\mathcal{L}$ encodes one logical qubit.

colorability conditions, Π_1 and Π_2 cannot share two consecutive edges, and thus their intersection has to contain an even number of vertices,

$$|\mathcal{Q}(\Pi_1) \cap \mathcal{Q}(\Pi_2)| \equiv 0 \mod 2. \tag{4.2}$$

For the case $\Pi_1 = \Pi_2 = \Pi$, due to 3-colorability and 3-valence, the number of vertices belonging to a face Π is even,

$$|\mathcal{Q}(\Pi)| \equiv 0 \mod 2. \tag{4.3}$$

Therefore, we obtain commutation of $X(\Pi_1)$ and $Z(\Pi_2)$ for arbitrary Π_1 and Π_2.

From the construction of the lattice, one obtains that each vertex belongs to exactly three faces, colored with three different colors. Thus, one can express the set of vertices in $\mathcal{L}_0^*$ as the disjoint union[3] of vertices belonging to red faces, and similarly for green and blue H. Bombin and M. Martin-Delgado, 2006; Bombín, 2013, namely

$$Q = \bigsqcup_{\Pi_R} \mathcal{Q}(\Pi_R) = \bigsqcup_{\Pi_G} \mathcal{Q}(\Pi_G) = \bigsqcup_{\Pi_B} \mathcal{Q}(\Pi_B), \tag{4.4}$$

where $\{\Pi_R\}$, $\{\Pi_G\}$ and $\{\Pi_B\}$ are the sets of all red, green and blue faces, respectively. This implies that not all the stabilizer generators we have defined are independent

$$\prod_{\Pi_R} X(\Pi_R) = \prod_{\Pi_G} X(\Pi_G) = \prod_{\Pi_B} X(\Pi_B), \tag{4.5}$$

$$\prod_{\Pi_R} Z(\Pi_R) = \prod_{\Pi_G} Z(\Pi_G) = \prod_{\Pi_B} Z(\Pi_B). \tag{4.6}$$

In fact, these are the only conditions Bombín and M. Martin-Delgado, 2007; Bombín, 2013 which relate the stabilizer generators to one another.

We can now verify that the color code which we have defined on the lattice $\mathcal{L}_0^*$ encodes no logical qubits. As before, using the Euler characteristic we obtain $F-2 = E-V$, and from 3-valence of vertices — $E = \frac{3}{2}V$. We have placed physical qubits at vertices, thus $|Q| = V$. There are $2F-4$ independent stabilizer generators, since there are two stabilizer generators for every face and four conditions (4.5) and (4.6). The number of logical qubits is equal to the number of physical qubits minus the number of independent stabilizer generators, and we obtain

$$|Q| - (2F-4) = V - 2(E-V) = 0. \tag{4.7}$$

Color code with one logical qubit

To obtain a color code with one encoded logical qubit, we can remove one vertex from the lattice $\mathcal{L}_0^*$, together with three edges and three faces it belongs to, obtaining a

[3] We use the *disjoint union* $A \sqcup B$ in place of the union $A \cup B$ of two sets A and B when their intersection is empty, $A \cap B = \emptyset$.

new lattice $\mathcal{L}^*$ (see Fig. 4.1b). By removing one vertex, we also discard six stabilizer generators associated with the removed faces, and thus the stabilizer generators no longer have to satisfy (4.5) and (4.6). One can check that this new code encodes one logical qubit, since there is one qubit more than independent stabilizer generators. By removing more vertices, one could encode more logical qubits, but we will not analyze that case. Note that the total number of qubits in $\mathcal{L}^*$ is odd, $|Q| \equiv 1 \mod 2$, which plays an important role in our considerations.

On physical grounds, it is of interest to consider stabilizer codes with stabilizer generators which are low-weight and geometrically local. In the construction we have presented, this can be achieved if each face in the lattice $\mathcal{L}^*$ is geometrically local and contains a small number of vertices, as in Fig. 4.1b. It can be shown that following this construction, the resulting color code has macroscopic distance H. Bombin and M. Martin-Delgado, 2006, and therefore is a topological stabilizer code.

Later, when we discuss color codes in d dimensions, we follow a similar construction. We briefly outline the procedure here, deferring detailed discussion to Section 4.3. We start with a tiling of a d-sphere, place qubits at vertices and define (gauge group) generators to be supported on suitable cells. Then, we remove one vertex and all the cells containing it. In particular, we discard generators supported on the removed cells. Such a code encodes only one logical qubit Bombín and M. Martin-Delgado, 2007.

Transversal gates

Consider a stabilizer code encoding one logical qubit, with the stabilizer group $\mathcal{S}$. In this setting, a *transversal gate* $\overline{U}$ on a single logical qubit is implemented as a tensor product of single physical qubit unitaries $U_1 \otimes \ldots \otimes U_{|Q|}$, which preserves the code space. On the other hand, a logical gate on two logical qubits requires two copies of the code, in which case we say that the *overall* code space is the $+1$ eigenspace of the elements in $\mathcal{S} \otimes \mathcal{S}$. A transversal gate on two logical qubits is implemented as a tensor product of two qubit gates on pairs of corresponding qubits in both copies of the code, which preserves the overall code space. Observe that transversal gates are fault-tolerant since they do not spread errors within each copy of the code.

We now show that in the two-dimensional color code described in the previous subsection, one can transversally implement the gate set $\{\overline{H}, \overline{\text{CNOT}}, \overline{R}_2\}$, which generates the (non-universal) Clifford group. The Clifford group, combined with

computational basis state preparation and measurement, can be simulated efficiently on a classical computer Gottesman, 1998; Aaronson and Gottesman, 2004. For each gate, $\overline{H}$, $\overline{\text{CNOT}}$ and $\overline{R}_2$, we verify that a particular transversal unitary implements the logical gate by showing that it has the correct action under conjugation on generators of the logical Pauli group, and that the stabilizer group is preserved[4].

This two-dimensional color code is a CSS stabilizer code encoding a single logical qubit with logical Pauli operators $\overline{X} = X(Q)$ and $\overline{Z} = Z(Q)$. In addition it is a *self-dual CSS stabilizer code* — a code with the same support for X- and Z-type stabilizer group elements (for each face, there is an X- and a Z-type generator). This implies that the logical Hadamard gate can be implemented transversally, as under conjugation by $H(Q)$, $\overline{X} \mapsto H(Q)X(Q)H(Q)^\dagger = \overline{Z}$ and similarly $\overline{Z} \mapsto \overline{X}$. Moreover, $X(\Pi) \mapsto Z(\Pi)$, $Z(\Pi) \mapsto X(\Pi)$, and thus $\mathcal{S}$ is preserved.

The logical gate $\overline{\text{CNOT}}$ can be implemented transversally between two identical copies of this color code by applying a physical gate CNOT to every pair of corresponding qubits in the first and the second copy. This can be verified by checking that under conjugation by $\overline{\text{CNOT}}$, $\overline{X}\,\overline{I} \mapsto \overline{X}\,\overline{X}$, $\overline{I}\,\overline{X} \mapsto \overline{I}\,\overline{X}$, $\overline{Z}\,\overline{I} \mapsto \overline{Z}\,\overline{I}$, $\overline{I}\,\overline{Z} \mapsto \overline{Z}\,\overline{Z}$ and $\mathcal{S} \otimes \mathcal{S}$ is preserved[5].

To show that $\overline{R}_2$ can be implemented transversally, we use the fact that the set of vertices in $\mathcal{L}^*$ is bipartite (see Fig. 4.2(a)). In other words, Q can be split into two subsets, T and $T^c := Q \setminus T$, such that vertices in T are connected only to vertices in T^c and vice versa. To prove this, first note that every face in $\mathcal{L}_0^*$ has an even number of edges. Moreover, every cycle in $\mathcal{L}_0^*$ (as a tiling of the 2-sphere) is contractible. This implies that every cycle in $\mathcal{L}_0^*$ is a boundary of faces and is therefore even. Using the following lemma

Lemma 4.1 (Graph Bipartition)**.** A graph containing only even cycles is bipartite Wilson, 1996.

we see that $\mathcal{L}_0^*$ must be bipartite, and so is the lattice $\mathcal{L}^*$ due to its construction from $\mathcal{L}_0^*$.

Now, we can show that $R = R_2^k(T)R_2^{-k}(T^c)$ implements $\overline{R}_2$, for some choice of integer k. We use the relations $R_2 X R_2^\dagger = iXZ$ and $R_2 Z R_2^\dagger = Z$. Since $|Q| \equiv 1$

[4]Preservation of the stabilizer group is a sufficient (but not necessary) condition that implies preservation of the code.

[5]Notice that generators of $\mathcal{S} \otimes \mathcal{S}$ are mapped under conjugation to a different generators, namely $X(\Pi) \otimes I(\Pi) \mapsto X(\Pi) \otimes X(\Pi)$, $Z(\Pi) \otimes I(\Pi) \mapsto Z(\Pi) \otimes I(\Pi)$, $I(\Pi) \otimes X(\Pi) \mapsto I(\Pi) \otimes X(\Pi)$ and $I(\Pi) \otimes Z(\Pi) \mapsto Z(\Pi) \otimes Z(\Pi)$.

$\mod 2$, then $|T| - |T^c| = 2|T| - |Q| \equiv \pm 1 \mod 4$, and picking $k = |T| - |T^c| \mod 4$ ensures that $k(|T| - |T^c|) \equiv 1 \mod 4$. With this choice of k, the action by conjugation of $R = R_2^k(T)R_2^{-k}(T^c)$ on the logical $\overline{X}$ and $\overline{Z}$ is

$$R\overline{X}\,R^\dagger = i^{k(|T|-|T^c|)}\overline{X}\,\overline{Z} = i\overline{X}\,\overline{Z}, \tag{4.8}$$

$$R\overline{Z}\,R^\dagger = \overline{Z}. \tag{4.9}$$

Furthermore, as every face Π in the lattice $\mathcal{L}^*$ has an equal number of vertices in T and T^c, under the action of R the stabilizer generators $X(\Pi)$ and $Z(\Pi)$ become:

$$RX(\Pi)R^\dagger = i^{k(|T\cap\Pi|-|T^c\cap\Pi|)}X(\Pi)Z(\Pi) \tag{4.10}$$

$$= X(\Pi)Z(\Pi) \in \mathcal{S}, \tag{4.11}$$

$$RZ(\Pi)R^\dagger = Z(\Pi), \tag{4.12}$$

implying that the stabilizer group $\mathcal{S}$ is preserved. This completes the verification that R implements $\overline{R}_2$.

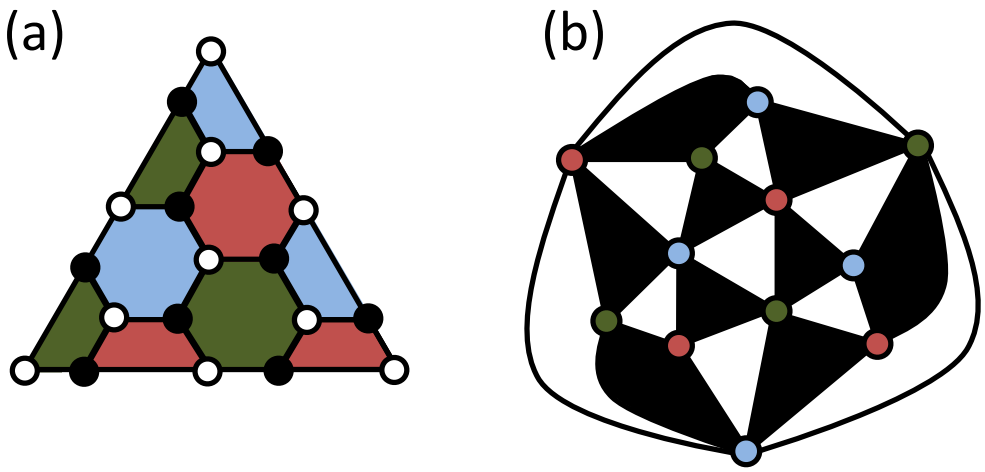

Figure 4.2: (Color online) (a) The set of vertices of $\mathcal{L}^*$, the lattice used to define the color code, is bipartite — it can be split into two subsets: T (hollow circles), and its compliment T^c (filled circles). Vertices in T are only connected to vertices in T^c and vice versa. The logical gate $\overline{R}_2$ can implemented by applying R_2^k to qubits in T, and R_2^{-k} to qubits in T^c, where $k \equiv |T| - |T^c| \mod 4$. (b) The dual lattice $\mathcal{L}$. Faces are bipartite.

Dual lattice picture

We can alternatively express the construction of color codes in the dual lattice picture, which we will use extensively for $d > 2$ dimensions. We use a two-dimensional

(dual) lattice $\mathcal{L}_0$, obtained from a tiling of the 2-sphere, and satisfying the following requirements

- all faces are triangles,
- vertices are 3-colorable, meaning two vertices belonging to the same edge are colored with different colors.

See Fig. 4.1(c) for a simple example. Note that these conditions are equivalent to the conditions of 3-valence of vertices and 3-colorability of faces required for the tiling $\mathcal{L}_0^*$ of the 2-sphere, where lattices $\mathcal{L}_0^*$ and $\mathcal{L}_0$ are dual to one another.

A qubit is placed on every face of $\mathcal{L}_0$, and an X- and a Z-type stabilizer generator is associated with every vertex, meaning they are supported on qubits corresponding to faces containing that vertex. The resulting color code is exactly the same as that described in Section 4.2, and therefore has zero logical qubits. To encode a single logical qubit, one should remove a face from $\mathcal{L}_0$, together with stabilizer generators associated with the vertices belonging to the removed face, see Fig. 4.1(d).

The bipartition of vertices in $\mathcal{L}^*$ corresponds to a bipartition of faces in $\mathcal{L}$, meaning that faces in $\mathcal{L}$ can be split into two sets, T and its compliment T^c, such that faces in T share an edge only with faces in T^c and vice-versa. See Fig. 4.2(b).

4.3 Color code in higher dimensions

Here we present a construction of color codes on d-dimensional lattices. In higher dimensions it is easier to describe the construction in the language of the dual lattice. The majority of this section is devoted to defining dual lattices satisfying certain conditions and analyzing their properties. The discussion is a generalization of that already presented for two dimensions. The basic idea of how to construct the dual lattice $\mathcal{L}$ is to first tile a d-sphere with d-simplices to form a lattice $\mathcal{L}_0$. We require that every vertex in $\mathcal{L}_0$ can be assigned one of $d+1$ distinct colors and two vertices belonging to the same edge have different colors. The lattice $\mathcal{L}$, used to define the color code, is formed by removing one d-simplex from $\mathcal{L}_0$, which results in a color code encoding one logical qubit Bombín and M. Martin-Delgado, 2007; H. Bombin, 2013.

Simplicial complexes and colorability

A d-simplex δ is a d-dimensional polytope which is a convex hull of its $d+1$ affinely independent vertices $v_0, v_1, \ldots, v_d$, namely

$$\delta = \left\{ \sum_{i=0}^{d} t_i v_i \,\middle|\, 0 \leq t_i \wedge \sum_{i=0}^{d} t_i = 1 \right\}. \tag{4.13}$$

In particular, 0-simplices are vertices, 1-simplices are edges, 2-simplices are triangles, 3-simplices are tetrahedra and so on.

A convex hull of a subset of vertices of size $k+1 \leq d+1$ is a k-simplex σ, which we call a k-face of δ, and $\sigma \subset \delta$. For example, the faces of a 3-simplex (a tetrahedron) are: four 0-simplices, six 1-simplices, four 2-simplices and a single 3-simplex. More generally, δ contains $\binom{d+1}{k+1}$ k-faces, since every k-face is uniquely determined by the choice of $k+1$ vertices spanning it. By $\Delta_k(\delta)$ we call the set of all k-faces of δ, namely

$$\Delta_k(\delta) = \{\sigma \subset \delta | \sigma \text{ is a } k\text{-simplex}\}. \tag{4.14}$$

Instead of having only one simplex, we can consider a collection of them. Moreover, we can create new objects, called simplicial complexes Hatcher, 2002, by gluing simplices along their proper faces of matching dimension. We restrict ourselves to simplicial complexes containing finitely many simplices. We will define a d-dimensional color code on a lattice $\mathcal{L}$ obtained by gluing together d-simplices. The technical name for such a lattice is a homogeneous simplicial d-complex.

Although $\mathcal{L}$ is formally a collection of simplices, by the same symbol we also denote the union of these simplices as a topological space. Notice that $\mathcal{L}$ is a manifold with a boundary, which we can think of as being embedded in real space. We denote by $\partial\mathcal{L}$ the set of simplices belonging to the boundary of $\mathcal{L}$, where the boundary of $\mathcal{L}$ is the set of points in the closure of $\mathcal{L}$ not belonging to the interior of $\mathcal{L}$. Moreover, by $\Delta'_k(\mathcal{L})$ we understand the set of all k-simplices belonging to $\mathcal{L} \setminus \partial\mathcal{L}$. Note that $\Delta'_d(\mathcal{L}) = \Delta_d(\mathcal{L})$.

We say that a simplicial d-complex $\mathcal{L}$ is $(d+1)$-colorable if we can introduce a function

$$\text{color} : \Delta_0(\mathcal{L}) \to \mathbb{Z}_{d+1}, \tag{4.15}$$

where $\mathbb{Z}_{d+1} = \{0, 1, \ldots, d\}$ is a set of $d+1$ colors, and two vertices belonging to the same edge have different colors. Moreover, by $\text{color}(\delta)$ we understand the set of

colors assigned to all the vertices of a simplex δ, namely

$$\mathrm{color}(\delta) = \bigsqcup_{v \in \Delta_0(\delta)} \mathrm{color}(v). \tag{4.16}$$

An example of a 3-colorable, homogeneous, simplicial 2-complex is the lattice $\mathcal{L}$ shown in Fig. 4.1(d). Note in particular that it is composed of nineteen 2-simplices (triangles). The exact shape of objects in $\mathcal{L}$ is not important due to its topological nature — the lattice is not rigid and can be smoothly deformed. In this example, $\Delta_0'(\mathcal{L})$ consists of the set of 9 vertices (the three vertices in the boundary are excluded). $\Delta_1'(\mathcal{L})$ is the set of 27 edges, (the three edges in the boundary are excluded). $\Delta_2'(\mathcal{L})$ is the set of all 19 triangular faces.

Definition of color code

Here we define color codes on a d-dimensional lattice $\mathcal{L}$, which must satisfy the following conditions

Condition 1. *$\mathcal{L}$ is a homogeneous simplicial d-complex obtained as a triangulation of the interior of a d-simplex.*

Condition 2. *$\mathcal{L}$ is $(d+1)$-colorable.*

One can obtain such a lattice $\mathcal{L}$ from any $(d+1)$-colorable tiling of the d-sphere with d-simplices, followed by the removal of one d-simplex. In $d = 2$ dimensions, this is precisely the procedure described in Section 4.2. An explicit construction of a family of lattices satisfying these conditions is outlined in Appendix **??**.

Qubits are placed on each and every d-simplex of $\mathcal{L}$, and thus the set of all qubits Q is equal to $\Delta_d(\mathcal{L})$. This motivates the next definition, namely for a simplex $\delta \subset \mathcal{L} \setminus \partial\mathcal{L}$ we define

$$\mathcal{Q}(\delta) = \{\sigma \in \Delta_d(\mathcal{L}) | \sigma \supset \delta\}. \tag{4.17}$$

In other words, $\mathcal{Q}(\delta)$ can be thought of as the set of qubits placed on d-simplices containing δ. We say that qubits $\mathcal{Q}(\delta)$ are supported on δ. By saying that an operator is supported on δ we mean that it is supported on the set $\mathcal{Q}(\delta)$, for example $X(\delta) := X(\mathcal{Q}(\delta))$.

A color code is a CSS subsystem code Poulin, 2005; Bacon, 2006. Recall that a CSS subsystem code is specified by its gauge group $\mathcal{G}$. Each X-type gauge group generator $X(G^x)$ consists of Pauli X operators applied to qubits G^x; similarly for

Z-type generators. The stabilizer group $\mathcal{S} \subset \mathcal{G}$ is the group generated by all Pauli operators $X(S^x)$ and $Z(S^z)$ contained in $\mathcal{G}$, which commute with every element of $\mathcal{G}$. Note that $-I \notin \mathcal{S}$. The codewords are $+1$ eigenvectors of all elements of $\mathcal{S}$.

We define a d-dimensional color code H. Bombin, 2013 on the lattice $\mathcal{L}$, where $d = \dim \mathcal{L}$, as the CSS subsystem code with X- and Z-type gauge generators supported on $(d-2-z)$- and $(d-2-x)$-simplices in $\mathcal{L}$,

$$\mathcal{G} = \langle X(\delta), Z(\sigma) | \forall \delta \in \Delta'_{d-2-z}(\mathcal{L}), \sigma \in \Delta'_{d-2-x}(\mathcal{L}) \rangle, \tag{4.18}$$

where $x + z \leq d - 2$. The X- and Z-type generators of the stabilizer group $\mathcal{S}$ are supported on x- and z-simplices, namely

$$\mathcal{S} = \langle X(\delta), Z(\sigma) | \forall \delta \in \Delta'_x(\mathcal{L}), \sigma \in \Delta'_z(\mathcal{L}) \rangle. \tag{4.19}$$

We refer to this code by $CC_{\mathcal{L}}(x, z)$. When context makes the lattice unambiguous, we sometimes use $CC_d(x, z)$ to emphasize the dimensionality of the lattice, $\dim \mathcal{L} = d$. Note that the generators of the gauge and stabilizer groups are supported on simplices which do not belong to $\partial\mathcal{L}$, the boundary of the lattice $\mathcal{L}$.

To illustrate the language introduced in this section, we revisit the two-dimensional color code described in Sections 4.2 and 4.2. We begin with the lattice $\mathcal{L}$ shown in Fig. 4.1d. Qubits are placed on 2-simplices (triangular faces). Since $x + z \leq \dim \mathcal{L} - 2 = 0$, there is only one color code on the two-dimensional lattice $\mathcal{L}$, namely $CC_{\mathcal{L}}(0, 0)$, which is a stabilizer code. Stabilizer generators are associated with 0-simplices (vertices). Note that no stabilizer generators are assigned to the three vertices belonging to the boundary of $\mathcal{L}$.

Properties of the lattice

Here we present some properties of any $(d+1)$-colorable homogeneous simplicial d-complex $\mathcal{L}$. We use these properties to verify that $CC_{\mathcal{L}}(x, z)$ is a valid code, and later that there is a transversal implementation of $\overline{R}_n$. We start with the following lemmas.

Lemma 4.2 (Intersection)**.** Let δ and σ be two simplices in $\mathcal{L} \setminus \partial\mathcal{L}$. If $\mathcal{Q}(\delta) \cap \mathcal{Q}(\sigma) \neq \emptyset$, then $\mathcal{Q}(\delta) \cap \mathcal{Q}(\sigma) = \mathcal{Q}(\tau)$, where τ is the smallest simplex containing both δ and σ.

Proof. If $\mathcal{Q}(\delta) \cap \mathcal{Q}(\sigma) \neq \emptyset$, then there exists $\epsilon \in \Delta_d(\mathcal{L})$ such that $\epsilon \supset \delta, \sigma$. Let $C = \text{color}(\delta) \cup \text{color}(\sigma)$ and set τ to be the unique $(|C| - 1)$-simplex in ϵ, colored

with the set of colors C. Since $\tau \supset \delta$, then $\mathcal{Q}(\tau) \subset \mathcal{Q}(\delta)$; similarly $\mathcal{Q}(\tau) \subset \mathcal{Q}(\sigma)$, and therefore $\mathcal{Q}(\tau) \subset \mathcal{Q}(\delta) \cap \mathcal{Q}(\sigma)$. As τ is the smallest simplex containing δ and σ, then $\mathcal{Q}(\tau) \supset \mathcal{Q}(\delta) \cap \mathcal{Q}(\sigma)$ and thus $\mathcal{Q}(\delta) \cap \mathcal{Q}(\sigma) = \mathcal{Q}(\tau)$. □

Lemma 4.3 (Disjoint Union)**.** Let $\mathcal{L}$ be a simplicial d-complex which is $(d+1)$-colorable. Then, for a simplex $\delta \subset \mathcal{L} \setminus \partial\mathcal{L}$ and a chosen set of colors C, such that $\mathrm{color}(\delta) \subset C \subset \mathbb{Z}_{d+1}$, there exists a partition of the set of qubits supported on δ into a disjoint union of sets of qubits supported on $(|C|-1)$-simplices containing δ, namely

$$\mathcal{Q}(\delta) = \bigsqcup_{\substack{\sigma \supset \delta \\ \sigma \in \Delta'_{|C|-1}(\mathcal{L}) \\ \mathrm{color}(\sigma) = C}} \mathcal{Q}(\sigma). \tag{4.20}$$

Proof. First note, that two different k-simplices δ_1 and δ_2 in $\mathcal{L} \setminus \partial\mathcal{L}$ colored with the same colors, $\mathrm{color}(\delta_1) = \mathrm{color}(\delta_2)$, cannot belong to the same l-simplex, $l \geq k$, thus do not share a qubit, $\mathcal{Q}(\delta_1) \cap \mathcal{Q}(\delta_2) = \emptyset$. Moreover, if $\mathcal{Q}(\epsilon) \subset \mathcal{Q}(\delta)$, where $\epsilon \in \Delta_d(\mathcal{L})$, then $\epsilon \supset \delta$ and there exists a unique simplex $\sigma \subset \epsilon$ colored with colors C. Since $\mathrm{color}(\sigma) = C \supset \mathrm{color}(\delta)$, then $\sigma \supset \delta$, which finishes the proof of the (Disjoint Union) Lemma 4.3. □

As a corollary of the (Disjoint Union) Lemma 4.3 we obtain the following

Lemma 4.4 (Even Support)**.** Let δ be a k-simplex not belonging to the boundary of the lattice, $\delta \subset \Delta'_k(\mathcal{L})$, with $0 \leq k < d$. Then

$$|\mathcal{Q}(\delta)| \equiv 0 \mod 2. \tag{4.21}$$

Before we prove the (Even Support) Lemma 4.4, we explain its consequences. For $CC_d(x,z)$ to be a subsystem code, where $x+z \leq d-2$, the stabilizer generators have to commute with each other, as well as with the gauge group generators. Notice that for two arbitrary X- and Z-type stabilizer generators to commute, the intersection of their supports has to contain even number of elements. By definition, X- and Z-type stabilizer generators be supported on $\delta \subset \Delta'_x(\mathcal{L})$ and $\sigma \subset \Delta'_z(\mathcal{L})$, respectively. If the intersection $\mathcal{Q}(\delta) \cap \mathcal{Q}(\sigma)$ is non-empty, then due to the (Intersection) Lemma 4.2 there exists a simplex τ such that $\mathcal{Q}(\delta) \cap \mathcal{Q}(\sigma) = \mathcal{Q}(\tau)$. Moreover, since δ is spanned by $x+1$ vertices and σ by $z+1$ vertices, then τ is spanned by at most

$x + z + 2 \leq d$ vertices. Thus, τ is a k-simplex with $k < d$, and the (Even Support) Lemma 4.4 applies, $|\mathcal{Q}(\delta) \cap \mathcal{Q}(\sigma)| = |\mathcal{Q}(\tau)| \equiv 0 \mod 2$, showing that $X(\delta)$ and $Z(\sigma)$ commute. The commutation of stabilizer generators with the gauge generators follows similarly.

Proof. The set of qubits supported on any k-simplex δ in $\mathcal{L} \setminus \partial\mathcal{L}$ with $k < d$ can be decomposed as a disjoint union of qubits supported on $(d-1)$-simplices σ containing δ and colored with a chosen set of d colors, $C \supset \mathrm{color}(\delta)$. Note that any $(d-1)$-simplex $\sigma \in \Delta'_{d-1}(\mathcal{L})$ separates two d-simplices, and then $|\mathcal{Q}(\sigma)| = 2$, which immediately yields

$$|\mathcal{Q}(\delta)| = \sum_{\substack{\sigma \supset \delta \\ \sigma \in \Delta'_{d-1}(\mathcal{L}) \\ \mathrm{color}(\sigma) = C}} |\mathcal{Q}(\sigma)| \equiv 0 \mod 2, \tag{4.22}$$

showing the (Even Support) Lemma 4.4. □

The property needed for the transversal implementation of the gate $\overline{R}_n$, presented in Section 4.4, can be encapsulated in the following lemma

Lemma 4.5 (Bipartition of Qubits)**.** The set of d-simplices in $\mathcal{L}$, $\Delta_d(\mathcal{L})$, is bipartite.

Let us first explain the (Bipartition of Qubits) Lemma 4.5 — the d-simplices in $\mathcal{L}$ can be split into two disjoint sets, where d-simplices in the first set share $(d-1)$-faces only with d-simplices from the second set, and vice versa.

Proof. First, construct a graph $G = (V, E)$ with the set of vertices $V = \Delta_d(\mathcal{L})$ and the set of edges $E = \Delta'_{d-1}(\mathcal{L})$. Two vertices $v, w \in V$ are connected by an edge $e \in E$ iff d-simplices corresponding to v and w share a $(d-1)$-face corresponding to e. Since for all $\delta \in \Delta'_{d-2}(\mathcal{L})$ the (Even Support) Lemma 4.4 gives $|\mathcal{Q}(\delta)| \equiv 0 \mod 2$, and every cycle in $\mathcal{L}$ is contractible, we obtain that every cycle in the graph G is even. Using the (Graph Bipartition) Lemma 4.1 we immediately obtain that G is bipartite. This shows that the set of d-simplices in $\mathcal{L}$, which is equal to the set of qubits, $\Delta_d(\mathcal{L}) = Q$, is bipartite. □

4.4 Transversal gates in color codes

As mentioned in the introduction, transversal gates are fault-tolerant. In this section, we first review some relevant features of a class of CSS subsystem codes, which includes the color codes defined in Section 4.3. Then, we examine transversal gates of codes in this class. We show that $\overline{\text{CNOT}}$ is transversal in any such code and under certain additional conditions the Hadamard and $\overline{R}_n$ can be transversal, too. Finally, we show that the additional conditions are satisfied by certain color codes.

Subsystem codes

A CSS subsystem code Poulin, 2005; Bacon, 2006 is specified by its gauge group $\mathcal{G}$, which is a subgroup of the Pauli group on physical qubits Q. Each X-type gauge group generator $X(G^x)$ consists of Pauli X operators applied to qubits G^x; similarly for Z-type generators. The stabilizer group $\mathcal{S} \subseteq \mathcal{G}$ is the group generated by all Pauli operators $X(S^x)$ and $Z(S^z)$ contained in $\mathcal{G}$, which commute with every element of $\mathcal{G}$. (Note that a stabilizer code is a special case of a subsystem code, for which $\mathcal{G} = \mathcal{S}$). The codewords are the $+1$ eigenvectors of all elements of $\mathcal{S}$. We say that two codewords are equivalent if they differ by application of a linear combination of elements of $\mathcal{G} \setminus \mathcal{S}$. This allows one to decompose the subspace of codewords into a tensor product of two spaces: *logical* qubits and *gauge* qubits. Elements of $\mathcal{G} \setminus \mathcal{S}$ have no effect on the state of the logical qubits, but may change that of the gauge qubits.

For a subsystem code, we say a unitary implements a *logical gate* if it preserves the space of all codewords, and has an action on the logical qubits which is independent of any action on the gauge qubits. A logical gate $\overline{U}$ can be implemented on the logical qubits $|\psi\rangle$ as a *bare* gate U_{bare} which leaves gauge qubits $|g\rangle$ unchanged, $U_{\text{bare}} : |\psi\rangle|g\rangle \mapsto (\overline{U}|\psi\rangle)|g\rangle$, or more generally as a *dressed* gate U_{dressed}, which can affect the gauge qubits too, $U_{\text{dressed}} : |\psi\rangle|g\rangle \mapsto (\overline{U}|\psi\rangle)|g'\rangle$.

Consider the class of CSS subsystem codes which

- encode one logical qubit,
- have bare logical $\overline{X}$ and $\overline{Z}$ implemented by $X(Q)$ and $Z(Q)$.

Note that these codes are defined on an odd number of physical qubits, $|Q| \equiv 1 \mod 2$, since $\overline{X}$ and $\overline{Z}$ anti-commute.

We can define a pair of inequivalent (and not normalized) codewords, which are representatives of logical $\left|\overline{0}\right\rangle$ and $\left|\overline{1}\right\rangle$, namely

$$|\overline{0}\rangle|g_X\rangle = \sum_{X(G)\in\mathcal{G}} X(G)\,|\mathbf{0}\rangle\,, \tag{4.23}$$

$$|\overline{1}\rangle|g_X\rangle = \overline{X}|\overline{0}\rangle|g_X\rangle, \tag{4.24}$$

where $|\mathbf{0}\rangle$ is a state with every physical qubit set to $|0\rangle$, and $|g_X\rangle$ is a fixed state of the gauge qubits. One can verify that the states $|\overline{0}\rangle|g_X\rangle$ and $|\overline{1}\rangle|g_X\rangle$ are $+1$ eigenstates of $\mathcal{S}$, and satisfy $\overline{Z}|\overline{0}\rangle|g_X\rangle = |\overline{0}\rangle|g_X\rangle$, $\overline{Z}|\overline{1}\rangle|g_X\rangle = -|\overline{1}\rangle|g_X\rangle$. They are also $+1$ eigenstates of every X-type generator of $\mathcal{G}$. All equivalent codewords can be generated from $|\overline{0}\rangle|g_X\rangle, |\overline{1}\rangle|g_X\rangle$ by application of a linear combination of elements from $\mathcal{G}\setminus\mathcal{S}$. An alternative pair of representatives of logical $\left|\overline{0}\right\rangle$ and $\left|\overline{1}\right\rangle$ is

$$|\overline{0}\rangle|g_Z\rangle = \sum_{X(S)\in\mathcal{S}} X(S)\,|\mathbf{0}\rangle\,, \tag{4.25}$$

$$|\overline{1}\rangle|g_Z\rangle = \overline{X}|\overline{0}\rangle|g_Z\rangle, \tag{4.26}$$

which are $+1$ eigenstates of all Z-type generators of $\mathcal{G}$.

Transversal gates in subsystem codes

Consider a CSS subsystem code with one logical qubit, and $\overline{X}$ and $\overline{Z}$ implemented by $X(Q)$ and $Z(Q)$. To check that a physical unitary U implements a dressed logical gate $\overline{U}$ in such a code, one can verify its action on $|\overline{0}\rangle|g\rangle$, and $|\overline{1}\rangle|g\rangle$ for every state $|g\rangle$ of the gauge qubits. Alternatively, it is sufficient to verify that U has the correct action by conjugation on $\overline{X}$ and $\overline{Z}$, and that it preserves[6] the gauge group $\mathcal{G}$.

The logical gate $\overline{\text{CNOT}}$ can be implemented transversally between two identical copies of this class of CSS subsystem codes by applying a physical gate CNOT to every pair of corresponding qubits in the first and the second copy. This can be verified by checking that under conjugation by $\overline{\text{CNOT}}$, $\overline{XI} \mapsto \overline{XX}$, $\overline{IX} \mapsto \overline{IX}$, $\overline{ZI} \mapsto \overline{ZI}$, $\overline{IZ} \mapsto \overline{ZZ}$ and $\mathcal{G}\otimes\mathcal{G}$ is preserved[7].

If the CSS subsystem code is also *self-dual*, namely it has X- and Z-type gauge group generators supported on the same sets of qubits, $\mathcal{G} = \langle X(G_i), Z(G_i)\rangle$, then a dressed logical Hadamard gate can be implemented transversally as $\overline{H} = H(Q)$. To

[6]Note that preservation of the gauge group under the action of a physical unitary U is a sufficient, but not a necessary condition for U to implement a dressed logical gate.

[7]Notice, that generators of $\mathcal{G}\otimes\mathcal{G}$ are mapped under conjugation to another set of generators, namely $X(G)\otimes I(G) \mapsto X(G)\otimes X(G)$, $Z(G)\otimes I(G) \mapsto Z(G)\otimes I(G)$, $I(G)\otimes X(G) \mapsto I(G)\otimes X(G)$ and $I(G)\otimes Z(G) \mapsto Z(G)\otimes Z(G)$.

see this, observe that under conjugation by $H(Q)$, $\overline{X} \mapsto \overline{Z}, \overline{Z} \mapsto \overline{X}$, $X(G) \mapsto Z(G)$ and $Z(G) \mapsto X(G)$, and thus $\mathcal{G}$ is preserved.

The last logical gate we analyze is $\overline{R}_n = \text{diag}\left(1, e^{\frac{2\pi i}{2^n}}\right)$, for an integer $n > 0$. We aim to implement $\overline{R}_n$ transversally as a bare logical gate by applying the same single-qubit unitary to some subset $T \subset Q$ of the physical qubits, and applying that unitary's inverse to the rest of the qubits $T^c := Q \setminus T$. Specifically, we now prove that $\overline{R}_n$ is implemented by $R = R_n^k(T)R_n^{-k}(T^c)$, for some suitably chosen $k \in \{1, 2, \ldots, 2^n - 1\}$, provided that T and $\mathcal{G}$ satisfy

$$\forall X(G) \in \mathcal{G} : |T \cap G| \equiv |T^c \cap G| \mod 2^n. \tag{4.27}$$

First, pick k such that

$$k(|T| - |T^c|) \equiv 1 \mod 2^n. \tag{4.28}$$

The existence of k is guaranteed by Bezout's lemma, since $|Q|$ is odd, $|T| - |T^c| = 2|T| - |Q| \equiv 1 \mod 2$, and thus $\gcd(|T| - |T^c|, 2^n) = 1$. Noting that $R_n^{\pm k}|0\rangle = |0\rangle$ and $R_n^{\pm k}X = e^{\pm\frac{2\pi i k}{2^n}} X R_n^{\mp k}$, we obtain

$$\begin{aligned}
R|\overline{0}\rangle|g_X\rangle &= \sum_{X(G)\in\mathcal{G}} R_n^k(T)R_n^{-k}(T^c)X(G)|\mathbf{0}\rangle && (4.29)\\
&= \sum_{X(G)\in\mathcal{G}} e^{\frac{2\pi i k}{2^n}|T\cap G|} e^{-\frac{2\pi i k}{2^n}|T^c\cap G|} X(G)\,|\mathbf{0}\rangle && (4.30)\\
&= \sum_{X(G)\in\mathcal{G}} X(G)|\mathbf{0}\rangle = |\overline{0}\rangle|g_X\rangle, && (4.31)\\
R|\overline{1}\rangle|g_X\rangle &= R_n^k(T)R_n^{-k}(T^c)X(Q)|\overline{0}\rangle|g_X\rangle && (4.32)\\
&= e^{\frac{2\pi i k}{2^n}|T|} e^{-\frac{2\pi i k}{2^n}|T^c|} X(Q)R|\overline{0}\rangle|g_X\rangle && (4.33)\\
&= e^{\frac{2\pi i}{2^n}} X(Q)|\overline{0}\rangle|g_X\rangle = e^{\frac{2\pi i}{2^n}}|\overline{1}\rangle|g_X\rangle, && (4.34)
\end{aligned}$$

which shows that R correctly implements logical $\overline{R}_n$ when the gauge qubits are in the state $|g_X\rangle$. It remains to show that R implements $\overline{R}_n$ for arbitrary states of the gauge qubits. However, all other states of the gauge qubits can be reached from $|g_X\rangle$ by application of linear combinations of Z-type operators from $\mathcal{G} \setminus \mathcal{S}$, which all commute with R (since it is diagonal in the Z-basis). Therefore for any state $|g\rangle$ of the gauge qubits, it must be that $R : |\overline{0}\rangle|g\rangle \mapsto |\overline{0}\rangle|g\rangle, |\overline{1}\rangle|g\rangle \mapsto e^{\frac{2\pi i}{2^n}}|\overline{1}\rangle|g\rangle$, verifying that R implements the bare logical gate $\overline{R}_n$.

It may not be obvious that there exists a set $T \subset Q$ satisfying (4.27) for a given code. Later we will find such a T for color codes in d dimensions, with $n \leq d$.

Condition (4.27) can be inferred from the following condition

$$\left| T \cap \bigcap_{i=1}^{m} G_i \right| \equiv \left| T^c \cap \bigcap_{i=1}^{m} G_i \right| \mod 2^{n-m+1}, \tag{4.35}$$

where $m = 1, \ldots, n$ and $\{X(G_1), \ldots, X(G_m)\}$ is any subset of the X-type generators of the gauge group $\mathcal{G}$. To see the implication (4.35) $\Longrightarrow$ (4.27) notice, that for any $X(G) \in \mathcal{G}$, we can write $X(G)$ as a product of generators, namely $X(G) = \prod_{i=1}^{m} X(G_i)$. Then

$$G = G_1 \veebar G_2 \veebar \ldots \veebar G_m, \tag{4.36}$$

where we used the symmetric difference of sets, $A \veebar B := (A \setminus B) \cup (B \setminus A)$. Using the Inclusion-Exclusion Principle for symmetric difference[8] we obtain

$$\begin{aligned} |T \cap G| &= |T \cap (G_1 \veebar G_2 \veebar \ldots \veebar G_m)| && (4.37) \\ &= \sum_i |T \cap G_i| - 2 \sum_{i \neq j} |T \cap (G_i \cap G_j)| + \\ &\quad 4 \sum_{i \neq j \neq k} |T \cap (G_i \cap G_j \cap G_k)| - \ldots \\ &\quad + (-2)^{m-1} |T \cap (G_1 \cap G_2 \cap \ldots \cap G_m)|, && (4.38) \end{aligned}$$

and a similar expression for $|T^c \cap G|$. Clearly, if condition (4.35) holds, then $|T \cap G| - |T^c \cap G| \equiv 0 \mod 2^n$, showing (4.27). Moreover, condition (4.35) is easier to verify than condition (4.27), since we only need to check it for the X-type generators of $\mathcal{G}$, rather than for every X-type element of $\mathcal{G}$.

We can summarize the discussion of the implementation of transversal $\overline{R}_n$ in the following lemma

Lemma 4.6 (Sufficient Condition)**.** Consider a CSS subsystem code encoding one logical qubit. Let the code be defined on a set of physical qubits Q, where $|Q|$ is odd and with bare logical operators $\overline{X} = X(Q)$ and $\overline{Z} = Z(Q)$. If there exists $T \subset Q$, such that for any $m = 1, \ldots, n$:

$$\left| T \cap \bigcap_{i=1}^{m} G_i \right| \equiv \left| T^c \cap \bigcap_{i=1}^{m} G_i \right| \mod 2^{n-m+1}, \tag{4.39}$$

for every subset $\{X(G_1), \ldots, X(G_m)\}$ of the X-type gauge generators of the code, then

$$R = R_n^k(T) R_n^{-k}(T^c) \tag{4.40}$$

[8] For sets $A_1, A_2, \ldots, A_m$, we have $|A_1 \veebar A_2 \veebar \ldots \veebar A_m| = \sum_i |A_i| - 2 \sum_{i \neq j} |A_i \cap A_j| + \ldots + (-2)^{m-1} |A_1 \cap A_2 \cap \ldots \cap A_m|$.

implements logical $\overline{R}_n$, where k is a solution to $k(|T| - |T^c|) \equiv 1 \mod 2^n$ and $T^c = Q \setminus T$.

Transversal implementation of $\overline{R}_n$ in color code

Here we show how to implement the logical gate $\overline{R}_n$ transversely in the color code $CC_{\mathcal{L}}(x, z)$, for any integer $n \leq d/(d-1-z)$, where $d = \dim(\mathcal{L})$. One applies $R = R_n^k(T)R_n^{-k}(T^c)$ for some integer k, where T and its compliment $T^c = Q \setminus T$ correspond to the bipartite decomposition of qubits Q specified in the (Bipartition of Qubits) Lemma 4.5. We make use of the following property

Lemma 4.7 (Property of T)**.** For any m-simplex σ in $\mathcal{L} \setminus \partial\mathcal{L}$ with $m < d$

$$|T \cap \mathcal{Q}(\sigma)| = |T^c \cap \mathcal{Q}(\sigma)|. \tag{4.41}$$

Proof. By the choice of the set T, every $(d-1)$-simplex δ has one qubit in T, and one qubit in $T^c = Q \setminus T$, which is equivalent to $|T \cap \mathcal{Q}(\delta)| = |T^c \cap \mathcal{Q}(\delta)|$. Using the (Disjoint Union) Lemma 4.3, we can decompose the set of qubits $\mathcal{Q}(\sigma)$ supported on an m-simplex σ, where $m < d$, as a disjoint union of qubits supported on $(d-1)$-simplices colored with a chosen set of d colors $C \supset \mathrm{color}(\sigma)$, and then we immediately obtain

$$|T \cap \mathcal{Q}(\sigma)| \quad -|T^c \cap \mathcal{Q}(\sigma)| = \tag{4.42}$$

$$\sum_{\substack{\delta \supset \sigma \\ \delta \in \Delta'_{d-1}(\mathcal{L}) \\ \mathrm{color}(\delta) = C}} |T \cap \mathcal{Q}(\delta)| - |T^c \cap \mathcal{Q}(\delta)| = 0, \tag{4.43}$$

which shows the (Property of T) Lemma 4.7.

□

Note that (4.39) in the (Sufficient Condition) Lemma 4.6 follows form the (Property of T) Lemma 4.7. To see this, observe first that every stabilizer generator $X(\delta_i)$ is supported on a $(d-2-z)$-simplex δ_i, thus $G_i = \mathcal{Q}(\delta_i)$ and for $m = 1, \ldots, n$ we obtain

$$\bigcap_{i=1}^{m} \mathcal{Q}(\delta_i) = \emptyset \quad \text{or} \quad \bigcap_{i=1}^{m} \mathcal{Q}(\delta_i) = \mathcal{Q}(\tau), \tag{4.44}$$

where τ is a simplex colored with colors $C = \bigcup_{i=1}^{m} \mathrm{color}(\delta_i)$, such that $\tau \supset \delta_1, \ldots, \delta_m$. The case of an empty intersection is trivial. Since $|\mathrm{color}(\delta_i)| = d-1-z$,

then obviously $|C| \leq m(d-1-z) \leq n(d-1-z)$, and for τ to be at most a $(d-1)$-simplex, we need $n \leq d/(d-1-z)$. Using the (Property of T) Lemma 4.7 we obtain that for any $m = 1, ..., n$:

$$\left| T \cap \bigcap_{i=1}^{m} \mathcal{Q}(\delta_i) \right| - \left| T^c \cap \bigcap_{i=1}^{m} \mathcal{Q}(\delta_i) \right| = \tag{4.45}$$

$$|T \cap \mathcal{Q}(\tau)| - |T^c \cap \mathcal{Q}(\tau)| = 0, \tag{4.46}$$

which implies (4.39). The (Sufficient Condition) Lemma 4.6 implies that R implements the logical $\overline{R}_n$. In particular, one can implement $\overline{R}_d$ using the code $CC_d(0, d-2)$, since $z = d-2$, and thus $\lfloor d/(d-1-z) \rfloor = d$.

4.5 Universal transversal gates with color codes

A finite set of gates which is universal can be used to implement any logical unitary, with arbitrary precision. In particular, due to the Solovay-Kitaev A Yu Kitaev, 1997; M. Nielsen and I. Chuang, 2010 theorem, the number of applied gates scales poly-logarithmically with the precision of approximation. Note that the set $\{\overline{H}, \overline{\text{CNOT}}, \overline{R}_n\}$ is universal for any integer $n > 2$.

In this section, we show how to achieve a universal transversal gate set with color codes by using the technique of *gauge fixing* to switch between different codes. This technique allows one to take advantage of the transversally implementable gates for different color codes. We first illustrate the method with a simple example of two 15-qubit codes Paetznick and Reichardt, 2013; Jonas T. Anderson, Duclos-Cianci, and Poulin, 2014. Then, we define a partial order between color codes. One can switch between color codes which are comparable with respect to the partial order to implement a universal gate set in three or higher dimensions.

Switching between codes using gauge fixing

First, let us define matrices H_1 and H_2 given by

$$H_1 = \begin{pmatrix} 1 & 1 & 1 & 1 & 1 & 1 & 1 & 1 & 0 & 0 & 0 & 0 & 0 & 0 & 0 \\ 1 & 1 & 1 & 1 & 0 & 0 & 0 & 0 & 1 & 1 & 1 & 1 & 0 & 0 & 0 \\ 1 & 1 & 0 & 0 & 1 & 1 & 0 & 0 & 1 & 1 & 0 & 0 & 1 & 1 & 0 \\ 1 & 0 & 1 & 0 & 1 & 0 & 1 & 0 & 1 & 0 & 1 & 0 & 1 & 0 & 1 \end{pmatrix}, \tag{4.47}$$

$$H_2 = \begin{pmatrix} 1 & 1 & 1 & 1 & 0 & 0 & 0 & 0 & 0 & 0 & 0 & 0 & 0 & 0 & 0 \\ 1 & 1 & 0 & 0 & 1 & 1 & 0 & 0 & 0 & 0 & 0 & 0 & 0 & 0 & 0 \\ 1 & 0 & 1 & 0 & 1 & 0 & 1 & 0 & 0 & 0 & 0 & 0 & 0 & 0 & 0 \\ 1 & 1 & 0 & 0 & 0 & 0 & 0 & 0 & 1 & 1 & 0 & 0 & 0 & 0 & 0 \\ 1 & 0 & 1 & 0 & 0 & 0 & 0 & 0 & 1 & 0 & 1 & 0 & 0 & 0 & 0 \\ 1 & 0 & 0 & 0 & 1 & 0 & 0 & 0 & 1 & 0 & 0 & 0 & 1 & 0 & 0 \end{pmatrix}. \tag{4.48}$$

These matrices have a property that each row in H_1 is orthogonal to every row in H_1 and H_2 (modulo 2). Moreover, for a binary matrix M, we define M^X to be a matrix obtained from M by the following substitutions, $0 \mapsto I$ and $1 \mapsto X$. Similarly for M^Z, we substitute $0 \mapsto I$ and $1 \mapsto Z$. Let $\mathcal{C}_A$ be the stabilizer code with the stabilizer group $\mathcal{S}_A$ generated by rows of H_1^X, H_1^Z and H_2^Z, which we denote by

$$\mathcal{S}_A = \langle H_1^X, H_1^Z, H_2^Z \rangle. \tag{4.49}$$

Let $\mathcal{C}_B$ be the subsystem code with the stabilizer group $\mathcal{S}_B$ and the gauge group $\mathcal{G}_B$ chosen as follows

$$\mathcal{S}_B = \langle H_1^X, H_1^Z \rangle, \;\; \mathcal{G}_B = \langle H_1^X, H_2^X, H_1^Z, H_2^Z \rangle. \tag{4.50}$$

We can consider both codes $\mathcal{C}_A$ and $\mathcal{C}_B$ to be defined on the same 15 physical qubits. One can check that $\mathcal{C}_A$ represents the $[[15, 1, 3]]$ quantum Reed-Muller (stabilizer) code MacWilliams and Sloane, 1977; Steane, 1999; Jonas T. Anderson, Duclos-Cianci, and Poulin, 2014 and $\mathcal{C}_B$ is a $[[15, 1, 3]]$ (subsystem) code, which can be thought of as the $[[15, 7, 3]]$ Hamming code, with six of the seven logical qubits treated as gauge qubits. Note also that $\mathcal{S}_B \subset \mathcal{G}_A = \mathcal{S}_A$ and $\mathcal{G}_B$ has X- and Z-type generators supported on the same qubits (i.e. $\mathcal{C}_B$ is a self-dual subsystem code).

Since the X-type generators of $\mathcal{S}_B$ coincide with the X-type generators of $\mathcal{S}_A$, the codewords of $\mathcal{C}_A$ and $\mathcal{C}_B$ are the same when the latter has a gauge state $|g_Z\rangle$. In other words, codewords $|\bar{0}\rangle$, $|\bar{1}\rangle$ for $\mathcal{C}_A$ are the same as codewords $|\bar{0}\rangle|g_Z\rangle$, $|\bar{1}\rangle|g_Z\rangle$ for $\mathcal{C}_B$, as defined in Eqs. (4.25) and (4.26). On the other hand the codewords $|\bar{0}\rangle|g_X\rangle$, $|\bar{1}\rangle|g_X\rangle$ for $\mathcal{C}_B$ (as defined in Eqs. (4.23) and (4.24)), are not valid codewords for $\mathcal{C}_A$.

Now we show that $R_3^{\otimes 15}$ implements $\overline{R}_3$ transversally in $\mathcal{C}_A$. Consider any three of the four X-type generators for $\mathcal{G}_A$, and specify their support on subsets of qubits G_1, G_2, G_3, which correspond to rows of H_1. One can verify that $|G_a| = 8 \equiv 0 \mod 2^3$, $|G_a \cap G_b| = 4 \equiv 0 \mod 2^2$, and $|G_a \cap G_b \cap G_c| = 2 \equiv 0 \mod 2$, where $\{a, b, c\} = \{1, 2, 3\}$. Therefore by the (Sufficient Condition) Lemma 4.6, and by setting T to be an empty set, $T = \emptyset$, we see that $R_3^{\otimes 15}$ implements $\overline{R}_3$ transversally in the code $\mathcal{C}_A$. In contrast for the code $\mathcal{C}_B$, the extra X-type generators in $\mathcal{G}_B \setminus \mathcal{G}_A$ do not satisfy these conditions, and thus one cannot show that $\overline{R}_3$ is implemented transversally in $\mathcal{C}_B$.

It is straightforward to verify that $\overline{H}$ is implemented transversally by $H^{\otimes 15}$ in $\mathcal{C}_B$. It swaps X and Z on any physical qubit, and therefore acts on the representative states as $H^{\otimes 15} : |\psi\rangle|g_Z\rangle \mapsto (\overline{H}|\psi\rangle)|g_X\rangle$. Since the state of the gauge qubits has changed, $H^{\otimes 15}$ is a dressed implementation of $\overline{H}$ in $\mathcal{C}_A$. Clearly, $H^{\otimes 15}$ does not implement $\overline{H}$ in $\mathcal{C}_A$, since it takes the state $|\psi\rangle|g_Z\rangle \in \mathcal{C}_A$ to $(\overline{H}|\psi\rangle)|g_X\rangle \notin \mathcal{C}_A$.

To implement $\overline{H}$ fault-tolerantly in $\mathcal{C}_A$, we use the technique of *gauge fixing*. First, one should apply $H^{\otimes 15}$, resulting in mapping $|\psi\rangle|g_Z\rangle$ to $(\overline{H}|\psi\rangle)|g_X\rangle$, which is a codeword of $\mathcal{C}_B$, but not of $\mathcal{C}_A$. Then, to switch from code $\mathcal{C}_B$ to $\mathcal{C}_A$, one should sequentially measure each of the six Z-type stabilizer generators generated by rows of H_2^Z, i.e. those in $\mathcal{S}_A \setminus \mathcal{S}_B$. Note that it is possible to fault-tolerantly measure the stabilizer generators M. Nielsen and I. Chuang, 2010. If the measurement reveals that a particular Z-type generator is not satisfied, then one should apply an X-type Pauli operator which commutes with all generators in H_2^Z and H_1^Z, except for the violated stabilizer generator (with which it must anti-commute). Such an X-type Pauli operator always exists. Following this, the Z-type generator will no longer be violated. Therefore, after this procedure is carried out for all six generators in H_2^Z, the state will have changed from $(\overline{H}|\psi\rangle)|g_X\rangle$ to $(\overline{H}|\psi\rangle)|g_Z\rangle$, as required. Specifically, we use the term *gauge fixing* to refer to the process of measuring and setting the gauge qubits to a desired state, without affecting the logical qubits.

To recap, in the $[[15, 1, 3]]$ Reed-Muller code $\mathcal{C}_A$, one can implement $\overline{H}$ fault-tolerantly with the following procedure

$$|\psi\rangle\,|g_Z\rangle \xmapsto{H^{\otimes 15}} (\overline{H}\,|\psi\rangle)\,|g_X\rangle \xmapsto{\text{gauge fixing}} (\overline{H}\,|\psi\rangle)\,|g_Z\rangle\,. \tag{4.51}$$

In combination with the transversal gates of $\mathcal{C}_A$, this allows one to implement a fault-tolerant universal gate set $\{\overline{H}, \overline{\text{CNOT}}, \overline{R}_3\}$. We will repeat essentially the same procedure for color codes later.

Partial order of color codes

Given a d-dimensional lattice $\mathcal{L}$, $\dim \mathcal{L} = d$, satisfying Conditions 1 and 2 in Section 4.3 B, we can catalog all color codes defined on $\mathcal{L}$. Namely, a pair of integers $x, z \geq 0$, such that $x + z \leq d - 2$, corresponds to a color code, denoted as $CC_{\mathcal{L}}(x, z)$, with X- and Z-type gauge generators supported on $(d - 2 - z)$- and $(d - 2 - x)$-simplices. Note that the X- and Z-type stabilizer generators of $CC_{\mathcal{L}}(x, z)$ are supported on x-simplices and z-simplices, respectively. In two dimensions, $d = 2$, there is only one color code, $CC_2(0, 0)$ — a stabilizer code, with both X- and Z-type stabilizer generators supported on 0-simplices, whereas in three dimensions, $d = 3$, there are three color codes, $CC_3(1, 0)$, $CC_3(0, 1)$ — stabilizer codes, and $CC_3(0, 0)$ — a subsystem code.

One can define a partial order for subsystem color codes defined on the same lattice $\mathcal{L}$ if each codeword of code $\mathcal{C}$ is also a codeword of the other code $\mathcal{C}'$. In particular, we say that $\mathcal{C} \succ \mathcal{C}'$ holds if

- $\mathcal{C}$ and $\mathcal{C}'$ encode the same number of logical qubits, with identical bare logical Pauli operators,
- the gauge group $\mathcal{G}$ of $\mathcal{C}$ is contained in the gauge group $\mathcal{G}'$ of $\mathcal{C}'$, $\mathcal{G} \subset \mathcal{G}'$.

Note that $\mathcal{G} \subset \mathcal{G}'$ implies $\mathcal{S}' \subset \mathcal{S}$, thus any codeword of $\mathcal{C}$ is also a codeword of $\mathcal{C}'$, and since the bare Pauli operators for the logical qubit are the same in both codes, it actually represents the same logical codeword in both codes. Observe, that the partial order we have just defined can be succinctly expressed as

$$CC_{\mathcal{L}}(x, z) \succ CC_{\mathcal{L}}(x', z') \iff x \geq x' \wedge z \geq z', \tag{4.52}$$

as illustrated in Fig. 4.3. This follows from the observation that due to the (Disjoint Union) Lemma 4.3 the X-type gauge generators of $CC_{\mathcal{L}}(x, z)$, which are supported on $(d - 2 - z)$-simplices, can be expressed as the product of the X-type gauge generators of $CC_{\mathcal{L}}(x', z')$ supported on $(d-2-z')$-simplices, since $z \geq z'$. Similarly for Z-type gauge generators. We represent the family of color codes in Fig. 4.3, and show their partial order using arrows.

Universal fault-tolerant gate set in color codes

Here we apply the techniques just discussed to color codes defined on the same lattice $\mathcal{L}$. One can switch back and forth between two codes which are *comparable*, $CC_{\mathcal{L}}(x, z) \succ CC_{\mathcal{L}}(x', z')$, as follows

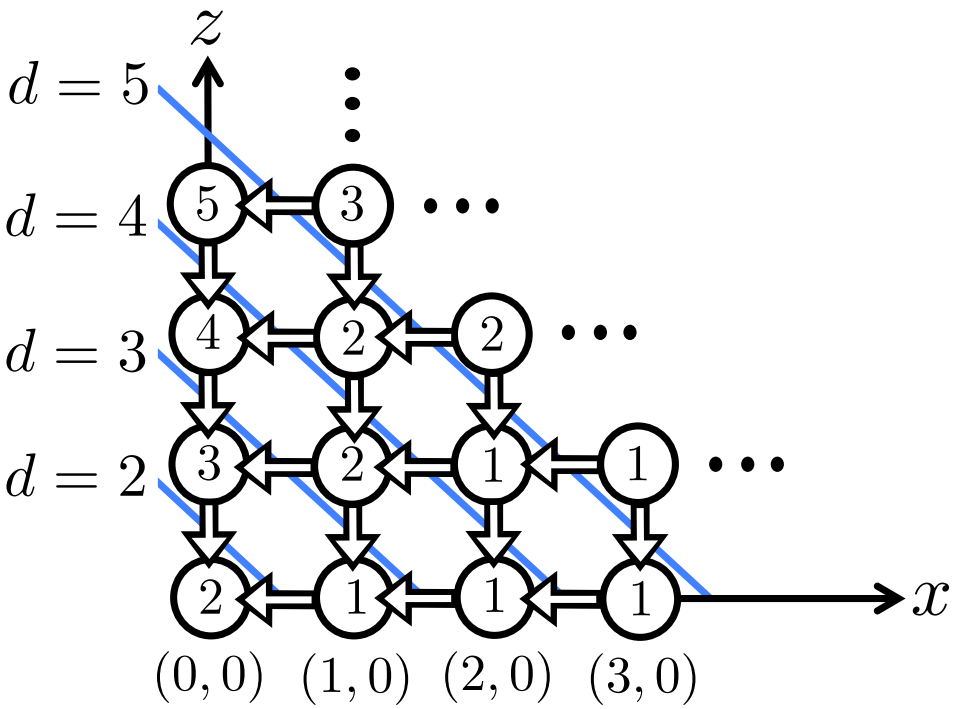

Figure 4.3: (Color online) Family of color codes. For a given lattice $\mathcal{L}$, only color codes below the d^{th} diagonal line can be realized, where $d = \dim \mathcal{L}$ and the point (x, z) corresponds to the color code $CC_{\mathcal{L}}(x, z)$. This constraint holds, since x and z have to satisfy $x + z \leq d - 2$. An arrow from code $\mathcal{C}$ to $\mathcal{C}'$ indicates partial order between them, $\mathcal{C} \succ \mathcal{C}'$. The number placed at (x, z) indicates the maximum gate $\overline{R}_n$ which can be implemented transversally with the stabilizer color code $CC_d(x, z)$, with $d = x + z + 2$, resulting in $n = \lfloor d/(d - 1 - z) \rfloor$.

- $CC_{\mathcal{L}}(x, z) \mapsto CC_{\mathcal{L}}(x', z')$: one does nothing, since codewords of $CC_{\mathcal{L}}(x, z)$ are codewords of $CC_{\mathcal{L}}(x', z')$,
- $CC_{\mathcal{L}}(x', z') \mapsto CC_{\mathcal{L}}(x, z)$: one can view the codewords of $CC_{\mathcal{L}}(x, z)$ as those for $CC_{\mathcal{L}}(x', z')$ with the additional gauge qubits present in $CC_{\mathcal{L}}(x, z)$ set to a particular state. To switch, one fixes the state of the additional gauge qubits to the appropriate state.

Given a three-dimensional lattice $\mathcal{L}$, $\dim \mathcal{L} = 3$, one can implement a universal gate set starting with the code $CC_{\mathcal{L}}(0, 1)$. As explained earlier, one can transversally perform the logical $\overline{\text{CNOT}}$ and $\overline{R_3}$ on that code. To form a universal gate set, it suffices to also implement logical $\overline{H}$. This gate cannot be implemented transversally in $CC_{\mathcal{L}}(0, 1)$, but can be in $CC_{\mathcal{L}}(0, 0)$. Note that $CC_3(0, 0) \prec CC_3(0, 1)$, therefore any codeword in $CC_3(0, 1)$ is a valid codeword in $CC_3(0, 0)$. In particular, we can

think of $|\psi\rangle \in CC_3(0,1)$ as $|\psi\rangle |g\rangle \in CC_3(0,0)$, where $|g\rangle$ is a state of the gauge qubits of $CC_3(0,0)$. By applying $H(Q)$ we perform the logical $\overline{H}$ on the logical qubits of $CC_3(0,0)$, which also changes the state of the gauge qubits, namely

$$H(Q)\left(|\psi\rangle |g\rangle\right) = \left(\overline{H}|\psi\rangle\right)|g'\rangle\,. \tag{4.53}$$

Note that the resulting codeword $\left(\overline{H}|\psi\rangle\right)|g'\rangle \in CC_3(0,0)$ is not a valid codeword of $CC_3(0,1)$, since the gauge qubits are in the state $|g'\rangle \neq |g\rangle$. To return to $CC_3(0,1)$, one needs to *fix the gauge qubits* to the correct state, namely $|g'\rangle \mapsto |g\rangle$, and we obtain a codeword $\overline{H}|\psi\rangle|g\rangle \in CC_3(0,1)$. Since $CC_3(0,1)$ is a stabilizer code, it is possible to measure and correct the violated stabilizers in a fault-tolerant way, just as in Section 4.5. Therefore, to fix the gauge, one should first measure all Z-type stabilizer generators supported on 1-simplices, and then apply the appropriate X-type Pauli operators in order to correct any violated stabilizer generators. After this, assuming no errors have occurred, all the stabilizer generators for $CC_3(0,1)$ are satisfied.

To summarize, we can perform the logical $\overline{H}$ on $CC_3(0,1)$ by first applying $H(Q)$ and subsequently fixing the gauge to return to the code space of $CC_3(0,1)$,

$$|\psi\rangle|g\rangle \xmapsto{H(Q)} \left(\overline{H}|\psi\rangle\right)|g'\rangle \xmapsto{\text{gauge fixing}} \left(\overline{H}|\psi\rangle\right)|g\rangle\,. \tag{4.54}$$

Since $\overline{\text{CNOT}}$ and $\overline{R}_3$ can be performed transversally in $CC_3(0,1)$, one can fault-tolerantly implement a universal gate-set $\{\overline{H}, \overline{\text{CNOT}}, \overline{R}_3\}$ in $CC_3(0,1)$. This procedure can be directly generalized to fault-tolerantly implement the universal gate set $\{\overline{H}, \overline{\text{CNOT}}, \overline{R}_d\}$ with the code $CC_d(0, d-2)$ in d dimensions.

4.6 Acknowledgements

We would like to thank Héctor Bombín for introducing us to color codes and taking the time to explain his results. We would like to thank Jeongwan Haah, Beni Yoshida, Olivier Landon-Cardinal, Gorjan Alagic and John Preskill for helpful comments on the manuscript. We thank Fernando Pastawski for pointing out bipartition as a possible construction of the set T. We acknowledge funding provided by the Institute for Quantum Information and Matter, an NSF Physics Frontiers Center with support of the Gordon and Betty Moore Foundation (Grants No. PHY-0803371 and PHY-1125565).

Chapter 5

OVERHEAD OF CODE SWITCHING AND STATE DISTILLATION

In the previous chapter, we explored a system in which a universal set of gates can be implemented in a three dimensional topological code in a fault-tolerant (transverse) way. Recall that the motivation for such a scheme was to reduce the large overhead involved in the known alternatives — in particular magic state distillation Sergey Bravyi and Alexei Kitaev, 2005; Austin G Fowler et al., 2012. In this chapter we study whether or not the scheme overcomes the problem that motivated it — does it significantly reduce the overhead requirements?

There are a number of difficulties to be expected in implementing the three dimensional color code described in Chapter 4. Recently, the three-dimensional color code has been flattened into psuedo two-dimensional schemes which still allow code switching Sergey Bravyi and Cross, 2015; Jochym-O'Connor and Bartlett, 2015; Jones, Brooks, and Harrington, 2015 to achieve universal transverse gates. These schemes seem much more experimentally feasible, but it is still unclear whether such a scheme has a threshold – in particular measurement errors may cause larger versions of the doubled color codes to perform worse rather than better than smaller versions. We will also comment on the resource requirements of these schemes.

Our analysis focuses on the two-dimensional color code, in which the Clifford gates can be implemented transversely. We also compare these techniques to the overhead requirements for the surface code. To achieve the non-Clifford $\pi/8$-gate that makes the gate set universal, a variant of code switching can be used to transforming from the two-dimensional color code to the three-dimensional stabilizer color code. In the three-dimensional code, the $\pi/8$-rotation is applied transversely, and then we imagine switching back to the two-dimensional code. In magic state distillation, many noisy magic states are injected into the code, and are distilled into fewer, higher fidelity magic states which can be used to implement the $\pi/8$ gate by an encoded Clifford circuit reminiscent of that used for teleportation.

As a part of this work, we found error thresholds of 0.3 % and 4.2 % under circuit-level and phenomenological noise for the two-dimensional color code on the hexagonal lattice using an efficient decoder based on that of Delfosse Delfosse,

2014. These are considerably higher than the thresholds for the previously analyzed 4.8.8 lattice, suggesting the performance of the color code may not be as far behind its cousin the surface code.

5.1 Quantum computing overhead

Accuracy threshold

An *accuracy threshold* Aharonov and Ben-Or, 1997, or *threshold* can be defined for a countably infinite quantum error correcting code family, where each code in the family is labelled (for example, by its distance d). The threshold is calculated for a code family assuming a simple specific noise model with a single parameter characterizing its strength. For example, the most common is to assume a depolarizing channel on each qubit, such that X, Y, Z are each applied with (independent) probability $p/3$ to each qubit during each time step. Then the threshold is probability p_T, such that provided $p < p_T$, then one can achieve arbitrarily good protection of the encoded qubits by increasing the distance of the code. For more general noise models, generalized notions of a threshold exist John Preskill, 2012.

Generically, the logical error probability p_L per time step[1] meaning of time-step at the logical level for the circuit level analysis is a for a code in the family of distance d will follow a form

$$p_L \approx \alpha(d)(p/p_T)^{d/2}, \tag{5.1}$$

where $\alpha(d)$ is a slow function of d which for practical purposes can sometimes be taken to be constant over "typical" distances. Clearly, a code family with a large threshold is advantageous as it means that the physical qubits required to use it for a code do not need to be as accurate, and the distance does not need to be increased as much to improve the logical error rate for a given $p < p_T$.

A relation such as Eq. (5.1) which relates the logical error rate to the physical error rate for each member of the code family can be used to infer the overhead. If a logical error rate of at most p_D can be tolerated for a logical qubit during each time step, then a sufficiently large member d_D must be used, such that $p_D < \alpha(d_D)(p/p_T)^{d_D/2}$. Then the overhead of that logical qubit is $n(d_D)$, where $n(d)$ is the number of physical qubits of family member d.

[1] Note that the word "time-step" could be misleading here. By it, we actually mean each round of stabilizer measurements, which may correspond to a number of physical time-steps in the circuit level analysis.

Treatment of measurement errors

Even assuming independent depolarizing noise on each qubit, more must be specified to fix the model and calculate a threshold. Such details can affect the threshold analysis of a code-family, for example the *syndrome decoder* and the model of the *syndrome measurement process*.

In the large class of stabilizer codes, the generic approach to perform error correction is to measure a set of low-weight stabilizer generators repeatedly, and record the measurement outcomes. Then, depending on the outcomes, a particular correction pauli operator is applied. The *syndrome decoder* is the classical algorithm which is used to choose which pauli to apply given the measurement outcomes. Typically, one focuses on either perfect decoders (which are not efficient to implement, but give an upper bound on the threshold), or on efficient decoders (which are expected be implementable in practice).

There are a number of standard models for the *syndrome measurement process*. In the *code capacity* model, measurements are assumed to be performed by a perfect quantum measurement device. In the *phenomenological noise* model, measurements are assumed to be performed by a perfect quantum measurement device, which feeds the decoder the incorrect syndrome with some probability. In the *circuit-level noise* model, additional (measurement) qubits are added to the (data) qubits, and are used to apply the syndrome measurements by sequentially applying CNOT gates between a measurement qubit and the data qubits involved in the syndrome measurement, before projectively measuring the measurement qubit.

It is generically the case that the syndrome decoder is qualitatively different in the setting of code capacity compared with phenomenological and circuit level noise. This is because (much) more information is usually needed to correct for the fact that measurement errors can occur in the latter two cases. This tends to significantly increase the classical complexity of the decoder, causing the classical processing to be quite slow. For example, in the surface code, one uses multiple rounds of syndromes to infer what correction should be applied when measurement errors are allowed in the model. In single shot error correction, which has been suggested occurs in the gauge version of the three-dimensional color code Hector Bombin, 2015, would avoid needing multiple rounds of syndrome data to identify the correction pauli. We will not consider single shot error correction in this work.

As an example of how these change the estimates, efficient decoders for Kitaev's surface code have been found to have thresholds of $\sim$ 10 % C. Wang, Harrington,

and John Preskill, 2003, ~ 3 % C. Wang, Harrington, and John Preskill, 2003, and ~ 0.6 % Austin G Fowler et al., 2012 for code-capacity, phenomenological and circuit-level noise respectively.

Circuit level noise model in our simulations

To give experimentally relevant estimates of performance and overhead, we consider circuit-level noise using an efficient syndrome decoder. For circuit-level noise, one must assign probabilities for errors of gates in each time-step in addition to the probability of errors of single idle qubits. Here we fix the model we will use in this paper. The precise noise model is defined by taking the original circuit for the code including syndrome measurements, and replacing gates as follows:

- A single-qubit gate $\{X, Y, Z, H, S, T\}$, or a single-qubit preparation, is replaced by itself followed by I with probability $1-p$, or X, Y, or Z each with probability $p/3$.
- A single-qubit measurement is replaced by itself, followed by I with probability $1-p$, or X, Y, or Z each with probability $p/3$.
- A single-qubit idle step I is replaced by itself, preceded by I with probability $1-p$, or X, Y, or Z each with probability $p/3$. (Note that the probability of error of an idle gate is often reduced from p to $p/10$ in threshold analysis. We will use p unless explicitly stated.)
- A two-qubit CNOT gate is replaced by itself followed by I with probability $1-p$, or each of XI, YI,..., ZY, or ZZ with probability $p/15$.

Note that in each time-step, each physical qubit is involved in a location: if no gate is applied to it then the identity location I is used.

A circuit-level threshold is given for a particular method of measuring the syndromes. The conceptually simplest approach to measure an X-type stabilizer generator is by preparing a measurement qubit in the $|+\rangle$ state, then sequentially applying a CNOT from the measurement qubit to each data qubit in the stabilizer generator, and then measuring the measurement qubit in the X basis. Similarly, one can measure a Z-type stabilizer generator by preparing the ancilla in a $|0\rangle$ state, applying a CNOT from each qubit in the stabilizer generator to the ancilla, and then measuring the ancilla qubit in the Z basis. Many CNOT gates can be applied in parallel, but to avoid generating errors, the circuit of CNOT gates must preserve all stabilizers of the

code state, in which case we say the schedule is 'valid'. For example, the circuit that applies CNOT gates between the data and the measurement ancilla qubits should propagate an X operator applied to any X-type measurement qubit to a stabilizer of the code space (where the stabilizer group here can act as X or Z on X and Z-type measurement qubits) Landahl, Jonas T Anderson, and Rice, 2011. Some valid schedules will propagate errors in a more benign way than others.

It is also possible to use Shor measurement (i.e. prepare and verify an m-qubit cat state to measures a weight m stabilizer). Hybrid approaches can be used where a number of smaller cat states are used to measure a single stabilizer. These cat-state based stabilizer measurement circuits would be expected to improve the threshold (through improved error propagation properties) but involve much more overhead.

Comparing overhead for state distillation and code switching

The encoded magic state $|T\rangle = |0\rangle + e^{i\pi/4}|1\rangle$ can be used to implement the encoded T gate through a small number of encoded Clifford operations. As the T gate generically dominates the overhead, we focus on the task of producing a magic state $|T\rangle$ as a proxy for the overall overhead of quantum computing. We compare the overhead required to produce a magic state of specified fidelity, encoded in a two-dimensional color code under realistic noise conditions, via: (1) code switching, and (2) state distillation.

To make this more precise, first consider each of the methods (1) and (2) as quantum circuits composed of preparation, measurement, and gates involving of the physical qubits. In particular the operations (locations) allowed are: I, X, Y, Z, H, S and T single-qubit operations, CNOT gates between pairs of qubits, and single-qubit measurements and preparations in the X and Z basis. Multi-qubit measurements are implemented within the circuit through entangling CNOT gates and single-qubit measurements. Noise is simulated by applying Pauli operators at each location of the circuit, with independent probabilities with a strength characterized by p (more details are given later). For each of the two approaches (1) and (2), we consider the circuit with the lowest width such that the final step in the circuit results in a magic state $|T\rangle$ encoded the hexagonal color code with logical error probability at most p_D. We are primarily interested in the qubit overhead (circuit width) of each technique, although to a lesser extent we also consider the time overhead (circuit depth).

5.2 Delfosse decoder

First we describe Delfosse's approach Delfosse, 2014 to decode the two-dimensional color code in the code capacity setting (i.e. when stabilizer measurements are assumed to be perfect). Then we describe the generalization of this decoder that can handle measurement error, which we later use to study the circuit level performance of the color code. It is neccesary to use an efficient decoder in order to calculate the threshold for the hexagonal color code and then the overhead requirements.

We use the Delfosse decoder due to its relative simplicity, although other decoders could be used, for example one could transform the two-dimensional color code by applying local unitaries into two decoupled copies of the toric code Hector Bombin, Duclos-Cianci, and Poulin, 2012; Kubica, Beni Yoshida, and Fernando Pastawski, 2015, and then one could running (for example) the renormalization group decoder Duclos-Cianci and Poulin, 2010 on each copy.

No measurement error

Consider a two-dimensional color code (either the 4.8.8, or the 6.6.6 lattice) with a triangular boundary [see figure 5.1(a)]. We refer to this as the *primal lattice*. The two-dimensional color code is a stabilizer code with qubits placed on vertices of the primal lattice, and two stabilizer generators for each face in the primal lattice: one generator consisting of X on each qubit in the face, and the other of Z on each qubit in the face. The primal lattices used for the color code have three-colorable faces, meaning that each face can be assigned one of three colors such that faces sharing an edge have distinct colors.

It is useful to construct the *dual lattice* [see figure 5.1(b)] by placing a dual vertex in each primal face (corresponding to stabilizer generators), connected by dual edges which intersect primal edges, to enclose dual faces around primal vertices (corresponding to data qubits). In the bulk, the dual of the regular hexagonal primal lattice is a regular triangular lattice. We add three "fictitious" vertices to the dual lattice, to terminate the edges in the dual lattice which intersect boundary edges in the primal lattice. Note that the vertices of the dual lattice inherit the coloring of the primal lattice (and therefore the dual lattice has three-colorable vertices). We describe the dual lattice by a graph G, consisting of the vertices V, and edges E. Each vertex in V corresponds to one X-type stabilizer generator and to one Z-type stabilizer generator.

Consider a state $|\psi\rangle$ in the codespace $\mathcal{C}$ (i.e. the $+1$ eigenspace of all stabilizer gen-

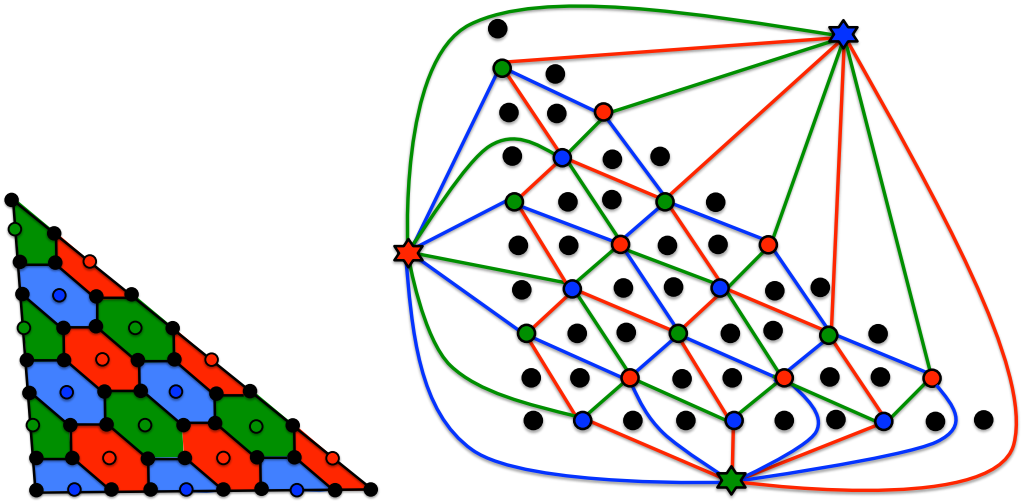

Figure 5.1: The dual lattice used to identify errors associated with stabilizer syndromes with the Delfosse decoder on the hexagonal color code with a triangular boundary. Vertices (corresponding to faces of the primal lattice) represent the measurements for the code, and are colored with three colors. A vertex (which does not correspond to any stabilizer generator) is added along each of the three boundaries, represented by a colored star. Edges in the dual lattice are colored with the complement of the colors of the vertices they connect. Black filled circles are placed in the faces of the dual lattice and represent data qubits for the code.

erators). Then consider the application of some unknown pauli error P_E, resulting in the state $P_E |\psi\rangle$ which will typically not be in the codespace. Measurement of all stabilizer generators gives a subset of "highlighted vertices" for each of X and Z generators, $V^{\mathrm{h}} \subset V$ (where each highlighted vertex also comes with a label of X or Z) which correspond to those stabilizer generators which do not yield a $+1$ measurement outcome.

A decoder $\mathcal{D}(V^{\mathrm{h}}) = P_C$ is a map from highlighted vertices sets to the Pauli group, and outputs the correction Pauli operator P_C that we should apply. In the setting of no measurement errors, we require that a decoder satisfies the condition that it returns the state to the codespace,

$$\mathcal{D}(V^{\mathrm{h}}(P_E)) \circ P_E |\psi\rangle \in \mathcal{C} \ \ \forall P_E \in \text{Pauli}. \tag{5.2}$$

This is equivalent to the statement that $\mathcal{D}(V^{\mathrm{h}}(P_E)) \circ P_E$ is in the normalizer of the stabilizer group for all pauli errors P_E. A good decoder will have the feature that $\mathcal{D}(V^{\mathrm{h}}(P_E)) \circ P_E$ is in the stabilizer group for a large class of "probable" pauli errors P_E, meaning that such errors return to the original codestate after the decoder is applied. An error for which $\mathcal{D}(V^{\mathrm{h}}(P_E)) \circ P_E$ is not in the stabilizer group implies

that the decoder will fail for that error (as it results in the application of a logical operator to the initial codestate).

We can divide the vertices V of G into their colors, and the edges into the complement of the pairs of colors they connect (i.e. a blue edge connects a green vertex and a red vertex):

$$V = V_{\mathrm{r}} \cup V_{\mathrm{g}} \cup V_{\mathrm{b}}, \tag{5.3}$$

$$E = E_{\mathrm{r}} \cup E_{\mathrm{g}} \cup E_{\mathrm{b}}. \tag{5.4}$$

We can consider three (non-disjoint) subgraphs of G. The "red" graph G_{r} consists of all green and blue vertices $V_{\mathrm{g}} \cup V_{\mathrm{b}}$ from G, and the edges in which connect them E_{r}. The "green" and "blue" graphs G_{g} and G_{b} are defined analogously. Note that each vertex from G appears in two sub graphs, but each edge in G appears in precisely one subgraph.

In the Delfosse decoder, the X and Z errors are treated independently. This is possible for the color code by virtue of the fact that the generators of the stabilizer group are purely X or Z type (it is a CSS code). As the X and Z type stabilizer generators have precisely the same support, the procedure for dealing with each is exactly the same. It is therefore sufficient to consider pure X-type errors. The algorithm is as follows:

1. The vertices associated with violated Z-type stabilizers are recorded as V^{h} and input into the decoder.

2. For the red graph G_{r}, the green and blue vertices $V_{\mathrm{g}}^{\mathrm{h}}$, $V_{\mathrm{b}}^{\mathrm{h}}$ from the set V^{h} are marked.

3. If the number of marked vertices $|V_{\mathrm{g}}^{\mathrm{h}}| + |V_{\mathrm{b}}^{\mathrm{h}}|$ in G_{r} is odd, the green fictitious vertex is also marked.

4. The marked vertices in G_{r} are paired together, and the two marked vertices in each pair are connected together along a path. All connecting "highlighted" edges are recorded as $E_{\mathrm{r}}^{\mathrm{h}}$. There real content of the algorithm is how to choose the pairing and the connecting path (see below).

5. The same process is applied to the other two colored subgraphs (with cyclic permutation of colors rgb in descriptions).

6. The set of all highlighted edges $E^{\mathrm{h}} = E^{\mathrm{h}}_{\mathrm{r}} \cup E^{\mathrm{h}}_{\mathrm{g}} \cup E^{\mathrm{h}}_{\mathrm{b}}$ are marked on the graph G. Note that since every highlighted vertex terminates a connecting string of edges in precisely two colors, the set of E^{h} must form a collection of closed loops.

7. The set of closed loops divides the surface into two disjoint regions. This divides the vertices of the direct graph (which correspond to qubits) into two subsets. The output of the decoder is the smaller of the two correction subsets – the correction Pauli P_C consists of X on every qubit in that subset.

For any choice of pairing and connecting paths, this algorithm is a valid decoder, in that it will return the state to the codespace. To prove this, it is sufficient to show that the correction pauli P_C flips the stabilizer outcomes of precisely those stabilizers corresponding to the V^{h}, and no others. This is ensured by the fact that a pair of edges in G connecting to a vertex v bisect the qubits of the stabilizer associated with v into two even subsets if the edges have the same color, and two odd subsets if the edges have distinct colors. The algorithm described ensures that highlighted vertices terminate an edge from two different colors, whereas non highlighted vertices can only have pairs of same-color edges which are part of connections between two (other) highlighted vertices.

Now we return to how the pairings and connections are decided. There is in fact a one-to-one correspondence between highlighted edges E^{h} in G and X-type pauli operators on the qubits. Therefore any decoder for the color code can be described in this framework, with all the differences contained in how the pairing and connection decisions are made. An efficient implementation of Delfosse's decoder makes the pairings by simply minimizing the total number of edges required to connect pairs through the colored sub graph (where edges to the fictitious vertex do not contribute to the sum). This set of included edges can be found efficiently (to the fourth power in the number of violated stabilizer generators) using the well-known Blossom algorithm.

An optimal decoder finds the most probable equivalence class of errors. In the surface code, minimum weight matching of pairs of violated stabilizer generators generates the most probable correction pauli (minimum weight), which may not be in the most probable equivalence class. Here, for the color code, the minimum weight matching does not necessarily find the minimum weight error[2]. Instead it

[2]However, a modification can be used to make the Delfosse decoder for the color code a maximum

find the minimum perimeter error, which of course is correlated with low weight errors.

With measurement error

Here we modify the above procedure in a similar way as Stephens did in Ashley M Stephens, 2014, but with some important differences. As we describe later, the decoder described in Ashley M Stephens, 2014 must fail for large distance codes.

We imagine that at time step $t = 0$, the code was in the the code space $|\psi\rangle \in \mathcal{C}$. In each time step, a set of Pauli errors are applied, and the overall pauli applied up to the current time step $t = T$ is $P_E(T)$. The input to the decoder is the set of the full history of (potentially faulty) stabilizer measurements up to the present time step T.

We define a "vertically extended" dual lattice, the graph $\tilde{G}$, which is constructed by stacking T layers of the graph G, and adding vertical edges to connect like-vertices (see figure 5.2).

We label vertices in $\tilde{G}$ by the pair $\tilde{v} = (v, t)$, where v is a vertex of G, and t the time step. The history of stabilizer measurements is given in the form of changes between round t and $t - 1$, which is a subset of vertices $\tilde{V}^{\mathrm{h}}(T) \subset \tilde{V}$.

The output of the decoder is a correction operator $P_C(T) = \mathcal{D}(\tilde{V}^{\mathrm{h}}(T))$, which should be applied to the system to try to correct the errors applied $P_E(T)$.

Only in the special case when there were no measurement errors[3] in the final round T of measurements will the decoder satisfy $\mathcal{D}(\tilde{V}^{\mathrm{h}}(T)) \circ P_E(T)$ is in the normalizer of the stabilizer group for all $P_E(T)$. However, the state will only deviate from the codespace by the effects of a thin layer of errors which occur in the most recent time steps.

As before, we can consider three (non-disjoint) subgraphs of $\tilde{G}$. The "red" graph $\tilde{G}_{\mathrm{r}}$ consists of all green and blue vertices $\tilde{V}_{\mathrm{g}} \cup \tilde{V}_{\mathrm{b}}$ from $\tilde{G}$, and the edges in which connect them E_{r} (including vertical edges). The "green" and "blue" graphs $\tilde{G}_{\mathrm{g}}$ and $\tilde{G}_{\mathrm{b}}$ are

likelihood decoder for this lattice (which importantly has trivial topology). The method would be to first form a pairing, and then in the full graph, move the connections (keeping their endpoints fixed) to minimize one of the two subsets, and then the other, and take the minimal subset. Note that any pairing could be used as the starting point.

[3] However in practice when measurement errors occur in the last step T, more information is gained about them - for example if we wanted to measure the logical state at time $t = T$, then we could simply measure all the qubits, which provides enough information to accurately identify errors in the last few rounds.

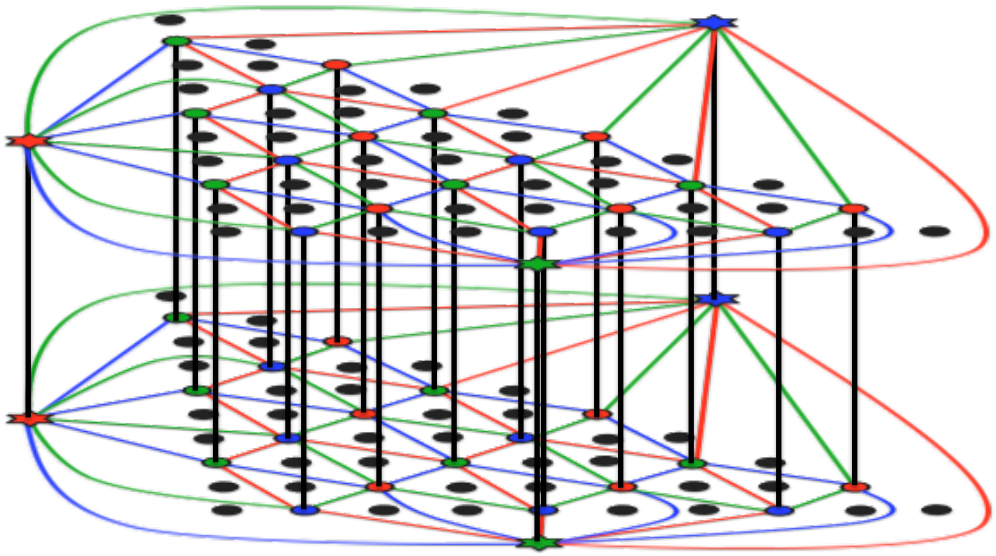

Figure 5.2: Two of the layers which are connected together to form a three-dimensional graph used to decode stabilizer measurement syndromes for the 2D color code when measurements are allowed to be faulty. The colors of the edges in-plane indicate which colored subgraph that edge belongs two. The vertical edges are placed in two of the subgraphs (the two colors that differ from the measurement site they connect).

defined analogously. Note that each vertex and vertical edge from $\tilde{G}$ appears in two sub graphs, whereas each horizontal edge in $\tilde{G}$ appears in precisely one subgraph.

Again we can just consider pure X-type errors and then treat the Z errors in an analogous way. The algorithm is as follows:

1. The vertices in the extended graph $\tilde{G}$ associated with changes in the Z-type stabilizer measurements are recorded as $\tilde{V}^{\mathrm{h}}$ and input into the decoder.

2. For the red graph $\tilde{G}_{\mathrm{r}}$, the green and blue vertices $\tilde{V}^{\mathrm{h}}_{\mathrm{g}}$, $\tilde{V}^{\mathrm{h}}_{\mathrm{b}}$ from the set $\tilde{V}^{\mathrm{h}}$ are marked.

3. If the number of marked vertices $|\tilde{V}^{\mathrm{h}}_{\mathrm{g}}| + |\tilde{V}^{\mathrm{h}}_{\mathrm{b}}|$ in $\tilde{G}_{\mathrm{r}}$ is odd, the green fictitious vertex at time $t = 0$ is also marked.

4. The marked vertices in $\tilde{G}_{\mathrm{r}}$ are paired together, and the two marked vertices in each pair are connected together along a path. All connecting "highlighted" edges are recorded as $\tilde{E}^{\mathrm{h}}_{\mathrm{r}}$. The pairing can be achieved (for example) by minimizing the number of connecting edges (excluding edges which involve fictitious sites).

5. The same process is applied to the other two colored subgraphs (with cyclic permutation of colors rgb in descriptions).

6. The set of all highlighted edges $\tilde{E}^{\mathrm{h}} = \tilde{E}^{\mathrm{h}}_{\mathrm{r}} \cup \tilde{E}^{\mathrm{h}}_{\mathrm{g}} \cup \tilde{E}^{\mathrm{h}}_{\mathrm{b}}$ are marked on the graph $\tilde{G}$. Note that since every highlighted vertex terminates a connecting string of edges in precisely two colors, the set of $\tilde{E}^{\mathrm{h}}$ must form a collection of closed loops.

7. Each connected component of highlighted edges is "collapsed" to the highest time step of vertices in the connected component. The meaning of collapse is that vertical edges are removed, and horizontal edges are added modulo two. This results in a set of E^{h} in a single layered graph G.

8. For each time step, the set of collapsed connected components are combined together (with edges combined modulo two). This gives a set of closed loops for the time step.

9. For each time step, the set of closed loops divides the surface into two disjoint regions. This divides the vertices of the direct graph (which correspond to qubits) into two subsets. The output of the decoder is the smaller of the two correction subsets – the correction Pauli P_C consists of X on every qubit in that subset.

To show that this is a valid decoder, it is sufficient to prove that the state is returned to the code space in the case where there are no measurement errors in the final round.

Comparison with Stephens' approach

Stephens proposes applying the above procedure, but instead of collapsing connected components and treating each time step separately as in (6), (7), and (8), he suggests collapsing the connections for all T times together modulo two, forming two subsets of qubits, and applying a correction pauli to the smaller of the two. In his paper, he studies the short time behavior: he considers an initially perfect state at time $t = 0$, and includes d rounds of stabilizer measurements, presumably followed by a single round of perfect syndrome measurements.

This approach clearly does not scale to large times or distances. The reason is that for a physical error rate p, after a time $\sim 1/p$ an error will have been applied to any given qubit with probability greater than half. After this time, the smaller of the two

subsets will not be correlated with the true correction operator (as both subsets will generically contain about half of the qubits). The typical error rates that he studied with this decoder were less than 3 %, and the largest distances were 21, so he did not explore the regime where this would be a significant problem (although it could have effected the precise value of his threshold estimates).

5.3 Two-dimensional color code thresholds

Previous analysis has been made for color code thresholds Ashley M Stephens, 2014; Hector Bombin, Duclos-Cianci, and Poulin, 2012; D. S. Wang et al., 2009; Landahl, Jonas T Anderson, and Rice, 2011; Andrist et al., 2011; Ohzeki, 2009; Katzgraber, H Bombin, and MA Martin-Delgado, 2009; Delfosse, 2014; Sarvepalli and Raussendorf, 2012. In Table 5.1 we summarize the threshold constants found using efficient decoders. Two conspicuous omissions from this list are phenomenological and circuit-level analysis for the color code on the hexagonal lattice. We suppose that a number of papers focus on the 4.8.8 lattice rather than the hexagonal lattice since it was not known during the time of their writing how to implement the full Clifford group of logical gates transversely in the latter (the S gate was known only for the color code on the 4.8.8 lattice). As we showed in Chapter 4, it is possible to implement the logical S gate transversely by applying S to one of the bipartition subsets of qubits in the color code lattice, and $S^\dagger$ to the other.

Code capacity threshold

The numerical simulation to find the threshold in the code capacity setting is very simple. Errors are applied to each qubit with probability p (i.e. X, Y and Z are each applied with probability $p/3$), then the decoder is applied, and the net pauli (consisting of the error and correction paulis) is identified. The weight of the X part and the Z will both be even if the decoder succeeded, but not otherwise. This process is repeated many times to estimate the probability of success, which is plotted for different distances (see figure 5.3). The threshold appears to be around 12.2 %, which is a little smaller that the threshold of 13.1 % Delfosse, 2014 calculated for the hexagonal lattice with the Delfosse decoder on the torus.

Phenomenological threshold

For the phenomenological threshold, the system is run for 10,000 consecutive time steps, with errors applied to each qubit in each step with probability p (i.e. X, Y and Z are each applied with probability $p/3$), and the exact stabilizer outcomes are

calculated given what errors have been applied, and then these outcomes are each flipped with probability p before being fed to the decoder.

The decoder is as almost as described in Section 5.2. The number of highlighted vertices that would occur during 10,000 time steps would make the matching prohibitively slow. Instead, after each time step, the decoder is run, and connected components of highlighted edges are recorded. After a connected component is observed d times, it is fixed, and the highlighted vertices in the component are removed from the history. This essentially implements a soft window through time to achieve a sub optimal matching but much more quickly.

Logical errors are identified by copying the system after each timestep, and running an additional round with no measurement errors. This returns the system to the codespace, and one can identify if the net effect of errors and the correction operation is a stabilizer or a logical operator. The mean number to time steps before a flip is calculated for the entire run and inverted to give an estimate of the logical error probability p_L. Repeating the procedure ten times gives a more accurate estimate of p_L along with an indication of its accuracy (via the standard deviation). See figure 5.4.

Thresholds with efficient decoders

Code	Code capacity	Phenomen.	Circuit
6.6.6	13.1 %*, [12.2%]	[4.2 %]	[0.3 %]
4.8.8	13.1 %**	3.12 %****	0.143 %****
4.4.4.4 (Kitaev)	15.46 %***	4.40 %***	1.1 %*****

Table 5.1: Threshold probability for 6.6.6 (hexagonal lattice), 4.8.8 (square-octagon lattice) color codes and the 4.4.4.4 (square lattice) surface code. Only those results found using efficiently implementable decoders are given. Our results presented in this paper are provided in square parenthesis. Note the circuit level threshold of 0.143% by Stephens uses a partial cat-state preparation, which trades extra qubits in order to achieve a higher threshold. (*) Delfosse, 2014, (**) Hector Bombin, Duclos-Cianci, and Poulin, 2012, (***) C. Wang, Harrington, and John Preskill, 2003, (****) Ashley M Stephens, 2014, (*****) A. G. Fowler, A. M. Stephens, and Groszkowski, 2009. All thresholds are given for depolarizing channels with strength p (if originally given for bit-flip channel, the threshold is multiplied by $3/2$). This rescaling actually overestimates the threshold for phenomenological noise since the measurement errors should not be rescaled, just the qubit errors. There can be no general formula to take this into account unfortunately.

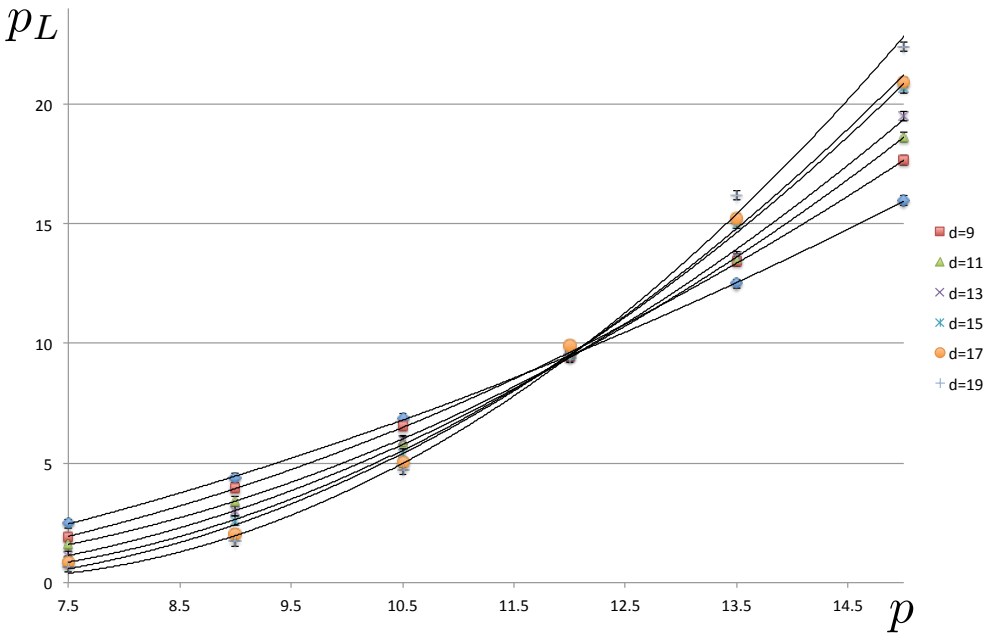

Figure 5.3: Logical error rate p_L versus physical error rate p under code capacity (perfect measurement) noise. This indicates the threshold value to be around 12.2 % for the color code. More data is needed to obtain a more accurate estimate.

Circuit level threshold

To measure stabilizers, one can consider using a single measurement qubit placed in each face of the lattice to measure both the X and the Z stabilizer associated with the face, one after the other. This requires that the order of the CNOT gates avoids any qubit being involved in two gates at once. Alternatively, two measurement qubits in each face allow for two CNOT gates to be applied per time-step in each face (one associated with the X, and the other with the Z measurement).

First we analyze the case of consecutive X and Z measurements, which is expected to have worse performance as it involves more steps in which errors can occur. The schedule for the CNOT gates is simply clockwise beginning from above. The analysis of the threshold is precisely the same as for the phenomenological case (we used the same decoder). During each time step, an error is applied to an idle qubit with probability p ($p/3$ for each of X, Y and Z). Measurements are flipped with probability p, and preparation of a state is replaced by the "flipped" state with probability p. The control gates are followed by each of the fifteen non-trivial two qubit paulis with probability p.

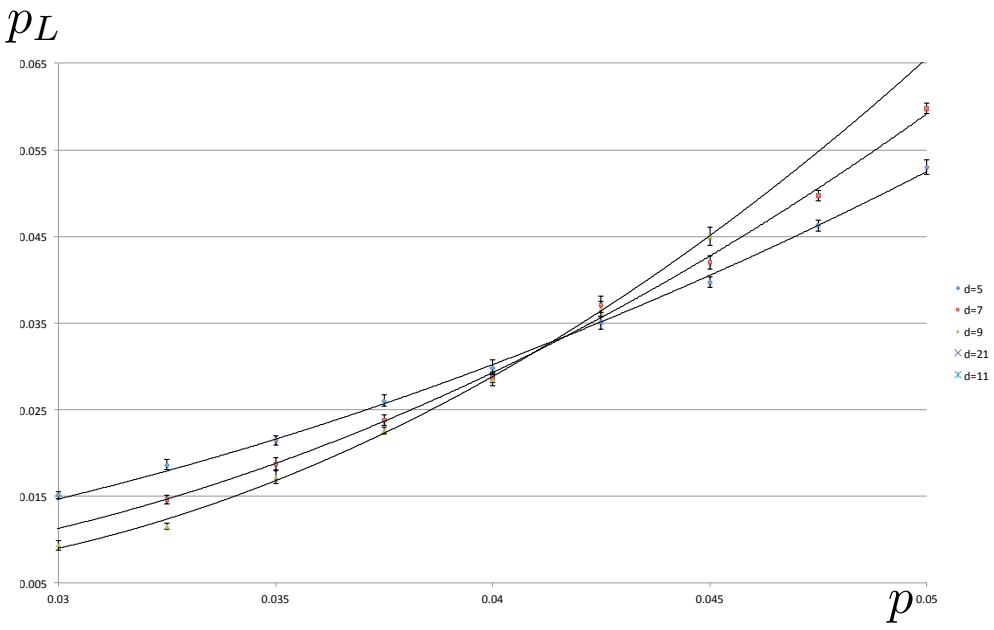

Figure 5.4: Logical error rate p_L versus physical error rate p under phenomenological noise. This indicates the threshold value to be around 4.2 % for the color code. More data is needed to obtain a more accurate estimate.

Circuit schedules

An alternative to measuring X and Z type stabilizers one after the other is to use two measurement qubits per face and to implement a circuit to measure both X and Z stabilizers simultaneously. Again, it is essential that each qubit is involved in at most one gate per time step, and there is an additional condition given in Landahl, Jonas T Anderson, and Rice, 2011: "any stabilizer generator for an error-free input state (including ancilla syndrome qubits) must propagate to an element of the stabilizer group for an error-free output state." For example, we must check that an X operator applied to an X measurement qubit (which stabilizes the $|+\rangle$ preparation state) at the beginning of the schedule must propagate through the circuit to give a stabilizer. If a schedule satisfies these conditions, we say it is *v*alid. Note that any schedule which involves measuring X and Z sequentially (i.e. in each round, all CNOT gates are applied before all control-Z gates) is valid.

A schedule for the color code can be specified by three pairs of integers for each physical qubit. Each pair corresponds to one of the three faces in contact with the qubit (for boundary qubits there can be fewer than three pairs). For a given pair, the first of the two integers specifies when a CNOT gate is applied between that qubit and the X-measurement qubit at the center of the corresponding face, and

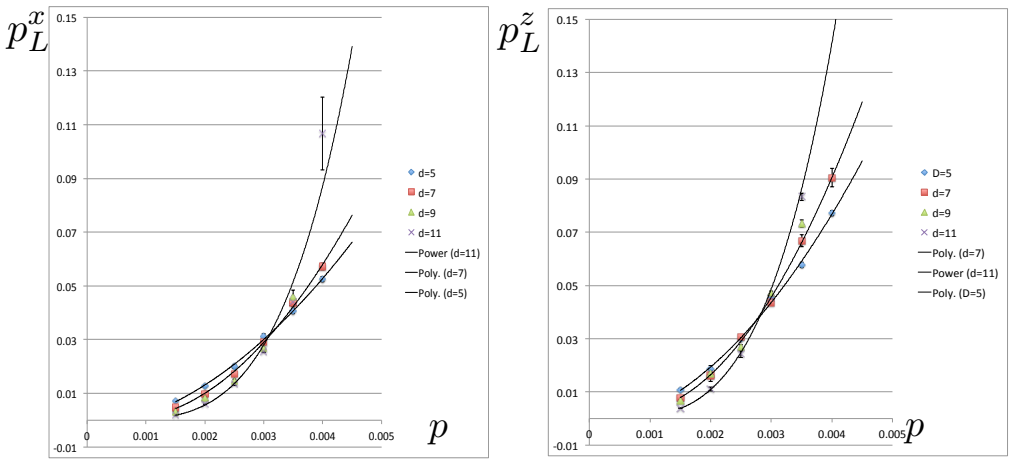

Figure 5.5: Logical error rate p_L versus physical error rate p under circuit-level noise. The logical error rate is calculated separately for X and Z type errors to point out that there is some asymmetry. This indicates the threshold value to be around 0.3 % for the color code. More data is needed to obtain a more accurate estimate.

the second specifies when a control-Z gate is applied between that qubit and the Z-measurement qubit. We focus on uniform schedules on regular lattices, such that only the pair for each data qubit in the unit cell of the lattice is specified, and the others are given by following the tiling.

Some uniform schedules that are valid for the color code are shown in figure 5.6. For the hexagonal lattice, the schedule for two qubits need to be specified to fix the schedule for the lattice. The approximate size of the search space for the hexagonal lattice for all length l schedules is $(l!)^2$, such that exhaustive search can be completed quickly for lengths $l = 6, 7$. Unfortunately there are no schedules of length six which satisfy all these constraints for the hexagonal lattice. However, there are 763 inequivalent schedules of length seven (where we consider two schedules to be equivalent if mapped by a symmetry of the lattice or by interchanging X and Z). A pair of integers for each of four qubits are needed to specify a uniform schedule for the square-octagon lattice. An exhaustive search for all length l schedules involves checking approximately $(l!)^4$ cases, which was computationally unfeasible for $l = 8$.

Some valid schedules will perform better than others. One generally expects short schedules to outperform long schedules since there are fewer opportunities for errors to occur per round of syndrome measurements. Two schedules of the same length can have different performance since they propagate errors differently. To compare the performance of valid schedules of length seven, one could consider the average total number of errors that result from a single error in the circuit. To calculate

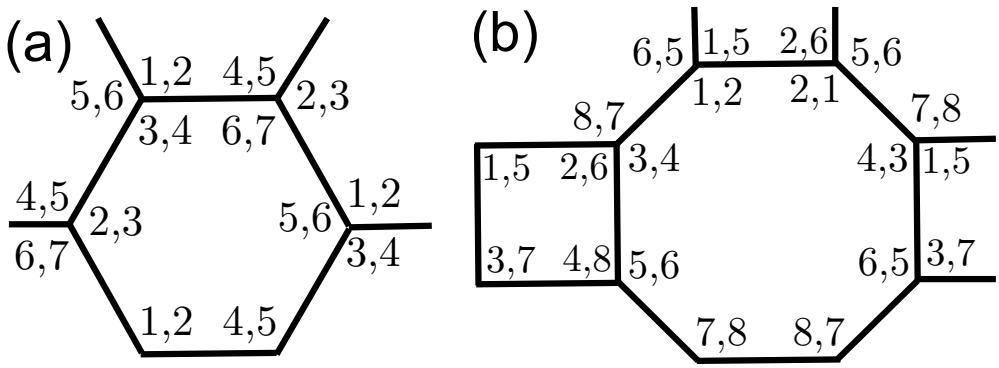

Figure 5.6: a) and b) Schedules for CNOT operations in the color code. The minimum number of steps for a valid schedule is 7 for the hexagonal lattice, and 8 for the 4.8.8 lattice. An exhaustive search for the hexagonal lattice yields 763 inequivalent valid schedules of length seven.

this, we should pick out two adjacent data sites in the bulk, and apply all single location errors to locations which involve the two qubits, propagate through the remainder of the circuit until measurement, and sum with the appropriate weight (the relative probability of that error occurring). As of yet, we have not performed such an analysis, and we hope there could be improvement on the 0.3% circuit level threshold if an optimized schedule is used.

5.4 Code switching – dimension jump

In chapter 4, we discussed code-switching between two three-dimensional color codes, one of which was a stabilizer code, and the other a subsystem code. Here we will be focused on an important variant of this scheme, which was first described for Reed-Muller codes in Jonas T. Anderson, Duclos-Cianci, and Poulin, 2014 and described for the topological color codes in H Bombin, 2014. The key observation is that it is possible to switch between a three-dimensional stabilizer code and a three-dimensional subsystem code in which the logical and gauge qubits can be decomposed from each other spatially, such that the logical qubits are completely confined to a portion of the two-dimensional boundary of the three-dimensional lattice, and the gauge qubits are completely confined to the remaining bulk. In this setting, code-switching is sometimes referred to as a "dimensional jump".

We describe the scheme using the example of the smallest three-dimensional color code, which is precisely the $[[15, 1, 3]]$ Reed-Muller code, which is switched to and from the smallest two-dimensional color code, the $[[7, 1, 3]]$ Steane code.

Distance three dimension jump with no errors

The seven qubit Steane and fifteen qubit Reed Muller codes are $d = 3$ color codes in two and three dimensions. Both of these codes can be described relatively easily visually (see figure 5.7).

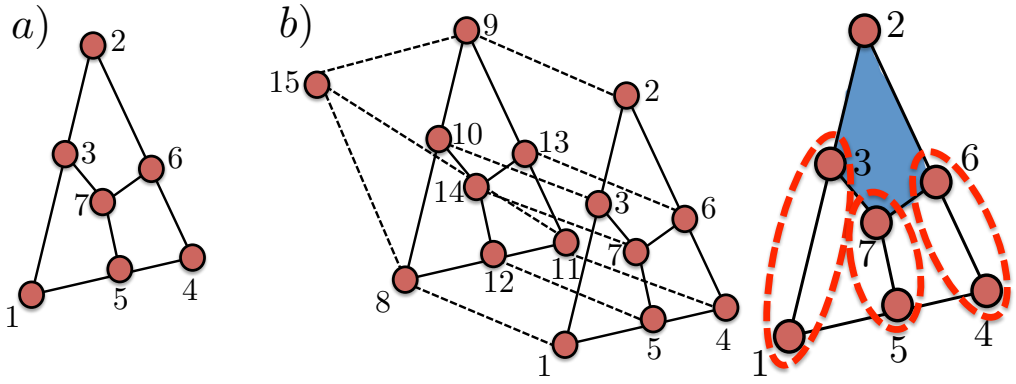

Figure 5.7: a) The $[[7, 1, 3]]$ Steane code has X and Z type stabilizer generators on faces. b) Volumes are X-type stabilizers, and faces are Z-type stabilizers in the fifteen qubit Reed-Muller code. The code can be interpreted as being constructed of two copies of the 7-qubit color code (aka the Steane code), one of which (at the back in this picture) is in a logical cat state $|\bar{0}0\rangle + |\bar{1}1\rangle$ with a single qubit. (c) The face operators (for example $Z_1Z_3Z_8Z_{10}$) have two qubits in the plane shown. Those which intersect with only a single qubit of the in-plane highlighted face are circled (corresponding to $Z_1Z_3Z_8Z_{10}$, $Z_5Z_7Z_{12}Z_{14}$, and $Z_4Z_6Z_{11}Z_{13}$). Each of these will have their value flipped if X's are applied to the highlighted face (i.e. $X_{11}X_{12}X_{13}X_{14}$), changing a from 1 to 0.

First we will describe the dimension jump procedure in an ideal error-free setting. To switch from the $[[7, 1, 3]]$ code (in physical qubits $1 - 7$), in some unknown codestate $|\psi\rangle = \alpha\,|\bar{0}\rangle + \beta\,|\bar{1}\rangle$, to the $[[15, 1, 3]]$ code (in physical qubits $1 - 15$), first prepare an additional eight ancilla qubits in the entangled state $|\bar{0}0\rangle + |\bar{1}1\rangle$, where qubits $8 - 14$ are encoded in a second $[[7, 1, 3]]$ code, entangled with qubit 15. Notice that this system of fifteen qubits already satisfies many of the stabilizers of the $[[15, 1, 3]]$ code. Following the labelling of figure 5.7(b), the four X-type stabilizer generators of the fifteen qubit code are all automatically satisfied, since three of the four volumes are composed of products of disjoint faces in the original pair of Steane codes, and the final volume (at the back) is satisfied by virtue of the state $|\bar{0}0\rangle + |\bar{1}1\rangle$. Moreover, all the Z-type generators corresponding to faces within the two Steane codes are satisfied, as are those on the back eight qubits (again since $|\bar{0}0\rangle + |\bar{1}1\rangle$). The only stabilizers which may not be satisfied are the nine Z-type face operators that span from the front $[[7, 1, 3]]$ code to the back $[[7, 1, 3]]$ code in

figure 5.7(b), such as $Z_1Z_3Z_8Z_{10}$ and $Z_6Z_7Z_{13}Z_{14}$. The strategy then is to measure these Z-stabilizer generators, and apply X-face operators to correct any which are not satisfied. As the logical pauli operators for origin $[[7,1,3]]$ code and the target $[[15,1,3]]$ code in figure 5.7(b) code can be chosen to be precisely the same, it is clear that applying these X-face operators will not alter the encoded information.

It is relatively straightforward that some X-face operators can be applied to correct any possible outcome of the Z-face measurements.. If all the Z-face measurements are satisfied, then the switch is complete. Only X-face operators for faces within the planes of the two $[[7,1,3]]$ codes in figure 5.7(b) need to be considered, as all other X-faces commute with the measured Z-faces. Without loss of generality, we can restrict our attention to X-faces in the front plane, since the parallel X-faces in the back have precisely the same commutation relations with the measured Z-faces as those in the front plane. Therefore we only need to consider three independent X-faces to correct the measured Z-faces. Although there are nine Z-faces we have discussed measuring, they are not independent as some combinations form (satisfied) Z-volumes,

$$Z_1Z_3Z_8Z_{10} = Z_5Z_7Z_{12}Z_{14} = Z_4Z_6Z_{11}Z_{13} = a, \tag{5.5}$$

$$Z_2Z_6Z_9Z_{13} = Z_3Z_7Z_{10}Z_{14} = Z_1Z_5Z_8Z_{12} = b, \tag{5.6}$$

$$Z_2Z_3Z_9Z_{10} = Z_6Z_7Z_{13}Z_{14} = Z_4Z_5Z_{11}Z_{12} = = c. \tag{5.7}$$

It is enough for us to measure three (one from each row) of these Z-face operators in order to determine (a,b,c), and then apply the appropriate X-face conditioned on (a,b,c). In summary, to switch from $[[7,1,3]]$ to $[[15,1,3]]$,

1. Measure Z-faces:

$$(Z_1Z_3Z_8Z_{10},\ Z_2Z_6Z_9Z_{13},\ Z_4Z_5Z_{11}Z_{12}) = (a,b,c). \tag{5.8}$$

2. Apply X-faces:

$$(X_9X_{10}X_{13}X_{14})^a\ (X_{11}X_{12}X_{13}X_{14})^b\ (X_8X_{10}X_{12}X_{14})^c. \tag{5.9}$$

Similarly, to switch from $[[15,1,3]]$ to $[[7,1,3]]$,

1. Measure X-faces:

$$(X_1X_3X_5X_7,\ X_2X_3X_6X_7,\ X_4X_5X_6X_7) = (d,e,f). \tag{5.10}$$

2. Apply Z-faces:

$$(Z_2Z_3Z_9Z_{10})^d\ (Z_1Z_3Z_8Z_{10})^e\ (Z_2Z_6Z_9Z_{13})^f \tag{5.11}$$

Distance three dimension jump with errors

We are interested in the procedure of switching from $[[7,1,3]]$ to $[[15,1,3]]$, then application of transverse T, followed by a switch from $[[15,1,3]]$ back to $[[7,1,3]]$. Now we consider the case where an arbitrary single qubit physical error occurs at some point throughout the procedure, but no measurement errors.

First note that every action involved in switching is transversal. Provided (a,b,c) and (d,e,f) are correct, a singe-qubit error at some point in the procedure will result in the correct final state up to a single qubit error on the same damaged qubit. The only danger then is that the error leads to an incorrect inference of (a,b,c) or (d,e,f) which the final state to differ by suppose the initial error occurs before we measure the three Z-type face operators, causing us to obtain a mistake in one of three numbers a,b or c. This can be avoided by measuring the redundant face operators, and then inferring (a,b,c) by majority vote.

For distance three, the code switching procedure can be made fault tolerant to a single unknown physical or measurement error by performing measurements using (for example) verified cat states. As this adds considerable overhead and should not be necessary for larger distances we will not elaborate on this further.

Scalable fault-tolerant dimension jump

These results generalize to arbitrary distance codes. By measuring faces only, and applying correction operations to fix the gauge, one can implement the switch between the two-dimensional color code and the three dimensional color code.

5.5 Overhead for code switching

The parameters for the lattices of the 4.8.8 (square-octagon) and 6.6.6 (hexagonal) two-dimensional color codes on triangular boundaries are given in Table 5.3. Note that for all distances $d > 3$, the number of vertices v for the hexagonal lattice is larger than that of the square-octagon lattice. The number of faces f is also larger for the hexagonal lattice.

For overhead calculations, the number of data qubits required is v, and the number of measurement qubits required depends on how one chooses to measure stabilizers. If there is one measurement qubit per stabilizer generator, then $2f$ data qubits are

required, whereas if a single measurement qubit is used to measure both X and Z stabilizers on the same face one after the other, then only f measurement qubits are required.

Two-dimensional Lattice parameters

	6.6.6 Hex. lattice	4.8.8 lattice
vertices v	$3(d^2-1)/4+1$	$(d-1)(d+3)/2+1$
faces f	$3(d^2-1)/8$	$(d-1)(d+3)/4$

Three*-dimensional Lattice parameters

	B.C.C lattice	Doubled Color code lattice
vertices v	$d(d+1)^2/2$	$(d^3+5d^2-d-9)/4$
faces f	$--$	$--$
volumes c	$--$	$--$

Table 5.2: The number of vertices v, faces f and (where relevant) volumes c of the different lattices we consider as a function of (odd) distance d. In two-dimensions, we consider the 4.8.8 (square-octagon) and 6.6.6 (hexagonal) lattices used for the color code. In three-dimensions, we consider the construction by Bombin, and the psuedo-two-dimensional lattice proposed by Bravyi and Cross Sergey Bravyi and Cross, 2015. Note that, like the three-dimensional color code, the Bravy-Cross flattened doubled color code (and the other flattened color code schemes Jochym-O'Connor and Bartlett, 2015; Jones, Brooks, and Harrington, 2015) have overhead which is cubic in the distance $v \sim$ constant $\times\, d^3$.

To estimate the overhead required for code switching with color codes to produce an encoded magic state of a desired quality (with logical error rate at most p_D), we consider the following steps:

1. Generate an encoded $|+\rangle$ state in a two-dimensional hexagonal color code of distance d. The error associated with this state can be estimated from $p_1(d) = \alpha(p/p_T)^d$ using the appropriate threshold parameters.

2. Prepare a distance-d three-dimensional color code (with hexagonal boundary) using ancilla qubits (or a flattened version of it) by measuring the appropriate stabilizers and applying correction operations. The code should have a boundary sheet missing (in the shape of the distance d, two-dimensional color code).

3. Apply the appropriate measurements to the two-dimensional color code and the three-dimensional color code such that they fuse resulting in an encoded

$|+\rangle$ in the three-dimensional color code. We call the error associated with this state $p_3(d)$.

4. Apply the transverse T gate, resulting in the encoded $|T\rangle$ in the three-dimensional color code. We call the error associated with this state $p_4(d)$.

5. Apply the appropriate measurements to "un-fuse" the two-dimensional code, leaving the encoded $|T\rangle$ in the distance d two-dimensional color code. We call the error associated with this state $p_5(d)$.

As the protection from noise improves with distance, each $p_i(d)$ monotonically decreases with d. To achieve the target state with the required accuracy with as low overhead as possible, we seek the smallest distance for which $p_5(d) \leq p_D$. Then the overhead $N(d)$ is the maximum number of physical qubits required at any time in steps (1) – (5). The most costly step involves the three-dimensional color code. The precise number of qubits required depends on the details. Taking the BCC lattice and assuming one measurement qubit per stabilizer generator results in $N(d) = d(d+1)^2 - 1$.

Each step can only reduce the quality of the encoded information, and therefore $p_5(d) \geq p_4(d) \geq p_3(d) \geq p_1(d)$. To estimate a lower bound on the overhead required for code switching, we make can consider the (unrealistic) case where steps (2) – (5) are perfect. In this case

$$p_5(d) = p_1(d) = \alpha(p/p_T)^d, \tag{5.12}$$

and we see that the lowest distance is $d = d_D$, such that $p_D = \alpha(p/p_T)^{d_D/2}$ (increased sufficiently such that it is an odd integer). See figure 5.8. As steps (2) – (5) are expected to introduce a significant amount of additional noise to the system, we expect this lower bound to be far from tight.

A more accurate estimate of code-switching overhead

Ideally, to obtain a good estimate of the code-switching overhead, one would need to implement a fault-tolerant decoder for the three-dimensional color code given circuit level noise (which is not yet well understood). Then one could simulate the two-dimensional code, and three dimensional bulk code in equilibrium, and then could find a threshold for the gadget which switches from one to the other. This would not account for the errors introduced by the transverse T gate, which cannot

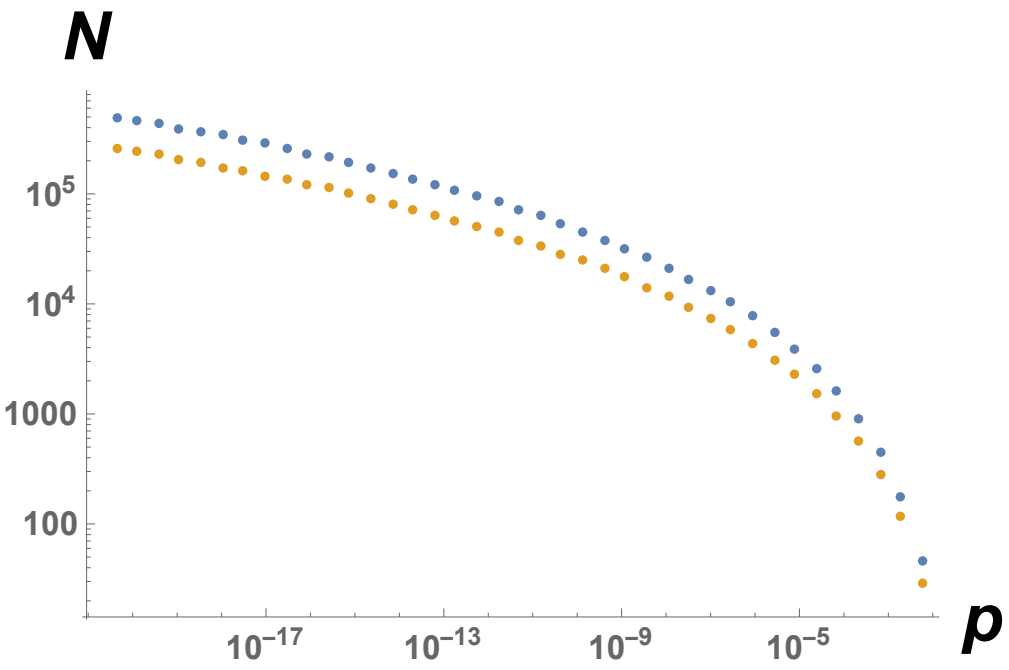

Figure 5.8: A lower bound on the qubit overhead for forming a magic state with logical error rate below p_L using code switching. In reality the actual overhead is expected to be significantly greater since here we assume that no additional noise is introduced by the switching process. The blue points are for the three dimensional color code, and the yellow points are for the doubled color code, where in each case we assume that there is one measurement qubit for each stabilizer generator for the code. [Note one would actually need more measurement qubits for the doubled color code, since in that case one should measure the (strictly larger) number of gauge generators as the stabilizer generators are not all local].

be easily simulated classically, but the (Clifford) phase gate could be applied instead to give an estimate of the behavior.

For the psuedo-three-dimensional color codes of Bravyi-Cross and Jochym-O'Connor-Bartlett, one would expect that there is no threshold leading to worse performance above some distance for a given error rate.

Alternatively, tighter bounds than that we have given could be achieved by keeping most of the three dimensional color code implementation perfect, but adding in extra noise associated with some of steps (2) – (5).

5.6 Magic state distillation

Universality through magic state distillation relies on the following two facts:

1. There is a Clifford circuit which takes an input qubit in arbitrary state $|\phi\rangle$, along with an ancilla qubit in the magic state $(|0\rangle + e^{i\pi/4}|1\rangle)/\sqrt{2}$, and outputs the state $T|\phi\rangle$ [see Fig. 5.9(a)].

2. For all sufficiently large m_{in} and f_{in}, there is a Clifford circuit which takes an input of m_{in} copies of the (fidelity f_{in}) magic state $(|0\rangle + e^{i\pi/4}|1\rangle)/\sqrt{2}$, and outputs m_{out} copies of the (fidelity f_{out}) magic state $(|0\rangle + e^{i\pi/4}|1\rangle)/\sqrt{2}$, such that $f_{\text{out}} > f_{\text{in}}$, but where $m_{\text{out}} < m_{\text{in}}$. Moreover, if the Clifford circuit is implemented without error, then there is a threshold fidelity f_{T} such that f_{out} can be made arbitrarily small for fixed m_{out} by increasing m_{in} provided $f_{\text{in}} < f_{\text{T}}$ [see Fig. 5.9(b)].

It is therefore possible to achieve universal fault-tolerant quantum computing using a fault-tolerant Clifford computer, provided one has access to a large number of encoded magic states of sufficiently high fidelity.

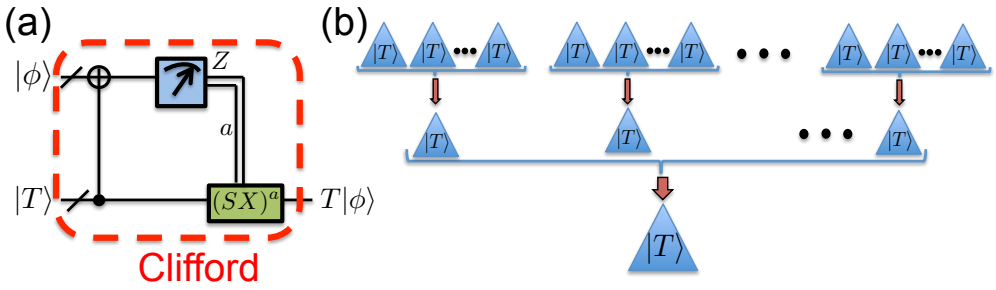

Figure 5.9: (a) A Clifford circuit that applies the T gate to its input qubit. (b) Magic state distillation is performed in consecutive rounds, with the output of one round forming the input to the next. In each round, a larger number of lower fidelity encoded magic states is transformed by a Clifford circuit into a smaller number of higher fidelity magic states.

An example of a Clifford circuit which can be used to implement state distillation is described below and in figure 5.10. In the description, we assume the circuit is perfect, and any noise is that associated with the noisy magic states.

1. Apply the encoding circuit for the [[15,1,3]] code on fifteen encoded qubits on one half of a Bell pair. The state of the system is $(|0\rangle|\bar{0}\rangle + |1\rangle|\bar{1}\rangle)/\sqrt{2}$.

2. Apply the transverse T gate (using 15 copies of the $|T\rangle$ state, each with an associated error rate p). If $p = 0$, the state of the system is $(|0\rangle|\bar{0}\rangle + e^{i\pi/4}|1\rangle|\bar{1}\rangle)/\sqrt{2} = ((|0\rangle - ie^{i\pi/4}|1\rangle)|\bar{+}\rangle + (|0\rangle + ie^{i\pi/4}|1\rangle)|\bar{+}\rangle)/2$.

3. Measure all the qubits comprising the [[15,1,3]] code in the X basis. The outcomes allow us to infer the measurement of the X-type stabilizers, and the X-type logical operator, which we denote $s = -1, 1$.

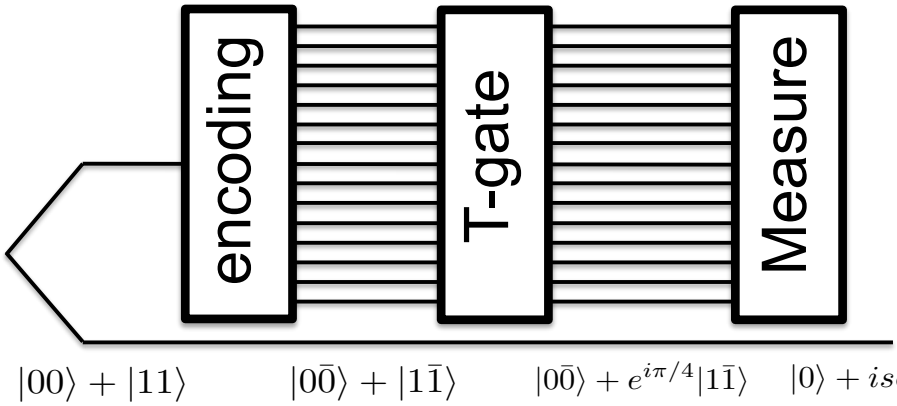

Figure 5.10: The circuit used for $|T\rangle$ distillation can be understood by first encoding one half of a Bell pair in the fifteen qubit code, using fifteen (noisy) $|T\rangle$ states to apply the transverse T gate in the fifteen qubit code, followed by measurement of the logical X operator giving outcome s. This forces the state of the other half of the Bell pair into something which differs from $|T\rangle$ by an s-dependent Clifford gate. By also measuring the X-stabilizers of the fifteen qubit code, and discarding the output of the process when the stabilizers are not satisfied, one can improve the fidelity of the output state. Note that since the encoding circuit is composed of Clifford gates, and the T gate preserves the Clifford group, we could pull the T gates through the encoding circuit to give a new circuit with equivalent action but where the ancilla states for the fifteen qubit code are $|T\rangle$ states rather than stabilizer states, and the encoding clifford circuit is replaced by a modified clifford circuit.

If $p = 0$, then the stabilizers must be satisfied, and the state of the only unmeasured qubit will be $(|0\rangle + ise^{i\pi/4}|1\rangle)\sqrt{2}$, and note that $|T\rangle \propto S^s(|0\rangle + ise^{i\pi/4}|1\rangle)\sqrt{2}$. For $p > 0$, since the fifteen qubit code has distance three, all weight one and two Z- type errors will result in some unsatisfied stabilizers. No X-type errors will affect the state since they commute with the X measurement. If we discard the state unless all the X-type stabilizers are satisfied, there can be contributions only from the logical Z operators of weight three and above. Neglecting $\mathcal{O}(p^4)$ terms, the 35 distinct weight-three logical Z operators result in an error rate in the post-selected state of $35p^3$. Note that the post-selection results in a reduction of yield: on average, approximately a fraction $15p$ of the states will be discarded. This circuit has an asymptotic rate $r = 1/15$, since (for $p \to 0$) fifteen input magic states are replaced by one magic state of higher fidelity in each round.

In an implementation one must produce an encoded resource state with a sufficient fidelity. In a topological stabilizer code such as the toric code or the color code, one can first prepare an unencoded magic state in a singe qubit, encode this in a small code, and then grow the code distance while preserving the encoded state. The result will be a (noisy) encoded magic state.

Note that there will be additional errors introduced by the Clifford circuit which is used to distill the magic states. The additional errors are reduced by encoding the information in a larger code, which increases the overhead.

5.7 Overhead for state distillation

We seek to estimate the qubit overhead for state distillation with two schemes the surface code and the color code. First we fix some notation which are common to both schemes.

The distillation protocol consists of k rounds, where the code in each round has distance $\{d_1, d_2, ..., d_k\}$, and the encoded magic states at the end of each round have error rate $\{p_1, p_2, ..., p_k\}$. At the beginning of the distillation protocol, the magic states are encoded into a distance d_1 color code, with error rate p_0. Each of these are formed by encoding the state $|T\rangle$ with error probability p into a distance d_1 code. At the end of the protocol, we should have a magic state $|T\rangle$ encoded in a distance d_k code with logical error rate at most p_D. We imagine that the qubits involved in each round can be reused - therefore the overhead of the distillation protocol with given set of distances $\{d_1, d_2, ..., d_k\}$ is simply the maximum overhead of any round. The overhead required to distill a p_D encoded magic state is simply

$$\max\{r^{-k+1}N(d_1), r^{-k+2}N(d_2), ..., r^{-1}N(d_{k-1}), N(d_k)\}, \tag{5.13}$$

minimized over all possible sets $\{d_1, d_2, ..., d_k\}$, such that $p_k \leq p_D$ (note that the number of rounds k is also allowed to vary).

To calculate the overhead for each scheme, we need to specify the overhead $N(d)$ of a single logical qubit at distance d, and a function $p_i = P_{\text{distillation}}(d_i, p_{i-1})$ which relates error rates of consecutive distillation rounds for $i = 1, 2, \ldots, k$. We must also specify a function which tracks the error introduced by encoding prior to the first round of distillation $p_0 = P_{\text{encoding}}(d_1, p)$. After the ith round of distillation, the magic state will be encoded with error rate p_i in a code of distance d_i. It then needs to be expanded into a code of distance d_{i+1} ready for the next round of distillation. We neglect additional noise added by the expansion process.

To estimate $P_{\text{encoding}}(d_1, p)$, we make the assumption that a two-stage process is used, where first the state $|T\rangle$ is encoded in a distance $d = 3$ code, and then that code is expanded to distance d_1. We assume that second stage does not contribute significantly to the noise. Then we encode the qubit into a distance d_1 color code. We take the error probability $p_1 = L_{\text{encoding}}p$, where L_{encoding} is the number of locations in the encoding circuit.

There are two contributions to error in the final encoded magic state: (1) that which originates from noise in the undistilled magic states, and (2) that which is introduced by the distillation circuit itself. We take the simple model that each contribute independently to p_i, such that we can take ideal reduction in noise due to state distillation to be $35p_{i-1}^3$, and that the the error rate associated with the distillation circuit given d_i is approximately $N_L(d_i)\alpha(p/p_T)^{d_i/2}$, where a single logical qubit encoded at distance d_i is $\alpha(p/p_T)^{d_i/2}$, and the number of locations in which an error can occur in the distillation circuit $L_{\text{distillation}}(d_i)$. Then we model the overall error rate as that consistent with overall success occurring only when there is no error in either (1) or (2), such that,

$$1 - p_i = 1 - P_{\text{distillation}}(d_i, p_{i-1}) = \left[1 - 35p_{i-1}^3\right]\left[1 - L_{\text{distillation}}(d_i)\alpha(p/p_T)^{d_i/2}\right]. \tag{5.14}$$

In order to estimate the overhead of state distillation, we must fix some details of the implementation and then identify L_{encoding} and $L_{\text{distillation}}$ in order to estimate the overhead as described above. The parameters we use for the calculation are given in table 5.3, and the corresponding overhead is plotted in figure 5.11.

Parameters for distillation circuits

Parameter	6.6.6 Color Code	4.8.8 Color Code	Surface Code
α	0.01	0.002	0.03
p_T	0.003	0.001	0.01
$N(d)$	$(9d^2 - 1)/8$	$(3d^2 + 6d - 5)/4$	$(2d)^2$
$L_{\text{encoding}}(d)$	5	5	5
$L_{\text{distillation}}(d)$	$10d$	$10d$	$10d$

Table 5.3: The constants relevant for estimating the overhead of state distillation with the hexagonal lattice and square-octagon lattice color codes, and the surface code. (Based on preliminary data).

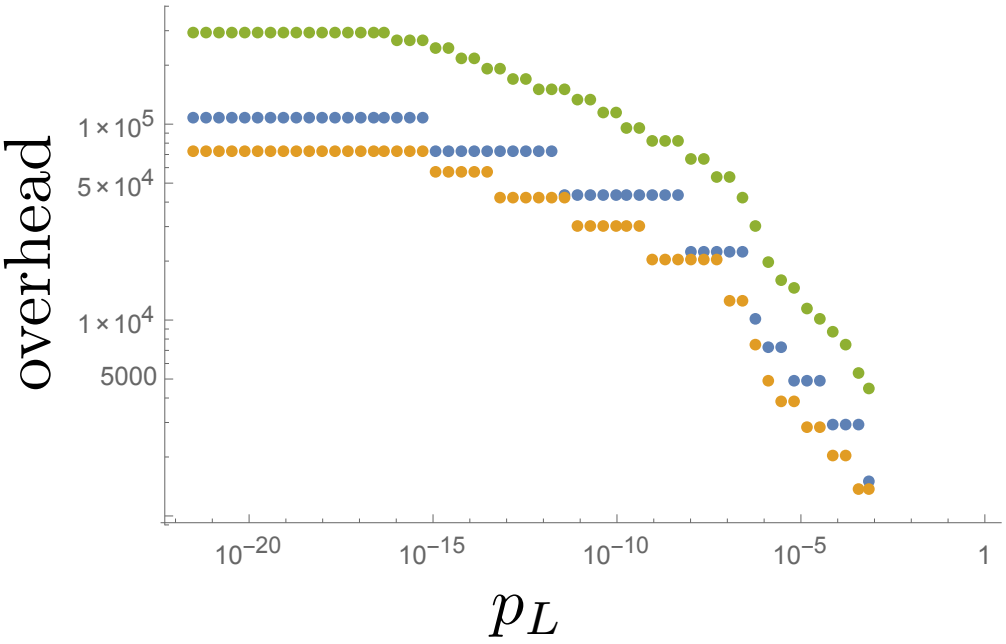

Figure 5.11: Approximate physical qubit overhead for forming a magic state with logical error rate below p_L with physical noise $p = 5 \times 10^{-4}$ by magic state distillation with (orange) the 6.6.6 color code, (green) the 4.8.8 color code, and (blue) the 4.4.4.4 Kitaev surface code. (Based on preliminary data).

5.8 Outlook

We have presented an analysis which shows that a lower bound of the overhead required for code switching for the known topological color codes and the overhead needed for state distillation are comparable. It is likely that lower bound is far from tight, suggesting that the overhead of code switching is actually significantly greater than the lower bound we present.

One would hope that other, currently unknown schemes for code switching exist with reduced overhead.

Despite the fact that the 4.8.8 code requires fewer qubits for a given distance, the hexagonal code has better threshold constants resulting in lower overhead for distillation at all target probabilities examined. On the other hand, the higher density of quibits required for a given distance for the surface code than the hexagonal color code overcomes the fact that the surface code has a better threshold for most values of p_T in this range.

BIBLIOGRAPHY

Aaronson, Scott and Daniel Gottesman (2004). "Improved simulation of stabilizer circuits". In: *Phys. Rev. A* 70, p. 052328.

Aharonov, Dorit and Michael Ben-Or (1997). "Fault-tolerant quantum computation with constant error". In: *Proceedings of the twenty-ninth annual ACM symposium on Theory of computing*. ACM, pp. 176–188.

Alex, Arne et al. (2011). "A numerical algorithm for the explicit calculation of SU(N) and SL(N,C) Clebsch–Gordan coefficients". In: *J. Math. Phys.* 52, p. 023507.

Alicki, R., S. Rudnicki, and S. Sadowski (1988). "Symmetry properties of product states for the system of N n-level atoms". In: *Journal of Mathematical Physics* 29.5, pp. 1158–1162.

Anderson, Jonas T., Guillaume Duclos-Cianci, and David Poulin (2014). "Fault-Tolerant Conversion between the Steane and Reed-Muller Quantum Codes". In: *Phys. Rev. Lett.* 113 (8), p. 080501.

Andrist, Ruben S et al. (2011). "Tricolored lattice gauge theory with randomness: fault tolerance in topological color codes". In: *New Journal of Physics* 13.8, p. 083006.

Aschauer, H., W. Dur, and H. -J. Briegel (2005). "Multiparticle entanglement purification for two-colorable graph states". In: *Phys. Rev. A* 71, p. 012319.

Atiyah, M. (1989). "Topological quantum field theories". In: *Inst. Hautes Études Sci. Publ. Math.* 68, pp. 175–186.

Bacon, Dave (2006). "Operator quantum error-correcting subsystems for self-correcting quantum memories". In: *Phys. Rev. A* 73, p. 012340.

Bacon, Dave, Isaac L. Chuang, and Aram W. Harrow (2007). "The Quantum Schur Transform: I. Efficient Qudit Circuits". In: *Proceedings of the eighteenth annual ACM-SIAM symposium on Discrete algorithms*, p. 1235.

Balents, Leon (2010). "Spin liquids in frustrated magnets". In: *Nature (London)* 464, p. 199.

Ballester, Manuel A (2006). "Estimating the spectrum of a density matrix with LOCC". In: *Journal of Physics A: Mathematical and General* 39.7, p. 1645.

Barnett, Ryan et al. (2006). "Quantum Magnetism with Multicomponent Dipolar Molecules in an Optical Lattice". In: *Phys. Rev. Lett.* 96, p. 190401.

Basko, D. M., I. L. Aleiner, and B. L. Altshuler (2006). "Metal–insulator transition in a weakly interacting many-electron system with localized single-particle states". In: *Ann. Phys.* 321, p. 1126.

Beckman, David et al. (2001). "Causal and localizable quantum operations". In: *Phys. Rev. A* 64, p. 052309.

Beigi, S., P. W. Shor, and D. Whalen (2011). "The Quantum Double Model with Boundary: Condensations and Symmetries". English. In: *Communications in Mathematical Physics* 306.3, pp. 663–694. ISSN: 0010-3616.

Beverland, Michael E et al. (2016). "Protected gates for topological quantum field theories". In: *Journal of Mathematical Physics* 57.2, p. 022201.

Beverland, Michael E. et al. (2016). "Realizing exactly solvable $\mathrm{SU}(N)$ magnets with thermal atoms". In: *Phys. Rev. A* 93 (5), p. 051601.

Bishof, M. et al. (2011). "Inelastic collisions and density-dependent excitation suppression in a 87Sr optical lattice clock". In: *Phys. Rev. A* 84, p. 052716.

Bloch, Immanuel, Jean Dalibard, and Sylvain Nascimbene (2012). "Quantum simulations with ultracold quantum gases". In: *Nature Phys.* 8, p. 267.

Bloch, Immanuel, Jean Dalibard, and Wilhelm Zwerger (2008). "Many-body physics with ultracold gases". In: *Rev. Mod. Phys.* 80, p. 885.

Bloom, B. J. et al. (2014). "An optical lattice clock with accuracy and stability at the 10^{-18} level". In: *Nature (London)* 506, p. 71.

Bollinger, J. J. et al. (1996). "Optimal frequency measurements with maximally correlated states". In: *Phys. Rev. A* 54, R4649.

Bombin, H. (2010). "Topological Order with a Twist: Ising Anyons from an Abelian Model". In: *Phys. Rev. Lett.* 105, p. 030403.

– (2013). "Optimal Transversal Gates under Geometric Constraints". In: arXiv:1311.0879.

Bombin, H (2014). "Dimensional Jump in Quantum Error Correction". In: *arXiv preprint arXiv:1412.5079*.

Bombín, H. (2013). "An Introduction to Topological Quantum Codes". In: *Topological Codes*. Ed. by Daniel A. Lidar and Todd A. Brun. Cambridge University Press.

Bombin, H. and M. Martin-Delgado (2006). "Topological Quantum Distillation". In: *Physical Review Letters* 97.18, p. 180501. ISSN: 0031-9007.

Bombín, H. and M. Martin-Delgado (2007). "Exact topological quantum order in D=3 and beyond: Branyons and brane-net condensates". In: *Phys. Rev. B* 75, p. 075103.

Bombin, H. and M. A. Martin-Delgado (2008). "Family of non-Abelian Kitaev models on a lattice: Topological condensation and confinement". In: *Phys. Rev. B* 78 (11), p. 115421.

Bombin, H. and M.A. Martin-Delgado (2007). "Topological Computation without Braiding". In: *Phys.Rev.Lett.* 98, p. 160502.

Bombin, Hector (2015). "Single-shot fault-tolerant quantum error correction". In: *Physical Review X* 5.3, p. 031043.

Bombin, Hector, Guillaume Duclos-Cianci, and David Poulin (2012). "Universal topological phase of two-dimensional stabilizer codes". In: *New Journal of Physics* 14.7, p. 073048.

Bonderson, P. H. et al. (2010). "A blueprint for a topologically fault-tolerant quantum computer". In: arXiv: 1003.2856.

Boyd, Martin M., Tanya Zelevinsky, Andrew D. Ludlow, Sebastian Blatt, et al. (2007). "Nuclear spin effects in optical lattice clocks". In: *Phys. Rev. A* 76, p. 022510.

Boyd, Martin M., Tanya Zelevinsky, Andrew D. Ludlow, Seth M. Foreman, et al. (2006). "Optical Atomic Coherence at the 1-Second Time Scale". In: *Science* 314, p. 1430.

Bravyi, S., M. Hastings, and F. Verstraete (2006). "Lieb-Robinson Bounds and the Generation of Correlations and Topological Quantum Order". In: *Physical Review Letters* 97.5, p. 050401. ISSN: 0031-9007.

Bravyi, S. and A. Y. Kitaev (1998). "Quantum codes on a lattice with boundary". In: arXiv:quant-ph/9811052.

Bravyi, Sergey and Andrew Cross (2015). "Doubled Color Codes". In: *arXiv preprint arXiv:1509.03239*.

Bravyi, Sergey and Alexei Kitaev (2005). "Universal quantum computation with ideal Clifford gates and noisy ancillas". In: *Phys. Rev. A* 71, p. 022316.

Bravyi, Sergey and Robert König (2013). "Classification of Topologically Protected Gates for Local Stabilizer Codes". In: *Phys. Rev. Lett.* 110, p. 170503.

Brell, Courtney G. et al. (2014). "Thermalization, Error Correction, and Memory Lifetime for Ising Anyon Systems". In: *Physical Review X* 4.3, p. 031058. ISSN: 2160-3308.

Britton, Joseph W et al. (2012). "Engineered two-dimensional Ising interactions in a trapped-ion quantum simulator with hundreds of spins". In: *Nature* 484.7395, pp. 489–492.

Brown, J.M. and A. Carrington (2003). *Rotational Spectroscopy of Diatomic Molecules*. Cambridge Molecular Science. Cambridge University Press. ISBN: 9780521530781.

Brown, R. C. et al. (2015). "Two-dimensional superexchange-mediated magnetization dynamics in an optical lattice". In: *Science* 348, p. 540.

Burton, Simon, Courtney G. Brell, and Steven T. Flammia (2015). "Classical Simulation of Quantum Error Correction in a Fibonacci Anyon Code". In: p. 5. arXiv: 1506.03815.

Calderbank, A. et al. (1997). “Quantum Error Correction and Orthogonal Geometry”. In: *Phys. Rev. Lett.* 78, pp. 405–408.

Cappellini, G. et al. (2014). “Direct Observation of Coherent Interorbital Spin-Exchange Dynamics”. In: *Phys. Rev. Lett.* 113, p. 120402.

Cazalilla, M. A., A. F. Ho, and M. Ueda (2009). “Ultracold gases of ytterbium: ferromagnetism and Mott states in an SU(6) Fermi system”. In: *New J. Phys.* 11, p. 103033.

Cazalilla, Miguel A and Ana Maria Rey (2014). “Ultracold Fermi gases with emergent SU(N) symmetry”. In: *Rep. Prog. Phys.* 77, p. 124401.

Chen, Xie, Zheng-Cheng Gu, and Xiao-Gang Wen (2010). “Local unitary transformation, long-range quantum entanglement, wave function renormalization, and topological order”. In: *Physical Review B* 82.15, p. 155138. ISSN: 1098-0121.

Childress, L. et al. (2005). “Fault-tolerant quantum repeaters with minimal physical resources and implementations based on single-photon emitters”. In: *Phys. Rev. A* 72, 052330, p. 052330.

Christandl, Matthias and Graeme Mitchison (2006). “The Spectra of Quantum States and the Kronecker Coefficients of the Symmetric Group”. In: 261.3, pp. 789–797.

Daley, Andrew J. (2011). “Quantum computing and quantum simulation with group-II atoms”. In: *Quantum Inf. Process.* 10, p. 865.

Daley, Andrew J. et al. (2008). “Quantum Computing with Alkaline-Earth-Metal Atoms”. In: *Phys. Rev. Lett.* 101, p. 170504.

Das, Arnab and Bikas K. Chakrabarti (2008). “Colloquium: Quantum annealing and analog quantum computation”. In: *Rev. Mod. Phys.* 80, p. 1061.

Delfosse, Nicolas (2014). “Decoding color codes by projection onto surface codes”. In: *Phys. Rev. A* 89 (1), p. 012317.

Deuretzbacher, F. et al. (2014). “Quantum magnetism without lattices in strongly interacting one-dimensional spinor gases”. In: *Phys. Rev. A* 90 (1), p. 013611.

Deutsch, C. et al. (2010). “Spin Self-Rephasing and Very Long Coherence Times in a Trapped Atomic Ensemble”. In: *Phys. Rev. Lett.* 105, p. 020401.

Devoret, M H and R J Schoelkopf (2013). “Superconducting circuits for quantum information: an outlook.” In: *Science* 339, pp. 1169–74.

Diaconis, Persi (1988). “Chapter 7: Representation Theory of the Symmetric Group”. In: *Group representations in probability and statistics*. Ed. by Shanti S. Gupta. Vol. Volume 11. Lecture Notes–Monograph Series. Hayward, CA: Institute of Mathematical Statistics, pp. 131–140.

Dicke, R. H. (1954). “Coherence in Spontaneous Radiation Processes”. In: *Phys. Rev.* 93, p. 99.

Duan, L. -M., E. Demler, and M. D. Lukin (2003). "Controlling Spin Exchange Interactions of Ultracold Atoms in Optical Lattices". In: *Phys. Rev. Lett.* 91, p. 090402.

Duclos-Cianci, Guillaume and David Poulin (2010). "Fast decoders for topological quantum codes". In: *Physical review letters* 104.5, p. 050504.

Dutta, T., M. Mukherjee, and K. Sengupta (2013). "Ramp Dynamics of Phonons in an Ion Trap: Entanglement Generation and Cooling". In: *Phys. Rev. Lett.* 111, p. 170406.

Eastin, B and E Knill (2009). "Restrictions on transversal encoded quantum gate sets". In: *Phys. Rev. Lett.* 102, p. 110502.

Eisert, J., M. Cramer, and M. B. Plenio (2010). "Colloquium: Area laws for the entanglement entropy". In: *Reviews of Modern Physics* 82.1.

Eisert, J., M. Friesdorf, and C. Gogolin (2015). "Quantum many-body systems out of equilibrium". In: *Nature Phys.* 11, p. 124.

Else, D. V. et al. (2012). "Symmetry-Protected Phases for Measurement-Based Quantum Computation". In: *Phys. Rev. Lett.* 108 (24), p. 240505.

Fowler, A. G., A. M. Stephens, and P. Groszkowski (2009). "High threshold universal quantum computation on the surface code". In: *Phys. Rev. A* 80, p. 052312.

Fowler, Austin G et al. (2012). "Surface codes: Towards practical large-scale quantum computation". In: *Physical Review A* 86.3, p. 032324.

Freedman, M. H., A. Y. Kitaev, and Z. Wang (2002). "Simulation of topological field theories by quantum computers". In: *Commun. Math. Phys.* 227, pp. 587–603.

Freedman, Michael H., Alexei Kitaev, et al. (2003). "Topological quantum computation". In: *Bull. Amer. Math. Soc.* 40, pp. 31–38.

Freedman, Michael H., Michael Larsen, and Zhenghan Wang (2002). "A Modular Functor Which is Universal for Quantum Computation". English. In: *Communications in Mathematical Physics* 227.3, pp. 605–622. ISSN: 0010-3616.

Freedman, M. et al. (2008). "On Picture (2+1)-TQFTs". In: *Topology and Physics*. Chap. 2, pp. 19–106.

Fukuhara, Takeshi et al. (2013). "Microscopic observation of magnon bound states and their dynamics". In: *Nature* 502, p. 76.

Fulton, William and Joe Harris (1991). "Representation Theory: A First Course (Graduate Texts in Mathematics)". In: Springer, New York.

Gibble, Kurt (2009). "Decoherence and Collisional Frequency Shifts of Trapped Bosons and Fermions". In: *Phys. Rev. Lett.* 103, p. 113202.

Gil, L. I. R. et al. (2014). "Spin Squeezing in a Rydberg Lattice Clock". In: *Phys. Rev. Lett.* 112, p. 103601.

González-Tudela, A. et al. (2015). "Subwavelength vacuum lattices and atom–atom interactions in two-dimensional photonic crystals". In: *Nature Photon.* 9.5, pp. 320–325.

Gorshkov, A. V., M. Hermele, et al. (2010). "Two-orbital SU(N) magnetism with ultracold alkaline-earth atoms". In: *Nature Phys.* 6, p. 289.

Gorshkov, A. V., S. R. Manmana, et al. (2011). "Tunable Superfluidity and Quantum Magnetism with Ultracold Polar Molecules". In: *Phys. Rev. Lett.* 107, p. 115301.

Gorshkov, A. V., A. M. Rey, et al. (2009). "Alkaline-Earth-Metal Atoms as Few-Qubit Quantum Registers". In: *Phys. Rev. Lett.* 102, p. 110503.

Gorshkov, Alexey V., Kaden R. A. Hazzard, and Ana Maria Rey (2013). "Kitaev honeycomb and other exotic spin models with polar molecules". In: *Mol. Phys.* 111, p. 1908.

Gottesman, Daniel (1996). "Class of quantum error-correcting codes saturating the quantum Hamming bound". In: *Phys. Rev. A* 54, pp. 1862–1868.

– (1998). "The Heisenberg Representation of Quantum Computers". In: arXiv: quant-ph/9807006.

Gottesman, Daniel and Isaac L. Chuang (1999). "Quantum Teleportation is a Universal Computational Primitive". In: *Nature* 402, pp. 390–393.

Greenberger, Daniel M., Michael A. Horne, and Anton Zeilinger (1989). "Going Beyond Bell's Theorem". In: *in 'Bell's Theorem, Quantum Theory, and Conceptions of the Universe', M. Kafatos (Ed.), Kluwer, Dordrecht*, pp. 69–72.

Greif, Daniel et al. (2013). "Short-Range Quantum Magnetism of Ultracold Fermions in an Optical Lattice". In: *Science* 340, p. 1307.

Gullans, M. et al. (2012). "Nanoplasmonic Lattices for Ultracold Atoms". In: *Phys. Rev. Lett.* 109 (23), p. 235309.

Haah, J. (2011). "Local stabilizer codes in three dimensions without string logical operators". In: *Phys. Rev. A* 83, p. 042330.

– (2014). *An invariant of topologically ordered states under local unitary transformations*. arXiv:1407.2926.

Hart, Russell A. et al. (2015). "Observation of antiferromagnetic correlations in the Hubbard model with ultracold atoms". In: *Nature (London)* 519, p. 211.

Hatcher, Allen (2002). *Algebraic Topology*. Cambridge University Press.

Hayashi, Masahito (2002). "Two quantum analogues of Fisher information from a large deviation viewpoint of quantum estimation". In: *Journal of Physics A: Mathematical and General* 35.36, p. 7689.

Hayes, David, Paul S. Julienne, and Ivan H. Deutsch (2007). "Quantum Logic via the Exchange Blockade in Ultracold Collisions". In: *Phys. Rev. Lett.* 98, p. 070501.

Hazlett, Eric L. et al. (2013). “s-Wave Collisional Frequency Shift of a Fermion Clock”. In: *Phys. Rev. Lett.* 110, p. 160801.

Hazzard, Kaden R. A. et al. (2012). “High-temperature properties of fermionic alkaline-earth-metal atoms in optical lattices”. In: *Phys. Rev. A* 85, p. 041604.

Hild, Sebastian et al. (2014). “Far-from-Equilibrium Spin Transport in Heisenberg Quantum Magnets”. In: *Phys. Rev. Lett.* 113, p. 147205.

Höfer, M. et al. (2015). “Observation of an Orbital Interaction-Induced Feshbach Resonance in $^{173}\mathrm{Yb}$”. In: *Phys. Rev. Lett.* 115, p. 265302.

Honerkamp, Carsten and Walter Hofstetter (2004). “Ultracold Fermions and the SU(N) Hubbard Model”. In: *Phys. Rev. Lett.* 92, p. 170403.

Horodecki, Ryszard et al. (2009). “Quantum entanglement”. In: *Rev. Mod. Phys.* 81, p. 865.

Hutter, Adrian and James R. Wootton (2015). “Continuous error correction for Ising anyons”. In: p. 8. arXiv: 1508.04033.

Jendrzejewski, F. et al. (2014). “...” In: *in preparation*.

Jochym-O’Connor, Tomas and Stephen D Bartlett (2015). “Stacked codes: universal fault-tolerant quantum computation in a two-dimensional layout”. In: *arXiv preprint arXiv:1509.04255*.

Jochym-O’Connor, Tomas and Raymond Laflamme (2014). “Using Concatenated Quantum Codes for Universal Fault-Tolerant Quantum Gates”. In: *Phys. Rev. Lett.* 112 (1), p. 010505.

Jones, Cody, Peter Brooks, and Jim Harrington (2015). “Gauge color codes in two dimensions”. In: *arXiv preprint arXiv:1512.04193*.

Jurcevic, P. et al. (2014). “Quasiparticle engineering and entanglement propagation in a quantum many-body system”. In: *Nature (London)* 511, p. 202.

K., Walker. (1991). *On Witten’s 3-manifold Invariants*. Lecture notes.

Katzgraber, Helmut G, H Bombin, and MA Martin-Delgado (2009). “Error threshold for color codes and random three-body ising models”. In: *Physical review letters* 103.9, p. 090501.

Keyl, M. (2006). “Quantum State Estimation and Large Deviations”. In: *Reviews in Mathematical Physics* 18.01, pp. 19–60.

Keyl, M. and R. F. Werner (2001). “Estimating the spectrum of a density operator”. In: *Phys. Rev. A* 64.052311.

Kitaev, A. Y. (2003). “Fault-tolerant quantum computation by anyons”. In: *Annals of Physics* 303.1, p. 2.

– (2006). “Anyons in an exactly solved model and beyond”. In: *Ann. Phys.* 321.1, p. 2.

Kitaev, A. Y. and L. Kong (2012). "Models for Gapped Boundaries and Domain Walls". In: *Communications in Mathematical Physics* 313.2, pp. 351–373. ISSN: 0010-3616.

Kitaev, A Yu (1997). "Quantum computations: algorithms and error correction". In: *Russ. Math. Surv.* 52.6, p. 1191.

Kitaev, A. and J. Preskill (2006). "Topological Entanglement Entropy". In: *Phys. Rev. Lett.* 96 (11), p. 110404.

Knap, Michael et al. (2013). "Probing Real-Space and Time-Resolved Correlation Functions with Many-Body Ramsey Interferometry". In: *Phys. Rev. Lett.* 111 (14), p. 147205.

Koller, A. P. et al. (2014). "Beyond the Spin Model Approximation for Ramsey Spectroscopy". In: *Phys. Rev. Lett.* 112, p. 123001.

Kong, L. and X.-G. Wen (2014). *Braided fusion categories, gravitational anomalies, and the mathematical framework for topological orders in any dimensions*. arXiv:1405.5858.

Koschorreck, Marco et al. (2013). "Universal spin dynamics in two-dimensional Fermi gases". In: *Nature Phys.* 9, p. 405.

Kubica, Aleksander and Michael Beverland (2015). "Universal transversal gates with color codes: A simplified approach". In: *Physical Review A* 91.3, p. 032330.

Kubica, Aleksander, Beni Yoshida, and Fernando Pastawski (2015). "Unfolding the color code". In: *New Journal of Physics* 17.8, p. 083026.

Landahl, Andrew J, Jonas T Anderson, and Patrick R Rice (2011). "Fault-tolerant quantum computing with color codes". In: *arXiv preprint arXiv:1108.5738*.

Lane, S. M. (1998). *Categories for the Working Mathematician*. Graduate Texts in Mathematics. Springer New York. ISBN: 9780387984032.

Levin, M. A. and X.-G. Wen (2005). "String-net condensation: A physical mechanism for topological phases". In: *Phys. Rev. B* 71, p. 045110.

– (2006). "Detecting Topological Order in a Ground State Wave Function". In: *Phys. Rev. Lett.* 96 (11), p. 110405.

Lieb, Elliott H. and Derek W. Robinson (1972). "The finite group velocity of quantum spin systems". In: *Communications in Mathematical Physics* 28.3, pp. 251–257.

MacWilliams, FJ and NJA Sloane (1977). *The theory of error-correcting codes*. North-Holland.

Maineult, Wilfried et al. (2012). "Spin Waves and Collisional Frequency Shifts of a Trapped-Atom Clock". In: *Phys. Rev. Lett.* 109, p. 020407.

Martin, M. J. et al. (2013). "A Quantum Many-Body Spin System in an Optical Lattice Clock". In: *Science* 341, p. 632.

Martinez de Escobar, Y. N. et al. (2008). "Two-photon photoassociative spectroscopy of ultracold Sr88". In: *Phys. Rev. A* 78 (6), p. 062708.

Micheli, A., G. K. Brennen, and P. Zoller (2006). "A toolbox for lattice-spin models with polar molecules". In: *Nature Phys.* 2, p. 341.

Michnicki, K. (2012). "3-d quantum stabilizer codes with a power law energy barrier". In: arXiv:1208.3496.

Moore, G. and N. Seiberg (1998). "Polynomial equations for rational conformal field theories". In: *Physics Letters B* 212.4, pp. 451–460.

Nayak, Chetan et al. (2008). "Non-Abelian anyons and topological quantum computation". In: *Rev. Mod. Phys.* 80 (3), pp. 1083–1159.

Nelson, Karl D., Xiao Li, and David S. Weiss (2007). "Imaging single atoms in a three-dimensional array". In: *Nature Phys.* 3, p. 556.

Nicholson, T. L. et al. (2014). "2e-18 total uncertainty in an atomic clock". In: *arXiv:1412.8261 [physics.atom-ph]*. eprint: arXiv:1412.8261.

Nielsen, MA and IL Chuang (2010). *Quantum Computation and Quantum Information*. Cambridge University Press.

Nielsen, Michael A. and Isaac L. Chuang (2000). *Quantum Computation and Quantum Information*. Cambridge University Press, Cambridge.

O'Donnell, Ryan and John Wright (2015). *Quantum Spectrum Testing*. eprint: arXiv:1501.05028.

Ohzeki, Masayuki (2009). "Accuracy thresholds of topological color codes on the hexagonal and square-octagonal lattices". In: *Physical Review E* 80.1, p. 011141.

Olmos, B. et al. (2013). "Long-Range Interacting Many-Body Systems with Alkaline-Earth-Metal Atoms". In: *Phys. Rev. Lett.* 110, p. 143602.

Paetznick, Adam and Ben W. Reichardt (2013). "Universal Fault-Tolerant Quantum Computation with Only Transversal Gates and Error Correction". In: *Phys. Rev. Lett.* 111 (9), p. 090505.

Pagano, Guido et al. (2014). "A one-dimensional liquid of fermions with tunable spin". In: *Nature Phys.* 10, p. 198.

Pagano, G. et al. (2015). "Strongly Interacting Gas of Two-Electron Fermions at an Orbital Feshbach Resonance". In: *Phys. Rev. Lett.* 115, p. 265301.

Pastawski, F. and B. Yoshida (2014). *Fault-tolerant logical gates in quantum error-correcting codes*. arXiv:1408.1720.

Pastawski, Fernando and Beni Yoshida (2014). "Fault-tolerant logical gates in quantum error-correcting codes". In: arXiv: 1408.1720.

Pechkis, H. K. et al. (2013). "Spinor Dynamics in an Antiferromagnetic Spin-1 Thermal Bose Gas". In: *Phys. Rev. Lett.* 111, p. 025301.

Pedrocchi, Fabio L. and David P. DiVincenzo (2015). “Majorana Braiding with Thermal Noise”. In: *Phys. Rev. Lett.* 115 (12), p. 120402.

Pielawa, Susanne et al. (2011). “Correlated phases of bosons in tilted frustrated lattices”. In: *Phys. Rev. B* 83.20.

Polkovnikov, Anatoli et al. (2011). “Colloquium: Nonequilibrium dynamics of closed interacting quantum systems”. In: *Rev. Mod. Phys.* 83, p. 863.

Poulin, David (2005). “Stabilizer Formalism for Operator Quantum Error Correction”. In: *Phys. Rev. Lett.* 95, p. 230504.

Preskill, J. (1998). “Reliable quantum computers”. In: *Proc. Roy. Soc. Lond.* 454, pp. 385–410.

– (2004). *Lecture notes on Quantum Computation*.

Preskill, John (2012). “Sufficient condition on noise correlations for scalable quantum computing”. In: *arXiv preprint arXiv:1207.6131*.

Reichenbach, Iris and Ivan H. Deutsch (2007). “Sideband Cooling while Preserving Coherences in the Nuclear Spin State in Group-II-like Atoms”. In: *Phys. Rev. Lett.* 99, p. 123001.

Rey, A. M., A. V. Gorshkov, C. V. Kraus, et al. (2014). “Probing many-body interactions in an optical lattice clock”. In: *Ann. Phys.* 340, p. 311.

Rey, A. M., A. V. Gorshkov, and C. Rubbo (2009). “Many-Body Treatment of the Collisional Frequency Shift in Fermionic Atoms”. In: *Phys. Rev. Lett.* 103, p. 260402.

Rey, A. M., L. Jiang, et al. (2008). “Many-body protected entanglement generation in interacting spin systems”. In: *Phys. Rev. A* 77, p. 052305.

Richerme, Philip et al. (2014). “Non-local propagation of correlations in quantum systems with long-range interactions”. In: *Nature* 511, p. 198.

Romero-Isart, O. et al. (2013). “Superconducting Vortex Lattices for Ultracold Atoms”. In: *Phys. Rev. Lett.* 111 (14), p. 145304.

Rose, M. E. (1957). *Elementary Theory of Angular Momentum*. Dover Publications Inc, New York.

Sackett, C. A. et al. (2000). “Experimental entanglement of four particles”. In: *Nature (London)* 404, p. 256.

Saffman, M. and K. Molmer (2009). “Efficient Multiparticle Entanglement via Asymmetric Rydberg Blockade”. In: *Phys. Rev. Lett.* 102, p. 240502.

Sagan, Bruce E. (2000). *The Symmetric Group*. Springer, New York.

Sarvepalli, Pradeep and Robert Raussendorf (2012). “Efficient decoding of topological color codes”. In: *Physical Review A* 85.2, p. 022317.

Scazza, Francesco et al. (2014). “Observation of two-orbital spin-exchange interactions with ultracold SU (N)-symmetric fermions”. In: *Nature Physics* 10.10, pp. 779–784.

Schauß, Peter et al. (2012). “Observation of spatially ordered structures in a two-dimensional Rydberg gas”. In: *Nature (London)* 491, p. 87.

Segal, G. (2004). “The definition of conformal field theory”. In: vol. 308. preprint. London Math. Soc. Lecture Note Ser., Cambridge University Press.

Shor, P.W. (1996). “Fault-tolerant quantum computation”. In: *Proceedings of 37th Conference on Foundations of Computer Science*. IEEE Comput. Soc. Press, pp. 56–65.

Simon, Jonathan et al. (2011). “Quantum simulation of antiferromagnetic spin chains in an optical lattice”. In: *Nature (London)* 472, p. 307.

Sommer, Ariel et al. (2011). “Universal spin transport in a strongly interacting Fermi gas”. In: *Nature (London)* 472, p. 201.

Sorensen, Anders and Klaus Molmer (1999). “Quantum Computation with Ions in Thermal Motion”. In: *Phys. Rev. Lett.* 82, p. 1971.

Steane, Andrew (1999). “Quantum Reed-Muller Codes”. In: *IEEE Trans. Info. Th.* 45, pp. 1701–1703.

Stephens, Ashley M (2014). “Efficient fault-tolerant decoding of topological color codes”. In: *arXiv preprint arXiv:1402.3037*.

Swallows, Matthew D. et al. (2011). “Suppression of Collisional Shifts in a Strongly Interacting Lattice Clock”. In: *Science* 331, p. 1043.

Taie, Shintaro et al. (2012). “An SU(6) Mott insulator of an atomic Fermi gas realized by large-spin Pomeranchuk cooling”. In: *Nature Phys.* 8, p. 825.

Traverso, A. et al. (2009). “Inelastic and elastic collision rates for triplet states of ultracold strontium”. In: *Phys. Rev. A* 79 (6), p. 060702.

Trotzky, S. et al. (2008). “Time-Resolved Observation and Control of Superexchange Interactions with Ultracold Atoms in Optical Lattices”. In: *Science* 319, p. 295.

Verlinde, E. (1988). “Fusion rules and modular transformations in 2D conformal field theory”. In: *Nucl. Phys. B* 300, pp. 360–376.

Volosniev, A. G. et al. (2015). “Engineering the dynamics of effective spin-chain models for strongly interacting atomic gases”. In: *Phys. Rev. A* 91, p. 023620.

Wang, Chenyang, Jim Harrington, and John Preskill (2003). “Confinement-Higgs transition in a disordered gauge theory and the accuracy threshold for quantum memory”. In: *Annals of Physics* 303.1, pp. 31–58.

Wang, David S et al. (2009). “Threshold error rates for the toric and surface codes”. In: *arXiv preprint arXiv:0905.0531*.

Wang, Z. (2010). *Topological Quantum Computation*. Regional Conference Series in Mathematics 112. Conference Board of the Mathematical Sciences.

Wecker, Dave et al. (2014). "Gate-count estimates for performing quantum chemistry on small quantum computers". In: *Phys. Rev. A* 90, p. 022305.

Wilson, Robin J. (1996). *Introduction to Graph Theory*. Longman.

Witten, E. (1989). "Quantum field theory and the Jones polynomial". In: *Comm. Math. Phys.* 121.3, pp. 351–399.

Wu, Congjun (2008). "Orbital Ordering and Frustration of p-Band Mott Insulators". In: *Phys. Rev. Lett.* 100, p. 200406.

Yan, Bo et al. (2013). "Observation of dipolar spin-exchange interactions with lattice-confined polar molecules". In: *Nature (London)* 501, p. 521.

Ye, Jun, H. J. Kimble, and Hidetoshi Katori (2008). "Quantum State Engineering and Precision Metrology Using State-Insensitive Light Traps". In: *Science* 320, p. 1734.

Yu, Zhenhua and C. J. Pethick (2010). "Clock Shifts of Optical Transitions in Ultracold Atomic Gases". In: *Phys. Rev. Lett.* 104, p. 010801.

Zhang, Ren et al. (2015). "Orbital Feshbach Resonance in Alkali-Earth Atoms". In: *Phys. Rev. Lett.* 115, p. 135301.

Zhang, X. et al. (2014). "Spectroscopic observation of SU(N)-symmetric interactions in Sr orbital magnetism". In: *Science* 345, p. 1467.